USAAEFA PROJECT NO. 73-01

(6)

LEVEL II

NW

HELICOPTER LIFT MARGIN SYSTEM AND LOW-SPEED PERFORMANCE EVALUATION

NUH-1M HELICOPTER

FINAL REPORT

FLOYD L. DOMINICK
PROJECT OFFICER

DAUMANTS BELTE
PROJECT ENGINEER

JAMES C. O'CONNOR
MAJ, CE
US ARMY
PROJECT PILOT

ALEXANDER J. KRYNYTZKY
PROJECT ENGINEER

ROBERT P. JEFFERIS
INSTRUMENTATION ENGINEER

WARREN E. GRIFFITH
LTC, AR
US ARMY
PROJECT PILOT

AUGUST 1977

Approved for public release; distribution unlimited.

UNITED STATES ARMY AVIATION ENGINEERING FLIGHT ACTIVITY
EDWARDS AIR FORCE BASE, CALIFORNIA 93523

DISCLAIMER NOTICE

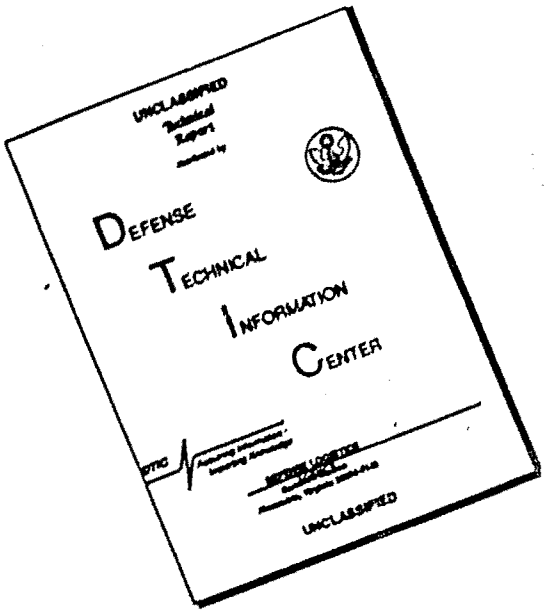

THIS DOCUMENT IS BEST QUALITY AVAILABLE. THE COPY FURNISHED TO DTIC CONTAINED A SIGNIFICANT NUMBER OF PAGES WHICH DO NOT REPRODUCE LEGIBLY.

DISCLAIMER NOTICE

The findings of this report are not to be construed as an official Department of the Army position unless so designated by other authorized documents.

DISPOSITION INSTRUCTIONS

Destroy this report when it is no longer needed. Do not return it to the originator.

TRADE NAMES

The use of trade names in this report does not constitute an official endorsement or approval of the use of the commercial hardware and software.

TABLE OF CONTENTS

UNCLASSIFIED

SECURITY CLASSIFICATION OF THIS PAGE *(When Data Entered)*

REPORT DOCUMENTATION PAGE

READ INSTRUCTIONS BEFORE COMPLETING FORM

1. REPORT NUMBER: USAAEFA PROJECT NO. 73-01	2. GOVT ACCESSION NO.
3. RECIPIENT'S CATALOG NUMBER	
4. TITLE *(and Subtitle)*: HELICOPTER LIFT MARGIN SYSTEM AND LOW-SPEED PERFORMANCE EVALUATION NUH-1M HELICOPTER,	5. TYPE OF REPORT & PERIOD COVERED: FINAL REPORT, 28 Sep 1973 – 10 Sep 1974
	6. PERFORMING ORG. REPORT NUMBER: USAAEFA PROJECT NO. 73-01
7. AUTHOR(s): FLOYD L. DOMINICK, DAUMANTS BELTE, MAJ JAMES C. O'CONNOR, ALEXANDER J. KRYNYTZKY, LTC WARREN E. GRIFFITH, ROBERT P. JEFFERIS	8. CONTRACT OR GRANT NUMBER(s)
9. PERFORMING ORGANIZATION NAME AND ADDRESS: US ARMY AVIATION ENGINEERING FLIGHT ACTIVITY, EDWARDS AIR FORCE BASE, CALIFORNIA 93523	10. PROGRAM ELEMENT, PROJECT, TASK AREA & WORK UNIT NUMBERS: None
11. CONTROLLING OFFICE NAME AND ADDRESS: US ARMY AVIATION ENGINEERING FLIGHT ACTIVITY, EDWARDS AIR FORCE BASE, CALIFORNIA 93523	12. REPORT DATE: AUGUST 1977
	13. NUMBER OF PAGES: 172
14. MONITORING AGENCY NAME & ADDRESS *(if different from Controlling Office)*: 12) 174 p.	15. SECURITY CLASS. *(of this report)*: UNCLASSIFIED
	15a. DECLASSIFICATION/DOWNGRADING SCHEDULE

16. DISTRIBUTION STATEMENT *(of this Report)*

Approved for public release; distribution unlimited.

17. DISTRIBUTION STATEMENT *(of the abstract entered in Block 20, if different from Report)*

18. SUPPLEMENTARY NOTES

19. KEY WORDS *(Continue on reverse side if necessary and identify by block number)*

Engineering flight evaluation
Helicopter lift margin system
NUH-1M helicopter
Sensor and computer system
Performance margin

20. ABSTRACT *(Continue on reverse side if necessary and identify by block number)*

The United States Army Aviation Engineering Flight Activity conducted an engineering flight evaluation of a helicopter lift margin system installed in an NUH-1M aircraft. The Trans-Sonics, Inc. helicopter lift margin system tested is a special-purpose sensor and computer system designed to continuously compute and display performance margin in terms of excess hover thrust available (lift margin). The prototype system evaluated approaches an operationally adequate (OVER)

DD FORM 1 JAN 73 1473 EDITION OF 1 NOV 65 IS OBSOLETE

409025

UNCLASSIFIED

SECURITY CLASSIFICATION OF THIS PAGE *(When Data Entered)*

20. ABSTRACT

system and represents a significant improvement over previous methods of presenting performance information. Fifty-eight productive flights were flown from 28 September through 23 December 1973 and from 25 June through 10 September 1974, resulting in 31 productive test hours. Tests were conducted at Edwards Air Force Base, Oxnard, Bishop, and Coyote Flats, California, to obtain a large variation in ambient conditions. Correction of the four deficiencies would result in an operationally suitable system. The deficiencies were (1) lack of consideration of low airspeed (wind) and its effects, (2) the requirement to hover out of ground effect prior to having lift margin available, (3) lack of a comprehensive failure warning, and (4) inadequate range of operational conditions considered in the design. The effects of winds could introduce errors as large as 2000 pounds. A significant portion of the tests was devoted to defining the effects of wind on helicopter performance, data not previously available. With the exception of wind effects, the system demonstrated an accuracy within 200 to 300 pounds, or approximately 2.5 to 4.5 percent of the aircraft gross weight range as tested. The goal of the system is 1 percent of aircraft gross weight. The 1-percent accuracy goal could be met with inclusion of low airspeed, modest improvement of the performance characterization and input parameter accuracy, and possible input of additional parameters that are available from the normal aircraft systems. The added complexity would probably make completely digital computation desirable rather than the hybrid method used in the prototype system. With the basic data input and performance characterizations, the computer could be tailored to provide performance information important to any aircraft type or mission in addition to lift margin. Although the initial justification of the lift margin system was to reduce takeoff and landing accidents due to insufficient thrust, a more probable benefit is increased aircraft productivity achieved by the safe use of the full performance potential of the helicopter.

INTRODUCTION

BACKGROUND

1. Numerous helicopter accidents have occurred in vertical or confined area takeoff and landing situations. A contributing factor to some of these accidents can be attributed to insufficient main rotor thrust when translating from in-ground-effect (IGE) hover to out-of-ground-effect (OGE) forward flight. Under Joint Army-Navy Aircraft Instrumentation Research (JANAIR) sponsorship, exploratory development was initiated to develop a system that would predict the aircraft lift margin prior to initiating these maneuvers. The direct availability of performance margins from such a computer can reduce accidents by helping the pilot avoid situations beyond the capability of his aircraft. Another benefit is increased mission effectiveness and productivity attained by allowing the pilot to safely use the full performance capability of the aircraft. A feasibility study for a lift margin system was reported in reference 1, appendix A, and evaluation of a manual input hover lift computer was reported in reference 2. The Office of Naval Research (ONR) contracted with Trans-Sonics, Inc. to provide a complete helicopter lift margin system (HLMS) for testing, and requested that the United States Army Aviation Engineering Flight Activity (USAAEFA) conduct an engineering flight evaluation. The United States Army Aviation Systems Command (AVSCOM)* directed USAAEFA to perform this test. A test plan (ref 3) to determine overall suitability of the system and to provide basic performance data in the hover environment was published in July 1973, and preliminary findings were reported in a letter report to ONR in August 1974 (ref 4).

TEST OBJECTIVES

2. The general objectives of the HLMS flight evaluation were as follows:

a. To determine overall accuracy and operational suitability of the system as an in-flight performance computer.

b. Evaluate the effects of wind speed, wind direction, humidity, and pilot control inputs on hover performance and HLMS indications.

3. Specific objectives were to evaluate individual and combined accuracies of the following parameters used in the lift margin computation:

a. Maximum available torque (Q_{ma}).

b. Maximum standard torque (Q_{ms}).

c. Effective gross weight (EGW)

*Since redesignated the Army Aviation Research and Development Command (AVRADCOM).

DESCRIPTION

Test Aircraft

4. The test helicopter, shown in photo A, was an NUH-1M, SN 63-8684. It is the small fuselage (9-seat capacity) model "Huey." The M series UH-1 incorporates a teetering main rotor which has a 44-foot diameter and two 27-inch chord blades. It is powered by a T53-L-13B turboshaft engine rated at 1400 shaft horsepower (shp) for sea-level, standard-day uninstalled conditions. The engine is derated to 1100 shp for the UH-1M installation due to drive train limits. The test aircraft was in standard configuration except for the test instrumentation and data installations described in appendix B. A detailed description of the UH-1M can be found in the operator's manual (ref 5, app A).

Air Data Systems

5. At the hover and ground test sites, sensors were available to record barometric pressure, temperature, and humidity at ground elevation. Wind speed information was furnished by sensors mounted on three 65-foot wind towers arranged symmetrically about and 400 feet from the hover site. Each tower provided readings of wind speed and direction at 6, 14, and 62-foot levels. Photo B shows the lower levels and sensors of one tower with a hover test being conducted in the background. A more detailed description of the ground instrumentation is contained in appendix C.

6. The standard test boom airspeed installation is inaccurate at airspeeds below 30 knots, where most of the testing was done. A dual-axis low airspeed system (Elliott LASSIE II) was installed in the aircraft, as shown in photo C, and was also tested in conjunction with the HLMS evaluation. Results of the airspeed systems test are reported in reference 6, appendix A. LASSIE II provided a direct presentation of forward, sideward, and rearward airspeed components in this low-speed regime, and also displayed pressure altitude and rate of climb. At skid heights of more than 65 feet where ground-recorded wind data were not applicable, LASSIE II was the only available source of low airspeed data.

Helicopter Lift Margin System

7. The HLMS is a special purpose hybrid (digital and analog) computer designed to present performance margin in terms of excess thrust available to hover. The HLMS computes aircraft EGW and maximum available hover lift (MAL) at existing or selected altitude and temperature conditions and displays the difference as lift margin to the pilot. Transducers input data concerning engine torque pressure, compressor inlet temperature (CIT), and ambient static air pressure. All computing, control, and display functions are contained in a single computer and display (C&D) unit, shown in photo D, which is mounted in the center instrument console.

Photo A. NUH-1M Test Aircraft.

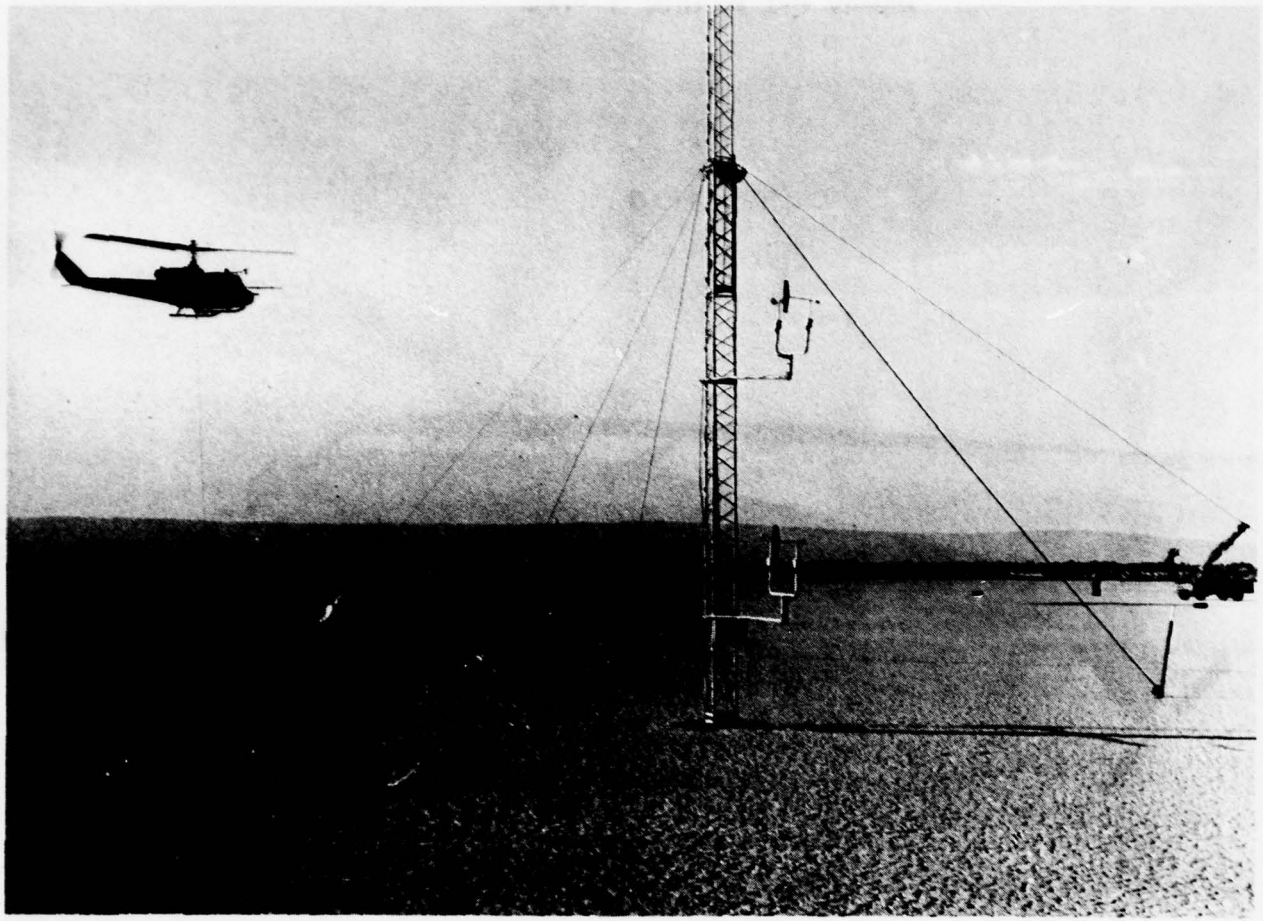

Photo B. Out-of-Ground-Effect Hover Testing and Lower Two Levels of One On-Site Wind Tower

Photo C. Test Aircraft Showing Installed LASSIE II Swivel-Mounted Air-Data Sensor

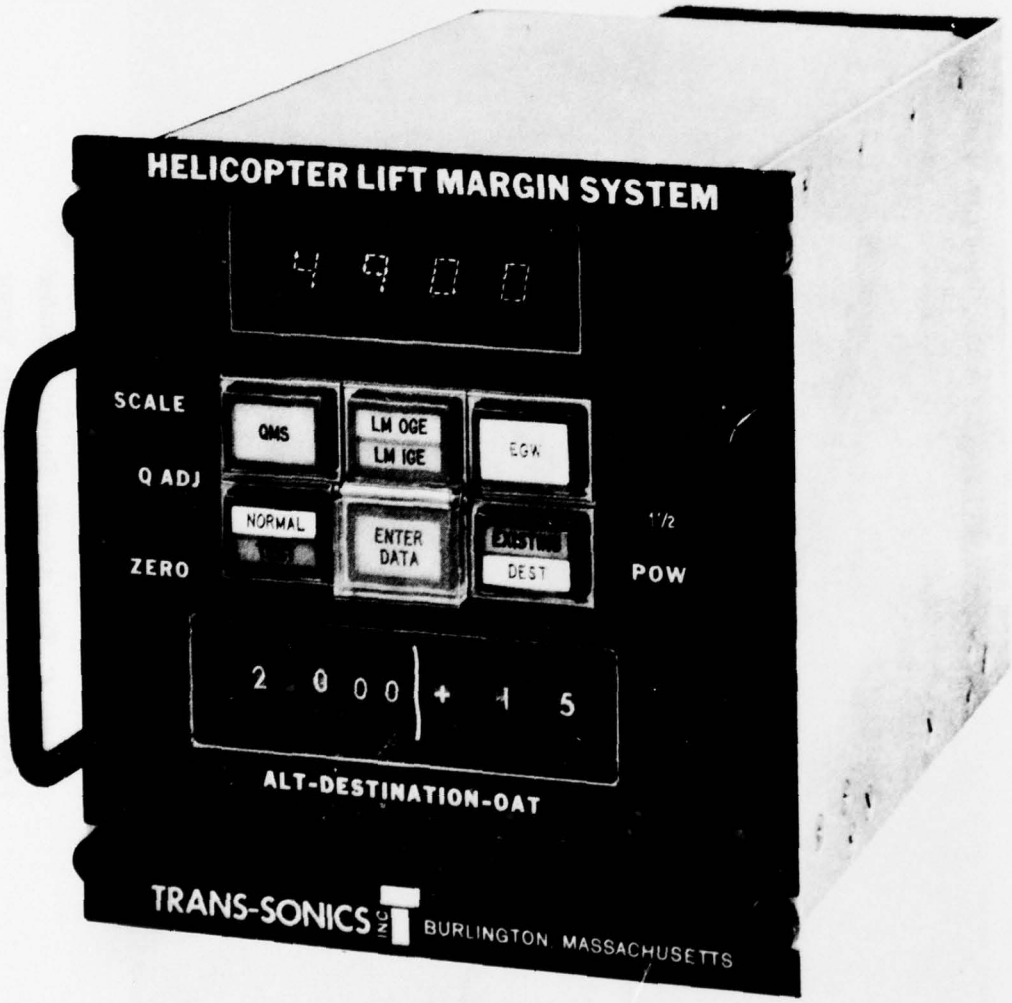

Photo D. Computer and Display Unit of the Helicopter Lift Margin System.

8. No formal accuracy specifications were stipulated. One percent overall accuracy was considered to be a desirable goal since in the UH-1, since this allows a decision on the number of troops to be carried.

9. Operation of the system requires two maneuvers to provide data to initialize the computer. A "topping maneuver" (demanding maximum power available) is performed to determine present condition Q_{ma}. From Q_{ma}, existing altitude, and temperature, the torque that would be available on a sea-level standard day (Q_{ms}) is computed and stored by the C&D unit. The Q_{ma} at any future condition is then continuously computed from this stored Q_{ms}. MAL is in turn continuously computed from Q_{ma}. The topping maneuver need not be performed on every flight since Q_{ms} should only change with a change in basic engine performance. A "weighing maneuver" is performed by hovering OGE at zero wind conditions to determine present aircraft EGW. EGW is continuously updated for computed fuel consumption based on existing torque and altitude. This value is stored and used to continuously compute and display lift margin based on the difference between EGW and MAL at existing or selected conditions. The weighing maneuver must be performed on initial takeoff and when the aircraft gross weight is changed by other than fuel consumption (*eg*, releasing sling load).

10. The HLMS has two general operating modes. In the "existing" mode, altitude and temperature information are input from transducers. In the "destination" mode, altitude and temperature are input manually via thumbwheels.

11. In addition to the C&D unit, a simulation and monitoring (S&M) test set was also available during the evaluation for functional checks and calibration of the HLMS. The input data, intermediate calculations, and final output were recorded by the data system. A more detailed description of the HLMS is included in appendix D.

TEST SCOPE

12. To obtain maximum practical variation in altitude, temperature, and humidity, four test sites were used: Edwards Air Force Base (field elevation 2270 feet), Oxnard (80 feet), Bishop (4120 feet), and Coyote Flats (9990 feet), California. Project flying comprised 58 test flights, resulting in 31 productive hours. Productive test flights took place during the periods between 28 September through 23 December 1973 and 25 June through 10 September 1974.

13. Test conditions were within the flight envelope contained in the operator's manual. All flights were conducted at a mid center of gravity (cg), and ballast was used to vary the aircraft weight from 6600 to 8300 pounds.

14. Tethered and free flight hover tests were conducted at all sites at 2 and 50-foot skid heights, with different relative winds of speeds from zero to 28 knots true airspeed (KTAS).

15. The parameters listed below were varied to evaluate their influence on aircraft hover performance and on the HLMS computed quantities.

a. Aircraft gross thrust.

b. Engine power output.

c. Wind speed.

d. Wind direction.

e. Ambient air density.

f. Ambient air temperature.

g. Rotor speed.

h. Vertical velocity.

i. Ambient air humidity.

j. Pilot control inputs.

k. Bleed air/anti-ice.

l. Ground effect (skid height).

16. At the Edwards test site, the aircraft was stabilized with reference to a calibrated ground pace vehicle in surface winds below 5 KTAS at 5 and 50-foot skid heights to obtain data for comparison with the hover test results. Forward flight data from hover to 50 KTAS were obtained. Rearward, sideward, and sideslip flights were limited to a maximum airspeed of 30 KTAS. Flights at altitude were conducted to obtain data for engine toppings, speed-power performance to 110 KTAS, hover ceiling determination, and vertical climb and descent at rates of up to ±500 feet per minute.

TEST METHODOLOGY

17. The flight tests defined one matrix for actual power available and another of power required at a variety of conditions. Where possible, nondimensional format was used in working with the performance parameters. The equations used are given in appendix E. Nondimensionalizing power (C_P), weight (C_T), and airspeed (μ) with respect to rotor speed and air density reduced the number of independent test variables and allowed more efficient analysis by cross-plotting and carpet plotting techniques. These data could then be converted to a form directly comparable to the following types of HLMS output:

a. Actual output as recorded in flight tests at various conditions.

b. Design output as defined by the lift margin computer equations.

c. Hardware output during bench testing with controlled transducer inputs.

The effects of parameters not included in the HLMS equations on available and required power could also be isolated.

18. Maximum power available was determined by engine topping maneuvers in free flight and in tethered hover. Variation of available shp with pressure altitude and outside air temperature was directly compared with the HLMS output. The HLMS Q_{ms}, and Q_{ma} outputs at varying conditions were then compared to the actual test data matrix values.

19. Power required to hover was defined during free and tethered hover tests. Effective gross thrust was changed by varying cable tension. The effect of wind on required power was correlated with the measured wind velocity. Low-speed pace flights simulated hover at constant gross weight with varving wind velocities. Accuracy of the EGW output from the HLMS was evaluated by comparison with altitude, temperature, gross weight, and required power from the test data matrix.

20. Bench testing of the HLMS hardware with known inputs of altitude, temperature, and engine torque allowed comparison of actual output to output calculated by the published lift margin equations.

RESULTS AND DISCUSSION

GENERAL

21. Correction of the deficiencies found in the prototype HLMS that was evaluated would result in an operationally suitable system. These deficiencies included (1) the lack of consideration of wind and its effects, (2) the requirement to hover OGE prior to having lift margin information available, (3) the lack of a comprehensive failure warning, and (4) the inadequate range of operational conditions considered in the design. Excluding the effects of wind, the HLMS demonstrated an accuracy within 200 to 300 pounds. The goal was 1 percent of aircraft gross weight. The unaccounted-for effects of wind could introduce errors as large as 2000 pounds. Operation at ambient conditions more extreme than those experienced during the tests would increase the error. The 1-percent accuracy goal can be met with inclusion of a low airspeed input, modest improvement of the performance characterization and input parameter accuracy, and possible input of additional parameters that are available from the normal aircraft systems. Consideration should be given to providing other performance information in addition to hover lift margin in future designs. With the basic data input and performance characterizations. the HLMS or similar on-board performance computer could be tailored to provide additional performance information such as range, endurance, maneuver capability, or other performance information critical to a given aircraft or mission.

22. The HLMS representation of actual aircraft performance depends on the validity of two basic characterizations:

a. The relation of engine torque and air density to helicopter lift (power required).

b. The effect of ambient pressure ratio and compressor inlet temperature on available engine torque (power available).

The analytical expressions modeled in the HLMS are described in appendix D, and the transformation equations applied to generate parameters directly comparable to flight test data summaries of actual aircraft performance are given in appendix E. Laboratory evaluation of the HLMS hardware showed good agreement between its actual output functions and its design analytical expressions. A detailed discussion of the flight tests and comparison between observed aircraft performance and the HLMS characterizations follows in the remainder of this section.

POWER REQUIRED AND EFFECTIVE GROSS WEIGHT

23. Performance tests were conducted to determine power required to hover at the conditions listed below. Paced flights were flown at similar atmospheric

conditions, with the exception that allowable wind velocities were limited to 5 knots.

a. Gross thrust (aircraft weight plus cable tension): 6000 to 10,300 pounds.

b. Rotor speed: 294 to 324 rpm.

c. Pressure altitude: -200 to 9700 feet.

d. Ambient temperature: -2 to 28°C.

e. Wind speed: Zero to 28 KTAS.

24. Analysis of power-required data was made in terms of the nondimensional parameters C_P, C_T, and μ. The validity of this analysis was checked by multiple correlation of the nondimensional relationships with each dimensional parameter. No significant residuals remained, which indicates that the analysis was valid for the range of data used. Rotor tip speed mach numbers were too low for compressibility effects to appear, as discussed in paragraph 36, appendix E. The influence of varying ambient conditions and aircraft configurations is discussed below.

Thrust

25. Aircraft thrust was varied in tethered hover by varying engine power and/or rotor speed and then measuring cable tension, or in free flight by changing the gross weight with ballast. The base-line condition at stabilized OGE hover in zero winds is shown in figure A (equation 18, app E), and the test data used to derive this curve are given in figure 2, appendix F.

26. The HLMS uses a measurement of engine torque at existing ambient conditions during the weighing maneuver to define the aircraft EGW. The HLMS power-required calculation in nondimensional format yields the straight line shown in figure A (equation 34, app E), where it is compared to the actual nonlinear function of power required versus thrust. In the central region between the two intersections, the HLMS calculated EGW is lower than actual, but is higher in the outside regions. At a fixed rotor speed of 324 rpm, the zone of maximum error is from C_T = .0040 to .0046 and represents an underestimate in gross weight of 140 to 180 pounds, depending on air density.

Air Density

28. The effect of air density variation can be calculated from the test nondimensional power-required curve of figure A. Taking a constant rotor speed of 324 rpm, figure B shows the power required at zero velocity for different density altitudes (equations 4, 5, and 18, app E).

Figure A. Nondimensional Comparison of Actual Out-Of-Ground Effect Hover Performance With the HLMS Model.

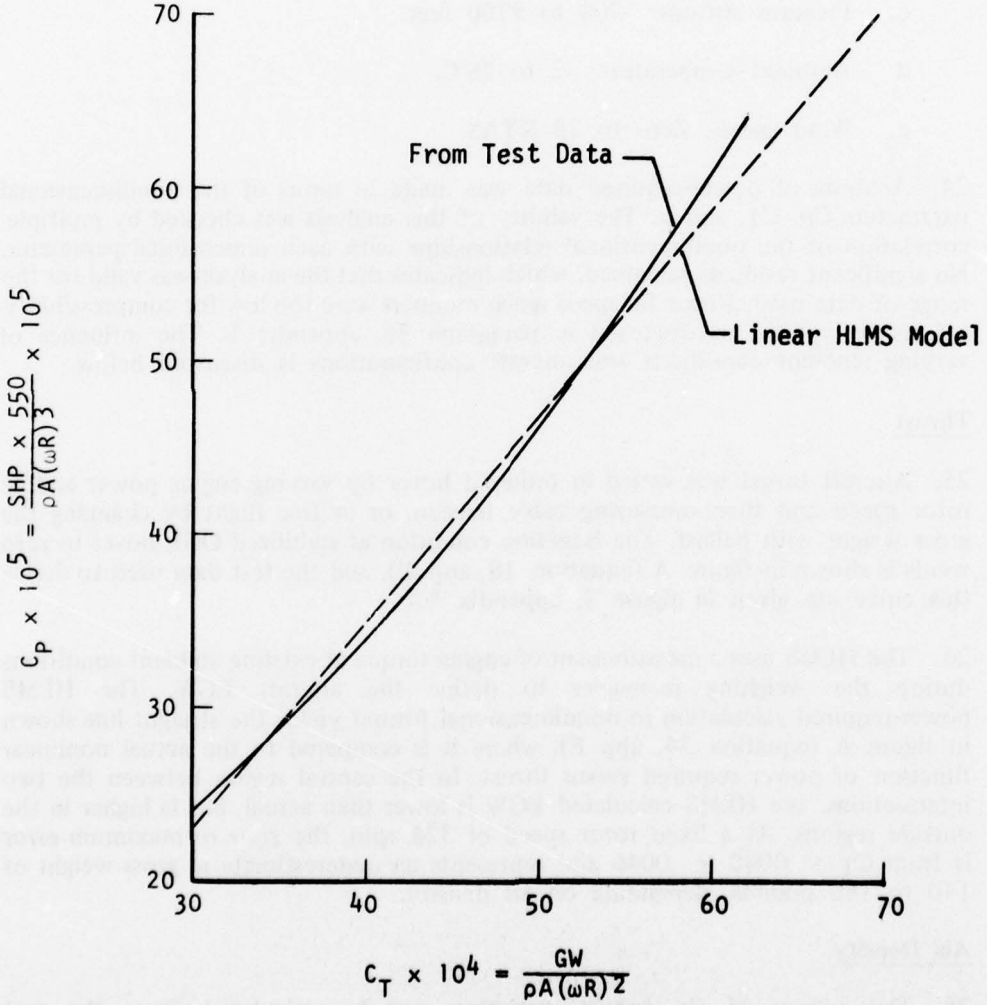

Figure B. Air Density Influence on Out-Of-Ground Effect Hover Performance.

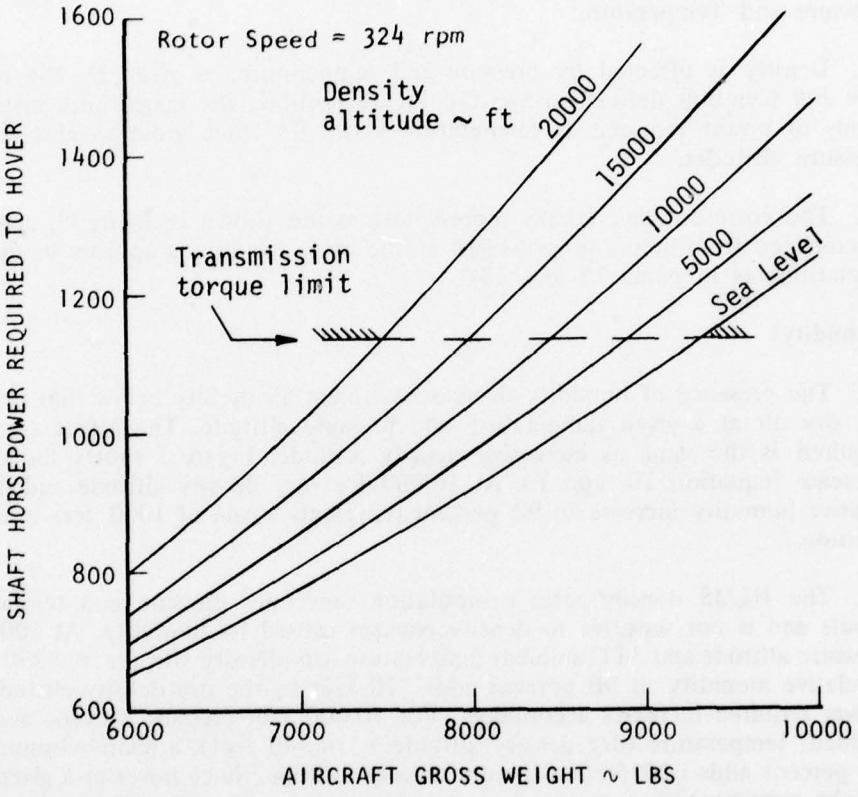

28. Similarly, the effect of the density term on EGW output can be extracted from the HLMS power-required function; figure C presents this dimensionally (equation 33, app E). The power-required differences between the HLMS model and the flight test summary are shown in figure D. From this, the difference between the HLMS linearization of EGW and the actual aircraft gross weight in OGE hover is illustrated in figure E (Δ lift from Δ power using dimensional form of equation 18, app E, as described in para 35, app E).

Pressure and Temperature:

29. Density is affected by pressure and temperature, as given by the relation $\sigma = \delta/\theta$ (symbols defined in app G). Figure F shows the magnitudes involved in terms of power required as temperature varies for three gross weights and five pressure altitudes.

30. The corresponding HLMS representations are shown in figure G, and EGW discrepancy from actual gross weight at the same conditions appears in figure H (equations as in paras 27 and 28).

Humidity:

31. The presence of humidity decreases ambient air density below that expected for dry air at a given temperature and pressure altitude. The effect on power required is the same as increasing density altitude. Figure I shows the density decrease (equation 10, app E). At 10,000 feet dry density altitude and 40°C, a relative humidity increase to 90 percent represents a gain of 1000 feet in density altitude.

32. The HLMS density ratio computation uses only pressure and temperature inputs and is not sensitive to density changes caused by humidity. At 5000 feet pressure altitude and 35°C ambient temperature (dry density altitude = 8330 feet), a relative humidity of 90 percent adds 770 feet to the dry density altitude, and power required increases accordingly. For 10,000 feet pressure altitude and 35°C ambient temperature (dry density altitude = 14,340 feet), a relative humidity of 60 percent adds 620 feet to the dry density altitude. Since hover at a given gross weight requires higher power for a humid condition than a dry one, the HLMS output EGW tends to be too high in the presence of humidity. Errors due to not considering humidity are small, and at most conditions do not have a significant effect on power required to hover. Figure J shows the effect of humidity on EGW due to power-required variation for an actual gross weight of 9500 pounds, where the basic HLMS function is represented by the zero humidity line (applying humidity/density relationship to equations of para 28).

Rotor Speed

33. Rotor speed effects on required power are presented in figure K at three density altitudes (Δ rotor speed applied to dimensional form of equation 18, app E). Rotor speeds of 324 and 294 rpm represent the limits of permissible operation.

Figure C. Air Density Influence on HLMS Model of Out-Of-Ground Effect Hover Performance.

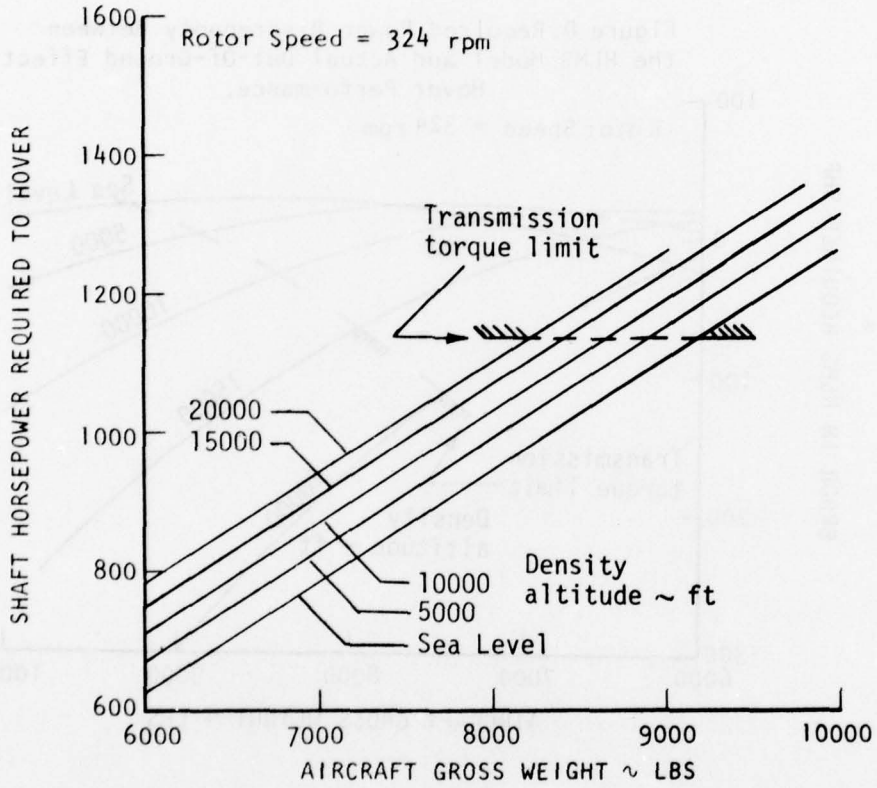

Figure D. Required Power Discrepancy Between the HLMS Model and Actual Out-Of-Ground Effect Hover Performance.

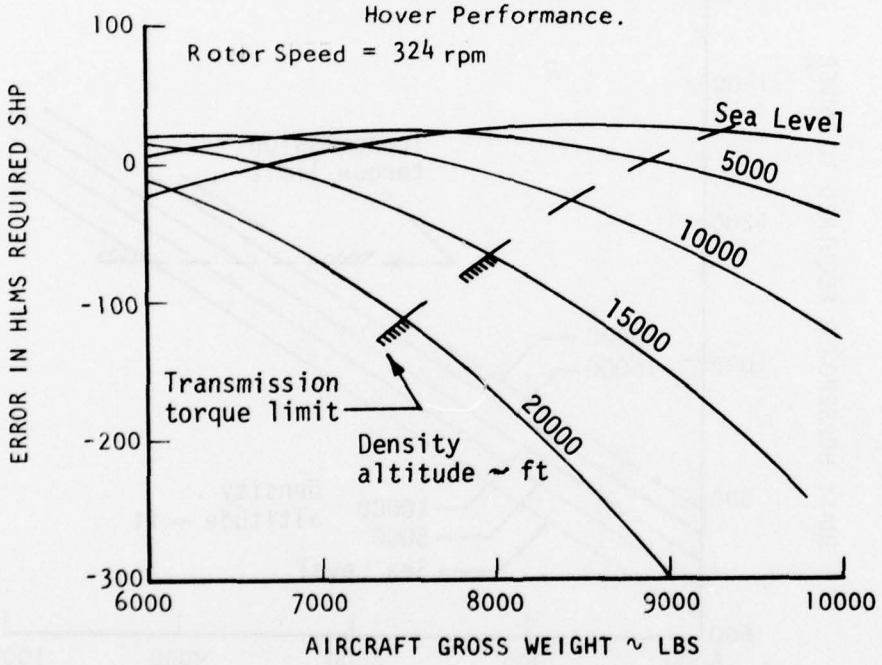

Figure E. Linearization Error in the HLMS Weighing Computation.

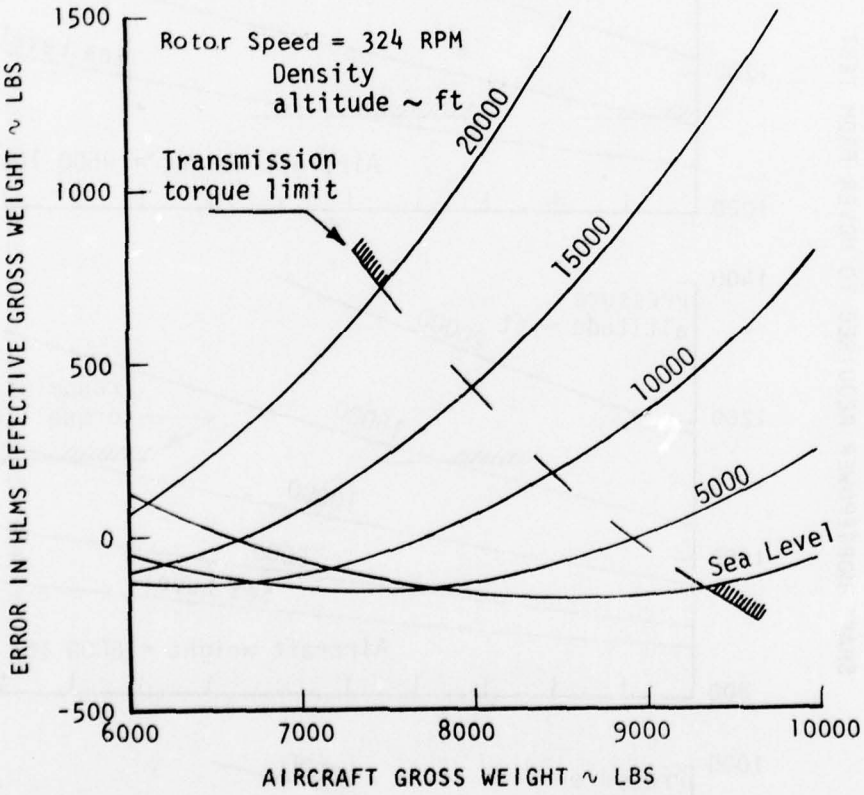

Figure F. Pressure and Temperature Influence
On Actual Out-of-Ground Effect Hover Performance

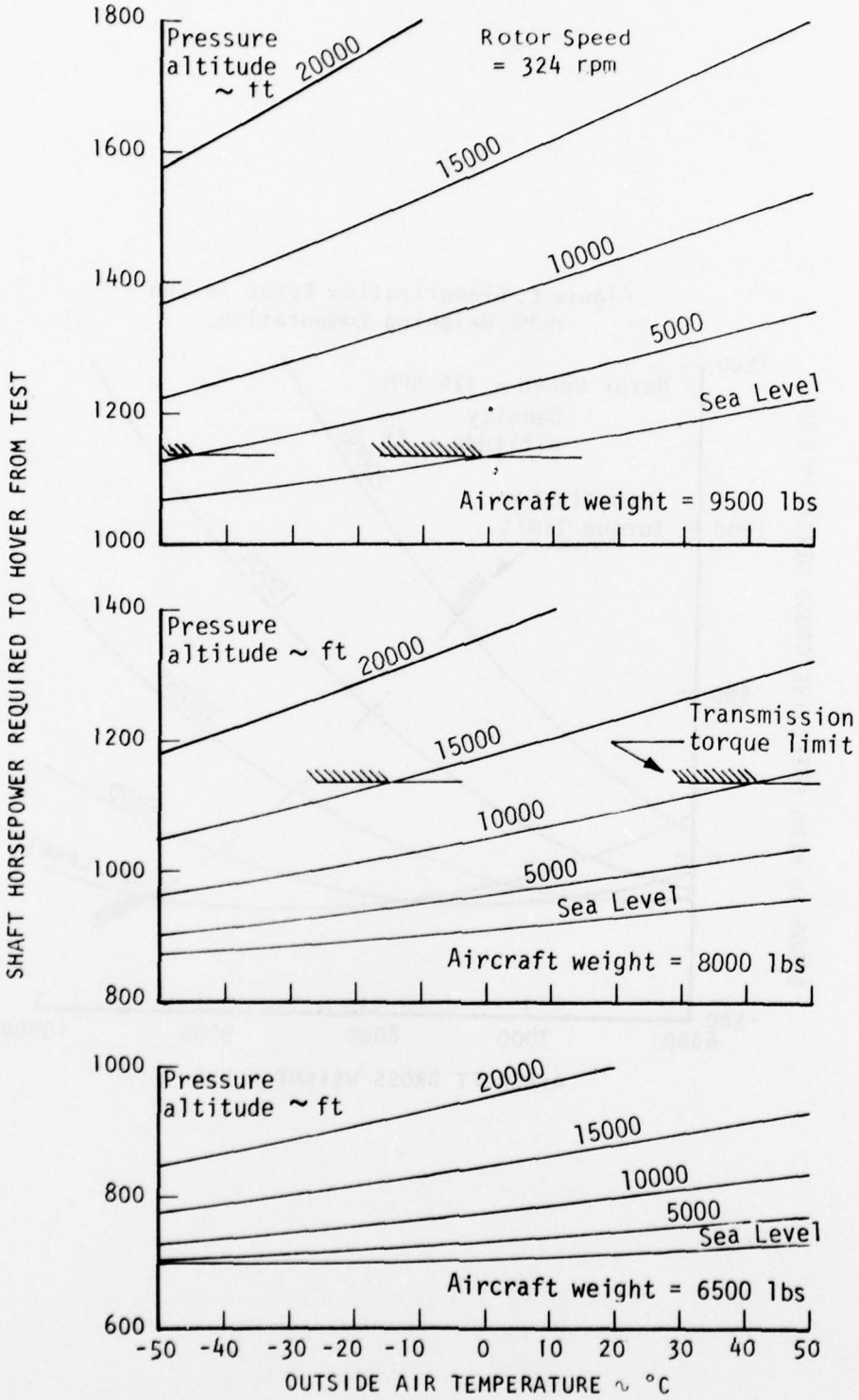

Figure G. Pressure and Temperature Influence On HLMS Model of Out-Of-Ground Effect Hover Performance.

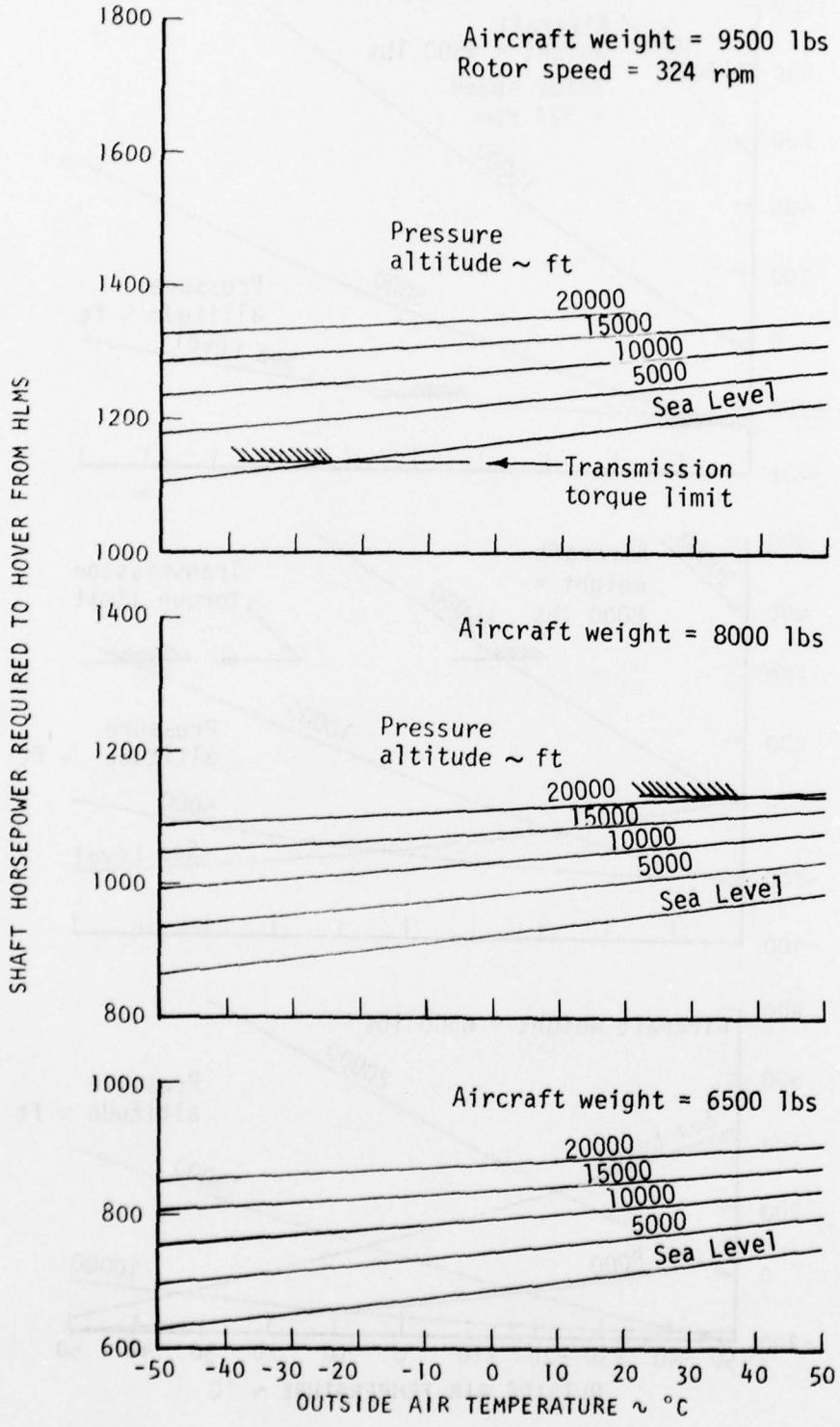

Figure H. Linearization Error in the HLMS Weighing Computation.

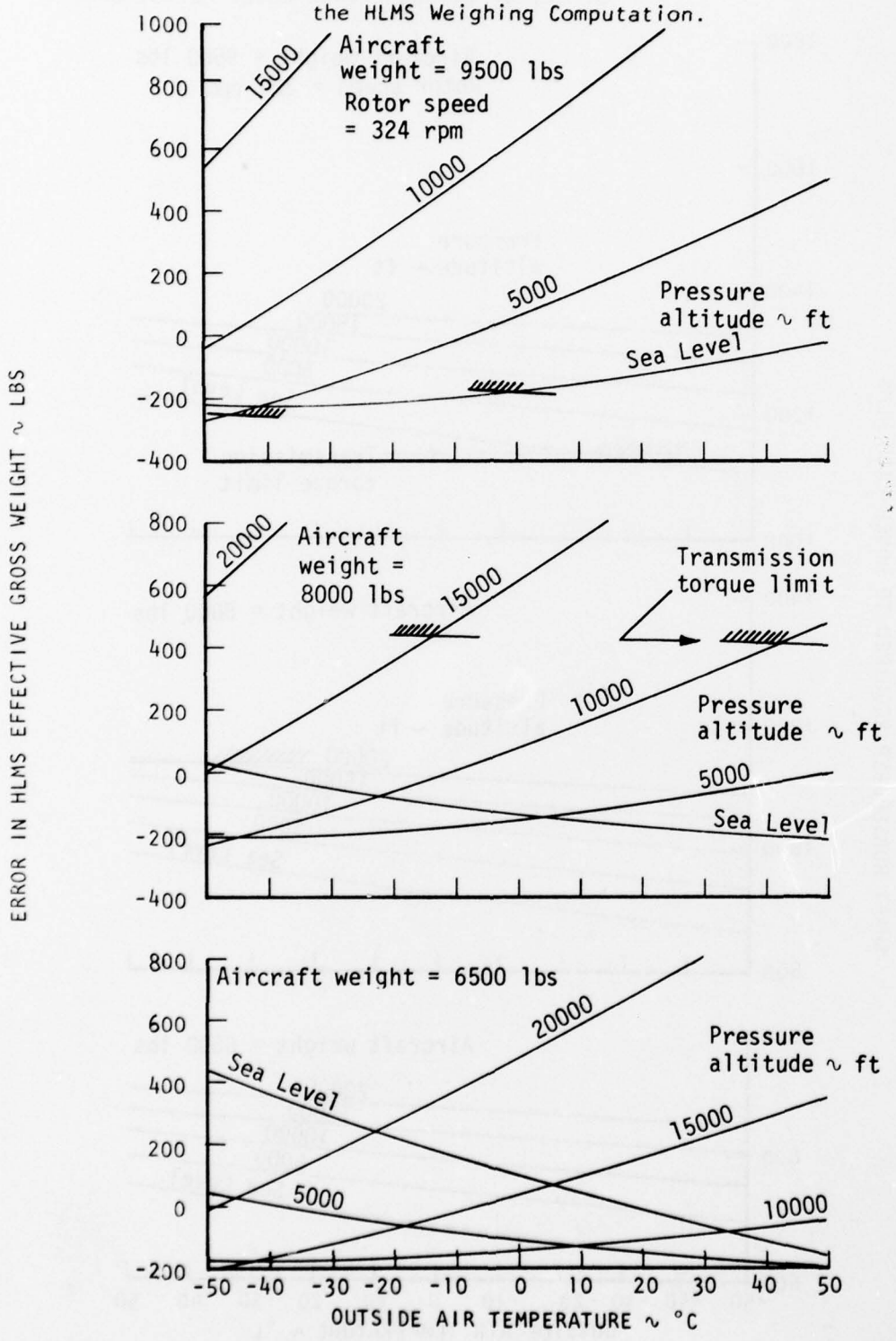

Figure 1. Effect of Relative Humidity on Air Density.

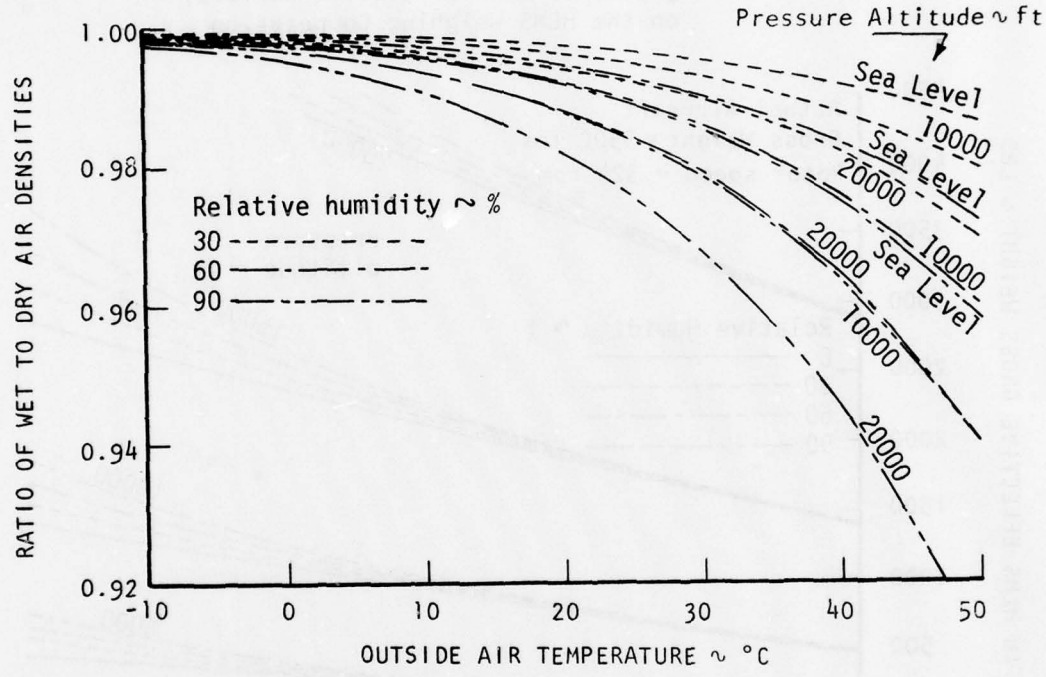

Figure J. Effect of Relative Humidity
on the HLMS Weighing Computation

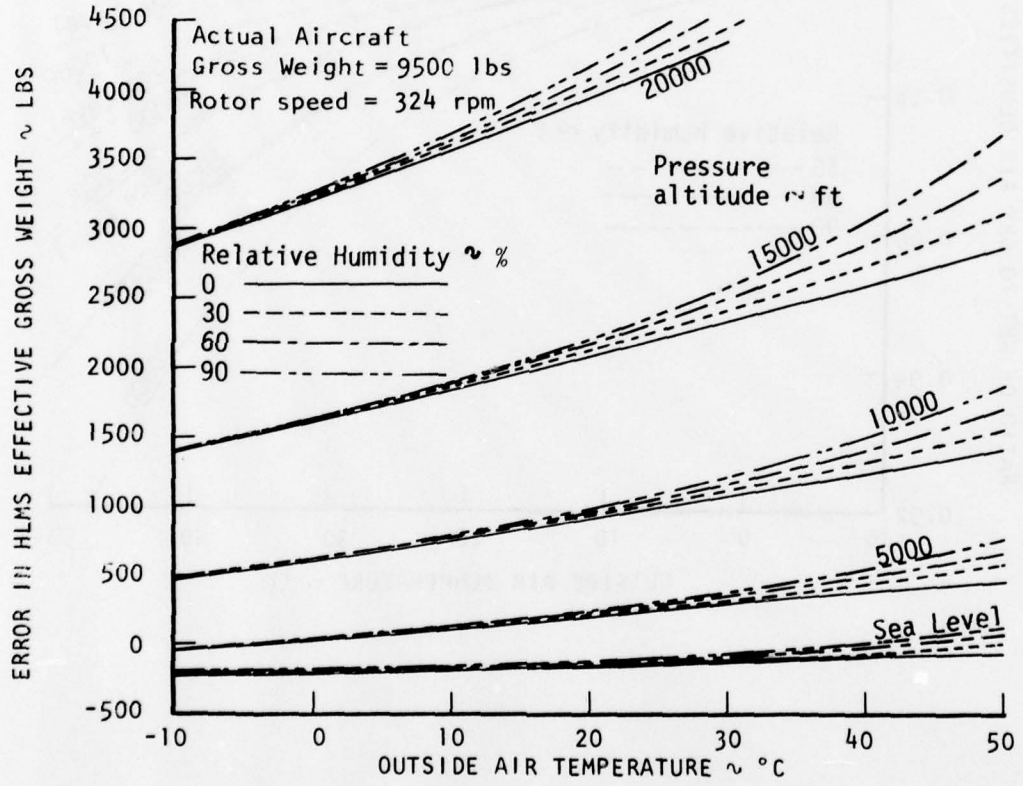

Figure K. Change in Required Power From Standard 324 Main Rotor RPM to Low Rotor Speed Conditions

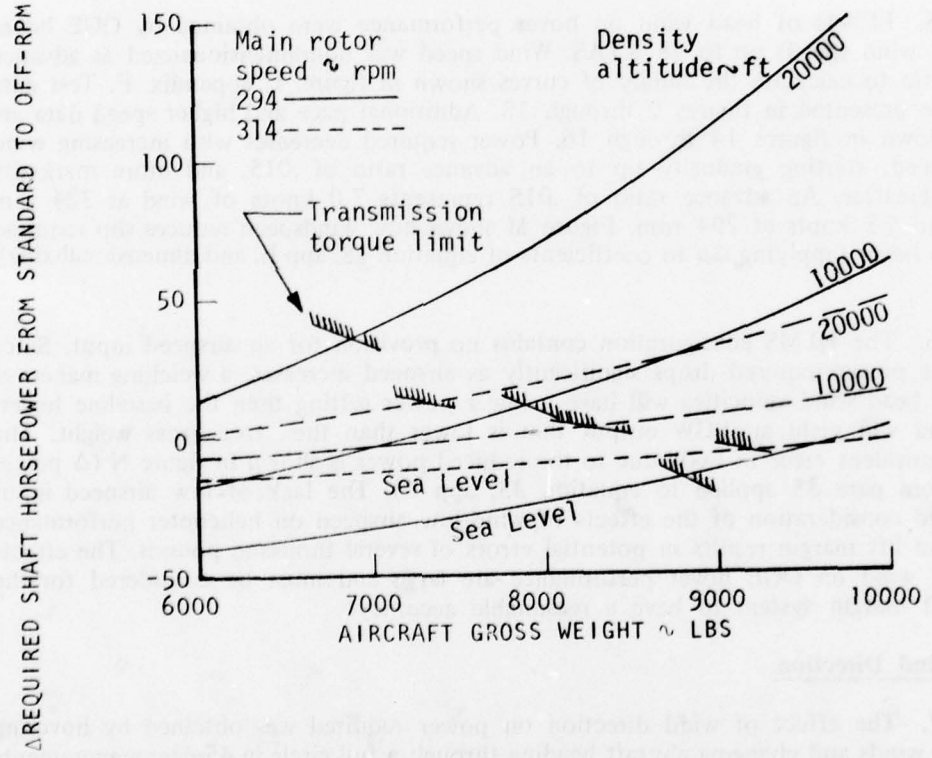

34. The rotor speed term in the EGW computation appears as engine speed (N_2). The value of N_2 is fixed at 6600 rpm, which corresponds to a main rotor speed of 324 rpm, and there is no adjustment in the function for off-rpm conditions. The resulting error between EGW and actual gross weight for rotor speeds of 314 and 294 rpm is shown in figure L (Δ rotor speed applied to equations of para 28). At 324 rpm, EGW error is due to linearization and can be zero (fig. E) but at 294 rpm rotor speed, EGW is always higher than actual gross weight by at least 200 pounds (fig. L).

Wind Speed

35. Effects of head wind on hover performance were obtained by OGE hover in wind speeds up to 28 KTAS. Wind speed was nondimensionalized as advance ratio to calculate the family of curves shown in figure 1, appendix F. Test data are presented in figures 2 through 13. Additional pace and higher speed data are shown in figures 14 through 16. Power required decreases with increasing wind speed starting gradually up to an advance ratio of .015, and more markedly thereafter. An advance ratio of .015 represents 7.0 knots of wind at 324 rpm and 5.5 knots at 294 rpm. Figure M shows how windspeed reduces shp required to hover (applying $\Delta\mu$ to coefficients of equation 18, app E, and dimensionalizing).

36. The HLMS configuration contains no provision for an airspeed input. Since the power required drops significantly as airspeed increases, a weighing maneuver at head wind velocities will have a lower power setting than the base-line hover, and will yield an EGW output that is lower than the true gross weight. The equivalent error in EGW due to the reduced power is shown in figure N (Δ power from para 35 applied to equation 33, app E). The lack of low airspeed input and consideration of the effects of wind/low airspeed on helicopter performance and lift margin results in potential errors of several thousand pounds. The effects of wind on OGE hover performance are large and must be considered for the lift margin system to have a reasonable accuracy.

Wind Direction

37. The effect of wind direction on power required was obtained by hovering in winds and changing aircraft heading through a full circle in 45-degree increments during both free and tethered hover. Data for several values of wind speed and gross thrust are shown in figures 29 through 34, appendix F. Pace flights with sideslips to 45 degrees in either direction in 15-degree increments defined the effects of small variations, and sideward and rearward pace data verified the influence of large directional changes on required power. The pace data appear in figures 35 through 37. The effects of wind direction are significant and increase with wind speed and rotor thrust.

38. Minimums in power required occur at relative wind azimuths from 340 to 350 degrees and 190 to 210 degrees, while maximums are from 70 to 80 degrees and 270 to 290 degrees. Change in power required with wind direction is attributed

Figure L. Error in HLMS Weighing Computation At Non-Standard Rotor Speeds.

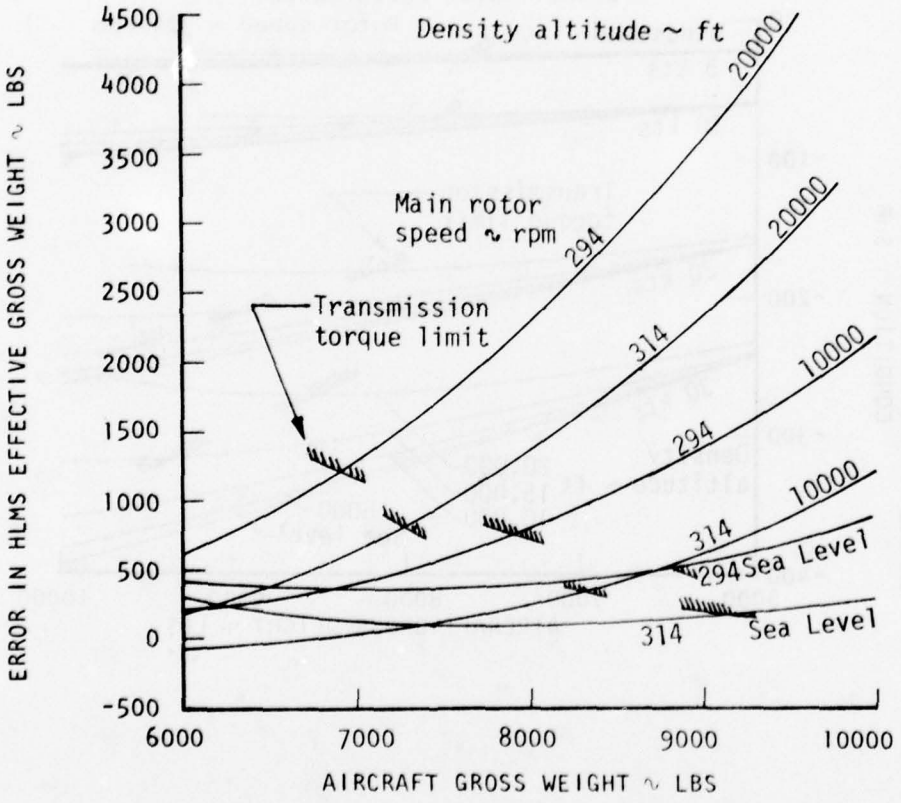

Figure M. Effect of Headwinds on Out-of-Ground Effect Hover Performance.

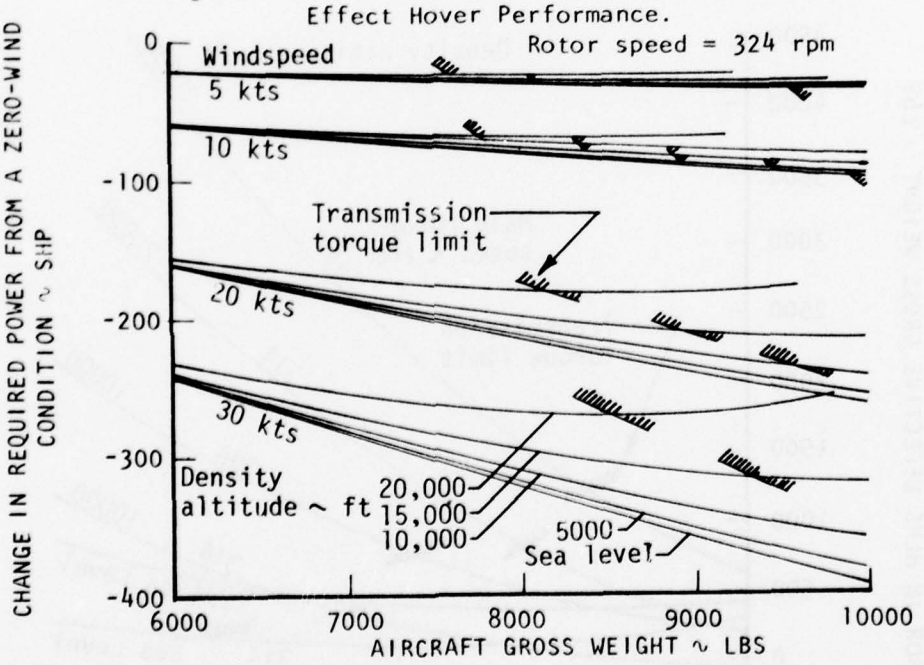

Figure N. Effects of Airspeed on the HLMS Weighing Computation.

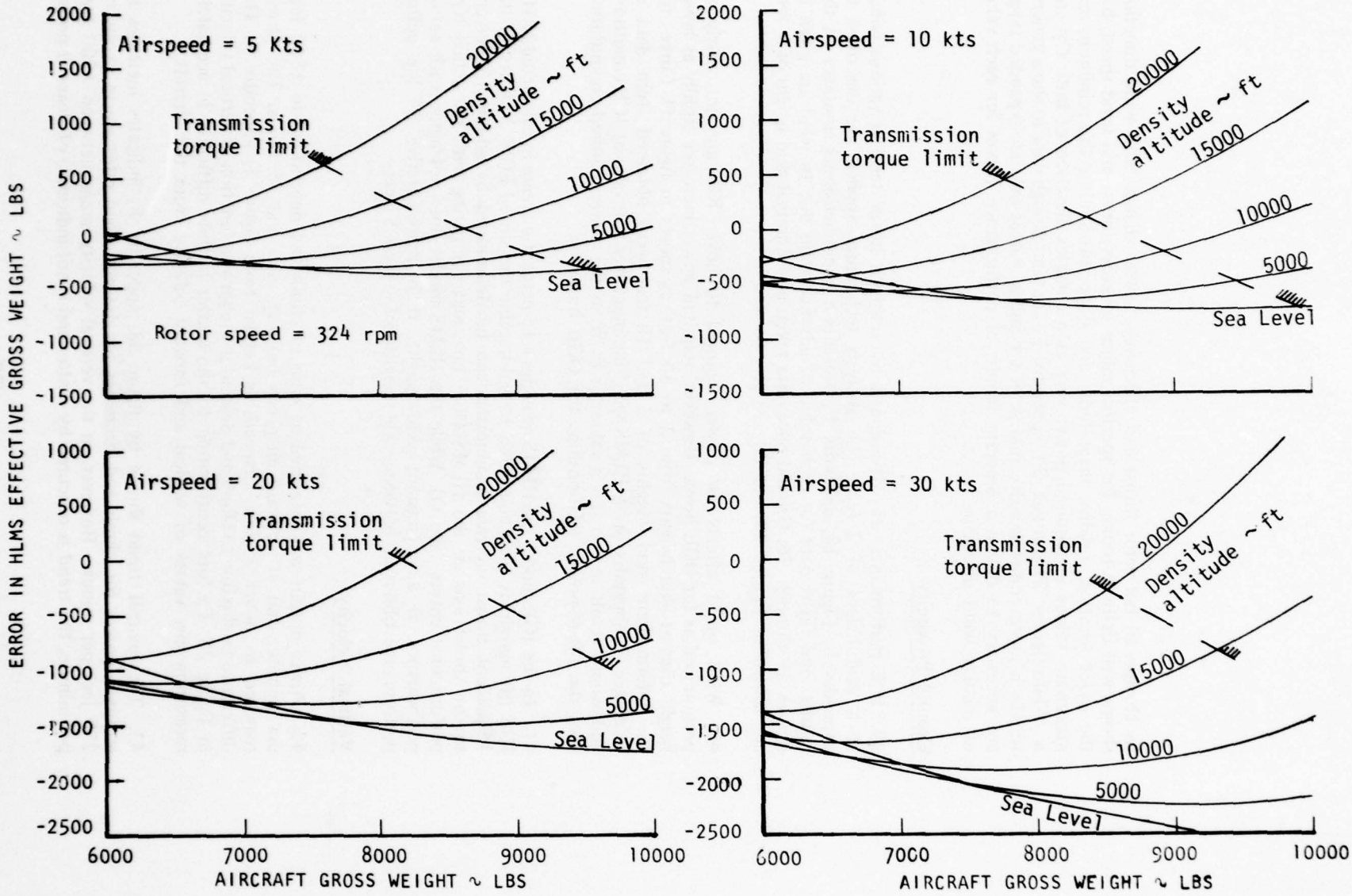

to changes in tail rotor thrust and efficiency. Power change with wind direction shows well defined trends for specific values of gross thrust and wind speed, but the exact location, relative magnitude, and slope surrounding the minimum and maximum values in required power vary as a complex function of both C_T and μ. While figures 29 through 34, appendix F, contain enough data to show general trends, a more comprehensive matrix of C_T and μ values over an expanded range are necessary to define a separate family of performance curves for each value of relative wind direction.

Ground Proximity

39. IGE performance was determined by tethered hover tests in various winds at a skid height of 2 feet. The analysis techniques applied are described in appendix E. Figure 18, appendix F, presents a nondimensional summary of the results, and flight data for each value of advance ratio due to wind are given in figures 19 through 26. Ground pace data taken at a nominal skid height of 5 feet are shown in figures 27 and 28.

40. Wind speed effects on power required to hover IGE are not nearly as pronounced as for OGE hover. However, required power increases rapidly as hover height rises at skid heights from 2 to 50 feet, as shown in figure O. Curves for the intermediate skid heights of 5 and 10 feet were obtained from data in reference 7, appendix A. A HLMS weighing maneuver is invalid at IGE conditions and would result in too low a value for EGW, as the power-required computation uses the lift-to-power relationships for OGE hover.

41. In the IGE mode, the HLMS provides a 15-percent increase in calculated MAL. IGE lift margin is then computed by subtracting the stored EGW. Validity of the 15-percent thrust increase assumption can be determined by adding 15 percent to the thrust axis of the HLMS OGE line, and comparing with the actual IGE performance curves (fig. O). While the HLMS model does not agree with actual performance at any constant skid height, it is representative of the actual performance observed between skid heights of 2 and 5 feet.

Vertical Velocity

42. Power output was measured at rates of climb and descent up to ±500 feet per minute, and at forward airspeeds between zero and 15 knots. The power required to hover at low airspeeds is known from figure 1, appendix F. The difference in shp due to climb and descent is shown as a function of vertical velocity in figure 38. Factors contributing to the scatter include difficulty in accurately measuring low values of vertical and forward velocity from the aircraft.

43. The general trend shown by figure 38, appendix F, indicates increases in required power for climb and decreases for descent when rates are in excess of 250 feet per minute. However, in the vertical velocity range between ±200 feet per minute, the trend is obscured by scatter and is not indicative of clear-cut power

Figure 0. Non-dimensional Hover Performance In and Out of Ground Effect and Comparison with the HLMS Model

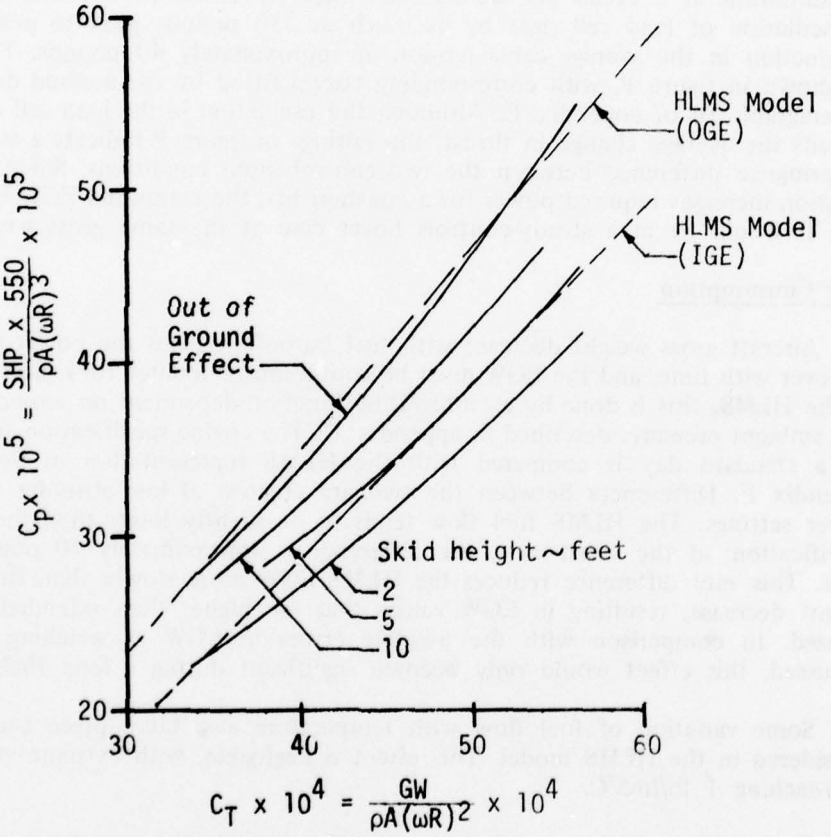

changes. This suggests that in practice, no appreciable difference in power is seen from hover to small rates of climb or descent. Thus, no systematic error in the HLMS EGW can be attributed to inadvertent low rates of climb or descent during the weighing maneuver.

Control Inputs

44. During one tethered hover test alternate data points were recorded with the cyclic control stabilized normally, and then with circular inputs of about 1-inch half-amplitude at 2 cycles per second. This stick movement produced an increase in oscillation of load cell data by as much as 350 pounds peak to peak, with a reduction in the average cable tension of approximately 40 pounds. The data are shown in figure P, with corresponding curves fitted by the method described in paragraph 14 of appendix E. Although the oscillation in the load cell data far exceeds the average change in thrust, the fairings in figure P indicate a statistical performance difference between the two control input conditions. Since control agitation increases required power for a constant lift, the computed EGW is higher than it would be in a steady-controls hover case at the same gross weight.

Fuel Consumption

45. Aircraft gross weight decrease with fuel burnoff reduces the power required to hover with time, and the EGW must be continuously updated for loss of weight. In the HLMS, this is done by an integrating function dependent on sensed torque and ambient pressure, described in appendix D. The engine specification fuel flow for a standard day is compared with the HLMS representation in figure 39, appendix F. Differences between the two are greatest at low altitudes and low power settings. The HLMS fuel flow tends to be slightly lower than the engine specification; at the worst case, the difference is approximately 40 pounds per hour. This rate difference reduces the HLMS EGW more slowly than the actual weight decrease, resulting in EGW values that are higher than intended as fuel is used. In comparison with the possible errors in EGW at weighing already discussed, this effect would only become significant during a long flight.

46. Some variation of fuel flow with temperature also takes place and is not considered in the HLMS model. This effect is negligible, with extreme variations approaching 1 lb/hrΔ°C.

47. During one test the aircraft had a lengthy ground idle, and it was observed that the HLMS output EGW began to increase, resulting in a final EGW value some 200 pounds higher than at the beginning. While the analytical integrating function does not permit this to occur, an offset in the analog integrator resulted in a sign change at very low measured torque values. Logic was installed in the HLMS circuitry to inhibit fuel flow integration when measured torque dropped below 5 psi, which is approximately the torque at ground idle. This switching value was later increased to 7 psi and eliminated the problem.

Figure P. Effect of Deliberate Continuous Cyclic Control Inputs on Hover Performance.

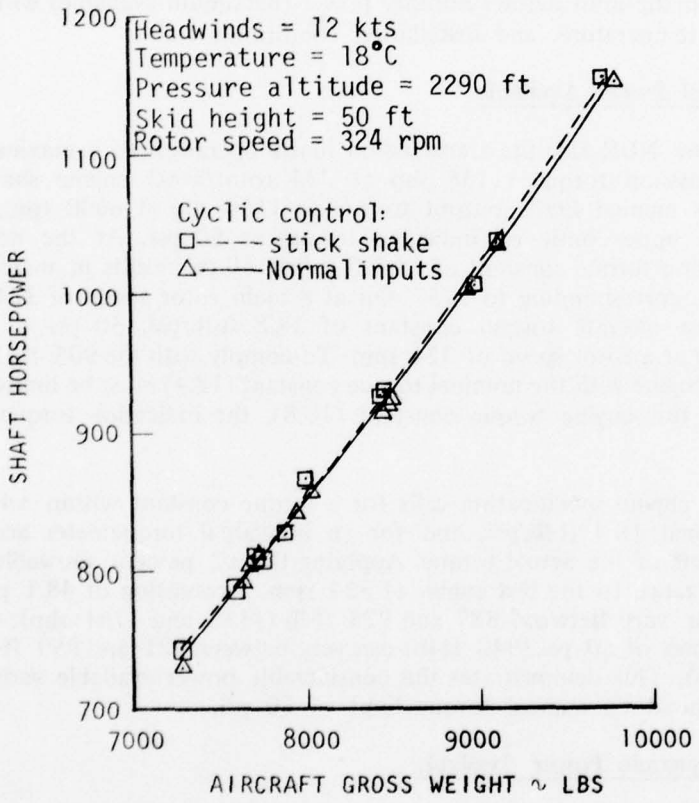

POWER AVAILABLE AND MAXIMUM STANDARD TORQUE

48. Power available in the test aircraft was determined by either the mechanical limits or the thermodynamic limits. The mechanical limits are fixed values of torque and rotational speed for which the drive system and rotors have been qualified. The thermodynamic limit on engine operation is 938°C turbine inlet temperature. In actual operation at nontorque-limited conditions, engine power output is limited by a fuel flow governor, which automatically follows a compressor inlet pressure/temperature profile to prevent exceeding the turbine temperature limit. This automatic limit defines military power (maximum available) which varies with altitude, temperature, and installation conditions.

Mechanical Power Available

49. In the NUH-1M, the transmission limits operation to a maximum 905 ft-lb of transmission torque (1138 shp at 324 rotor/6603 engine shaft rpm). The operator's manual limits output torque to 1100 shp at 6600 rpm, and sets the allowable upper limit of indicated torque at 50 psi. At the nominal engine specification torque constant of 18.4 ft-lb/psi, 50 psi results in an actual torque of 920 ft-lb, corresponding to 1157 shp at a main rotor speed of 324 rpm. At the actual test aircraft torque constant of 18.8 ft-lb/psi, 50 psi is 940 ft-lb, or 1182 shp at a rotor speed of 324 rpm. To comply with the 905 ft-lb transmission limit, an engine with the nominal torque constant (18.4) must be limited to 49.2 psi; with the test engine torque constant (18.8), the indication torque limit is 48.1 psi.

50. The engine specification calls for a torque constant within ±4.4 percent of the nominal 18.4 ft-lb/psi, and for an individual torquemeter accuracy within ±2 percent of the actual torque. Applying the ±2 percent allowable torquemeter accuracy range to the test engine at 324 rpm, a condition of 48.1 psi (905 ft-lb) torque can vary between 887 and 923 ft-lb (1115 and 1161 shp); the operator's manual limit of 50 psi (940 ft-lb) can vary between 921 and 959 ft-lb (1158 and 1206 shp). This demonstrates the considerable power available variation possible at the operator's manual torque limit of 50 psi.

Thermodynamic Power Available

51. Installed T53-L-13B engine SN LE 14420 military power available was evaluated between 5 and 35°C ambient temperature, and 2000 to 10,000 feet pressure altitude. The following sections present the results of several methods used to analyze and summarize the test results.

Power Available Analysis

Engine Model Specification:

52. As a basis for comparison with flight data and the HLMS model, military power was calculated from the manufacturer's engine model specifications (ref 8,

app A) for a matrix of ambient temperature from -50 to +50°C, and pressure altitude from sea level to 20,000 feet. The computer program for Lycoming performance specification No. 104.33 was used and resulted in the power available shown in figure 40. appendix F, for the following operating conditions and installation losses:

a. Power turbine rotor speed (N_2): 6,600 rpm.

b. Compressor inlet temperature rise over ambient: 2°C.

c. Compressor inlet pressure ratio: .992.

d. Exhaust gas pressure ratio: 1.0.

e. Mechanical power extraction from the gas producer train: zero horsepower.

f. Air bleed loss: .005 percent.

g. Anti-ice: Off.

53. At sea level and 15°C outside air temperature (OAT), power available at 324 rpm main rotor speed (1373 shp) corresponds to a torque indication of 58.1 psi, and is the Q_{ms} defined by the nominal engine specification. Theoretically, the value of Q_{ms} serves as a fundamental measure of engine output capability, and should remain essentially constant for a given engine. However, Q_{ms} is expected to show a long-term gradual decrease as engine performance deteriorates with use.

Helicopter Lift Margin System Engine Representation:

54. While shp does not appear explicitly in the HLMS functions, it can be calculated from known HLMS quantities, as described in paragraph 34 of appendix E, for comparison with power-available data from other sources. Fixing Q_{ms} at the nominal specification of 58.1 psi, the HLMS power-available function (equation 5, app D, and equations 32 and 33, app E) produces the curves shown in figure 41, appendix F, which are directly comparable to the engine specification representation of figure 40.

55. Difference in available shp between the HLMS model and the engine specification is shown in figure Q for several pressure altitudes. The greatest discrepancy occurs at temperatures below -20°C, but within the transmission torque limited operating range (power below 1138 shp at 324 rpm) the differences above -20°C do not exceed 43 shp. The HLMS analytical expressions for power available accurately duplicate that of the model specification over the present operating range.

56. The operator's manual torque limit of 50 psi is used for the upper allowable power output in the HLMS model formulation (940 ft-lb, or 1182 shp at

Figure Q. Power Available Difference
Between the HLMS Model and the L-13 Engine Specification.

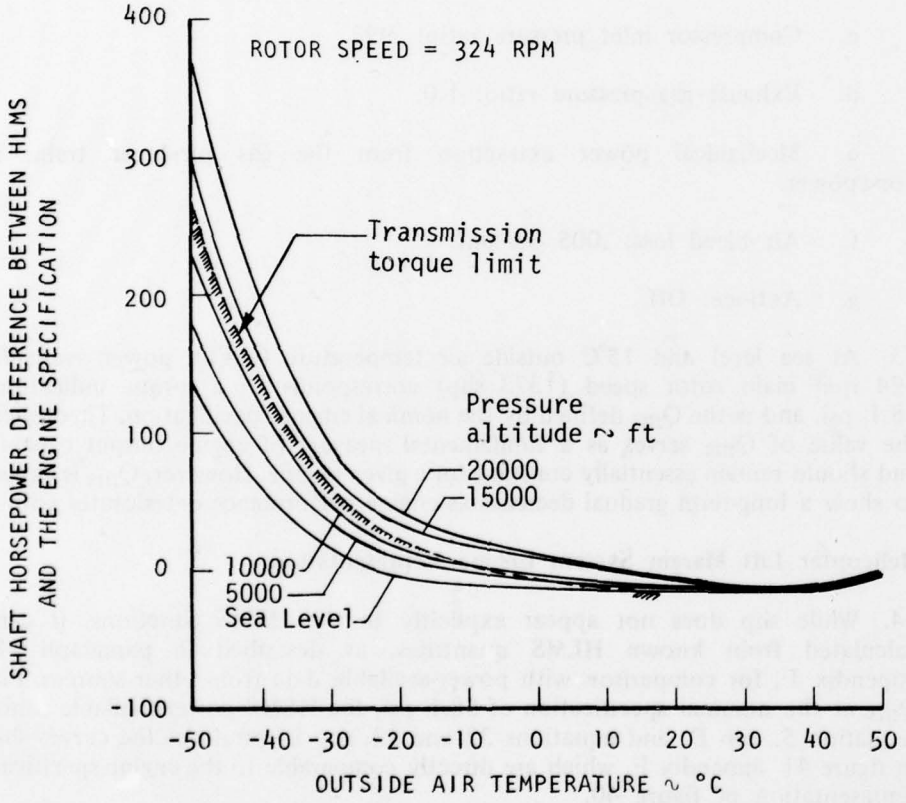

324 rotor rpm). If the 905 ft-lb transmission limit torque is applied to the test engine, the resulting maximum power output is 1138 shp, 44 shp below that of the HLMS model. Adding the possible ±24 shp torquemeter inaccuracy at topping conditions introduces ambiguity in defining the actual maximum permissible power without overtorquing in this operating range.

57. The N_2 that produces 324 rpm main rotor speed is 6600 rpm in the HLMS model. The actual gearing ratio results in an N_2 of 6603 rpm for this rotor speed. This effect on accuracy is negligible compared to the torquemeter limit uncertainties. At 50 psi torque, there is a difference of only 0.5 shp between N_2 values of 6603 and 6600 rpm.

Statistical Fit of Flight Data:

58. The two statistical techniques described in paragraphs 19 through 31, appendix E, were applied to the topping flight data to determine power available characteristics for the test engine. The range of flight data available for this analysis was from 5 to 35°C ambient temperature, and 2000 to 10,000 feet pressure altitude.

59. One method found coefficients for power available as a function of ambient pressure ratio and compressor inlet temperature (CIT) in a format that allowed direct comparison with corresponding HLMS coefficients. To show engine performance for ambient conditions, the CIT term in this function was converted to equivalent OAT by assuming a constant compressor inlet temperature rise over ambient. The value used was 2°C, which is the same as that assumed in the HLMS. In fitting the flight data, coefficients were found using both measured CIT and OAT + 2 for the inlet temperature term. The resulting engine characteristics are shown in figures 42 and 43, appendix F.

60. These statistical functions allow available power to be extrapolated for conditions well beyond the actual range of temperature and altitude in which the data were obtained, as well as for conditions where torque limitations preclude taking topping data.

61. To avoid convergence at a point, the function was modified as described in paragraphs 23 through 26, appendix E, and referred shp was incorporated in the calculations to provide interdependent altitude-temperature engine characteristics. Both CIT and OAT + 2 were again used for the inlet temperature term, and the resulting performance curves are given in figures 44 and 45, appendix F, respectively. These are more representative of engine characteristics over the entire range than the previous fit to the data using the HLMS format.

62. Because of the pitfalls in extrapolating the statistical fit functions of the topping points, a referred power method using a larger volume of data at a variety of power settings was also used. As described in paragraphs 27 through 31, appendix E, this method established a direct relation between referred power and

referred gas producer speed. These data sets are shown in figures 48 through 51, appendix F. Deviation of test topping N_1 from maximum available from the engine specification is shown by the curve in figure 52. The linear portion of this curve corresponds to the test engine acceptance run value of 99.5 percent N_1. A constant inlet temperature rise is assumed to provide correspondence between OAT and CIT. This analysis used an inlet temperature rise of 2.9°C for the best available estimate, as described in paragraph 69. Figure 52 defines a maximum available N_1 for each ambient temperature, and by referring this N_1 to standard sea-level conditions, it can then be used to find a corresponding referred shp from figures 48 through 51. At the temperature for which maximum N_1 was determined, actual shp can be computed from the referred shp for any altitude.

63. The performance curves obtained by this process are shown in figure 46, appendix F, and are used as the base line power available for comparison with the HLMS model. At standard sea-level conditions and 324 rpm, this function shows Q_{ms} to be 54.4, equivalent to 1022 ft-lb torque, or 1285 shp. The actual test engine performance is significantly different from the model specification engine performance from which the lift margin system power available expression was derived.

64. With this Q_{ms}, the HLMS model produces the performance curves shown in figure 47, appendix F (equations as in para 54). The HLMS power-available model for both the engine specification Q_{ms} of 58.1 and the flight-determined Q_{ms} of 54.4 are compared to the flight-determined performance model in figure R as a function of temperature and in figure S as a function of altitude. These show that at 54.4 Q_{ms}, the model is representative of actual power available within ±30 shp for most conditions. At 58.1 Q_{ms}, however, predicted power is always too high, and approaches an error of 100 shp at a number of nontorque-limited conditions.

65. The HLMS model of power change with temperature is correct at some ambient conditions, with power change slopes (Δ shp/°C) overlapping the observed range. The HLMS altitude effects (Δ shp/ft) are always larger than those observed in flight tests, indicating that the engine tested was not as sensitive to altitude as represented by the HLMS model. Because of the differences in temperature and altitude slopes between the actual and HLMS power-available functions, the HLMS-calculated Q_{ms} at topping will not always result in the same value. Observed topping torque, for an "actual" Q_{ms} of 54.4, will result in an HLMS Q_{ms} anywhere from 53.7 to 55.7 for nontorque-limited conditions, depending on ambient conditions at topping (equation 5, app D). At 10,000 feet pressure altitude, HLMS Q_{ms} varies from 54.2 at -10°C OAT to 55.7 at +40°C; at 5000 feet, Q_{ms} ranges from 54.6 at +10°C to 54.2 at 50°C, and at sea-level, from 54.2 at 30°C to 53.7 at 50°C; all based on predicted measured topping torque from figure 46, appendix F. Only topping at certain altitude-temperature conditions will result in the "correct" Q_{ms} of 54.4 output from the HLMS.

Figure R. Difference in Power Available Between the HLMS Model and Flight Determined Engine Characteristics

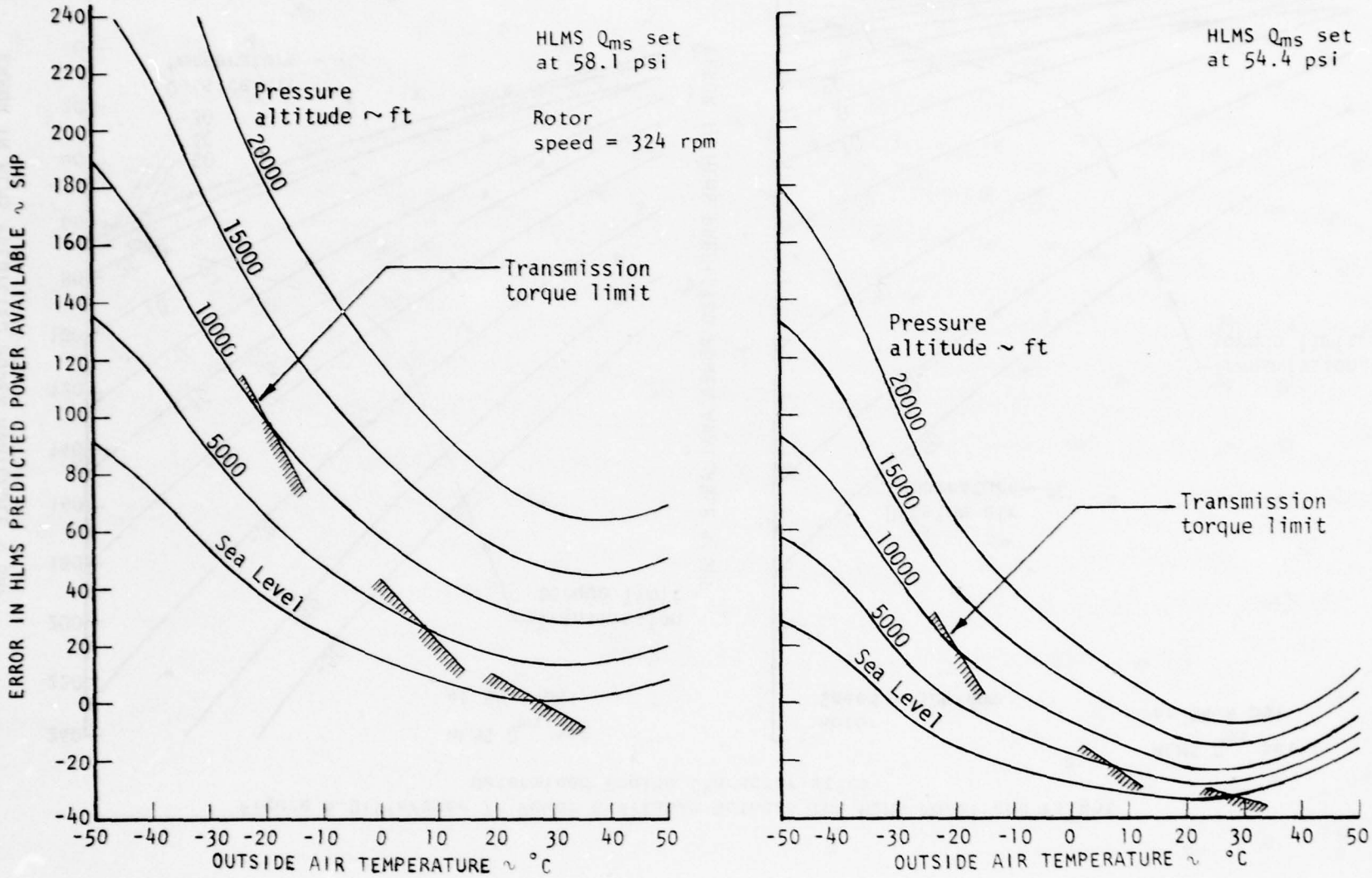

Figure S. Difference in Power Available Between the HLMS Model and Flight Determined Engine Characteristics.

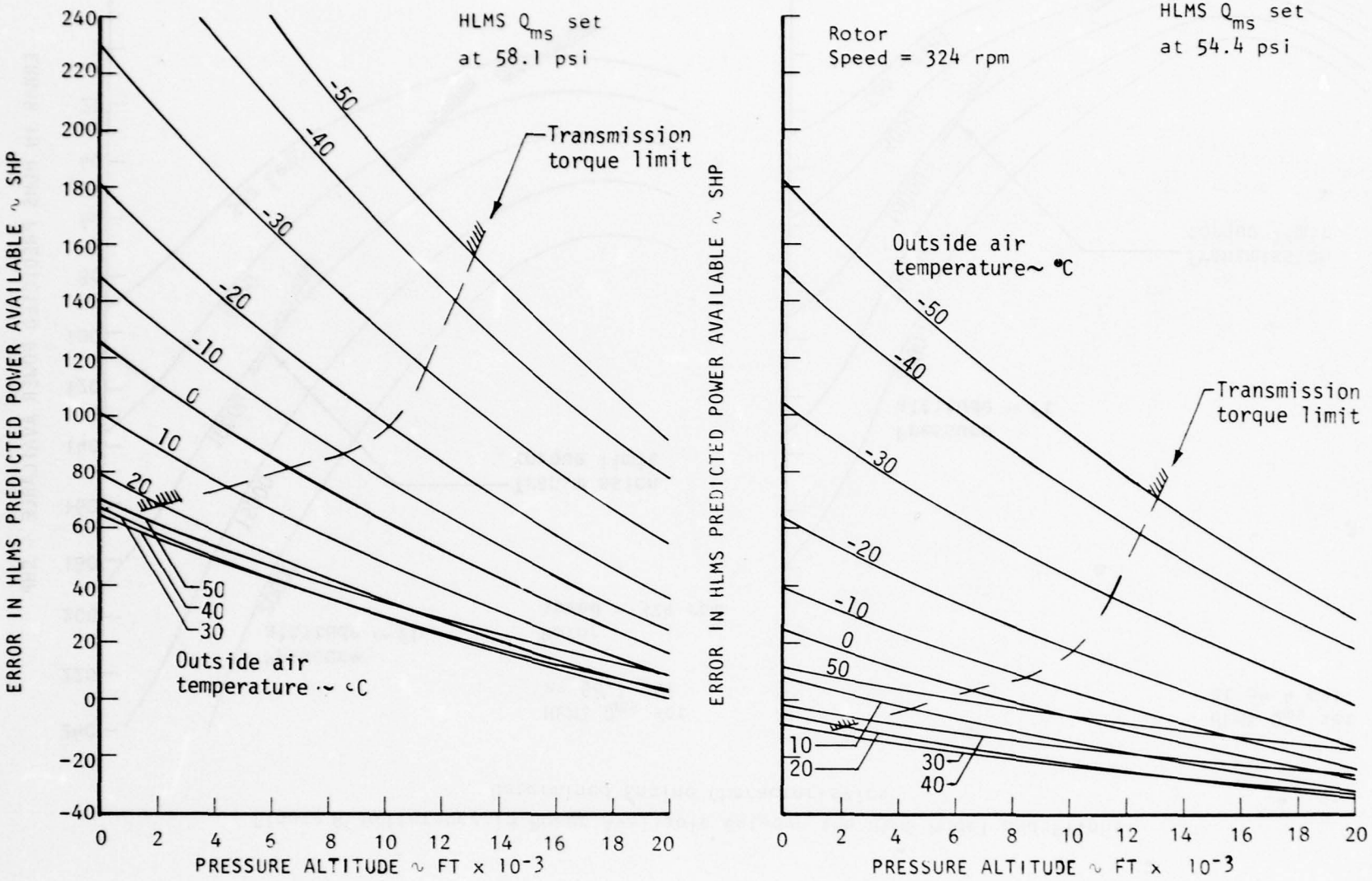

Effects on Power Available

66. The influence of ambient conditions and operating variables on actual power available, the HLMS model, and Q_{ms} is discussed in the following sections.

Temperature:

67. The characteristics of power loss with increasing temperature are seen from the individual temperature lines of figure 46, appendix F. This shows that the rate of power loss in shp/°C increases as OAT increases. Pressure altitude also influences the power variation with temperature: the power loss rate with increasing temperature is greater at low altitude than at high altitude.

68. Both the HLMS model and the flight data analysis require a CIT measurement for computation of the power-available function. Accuracy of this measurement can have significant effects on the computed engine characteristics, as was demonstrated by differences in figures 42 through 45, appendix F. Power available computations are extremely sensitive to CIT, and small errors in CIT measurement can have a large impact on overall accuracy of the HLMS. The test L-13 engine had only one compressor inlet temperature probe *mounting location, and the* transducer for this sensor was used directly in the HLMS hardware as a variable resistor in a feedback loop. Thus, direct measurement of the CIT input to the HLMS was not available.

69. The CIT output from the HLMS was recorded. Measured OAT corrected for compressibility during topping maneuvers is plotted against HLMS output CIT in figure 53, appendix F. Scatter is significant, with a maximum discrepancy of 6°C from the CIT = OAT + 2 line. The HLMS was removed and the CIT transducer output was recorded. Figure 54 shows the CIT output for two values of probe recovery factor (K, as defined in paragraph 8, app E). The scatter band is less than 1.2°C. In correcting CIT by substituting different values of K into equation 14, appendix E, the correlation coefficient of a linear fit to the data is maximized at approximately K = 0.5. This minimum scatter fit results in an inlet temperature rise of about 2.9°C. The large improvement in data between the two figures shows the consistent quality of the initial CIT transducer output, and demonstrates that transmission of this signal via the HLMS introduces noise to the point that the original CIT value is lost in the scatter and cannot be recovered.

70. The effects of temperature variation on Q_{ms} and the subsequent HLMS model it defines can be seen by varying the CIT inputs to the HLMS equations. In a topping maneuver, Q_{ms} is derived from the measured pressure ratio, CIT and torque (Q_{ma}). Figure T shows the Q_{ms} resulting at three pressure altitudes for several values of input torque over a range of CIT values (equation 5, app D). The slopes of Q_{ms} as a function of CIT vary from 0.24 to 0.77 psi/°C as conditions change, with a representative value for typical topping conditions at 0.5 psi/°C, or 1 psi of Q_{ms} for each 2°C change in CIT.

Figure T. Compressor Inlet Temperature Effects on the HLMS Maximum Standard Torque Calculation.

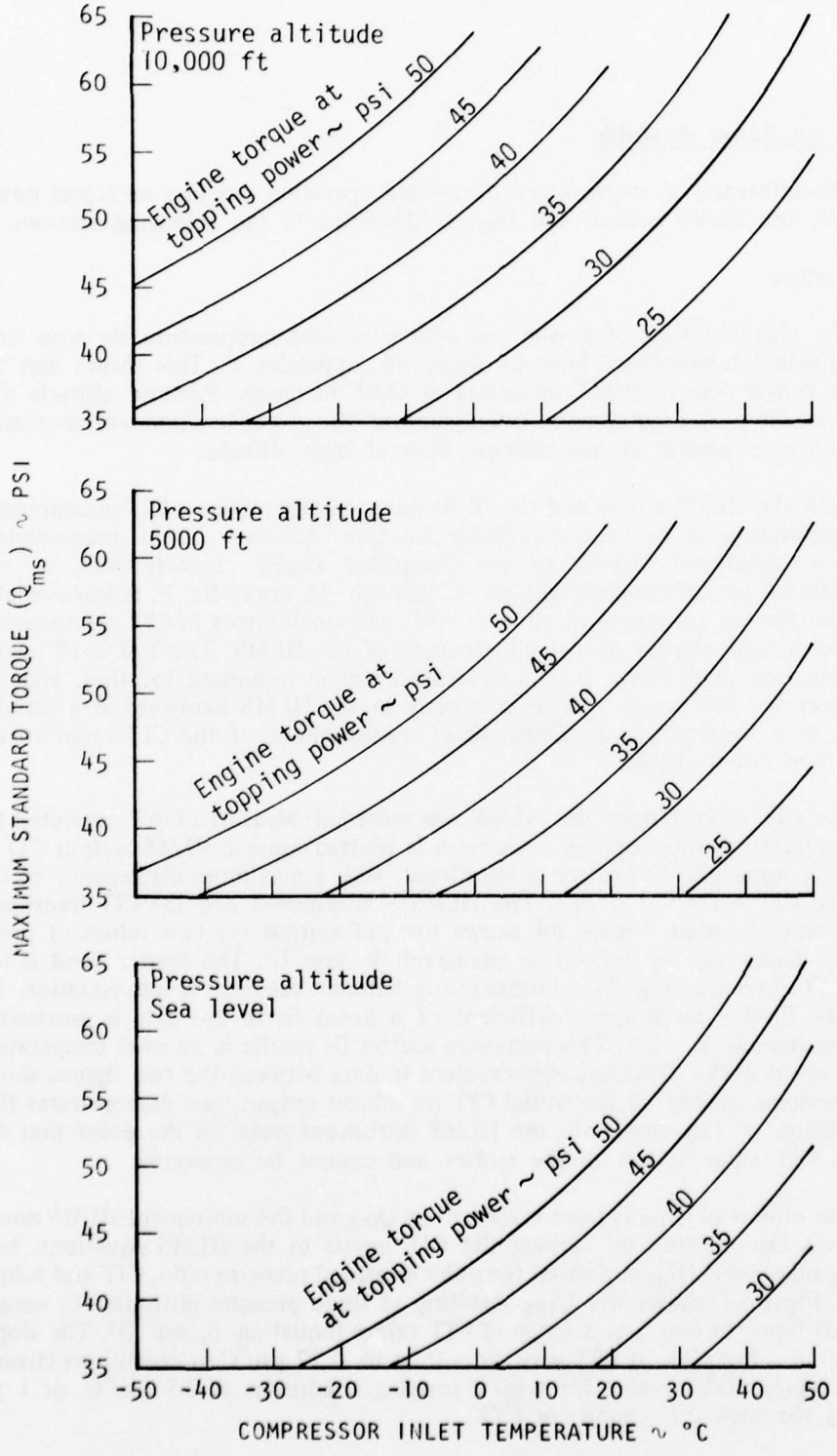

71. During the in-flight topping maneuvers recorded Q_{ms} varied significantly from test to test, as shown in figure 55, appendix F, and prevented evaluating the ability of the HLMS to monitor engine performance degradation. The majority of Q_{ms} values were spread fairly uniformly between 56 and 59 psi, with extremes of scatter to 54.7 and 61.5 psi. This variation is larger than that expected from changes due to ambient conditions only. Taking a ±2-psi shift of Q_{ms} from the nominal 58.1 produces the equivalent power-available changes in the HLMS model shown in figure U (equations as in para 54). Maximum power variation is ±75 shp from the value calculated with the base line Q_{ms}. This is representative of the random variation in HLMS power available due to inconsistency in Q_{ms} between tests.

72. The observed values of Q_{ms} at topping could not be duplicated by applying the HLMS equations to measured values of torque, CIT, and pressure. The flight Q_{ms} values ranged from 2 psi below to 7 psi above those calculated for the existing conditions. Differences in the three parameters sensed by the HLMS and those recorded by the PCM system could account for the discrepancy.

73. If the entire difference is assumed to be inaccuracy in CIT, an artificial value of CIT can be calculated which when combined with the measured torque and pressure, yields the observed Q_{ms} (equation 5, app D). This was done for the topping data and the results are shown in figure V. The artificial CIT computed is compared to measured CIT, and shows a well-defined slope shift. This indicates that a systematic variation between HLMS-sensed CIT and the flight-recorded CIT could account for a large portion of the observed Q_{ms} variations. However, variations in the HLMS-sensed torque and pressure would act simultaneously. With the existing test design, it was impossible to separate their individual effects.

74. Bench tests of the HLMS hardware in the Q_{ms} mode, with controlled electrical inputs of torque, pressure, and altitude, yielded the Q_{ma}/Q_{ms} ratios shown in figure 57, appendix F, where the analytical HLMS expressions are also shown for comparison. The torque ratios determine the output Q_{ms} for the existing conditions. This figure shows that by including a CIT shift of approximately +2°C in the HLMS output points agreement with the analytical functions is greatly improved. A similar improvement is seen if the vertical scale is shifted, representing pressure measurement effect. Neglecting these biases, the lift margin hardware accurately performs the programmed analytical expressions. This confirms that sensed parameter shifts are a likely cause of excessive Q_{ms} scatter.

Altitude:

75. The amount of available power lost with increasing altitude is shown in figure 46, appendix F. The rate of available power decrease is obtained from the slopes of the constant temperature curves. Rate of power decrease is greatest at low altitudes and decreases for higher altitudes.

76. In addition to CIT, compressor inlet pressure ratio is necessary for generating power-available characteristics. The output of the test boom pressure transducer

Figure U. Effect of a ±2 psi Change in Maximum Standard Torque on HLMS Calculated Power Available.

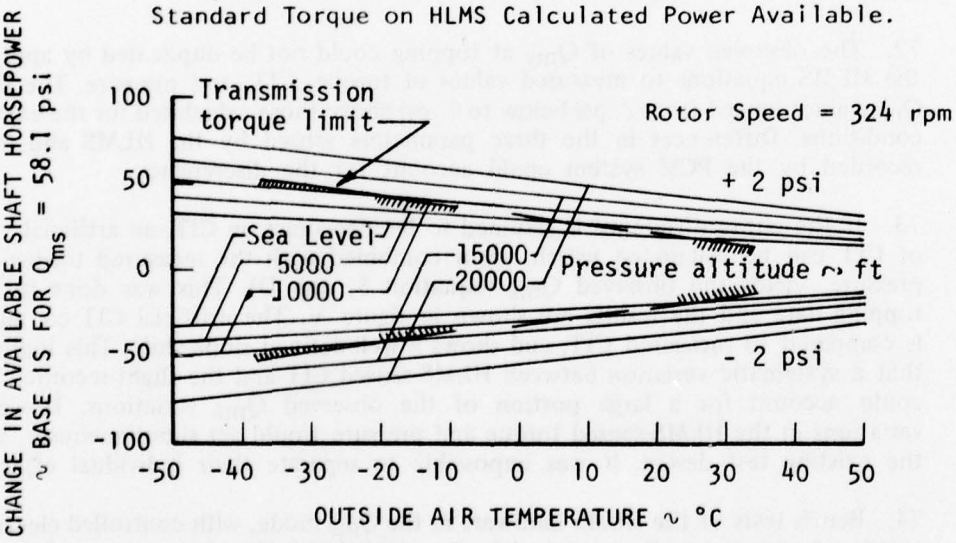

Figure V. Compressor Inlet Temperature Comparison: Measured Values at Topping and Calculated Values Required for the Observed HLMS Maximum Standard Torque.

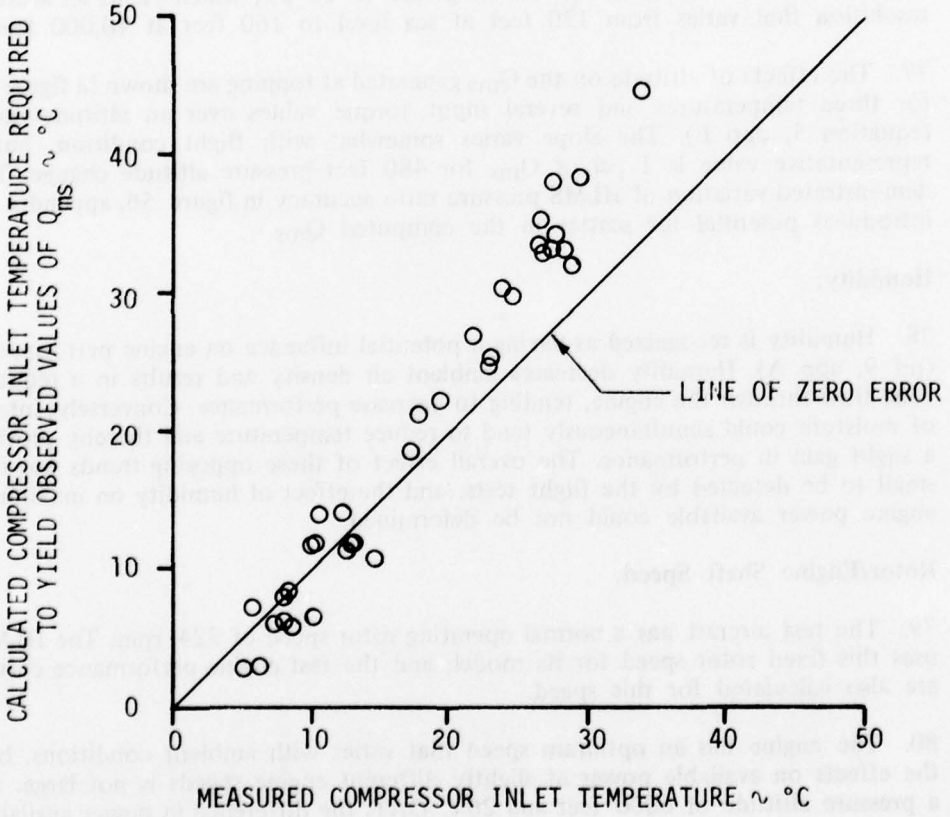

to the HLMS was available both directly from the transducer and from the HLMS as one of the recorded outputs of the S&M unit. Figure 56, appendix F, compares the differences between the HLMS altitude and the transducer altitude for the topping maneuver data. As with CIT, disagreement exists between the original transducer output and the HLMS output of the same quantity. One source of discrepancy is the degraded resolution of the HLMS output. The initial boom signal is split into three altitude ranges and recorded on separate PCM channels, resulting in a test altitude resolution of approximately 20 feet. The HLMS uses the same pressure signal in a single range covering zero to 16 psi, which yields an altitude resolution that varies from 120 feet at sea level to 160 feet at 10,000 feet.

77. The effects of altitude on the Q_{ms} generated at topping are shown in figure W for three temperatures and several input torque values over an altitude range (equation 5, app E). The slope varies somewhat with flight condition, but a representative value is 1 psi of Q_{ms} for 480 feet pressure altitude change. The demonstrated variation of HLMS pressure ratio accuracy in figure 56, appendix F, introduces potential for scatter in the computed Q_{ms}.

Humidity:

78. Humidity is recognized as having a potential influence on engine performance (ref 9, app A). Humidity decreases ambient air density and results in a reduced mass flow through the engine, tending to decrease performance. Conversely, intake of moisture could simultaneously tend to reduce temperature and thereby provide a slight gain in performance. The overall effect of these opposing trends was too small to be detected by the flight tests, and the effect of humidity on maximum engine power available could not be determined.

Rotor/Engine Shaft Speed:

79. The test aircraft has a normal operating rotor speed of 324 rpm. The HLMS uses this fixed rotor speed for its model, and the test engine performance curves are also calculated for this speed.

80. The engine has an optimum speed that varies with ambient conditions, but the effects on available power at slightly different engine speeds is not large. At a pressure altitude of 6000 feet and 20°C OAT, the difference in power available between 300 and 324 rpm main rotor speeds is approximately 10 shp.

Airspeed:

81. Power-available changes with airspeed became noticeable only for airspeeds in excess of 60 KTAS, beyond which a slight decrease was observed. At 100 KTAS available power was reduced approximately 15 shp from that at 60 KTAS and below. Since the HLMS performance is concerned only with considerably lower airspeeds, no compensation of power with airspeed is needed.

Figure W. Pressure Altitude Effects on the HLMS Maximum Standard Torque Calculation.

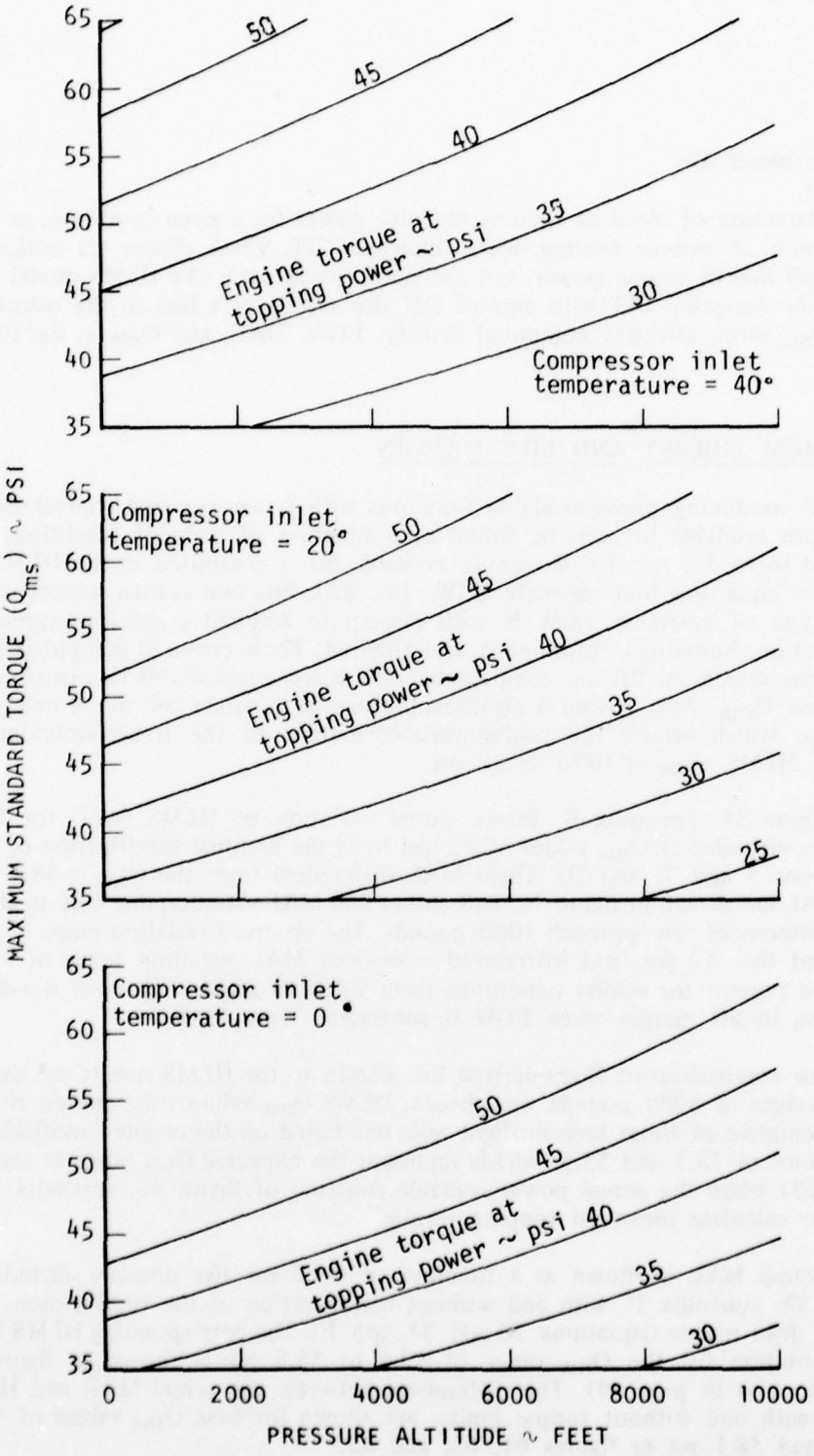

Anti-Ice/Bleed Air:

82. Extraction of bleed air reduces available power for a given condition, as does application of anti-ice heating, which increases CIT. These effects are noticeable in overall loss of engine power, but are not considered in the HLMS model. The artificially increased CIT with anti-ice ON also results in a bias in the calculated Q_{ma}/Q_{ms} ratio, affecting computed density, EGW, MAL, and Q_{ms} in the HLMS output.

MAXIMUM THRUST AND LIFT MARGIN

83. By combining power-available functions with power-required characteristics, maximum available lift can be found as a function of ambient conditions and airspeed (para 32, app E). Maximum available lift is computed in the HLMS by the same equations that calculate EGW. The MAL function is then subject to the same type of errors as EGW is with respect to ambient conditions (pressure, temperature, humidity), rotor speed, and airspeed. These errors in computed MAL from true maximum lift are compensated for at some conditions by errors in the predicted Q_{ma}. Also having a significant effect is accuracy of the stored value of Q_{ms}, which affects the power-available matrix. In the transmission-limited regime, HLMS Q_{ma} is fixed at 50 psi.

84. Figure 58, appendix B, shows actual variation of HLMS MAL for three pressure altitudes at Q_{ms} values of ±2 psi from the nominal specification of 58.1 (equations 5 and 7, app D). These MAL differences from the Q_{ms} = 58.1 base line MAL are shown in figure X. This shows that MAL variation due only to stored Q_{ms} differences can approach 1000 pounds. The observed variation range of Q_{ms} exceeded this ±2 psi, and introduced a random MAL variation range of several hundred pounds for similar conditions from flight to flight. This error is a direct variation in lift margin when EGW is subtracted from MAL.

85. For comparison of flight-derived lift margin to the HLMS results, an aircraft gross weight of 8000 pounds was chosen. HLMS Q_{ms} values were chosen at 58.1 (representative of those seen in flight tests and based on the engine specification), and values of 53.5 and 55.5, which represent the expected Q_{ms} range at topping (para 65) when the actual power-available function of figure 46, appendix F, is used to calculate measured topping torque.

86. Actual MAL is shown as a function of OAT for five pressure altitudes in figure 59, appendix F, with and without consideration of the transmission limit of 905 ft-lb torque (equations 30 and 31, app E). The corresponding HLMS MAL representation for the Q_{ms} range of 53.5 to 55.5 psi is shown in figure 60 (equations as in para 84). The differences between the actual MAL and HLMS MAL, with and without torque limits, are shown for base Q_{ms} values of 53.5, 55.5, and 58.1 psi in figures 61, 62, and 63.

Figure X. Effect of a ±2 psi Change in Maximum Standard Torque on HLMS Calculated Maximum Available Lift

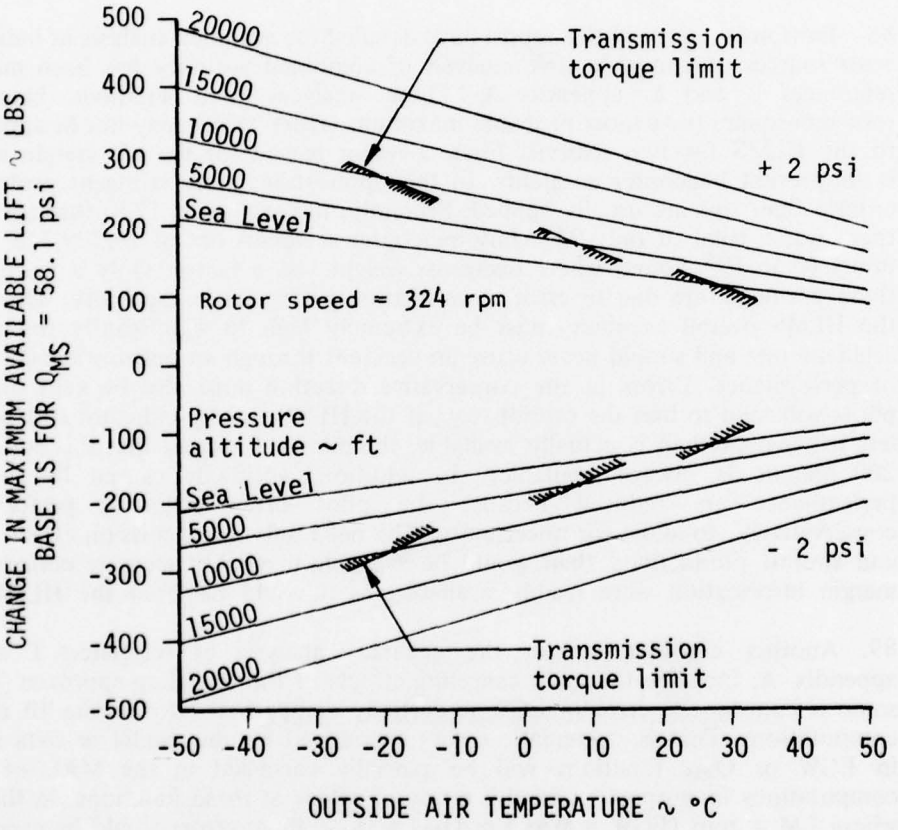

87. For an aircraft gross weight of 8000 pounds, actual lift margin is shown in figure 59, appendix F (equations 30 and 31, app E), and the HLMS computation results in figure 64 (equation 11, app D). These include effects of both EGW linearization as well as the MAL errors. Total error in lift margin, with and without torque limits, are shown for the three Q_{ms} values in figures 65, 66, and 67.

Accuracy Considerations

88. Previous sections of this report have detailed the accuracy analysis of individual error sources. A comprehensive analysis of combined accuracy has been made in references 1 and 2, appendix A. These analyses used methods based on root-sum-square (r-s-s most probable maximum error), which may not be applicable to the HLMS for two reasons. First, a major reason for the lift margin system is to prevent helicopter accidents. In this application, more stringent probability criteria than r-s-s are usually applied. Secondly, in fiscal years 1970 through 1975 there was a total of only 94 Army helicopter accidents out of 16,729,712 flying hours ($0.56/10^5$ hours) where overgross weight was a factor. Only a fraction of these accidents are due to error in estimating performance capability. Therefore, the HLMS overall accuracy must be extremely high to significantly reduce the accident rate and should never cause an accident through an optimistic calculation of performance. Errors in the conservative direction must also be kept small or pilots will tend to bias the output (e.g., if the HLMS usually indicates 200 pounds less lift margin than is actually available, the pilot will expect that this additional 200 pounds is always available). In addition, accidents caused by lack of performance are reduced because the pilot often estimates performance conservatively, to allow for uncertainty. The net result is less mission effectiveness and aircraft productivity than would be available if reliably accurate performance margin information were readily available, as it could be from the HLMS.

89. Another consideration in the accuracy analysis of references 1 and 2, appendix A, includes the error canceling effects of the modeling approach. Under some circumstances, error in EGW is partially compensated for in the lift margin computations. That is, systematic errors introduced by the model or data inputs in EGW or Q_{ms} functions will be partially cancelled in the MAL or Q_{ma} computations in proportion to the ratios of values of these functions. In the case where LM = zero (EGW = MAL) or $Q_{ms} = Q_{ma}$, these errors would be cancelled, since the same function is used to transfer from one parameter to the other. However, this is only true if topping, weighing, and lift margin are determined at identical conditions. This was generally the case during the tests; however, it would generally not be the situation during operational use of the system. Therefore, accuracy of the system in operational use could be substantially reduced from that demonstrated during this evaluation.

90. Three general areas must be considered in determining overall accuracy of the lift margin system. These are (1) the accuracy of the base line data from which the computer modeling functions are derived, (2) the modeling accuracy, including both the analytical functions and the hardware that performs them, and (3) the

accuracy of the measured input data. Of these, only the last was considered in detail in the error analysis of the HLMS in references 1 and 2, appendix A.

Base-line Data:

91. The ultimate accuracy of the HLMS or any performance computer can be no more accurate than the data upon which it is based. Unfortunately, base-line performance data accuracy is not well known or documented. The effects of winds on power required to hover the test aircraft were not known prior to this project. For other power-required flight test data, the present measured parameters are limited to a resolution of 0.4 percent. This generally determines an upper limit on their accuracy. However, numerous manipulations made to the measured raw data prior to its reaching final form will degrade the original accuracy. Another factor that can affect accuracy at extreme conditions is the range of conditions for which the data was gathered. During future flight characteristics tests, data should be obtained over an adequate altitude, temperature, and airspeed range to accurately predict performance at the extreme conditions that might be encountered operationally. Power-available data have usually been obtained from the engine model specification and corrected for installation losses as determined from flight test data. Actual engine performance has varied significantly from the model specification, usually in the conservative direction. Sufficient engines are not tested to determine variations between engines. The other factor not determined is the effect of engine running time or condition on engine performance. Engine-to-engine performance variation and variation with running time/condition should be determined during future tests.

Modeling Accuracy:

92. The modeling accuracy was generally quite good considering the linearized analog functions used. The power-available function matched the engine model specification from which is was derived. Actual engine power available was more sensitive to temperature than predicted. A more complex model might be necessary to account for the different temperature sensitivity of engines. Adequate accuracy over the extreme range of conditions may also require more model complexity. The power-required function linearization caused lift errors as large as 180 pounds, which prevented obtaining the desired accuracy. The effects of wind/airspeed are quite large and complex and were not considered in the HLMS. They must be included in future performance computers. Additional modeling complexity may make it desirable to use completely digital computations.

Input Parameter Accuracy:

93. Detailed analyses of the effects of input parameter accuracy have been made in references 1 and 2, appendix A. These are generally correct except for the r-s-s method used. A worst-case method is considered more appropriate. In an operational installation the test transducers used for the prototype systems would probably not be an economic feasibility. Most of the required parameter signals are available from standard aircraft instrument systems. Future performance computers should use inputs from standard aircraft instruments where practical.

OPERATIONAL CONSIDERATIONS

94. In addition to accuracy, several other areas influence the operational suitability of the lift margin system. These include operation of the system, range, limits, human engineering aspects, documentation, and reliability.

Operation

95. To compute lift margin, initial values of maximum standard torque (Q_{ms}) and effective gross weight (EGW) must be obtained and stored in the system.

Maximum Standard Torque:

96. Maximum standard torque is obtained by flying the aircraft at a condition that requires maximum available power. With the lift margin system in the Q_{ms} mode, the enter-data switch is depressed when conditions are stable. This maneuver is a routine maintenance test flight maneuver; however, it is normally not performed operationally. No instructions were provided as to how the maneuver was to be accomplished. Consideration has been given to a means of obtaining Q_{ms} at low power conditions. This would probably require input of other engine parameters (i.e., N_1, EGT, or fuel flow). Further study should be conducted on initializing the power-available function at less than maximum power. In theory, only engine deterioration should affect the value of Q_{ms}; therefore, it only needs to be checked or updated periodically. The Q_{ms} value is displayed on the C&D unit. Maximum torque available at present ambient conditions (Q_{ma}) would be of more value to the pilot. This was available by selection on the S&M unit. Q_{ma} should be continuously available on the C&D unit. For example, Q_{ms} could be available while the switch is depressed, as is IGE lift margin.

Effective Gross Weight:

97. Present aircraft weight needs to be obtained and stored at the beginning of each flight, and any time the aircraft loading is changed (i.e., cargo, personnel, or ordnance loaded or unloaded) or when the aircraft is refueled. Fuel consumed is the only weight change accounted for automatically. EGW is obtained by stabilizing the aircraft at a zero wind OGE hover. With the HLMS in EGW mode, the enter-data switch is depressed. EGW is then computed on the basis of torque required to hover at existing ambient conditions. The requirement to hover OGE prior to having lift margin information available might be acceptable for sling-load operations where the aircraft will normally be hovering OGE both prior to and after picking up the sling load. For most missions this requirement is unacceptable, since the most important information is the hover capability (lift margin) prior to initial takeoff of a flight or after changing the load. The requirement to hover OGE on the initial takeoff of each flight or any time a loading change is made, prior to having lift margin information available, is a deficiency. Input from a landing gear weighing system is the most direct solution to this problem. Such systems are under development; however, none have been completely successful.

Another solution would be to manually input gross weight information. It is presently required that a gross weight and balance calculation be made for all flights, so gross weight information should be available. However, the accuracy of these calculations and the resulting impact on lift margin accuracy is questionable. There are many cases where a weight change is known with acceptable accuracy, such as ordnance loaded or expended, cargo loaded or unloaded, etc. A manual weight change input could, therefore, reduce the requirement for weighing maneuvers. The in-flight weighing capability should be retained even if ground weighing information is available, since in-flight weighing includes rotor efficiency, individual aircraft differences, and other error-canceling factors. With the input of airspeed from a low airspeed system, which will be required for reasonable accuracy, weighings could be conducted in forward flight. This would be useful to check/update EGW prior to landing at critical conditions. Another improvement would be to use the measured fuel quantity in weight determination as opposed to the present method of computing fuel consumption rate. Fueling operations would then not require reweighing. Additionally, if the fuel consumption computation were retained or fuel flow rate were measured, the two could be compared to provide endurance information. This, combined with airspeed or INS/doppler/DME ground-speed information, could provide range data. One other possible solution to the problem of having to hover OGE before the HLMS can predict hover capability is to perform the weighing maneuver by hovering IGE. This is the present method used to estimate performance capability (i.e., go, no-go, check). One problem associated with IGE weighing is the sensitivity of power to hover height. For example, at a 2-foot skid height power required varies approximately 3 shp per inch, which is equivalent to approximately 20 pounds per inch. Therefore, for IGE weighings to give reasonable accuracy, skid height would have to be controlled and/or determined very accurately. One advantage of the IGE weighing maneuver is the helicopters insensitivity to winds up to approximately 15 knots Therefore, errors introduced by wind/airspeed measurement would be minimal.

Operating Range

98. In the "destination" mode, the HLMS was limited to ambient temperatures of ±49°C and pressure altitudes from sea level to 9900 feet. The accuracy of the analog functions deteriorated rapidly beyond those conditions. Although this range of conditions encompasses the maiority of probable conditions to be encountered operationally, operations beyond these conditions will be required. Additionally, at these extreme conditions helicopter performance will be more critical. Inadequacy of the altitude and temperature range over which the HLMS was designed to operate accurately is a deficiency. When these factors were considered during the operator's manual revision program, conditions of ±60°C and sea level to 20,000 feet were chosen as the maximum probable conditions to be encountered in helicopter operations. Future helicopter performance computers should be designed to function accurately over this range of conditions.

Limits

99. The HLMS considered two limits in computing lift margin. Primarily, maximum engine power available (Q_{ma}) determined maximum available lift (MAL), and in turn, lift margin. Additionally, the transmission torque limit was used for maximum power if engine power available was larger at the existing conditions. Other factors that limit the aircraft performance should be considered and included in future helicopter performance computers. For example, on several occasions at the high-altitude test site the HLMS accurately predicted additional lift capability based on engine power available. However, there was insufficient directional control authority to safely use the total lift capability (i.e., if maximum power had been used to obtain maximum lift, the aircraft would be turning uncontrollably). The maximum allowable gross weight limit was not considered in the HLMS and should be included for future designs. Any other limits or capabilities which may determine maximum performance of any specific helicopter should also be considered in future helicopter performance computers.

100. It would be desirable that the applicable limit that determines lift margin be indicated so the pilot will know which parameter to monitor. Additionally, the pilot should be able to select a limit and obtain the performance capability if he chose to exceed the limit in an emergency or critical situation.

Human Engineering Aspects

101. Several human engineering features degraded the system. Although the contractor was aware of most of them, they were not corrected on the prototype systems because of time and cost considerations. These shortcomings had little impact on the operation of the prototype system, but would require correction in a design intended for operational use. These areas included display, lighting, switching, and control logic.

102. The primary display of the C&D unit was with numerical light-emitting diodes (LEDs) with no provision for intensity variation. In daylight they were marginally bright enough to read. A cardboard glare shield was locally fabricated, and when shielded by hand from direct sunlight, the display was readable from the copilot position. At night the display was much too bright. The 3/8-inch numbers were adequate. Under flight conditions where the displayed values were fluctuating, it was difficult to determine an average. The C&D unit had an update rate of approximately once per second.

103. The display and operating mode selection was made via backlighted, alpha-coded, pushbutton switches. These suffered the same lighting problems as the data display. The predominately yellow color used was less visible in daylight than the red LED data display. The lift margin system lighting is inadequate for operational use. A future system should have sufficient intensity of both the data display and mode indications to be readable in direct sunlight. It should have a dimming control, automatic intensity control, or be wired into the master aircraft light intensity control.

104. Another problem associated with mode control was the switching and display logic, which was confusing and needs improvement for operational use. The system displays EGW, lift margin, or Q_{ms} at all times. Q_{ms} can be obtained directly at any time regardless of which parameter is being displayed. To obtain EGW or lift margin, the signal being displayed must be canceled before the selection is made. When a signal is canceled, the system will display the previous selection. A production system should have each mode directly selectable. Another minor shortcoming was the lack of an ON/OFF switch. A panel-mounted circuit breaker was used for this function. A production system should have an ON/OFF switch with the circuit breaker mounted remotely on the aircraft circuit breaker panel. The TEST/NORMAL mode switch could be deleted on a production system. This function could be accomplished by plugging in the test set (S&M unit).

105. The HLMS C&D unit had several desirable features that should be retained in a production design. The ENTER DATA switch was guarded to preclude inadvertent data entry. The mode selected and data displayed were positively indicated. The data displayed and DESTINATION data inputs were in correct units and had proper resolution. Nomenclature and display labels were generally clear and easily understood. The C&D unit was light, relatively compact, and fitted directly into available console mounting space.

Documentation

106. There were no operator or maintenance manuals provided for the HLMS. Additionally, design specifications and drawings provided were incomplete. This, combined with the lack of a full-time technical representative from the manufacturer, caused problems in conducting the test, analyzing the data, and delays when attempting to troubleshoot the system when failures or problems occurred. Future test projects of this nature should require a complete set of engineering drawings, and draft operating and troubleshooting manuals or instructions for use and review of their adequacy. If practical, full-time technical representation from the manufacturer will help minimize delays and will facilitate improvements and modifications.

Reliability

107. Several failures occurred during the test. One failure was traced to partial failure of the CIT probe. Most of the other failures were attributed to the internal battery used to power a circuit for retaining the stored values of Q_{ms} and EGW after aircraft electrical power was removed. The long-term memory of the HLMS was unreliable. One C&D unit was modified to eliminate the battery. This required the values of Q_{ms} and EGW to be entered manually via the S&M unit prior to each flight. Other means of long-term storage should be investigated.

Failure Warning

108. Most of the failures were not readily apparent. Even when not operating properly, the HLMS would still display reasonable values for lift margin and other

parameters. The failures were detected primarily because the operator was familiar with the expected output. This type of failure would be extremely hazardous operationally, since it would mislead the pilot as to the performance margin. The lack of a failure warning system to positively indicate all possible failure modes is a deficiency. A production system must have a positive failure warning system that will detect all possible failure modes. It should include some means of indicating the type of failure to aid repair.

CONCLUSIONS

GENERAL

109. An on-board performance computer for helicopters such as the Helicopter Lift Margin System is feasible and desirable. The direct availability of performance margins can reduce accidents by helping the pilot avoid situations beyond the capability of his aircraft. Another benefit is increased aircraft productivity attained by safe use of the full performance capability of the aircraft.

110. The following conclusions were reached as a result of these tests:

a. The lift margin hardware accurately performs the programmed analytical expressions (paras 22 and 74).

b. Errors due to not considering humidity (on the test aircraft) were small, and at most conditions will not have a significant effect on power required to hover (para 32).

c. The effects of wind on OGE hover performance are large and must be considered for the lift margin system to have a reasonable accuracy (para 36).

d. The effects of wind direction are significant and increase with wind speed and rotor thrust (para 37).

e. The analytical expression for power available (maximum available torque) accurately duplicates that of the model specification over the present operating range (para 55).

f. Actual test engine performance is significantly different from the model specification engine performance from which the lift margin system power-available expression was derived (para 63).

g. Power-available computations (maximum available torque, maximum standard torque, maximum available lift) are extremely sensitive to compressor inlet temperature. Small errors in compressor inlet temperature measurement can have a large impact on the overall accuracy of the lift margin system (para 68).

h. The effect of humidity on maximum engine power available could not be determined (para 78).

i. Under some circumstances, error in equivalent gross weight is partially compensated for in the lift margin computations (para 89).

j. Four deficiencies and four shortcomings were noted.

DEFICIENCIES AND SHORTCOMINGS

111. The following deficiencies, presented in order of importance, must be corrected in a lift margin system intended for operational use:

a. The requirement to hover OGE on the initial takeoff of each flight or any time a loading change is made, prior to having lift margin information available (para 97).

b. The lack of low airspeed input and consideration of the effects of wind/low airspeed on helicopter performance and lift margin results in potential errors of several thousand pounds (para 36).

c. The lack of a failure warning system to positively indicate all possible failure modes would be extremely hazardous operationally. Failures were experienced which allowed the HLMS to indicate erroneous but reasonable values of lift margin (para 108).

d. The range of altitude and temperature for which the HLMS was designed to operate accurately was inadequate. The need for adequate performance information is most critical at extreme conditions (para 98).

112. The following shortcomings, presented in order of importance, should be corrected in a production design intended for operational use:

a. The linearized function for power required (equivalent gross weight) does not adequately represent the nonlinear function of power required versus thrust, resulting in a possible error in equivalent gross weight of 180 pounds and a proportionate error in lift margin (para 26).

b. The lift margin system lighting is inadequate for operational use (paras 102 and 103).

c. The lift margin switching and display logic is confusing and needs improvement for operational use (para 104).

d. The long-term memory of the lift margin system is unreliable (para 107).

RECOMMENDATIONS

113. An in-flight performance computer represents a significant improvement in providing the pilot information needed to increase safety and enhance mission accomplishment. Development of an operational system should be continued. In addition:

a. Consideration should be given to providing other performance information in addition to hover lift margin in future designs (para 21).

b. Future performance computers should use inputs from standard aircraft instrument systems where practical (para 93).

c. The prototype HLMS incorporated many desirable features which should be retained in future designs (para 105).

d. The deficiencies and shortcomings identified in these tests should be corrected in future designs.

APPENDIX A. REFERENCES

1. Final Report, JANAIR, No. 690107, *Final Report for Helicopter Lift Margin System, Volume I,* February 1969.

2. Final Report, JANAIR, No. 701218, *Final Report for Helicopter Lift Margin System, Volume II,* December 1970.

3. Test Plan, US Army Aviation Systems Test Activity (USAASTA), Project No. 73-01, *Engineering Flight Evaluation, Helicopter Lift Margin System,* July 1973.

4. Letter, USAAEFA, 19 August 1974, subject: Status Report, Helicopter Lift Margin System Evaluation.

5. Technical Manual, TM-1520-220-10, *Operator's Manual Army Model UH-1C/M Helicopter,* November 1968.

6. Final Report, USAAEFA project No. 71-30-6, *Flight Evaluation, Elliott Dual-Axis Low Airspeed System, LASSIE II,* September 1975.

7. Test Report, US Army Aviation Test Activity, Project No. 64-28, *Engineering Flight Test of the UH-1B Helicopter Equipped with the Model 540 Rotor System, Phase D,* December 1966.

8. Specification, Lycoming Division of Avco Corporation, No. 104.33, *Model Specification T53-L-13 Shaft Turbine Engine (Lycoming Model LTCIK-4),* revised May 1966.

9. Technical Note, NACA, No. 2119, *Effect of Humidity on Performance of Turbojet Engines,* March 1950.

10. Final Report, JANAIR, No. 731003, *Final Report for Helicopter Lift Margin System,* December 1974.

11. Technical Report, Trans-Sonics, Inc., No. 74-56, *Helicopter Lift Margin System,* February 1974.

12. Final Report, JANAIR, No. 721201, *Air Density and Helicopter Lift,* January 1973.

13. Textbook Gessow, G; Myers, G. C. Jr, *Aerodynamics of the Helicopter,* Frederic Ungar Publishing Company, New York, 1952.

14. Final Report, USAASTA, Project No. 66-04, *Engineering Flight Test YUH-1H Helicopter, Phase D (Limited),* November 1970.

15. Report, NACA, No. 824, *Summary of Airfoil Data,* 1945.

16. Report, Air Force Flight Test Center, AFFTC-TR-65-17, *Determination of the Effects of Compressibility on the Performance of the UH-1F,* July 1965.

17. Final Report, USAAEFA, Project No. 74-87, *Flight Evaluation of Nondimensional Static Longitudinal Stability Test Methods,* June 1977.

APPENDIX B. INSTRUMENTATION

1. The test aircraft was equipped with an on-board PCM data system to record the parameters listed below on magnetic tape. A selection of the same parameters could also be transmitted to ground strip-chart recorders via telemetry. Each channel consists of 255 discrete counts, which determines the attainable resolution of a given parameter as 1/255 of its full calibration range. Exceptions are the discrete counter or ON/OFF flag-type channels, and the multichannel parameters. While a few changes in the available parameters were made early in the program, those listed below remained constant for most of the flights and represent the final configuration. The following notation identifies appropriate channels:

(B) Bi-level channel (all others zero to 5-volt DC analog)
(E) Signal provided by E-A Industrial Corporation (LASSIE II)
(N) Signal provided by National Bureau of Standards
(T) Signal provided by Trans-Sonics Inc. as output from HLMS

Parameter	Calibration Range
(B) Time of day	Days, hours, min, sec, millisec
(B) Correlation counter	Zero to 127 counts
(B) Event	Off/zero, pilot/64, engr/128 counts
Cargo hook load (low range)	Zero to 2500 pounds
Cargo hook load (high range)	1880 to 4250 pounds
(B) Fuel used (fine)	Zero to 25.5 gallons
(B) Fuel used (coarse)	25.5 gallons/count
Fuel temperature	-10 to +61°C
Outside air temp (total)	-10 to +61°C
Altitude #1 (boom)	-500 to 5000 feet (nonlinear)
Altitude #2 (boom)	4500 to 10,000 feet (nonlinear)
Altitude #3 (boom)	9000 to 18,000 feet (nonlinear)
Airspeed (boom)	20 to 135 knots (nonlinear)
Radar altitude (fine)	Zero to 136 feet (AGL)
Radar altitude (coarse)	Zero to 975 feet (AGL)
Radar vertical velocity	±600 feet per min
Longitudinal acceleration	±1.2g
Lateral acceleration	±1.2g
Vertical acceleration	-.1 downward to +4.7g
Longitudinal cyclic position	Zero (forward) to 100 percent
Lateral cyclic position	Zero (left) to 100 percent
Pedal position	Zero (left) to 100 percent
Collective position	Zero (down) to 100 percent
Twist grip position	Off, flight idle, flight governing
Rotor speed select position	Zero (full decrease) to 100 percent
Angle of attack (boom)	-30 (vane nose up) to +30 degrees
Angle of sideslip (boom)	-30 (vane nose left) to +30 degrees

Pitch attitude	-32 (nose down) to +32 degrees
Roll attitude	-62 (bank left) to +62 degrees
(B) Aircraft heading (magnetic)	Zero to 360 degrees, 255 counts/quadrant
Yaw rate	-61 (nose left) to +61 deg/sec
Fuel flow rate	Zero to 247 gallons per hour
Exhaust gas temperature	443 to 653°C
Engine torque pressure	Zero to 70.9 psi
Output shaft speed (N_2)	2538 to 7175 rpm
(N) Dew point temperature	-54 to +53°C
Delta Static pressure, Elliott	-.32 to +.59 psi
(E) Longitudinal CAS (coarse, uncorrected)	-50 to +205 KCAS
(E) Longitudinal CAS (coarse, corrected)	-50 to +205 KCAS
(E) Lateral CAS (uncorrected)	-30 (left sideward) to +30 KCAS
(E) Lateral CAS (corrected)	-30 (left sideward) to +30 KCAS
(E) Transition monitor	ON/OFF signal for high/low speed flight
(E) Sin alpha	-1 to +1
(E) Cosine alpha	-1 to +1
(E) Sin beta	-1 to +1
(E) Cosine beta	-1 to +1
(E) Total velocity	Zero to 205 knots
(E) Downwash velocity	Zero to 51 knots
(E) Altitude (coarse)	-590 to 20,930 feet
(E) Altitude (fine #1)	2198 feet/turn
(E) Altitude (fine #2)	2198 feet/turn
(E) Altitude "E-Coil"	2.4 volts/100 feet
(E) Vertical velocity	-3125 to +3250 feet/minute
(E) Vertical speed indicator feedback	±2.5 volts
(TB) Lift margin or effective gross weight or maximum standard torque	LM: -980 to 9980 pounds EGW: 4900 to 9980 pounds QMS: 39.9 to 65.5 psi
(TB) HLMS flag	LM, EGW, or Q_{ms}; OGE or IGE
(T) Air density ratio, calculated	Zero to 1.289
(T) Effective gross weight	Zero to 10,625 pounds
(T) Compressor inlet temperature, numerator	Voltage signal
(T) Compressor inlet temperature, denominator	Voltage signal

2. The cockpit panel display is shown in photo 1, and the numbered key identifies the separate indicators corresponding to the following list:

Parameter		Display Range
1.	Tethered thrust (cable tension)	Zero to 4000 pounds
2.	Boom angle of sideslip	-45 (vane nose left) to +45 deg
3.	Airspeed (Rosemount, Inc.)	-40 to +40 knots
4.	Tail rotor blade angle	Zero to 100 percent
5.	Shuping meter (cable angle)	Zero to 30 deg
6.	Ship's airspeed	Zero to 130 knots
7a.	Fuel flow rate	Zero to 240 gallons/hour
7b.	Fuel used	Zero to 999.9 gallons
8.	Radar altitude	Zero to 1000 feet
9.	Outside air temperature (total)	-20 to +50°C
10.	Ship's altitude	Sea level to 12,000 feet
11.	Altitude (LASSIE II)	-1000 to 70,000 feet
12.	PCM system: power, event, record indicators; cumulative event counter	On/off indicators, digital counter
13.	PCM system recorded time	Hours, min, sec
14.	Ship's fuel pressure	Zero to 50 psi
15.	Ship's fuel quantity	Zero to 1150 pounds
16.	Ship's engine oil pressure	Zero to 100 psi
17.	Ship's engine oil temperature	-70 to +150°C
18.	Ship's transmission oil pressure	Zero to 100 psi
19.	Ship's transmission oil temperature	-70 to +150°C
20.	Ship's main generator load	Zero to 1.2 maximum
21.	Ship's main generator DC voltage	Zero to 30 volts
22.	Ship's stby generator load	Zero to 1.2 maximum
23.	Ship's stby generator AC voltage	Zero to 150 volts
24.	Lateral airspeed (LASSIE II)	-40 (left sideward) to +40 knots
25.	Vertical speed (LASSIE II)	-3000 to +3000 ft/min
26.	Longitudinal airspeed (LASSIE II)	-40 to +40 knots
27.	Exhaust gas temperature	Zero to 1200°C
28.	Compressor speed	60 to 110 percent
29.	Engine torque pressure	Zero to 50 psi
30.	Ship's rotor/engine speed	Zero to 7200 rpm
31.	Rotor speed (sensitive)	250 to 350 rpm
32.	Ship's turn rate and slip ball	Standard display
33.	Ship's pitch and roll attitude	Standard display
34.	Magnetic aircraft heading	Zero to 360 degrees
35.	Ship's vertical speed	-3000 to +3000 ft/min
36.	Boom altitude	Sea level to 12,000 feet
37.	Boom airspeed	Zero to 130 knots
38.	Clock	Hours, min, sec

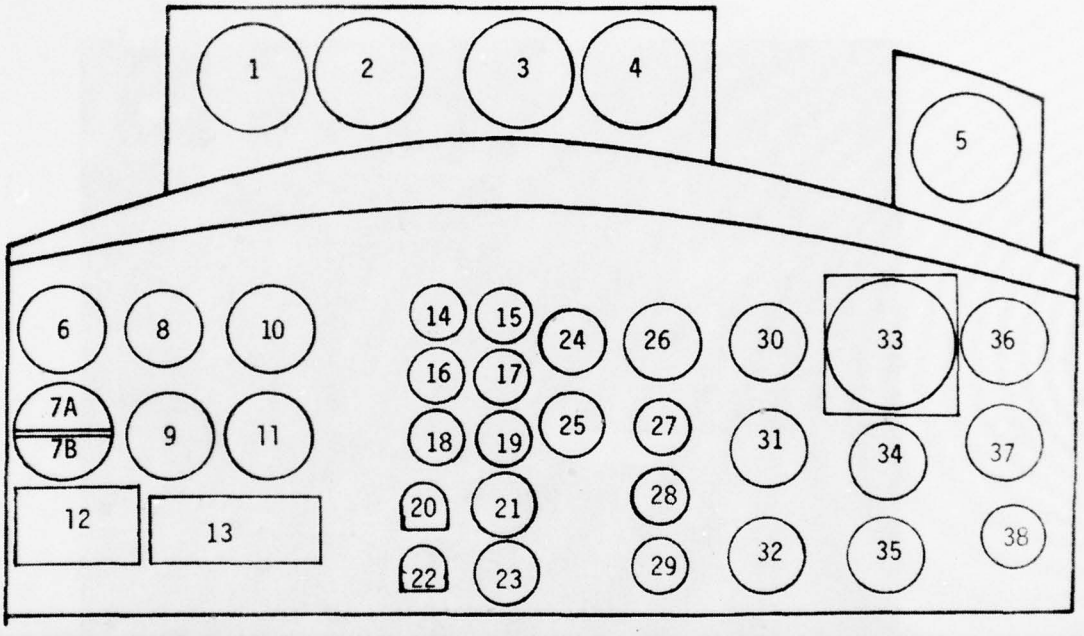

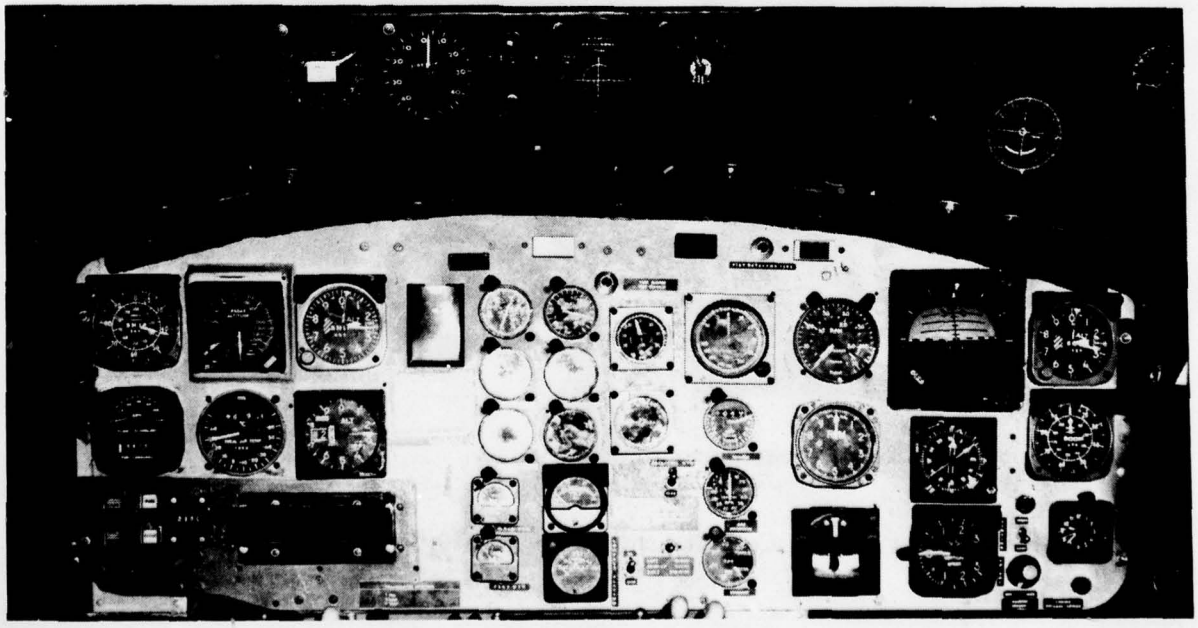

Photo 1. Main Cockpit Panel Display of Test Aircraft.

Photo 2. Test Aircraft Cockpit Center Console With Insets A and B (following page).

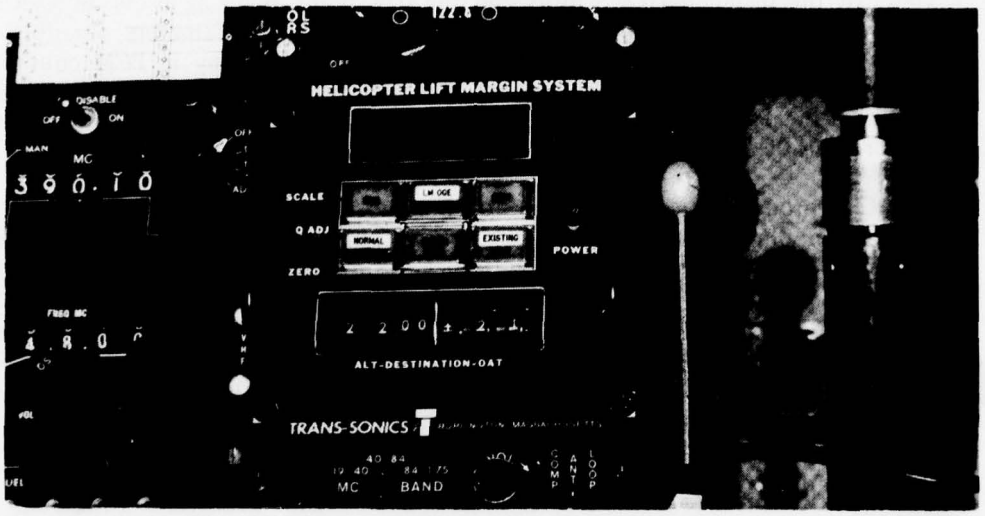

Inset A. HLMS C&D Unit.

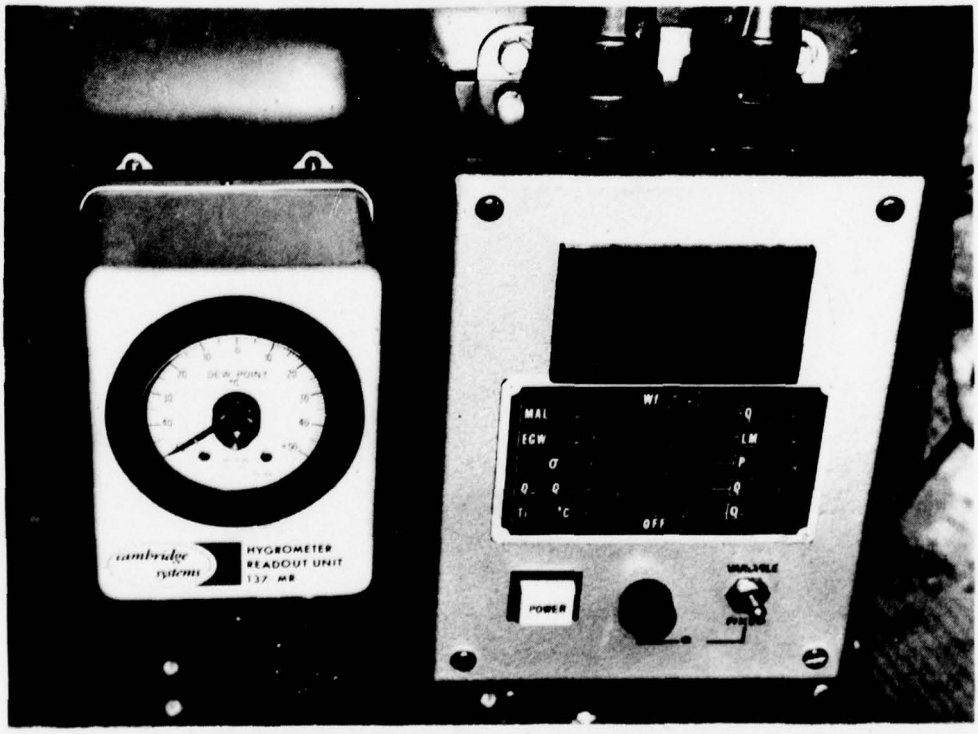

Inset B. Dew Point Meter and HLMS S&M Unit

3. An overall view of the cockpit center console is shown in photo 2 with closer views of the installed HLMS units and the dew point meter as insets. In addition to the dew point and all the HLMS C&D and S&M parameters described in appendix C, the center console also provided a digital display in PCM counts of any of the PCM channels, selected by means of a thumbwheel. This data display unit and the PCM tape drive switches are located in the upper left corner of the center console.

4. Gas producer (N_1) and main rotor speeds were extracted from respective tachometer blips recorded on the flight tape. These signals, on a separate channel from the PCM parameters, were electronically timed during the event-on segments while the flight tape was being formatted into engineering units. These resulting counter values were directly converted to N_1 percent speed and main rotor rpm for use with the corresponding flight data records in further analysis. The resolutions of N_1 and main rotor speed were 0.14 percent and 0.4 rpm, respectively.

APPENDIX C.
GROUND INSTRUMENTATION

1. Two barometers were available at the test sites for measuring ambient atmospheric pressure at ground elevation. Their combined range covered 10 to 34 inches of mercury. Both instruments had scales graduated in increments of 0.02 inch of mercury, permitting estimation of the observed reading within 0.002 inch of mercury. Both instruments included built-in removable thermometers and individual calibrated correction curves for temperature.

2. An electronic solid-state hygrometer indicator supplied readings of humidity and temperature, with 115-volt AC power furnished by the computer van. Then separate sensors, each with its own sensitivity range, could be individually connected via cable to provide a total measured relative humidity range from 1.6 to 99 percent, and the temperature range measured by the same sensors was -18 to +60°C. Manufacturer's specified accuracies were ±1.5 percent for relative humidity, and ±1.1°C for temperature.

3. Three wind towers were erected at each test site to gather wind data. The towers were symmetrically arranged about the hover pad at distances of 400 feet. Wind speed and direction were measured with a six-cup anemometer and a wind vane set mounted together, as shown in photo 1. Each tower was equipped with three such wind sets, located at approximate elevations of 6, 14, and 62 feet. a complete tower is shown in photo 2. Instrumentation on the lower two levels was mounted on 10-foot long booms that extended horizontally from the tower. For structural reasons, the top level sensors were mounted directly onto the wind tower with no horizontal offset, and reached their 62-feet elevation only at full tower extension. Collapsed tower height, for normal storage between flights, was 22 feet.

4. Each of the nine sensor stations had transducers directly wired to the computer van. Wind data analog signals were formatted on magnetic tape during the flight, for later correlation with the aircraft flight data tape. Three sets of wind speed and direction gages, shown in photo 3, could display the output of any combination of levels and towers. These were used to hand-record average wind data during each data point taken, and to monitor gust velocity spread and direction differences between levels and towers. A 2-knot gust spread in speed and a 10-degree spread in direction were the steadiness criteria for acceptable data-producing flight conditions.

5. For the best estimate of winds at rotor height, the outputs of top tower levels were recorded during OGE flying, and from the center levels during IGE flight. Comparison of wind tapes with hand-recorded data for the same flights showed good correlation. Averaged wind speeds agreed within 0.5-knot and averaged directions within 5 degrees.

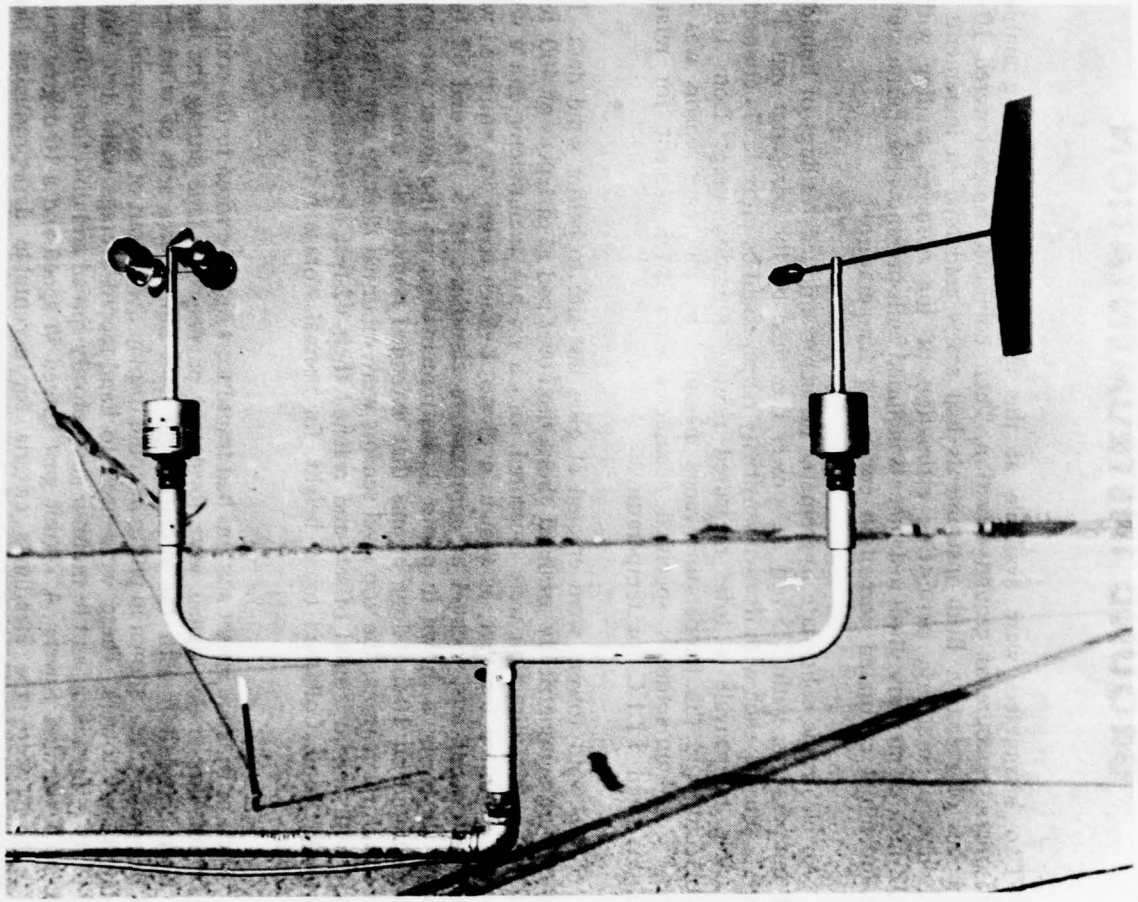

Photo 1. Anemometer and Wind-Vane Sensors Mounted on Bottom Wind Tower Level.

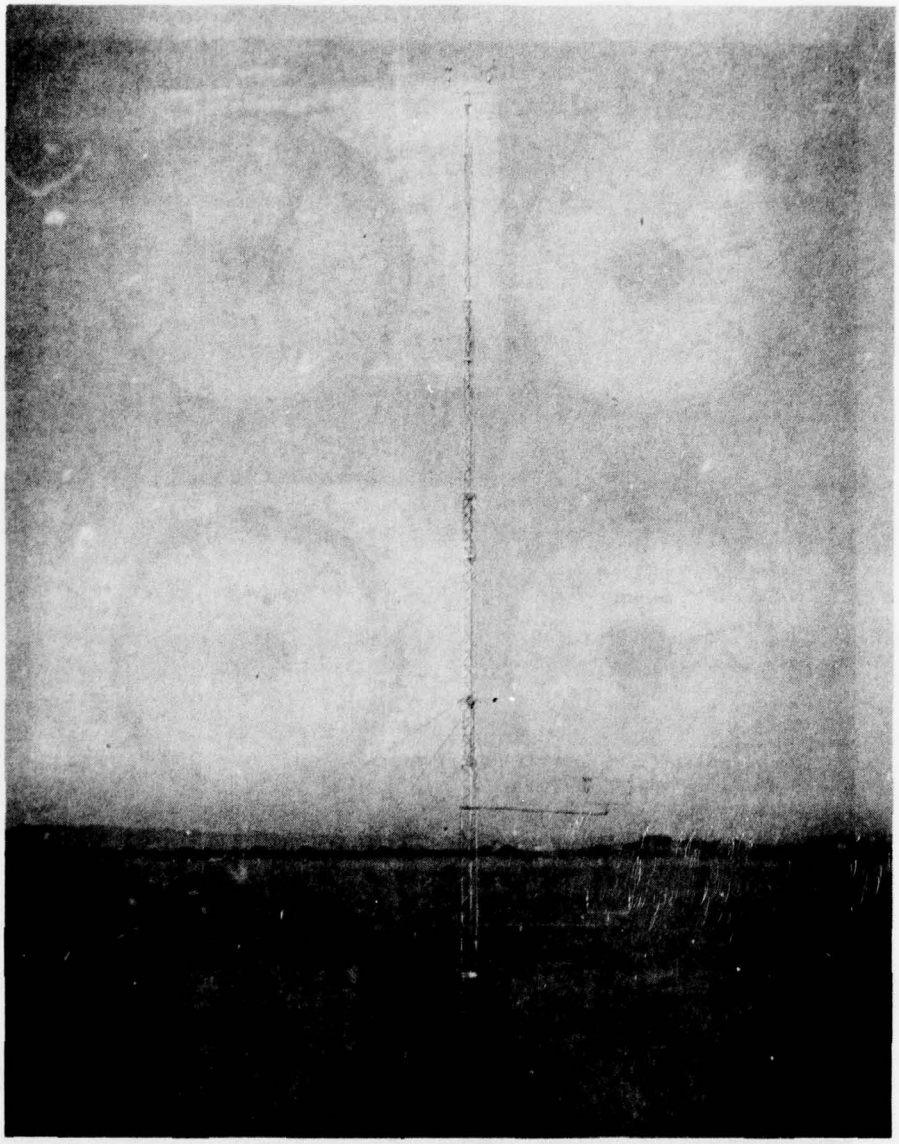

Photo 2. Extended Wind Tower Showing All Three Sensor **Levels.**

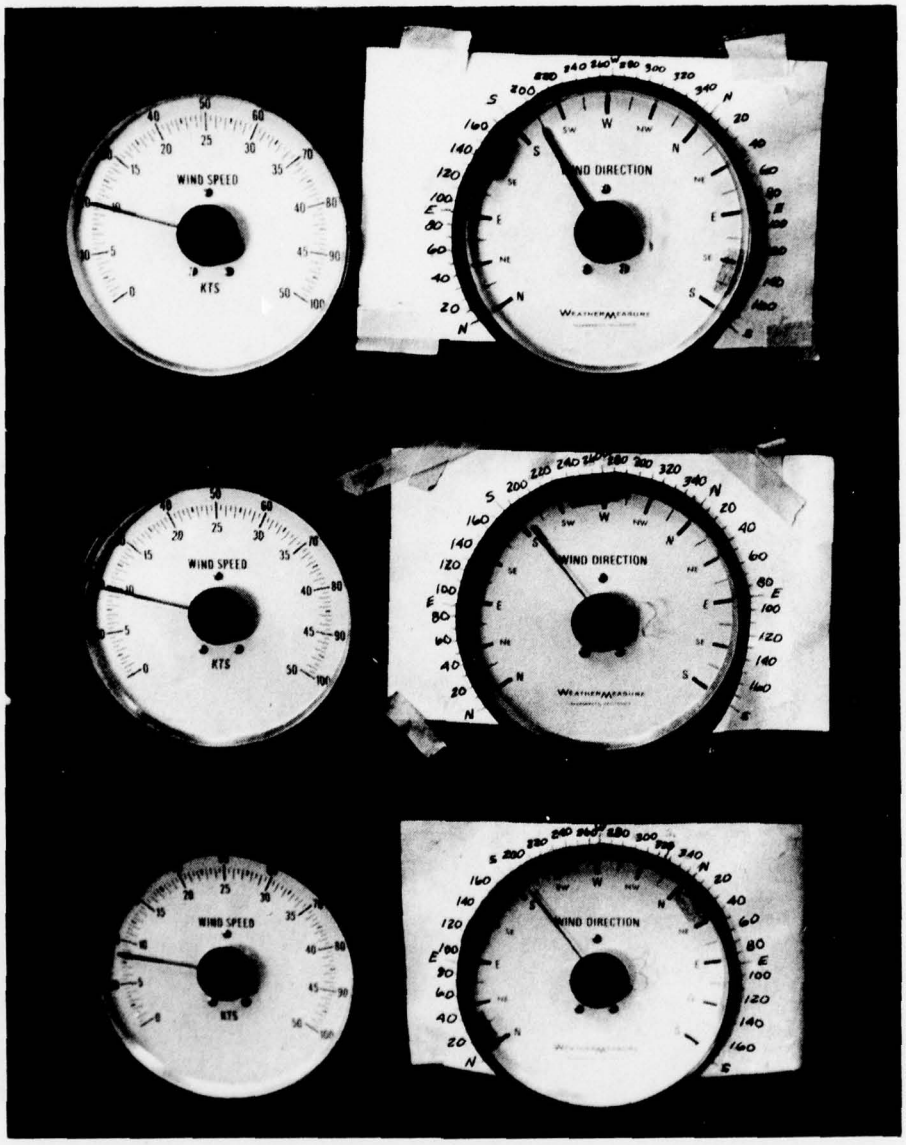

Photo 3. Selectable Wind-Data Displays in the On-Site Computer Van.

APPENDIX D. HELICOPTER LIFT MARGIN SYSTEM DESCRIPTION AND OPERATION

GENERAL

1. The HLMS presents the pilot a digital display of the potential extra lift (lift margin) available for a hover or vertical climb. Additional descriptions of the Type 5606 system are given in reference 10 and 11.

2. Lift margin is determined as the excess of maximum available lift (MAL) over the effective gross weight (EGW). These two quantities are derived from (1) the stored value of maximum available torque at standard conditions (Q_{ms}), and (2) the updated (corrected for fuel depletion) value of the stored gross weight at hover (EGW). In order that Q_{ms} and EGW be determined correctly from maximum power available (topping) and hover power required, the relation between Q_{ms} and maximum available torque (Q_{ma}) is stored analytically, and the relationship between lift, power and air density is likewise stored. The governing analytic expressions are given later in this appendix.

COMPUTER AND DISPLAY UNIT (TYPE 5606)

3. The C&D unit performs all computations and has the capability of presenting lift margin, Q_{ms}, or EGW as a four-digit display. Their ranges and resolution are as follows:

Lift margin: -980 to 9980 pounds (20-pound increments)
Q_{ms}: 39.9 to 65.5 psi (0.1 psi increments)
EGW: 4900 to 9980 pounds (20-pound increments)

In its enter-data mode, both Q_{ms} (at topping) and EGW (at weighing) can be entered into the appropriate memory. The memory is intended to retain these values even with power off. Display of Q_{ms} affords a means of monitoring the long-term degradation of the engine; display of EGW monitors both the long-term degradation of the lifting surfaces of the aircraft, and the changes in weight occasioned by fuel consumption. Controls on the front panel of the C&D unit permit both the introduction of ground effect into the calculation of lift margin (IGE mode) and the prediction of lift margin at a contemplated destination. The "destination" mode thumbwheel inputs are limited to ±49°C OAT, and sea level to 9900 feet pressure altitude. The destination altitude limitation occurs because of modeling accuracy in conversion of the altitude input to an equivalent pressure ratio; the error becomes significant at higher altitudes.

4. For the determination and display of lift margin to be available continuously and automatically, the necessary input parameters of torquemeter differential pressure, Q_E, static pressure, P, and engine compressor air inlet temperature, CIT,

are sensed by transducers. These inputs are delivered to the C&D unit mounted in the center instrument console for presentation of the data. The zero and the scale factor of the torque channel are adjustable from the front panel of the C&D unit.

SIMULATOR AND MONITOR UNIT (Type 5607)

5. For engineering personnel to monitor the operation of the C&D unit and to provide signals to adjust the C&D unit, an S&M unit was furnished for the flight tests. The following parameters can be selected for digital display on the S&M unit:

CIT	°C
Q_{ma}/Q_{ms}	Torque ratio
σ calculated	Density ratio
EGW	Pounds
MAL	Pounds
W_f	(fuel flow, lb/hr)
Q_n	(measured engine torque in "normal" mode or test torque in "test" mode, psi)
LM	Pounds
P	Inches of mercury
Q_T	(test torque, 50 or 65.5 psi)
Q_{ms} or Q_{ma}	psi

6. In addition, Q_E input and Q_{ms} and EGW memory output on the C&D unit can be arbitrarily adjusted by means of S&M controls. The following four adjustable analog parameters were recorded on the PCM flight recorder via the S&M unit: calculated ambient air density ratio (σ), EGW, CIT numerator, and CIT denominator. The quotient of the CIT numerator and denominator outputs equals engine CIT plus 50, and this output was the only measure of CIT available to record on the PCM system.

Helicopter Lift Margin System Computation

7. Two basic performance relations are required for the HLMS function:

a. Power required: relation of engine torque to helicopter lift (variable with air density and rotor speed).

b. Power available: relation of atainable engine torque to ambient conditions (pressure ratio and inlet temperature).

Lift is assumed related to engine torque (Q_E), engine speed (N_2), and density ratio (σ) by the following linear expression (power required):

$$\text{Lift (lb)} = K_1 N_2 Q_E + K_2 \sigma \qquad (1)$$

Where K_1 and K_2 are constants determined by the particular helicopter and engine. In the HLMS mechanization N_2 is not an input variable, but a constant taken at the nominal standard rotor speed of 324 rpm (an N_2 of 6600 rpm is approximately equivalent to 324 rpm). The density ratio is indirectly computed from the maximum available torque equation given later in this appendix.

8. The basic lift relation of equation 1 is used for two functions in the lift margin computation: Maximum available lift (MAL), and equivalent gross weight (EGW). The difference between the two is the lift margin in pounds. For EGW, the torque in equation 1 is that measured in flight at the time of weighing. This lift is stored as EGW and is compensated for weight loss due to fuel consumption by the following integrating function.

$$\int \left(K_1 N_2 Q_E + K_2 \frac{P}{P_o}\right) dt = \text{weight of fuel used} \qquad (2)$$

K_1 and K_2 are specific constants for the helicopter and engine, Q_E is the continuously measured torque, and P/P_o is the measured static pressure ratio. Since N_2 is fixed, off-rpm conditions will introduce errors. The integrating function only operates above a minimum sensed torque.

9. For MAL, the torque in equation 1 is the predicted maximum available torque (Q_{ma}) at existing pressure and temperature. Q_{ma} is continuously generated by the second basic linear HLMS function (power available):

$$\frac{Q_{ma}}{Q_{ms}} = \left(K_1 + K_2 \frac{P}{P_o}\right) (K_3 + K_4 \text{ CIT}) \qquad (3)$$

10. The constants are specific for the aircraft, CIT is the measured compressor inlet temperature, and Q_{ms} is a stored maximum standard reference torque, i.e.,

the maximum available torque at standard sea-level conditions. Q_{ms} should remain essentially constant, decreasing with engine performance degradation over a long period of time.

11. The ratio given by equation 3 influences several variables in the lift margin equations. The ratio of Q_{ma} to Q_{ms} in equation 3 at topping power defines Q_{ms}, since Q_{ma} at topping is the measured engine torque. This value of Q_{ms} must be stored in the HLMS for proper operation in other modes.

12. Except at topping, the Q_{ma}/Q_{ms} ratio is continuously changing with the measured values of P/P_O and CIT. In calculating MAL with equation 1, the torque used is Q_{ma}, generated as the product of the stored Q_{ms} and the instantaneous Q_{ma}/Q_{ms} ratio.

13. In addition to the above functions, the Q_{ma}/Q_{ms} ratio is used to produce the density ratio needed in equation 1 for MAL and EGW. The form of this approximation is:

$$\sigma_c = K_1 \left(K_2 \frac{Q_{ma}}{Q_{ms}} + K_3 \frac{P}{P_o}\right) \tag{4}$$

14. P/P_O is continuously measured, and the constants in equation 4 depend on the aircraft. Temperature effects are included in the Q_{ma}/Q_{ms} ratio, where CIT is a factor in equation 3. The assumption is made that static temperature (OAT) is always 2°C lower than the measured CIT; OAT as such is not input separately into the HLMS.

15. Using the Trans-Sonics, Inc., subscript notation for the actual constants of the preceding expressions, the design equations for the HLMS follow (P/P_O, Q_E, and CIT are continuously measured, and Q_{ms} is stored at topping from equation 5).

$$\frac{Q_{ma}}{Q_{ms}} = \left(K_{51} + K_{52} \frac{P}{P_o}\right) \left(K_{1i} + K_2 \text{ CIT}\right) \tag{5}$$

$$\sigma_c = K_{11} \left(\frac{Q_{ma}}{Q_{ms}}\right) + K_{12} \frac{P}{P_o} \tag{6}$$

$$\text{MAL} = K_7 K_6 N_2 (Q_{ms}) \left(\frac{Q_{ma}}{Q_{ms}}\right) + K_8 \sigma_c \text{ ~lb} \tag{7}$$

$$\text{Fuel used} = \int \left(K_{91} N_2 K_6 Q_E + K_{92} \frac{P}{P_o}\right) (F(Q_E)) \, dt \text{ ~lb} \tag{8}$$

$$F_{(Q_E)} = \text{zero if } Q_E \text{ is below } 4.65 \pm .35 \text{ psi},$$
$$F_{(Q_E)} = 1 \text{ otherwise} \tag{9}$$

$$EGW = K_7 K_6 N_2 Q_{E_W} + K_8 \sigma_{c_w} - \text{Fuel used} \sim \text{lb} \tag{10}$$

$$LM = MAL - EGW \sim \text{lb} \tag{11}$$

16. The subscript W in equation 10 refers to the parameter values at the time of weighing. Values of the constants and their units are listed below:

CONSTANT	VALUE	UNITS
K_{1i}	1.1649	—
K_2	-0.0097	1/°C
K_{51}	-0.0480	—
K_{52}	1.0480	—
K_6	.00352	shp/rpm-psi
K_7	6.4144	lb/shp
K_8	2023.9	lb
K_{91}	0.43	lb/shp-hr
K_{92}	230	lb/hr
K_{11}	0.400	—
K_{12}	0.600	—
N_2	6600	engine rpm

APPENDIX E. DATA ANALYSIS METHODS

Index

PERFORMANCE EQUATIONS

1. The equations used in deriving performance parameters from the measured quantities are given below.

2. Engine output power is found from measured output shaft speed and torque:

$$shp = \frac{2\pi \times Q_E \times N_2}{33{,}000} = (1.904 \times 10^{-4}) \times Q_E \times N_2 \qquad (1)$$

Where:

Q_E = output shaft torque (ft-lb)

N_2 = output shaft speed (rpm)

3. Differential hydraulic pressure as measured in psi defines the output shaft torque (ft-lb) by means of a torque constant calibrated for the specific engine:

$$Q_E = K_Q \times \Delta P, \text{ ft-lb} \qquad (2)$$

Where:

ΔP = differential hydraulic pressure (psi)

K_Q = torque constant (ft-lb/psi)

For the engine used in the flight tests, K_Q = 18.8 ft-lb/psi.

4. Output shaft speed was calculated from the known main rotor speed and the gearing ratio:

$$N_2 = 20.3704 \times \text{rotor speed (rpm)} \quad (3)$$

Where:

324 rpm rotor speed = 6603 engine rpm (N_2)

5. Nondimensional performance parameters for power, thrust (weight), and airspeed were found using:

$$\text{Power coefficient: } C_P = \frac{550 \text{ shp}}{\rho A(\Omega R)^3} \quad (4)$$

$$\text{Thrust coefficient: } C_T = \frac{\text{Thrust}}{\rho A(\Omega R)^2} \quad (5)$$

$$\text{Advance ratio: } \mu = \frac{1.6878 V_T}{\Omega R} \quad (6)$$

Where:

ρ = Ambient air density (slug/ft^3)

A = Rotor disc area (1520.53 ft^2)

Ω = Rotor rotational speed (rad/sec) (Ω = .10472 x rpm)

R = Rotor radius (22.0 ft)

V_T = True airspeed (kt)

HUMIDITY EFFECTS ON AIR DENSITY

6. The effects of humidity on air density were calculated from the relationships given in reference 12, appendix A. The exponential element in the equations, a, must be calculated for both OAT and dew point temperature (TDP):

$$a_{TDP} = \frac{-7246.6}{TDP} + 73.036 + .0057449(TDP) - 9.2470 ln(TDP) \quad (7)$$

$$\alpha_{OAT} = \frac{-7246.6}{OAT} + 73.036 + .0057449(OAT) - 8.2470 ln(OAT) \quad (8)$$

Where:

TDP and OAT are in °K

From these quantities, relative humidity is given by:

$$\text{Relative humidity} = \frac{e^{\alpha_{TDP}}}{e^{\alpha_{OAT}}} \times 100 \quad (9)$$

Density ratio of humid air is obtained from:

$$\sigma_{WET} = 9.630191 \left(\frac{P - .011163\, e^{\alpha_{TDP}}}{OAT}\right) \quad (10)$$

Where:

P = ambient pressure in inches of mercury

OAT is in °K

CIT PROBE RECOVERY FACTOR

7. The commonly used form of ram-rise temperature correction is obtained by combining the following equations:

$$\frac{T_{total}}{T_{static}} = 1 + \frac{Mach^2}{5} \quad (11)$$

$$\text{Mach Number} = \frac{V_T}{38.967 \sqrt{T_{static}}} \quad (12)$$

8. A probe recovery factor (K) is applied to the measured total temperature to account for instrument inaccuracy, such that:

$$\frac{T_{measured}}{T_{static}} = 1 + K \frac{Mach^2}{5} \quad (13)$$

Combining the above yields:

$$T_{total} = T_{measured} + (1-K)\left(\frac{V_T^2}{7592.1}\right) \tag{14}$$

Where:

T is in °K

V_T is true airspeed (kt)

K is the probe recovery factor

9. For conditions at the compressor inlet probe location, the relation between V_T and gas producer speed shown in figure 1 was used.

Required Power

10. The procedure followed to find an analytic function describing hover performance in winds is given below.

11. Normally, C_P and C_T define hover performance for a given configuration. Since wind effects can be substantial, an airspeed term must also be considered in the analysis. Advance ratio (μ) was included as an independent variable, and calculated by substituting measured wind speed for the airspeed.

12. From momentum theory, induced power at hover (ref 13, app A) is given by:

$$shp = \frac{Thrust\sqrt{\frac{Thrust}{2\rho\pi R^2}}}{550} \tag{15}$$

13. If no losses are present, this represents the basic proportionality between thrust (weight) and power required to hover, and reduces to:

$$shp \sim \frac{Thrust^{3/2}}{\rho^{1/2}} \tag{16}$$

Nondimensionally:

$$C_P \sim C_T^{3/2} \tag{17}$$

14. Retaining this major term and grouping profile, parasite, tail rotor, and other power losses that vary with C_T into a higher order term, the relationship of C_P to C_T at a fixed advance ratio can be given as:

Figure 1. Nominal Variation of Airspeed at the Compressor Inlet Probe Location With Gas Producer (N_1) speed.

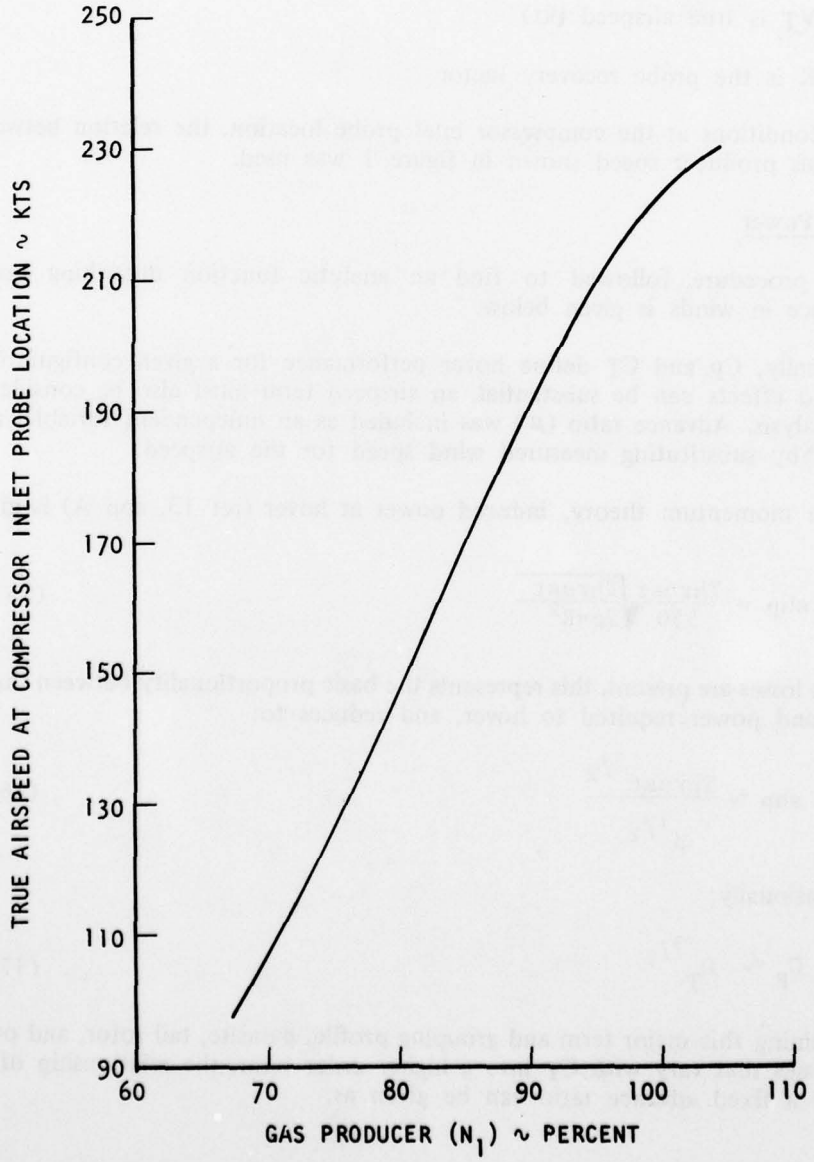

$$C_P = B_o + B_1 C_T^{3/2} + B_2 C_T^3 \qquad (18)$$

Where the B coefficients have values extracted from the flight data. Essentially, equation 18 is a second-order equation with C_P and $C_T 3/2$ as the variables. While the original derivation was for hover in still air ($\mu = 0$), it is assumed that the format using the same power terms of C_T remains valid as airspeed gradually increases.

15. By dividing the flight data into separate μ ranges and considering each range individually, a different set of coefficients for equation 18 is determined for increasing values of μ. By assuming a smoothly varying family of C_P versus C_T curves as μ changes, each coefficient of equation 18 can be expressed by a continuous function of μ.

16. Two techniques were combined to arrive at the final hover performance curves:

a. The first technique was iterative and used standard carpet and cross-plotting techniques. Initially, nominal values of μ from zero to .055 are taken in increments of .005, and all data falling within ±.005 of the nominal value are combined to fit a curve using equation 18. The smoothness of the resultant family is checked by carpet-plotting C_P against C_T and μ. A slope of C_P in μ, $\delta C_P/\delta\mu$, as a function of C_T is found from the smoothed family and applied to the original data sets to correct for variations in μ. In effect, the same nominal values of μ are again chosen, but now C_P is corrected in the data for individual variation in μ from the base value. This creates a new family which can again be carpet-plotted and smoothed. By carpet-plotting, any unusual curves of equation 18 resulting from gaps in the data are corrected to form a continuous family.

b. The second technique used all the data simultaneously, eliminating the need for overlapping ranges of μ and subsequent corrections of C_P to base μ values. By setting the coefficients of equation 18 as third-order functions of μ:

$$B_o = A_o + A_1\mu + A_2\mu^2 + A_3\mu^3$$

$$B_1 = A_4 + A_5\mu + A_6\mu^2 + A_7\mu^3 \qquad (19)$$

$$B_2 = A_8 + A_9\mu + A_{10}\mu^2 + A_{11}\mu^3$$

and substituting them into equation 18, a general equation results with twelve terms and six cross-products in powers of μ and C_T. Any standard regression analysis program can be used to find the A coefficients of this resulting equation. Difficulties arise from uneven distribution of data in μ and C_T. Because certain ranges of μ and C_T may not have enough data to adequately define the corresponding C_P values, the B coefficients in equation 19 can show extreme variation with μ. Constraints must be put on some of the terms in equation 19 to obtain a smooth family of curves from equation 18.

17. The final OGE hover data are shown in figures 2 through 13, appendix F. The individual curves for each μ are from the family shown in figure 1 and conform to the format given by combining equations 18 and 19. The IGE data are presented in figures 19 through 26, and summarized in figure 18.

18. For convenience in manipulating the nondimensional parameters, they were redefined by increasing their orders of magnitude as follows:

$C_P5 = C_P \times 10^5$ (e.g. $C_P = .0004$, $C_P5 = 40.$)

$C_T4 = C_T \times 10^4$ (e.g. $C_T = .0056$, $C_T4 = 56.$)

$MU3 = \mu \times 10^3$ (e.g. $\mu = .0250$, $MU3 = 25.$)

With these quantities, equation 18 can be rewritten as:

$$C_P5 = B_o + B_1 C_T4^{3/2} + B_2 C_T4^3 \qquad (20)$$

Values of these coefficients at $\mu = 0$ are:

$B_o = 7.4459$

$B_1 = 9.2701 \times 10^{-2}$

$B_2 = 4.8184 \times 10^{-5}$

Variations of these B coefficients as μ changes are shown in figure 2. Rewriting equation 19 to use MU3 gives:

$$B_o = A_o + A_1 MU3 + A_2 MU3^2 + A_3 MU3^3$$

$$B_1 = A_4 + A_5 MU3 + A_6 MU3^2 + A_7 MU3^3 \qquad (21)$$

$$B_2 = A_8 + A_9 MU3 + A_{10} MU3^2 + A_{11} MU3^3$$

The A coefficients of equation 21 are:

$A_o = 7.4459$ $\qquad A_4 = 9.2701 \times 10^{-2}$ $\qquad A_8 = 4.8184 \times 10^{-5}$

$A_1 = -1.2095 \times 10^{-2}$ $\qquad A_5 = -1.7486 \times 10^{-4}$ $\qquad A_9 = 1.1140 \times 10^{-7}$

$A_2 = -5.8732 \times 10^{-4}$ $\qquad A_6 = -1.9705 \times 10^{-5}$ $\qquad A_{10} = 1.4080 \times 10^{-8}$

$A_3 = 4.1449 \times 10^{-6}$ $\qquad A_7 = 1.7963 \times 10^{-7}$ $\qquad A_{11} = -1.2671 \times 10^{-10}$

Figure 2. Coefficients for Non-Dimensional OGE Performance

COEFFICIENTS APPEAR IN THE EQUATION:

$$C_p \times 10^5 = B_0 + B_1(C_T \times 10^4)^{3/2} + B_2(C_T \times 10^4)^3$$

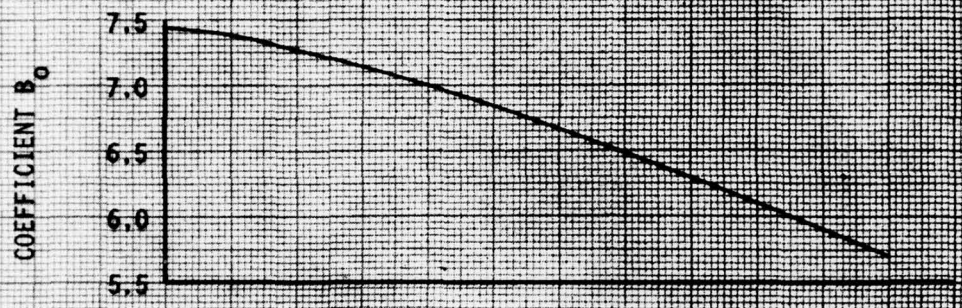

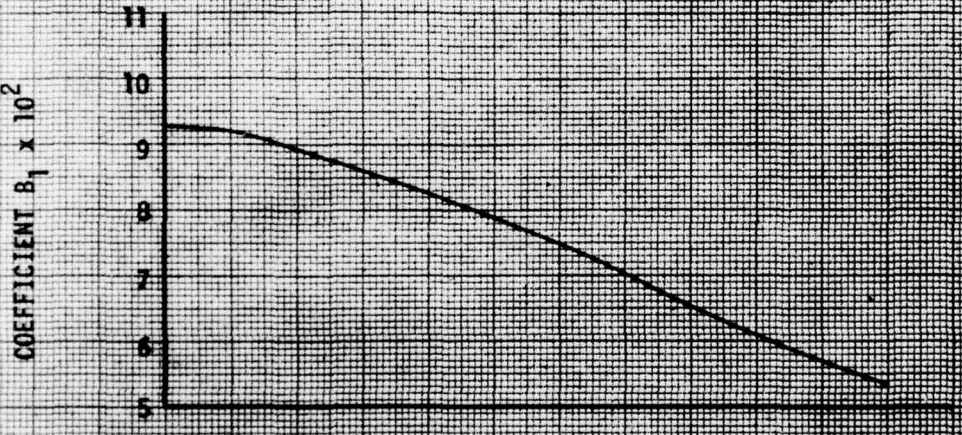

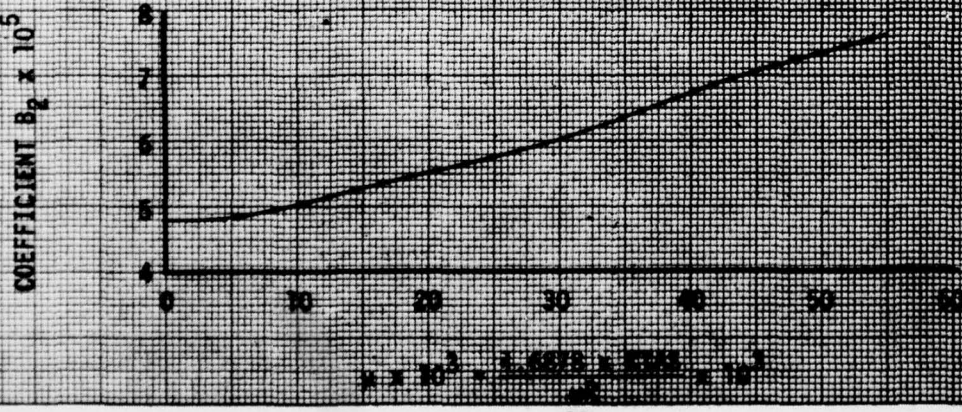

For IGE conditions at a 2-foot skid height, values of the B coefficients for use in equation 18 are shown in figure 3.

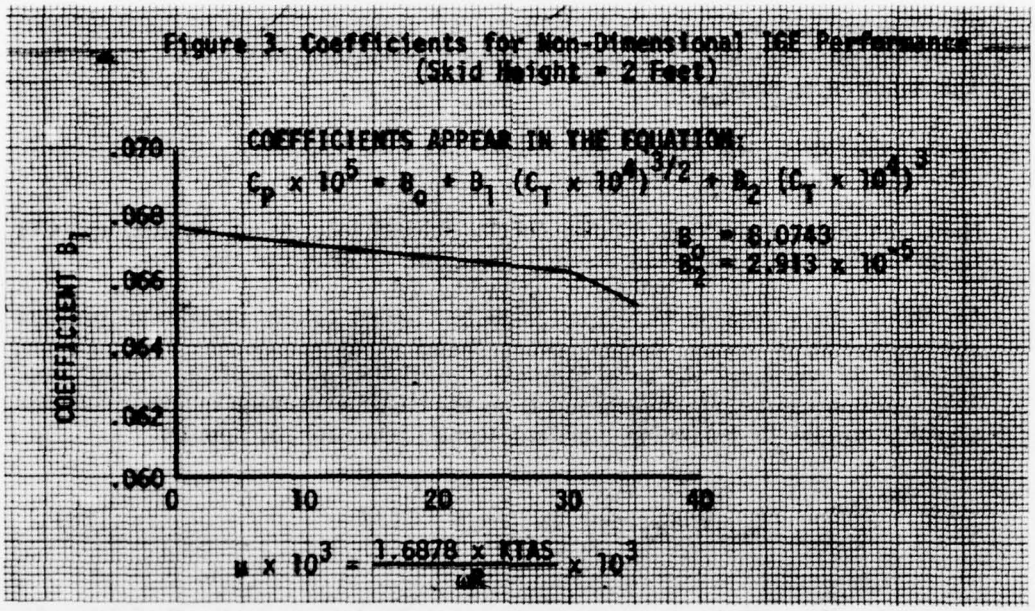

Figure 3. Coefficients for Non-Dimensional IGE Performance (Skid Height = 2 Feet)

Power Available

19. Two techniques, a statistical fit and the referred power method, were used to establish available engine power output as a function of flight condition from topping maneuver data, and are described below.

Statistical Fit:

20. One method applied to a multiple linear regression routine to the flight data to determine coefficients for a best-fit as a function of altitude and temperature. The function is given by:

$$\text{Max available shp} = A_o + A_1\ P/P_o + A_2\ CIT + A_3\ P/P_o\ CIT \qquad (22)$$

Here, the ambient pressure ratio is directly related to pressure altitude, and CIT to ambient conditions by an assumed constant temperature rise.

21. While the regression technique could be applied to any function of pressure and temperature using higher order terms and additional cross-products, equation 22 represents the same format as the HLMS power-available computation. This function can be directly derived from the HLMS expression relating maximum available torque to maximum standard torque (equation 5, app D):

$$\frac{Q_{ma}}{Q_{ms}} = (K_{51} + K_{52}\frac{P}{P_o})\ (K_{1i} + K_2\ CIT) \qquad (23)$$

Where the K coefficients are constants as defined in appendix C. Solving for maximum available torque and multiplying the right-hand factors in equation 23 together, we get:

$$Q_{ma} = Q_{ms}\ (K_{51}\ K_{1i} + K_{1i}\ K_{52}\frac{P}{P_o} + K_{51}\ K_2\ CIT + K_2\ K_{52}\frac{P}{P_o}\ CIT) \qquad (24)$$

By definition, at topping power the measured torque is Q_{ma}, The maximum available. Maximum available shp is then directly obtained from the torque proportionally at a known rotor speed (equations 1, 2, and 3). Since Q_{ms} is defined by the engine, its value presumably remains constant throughout the topping data. Using the torque proportionality, setting Q_{ms} constant, and consolidating these quantities with the K coefficients into new constants, equation 23 becomes identical to equation 22, the function used in the statistical fit.

22. The coefficients resulting from fitting the topping maneuver data to the format of equation 22 are given in table 1; statistical fits using both measured CIT and measured OAT + 2 as the temperature term were made. The corresponding power-available plots are shown in figures 42 and 43, appendix F, respectively. For comparison, the values of the equivalent HLMS model coefficients, appropriately multiplied to fit the format of equation 22, are also presented in table 1.

Table 1. Comparison of Power-Available Function Coefficients (equation 22).

Coefficients:	Statistical Fit, with temperature term used:		HLMS Model with Q_{ms} = 58.1 psi
	CIT	OAT + 2	
A_o	-331.4380	-78.89640	-3.24867 = $(Q_{ms}K_{51}K_{1i})$
A_1	31.17690	9.26237	70.92936 = $(Q_{ms}K_{1i}K_{52})$
A_2	18.85059	15.95741	0.02705 = $(Q_{ms}K_{51}K_2)$
A_3	-.48489	-.23541	-.59062 = $(Q_{ms}K_2K_{52})$

23. The families of curves produced by fitting the data to this function do not accurately represent actual power-available characteristics beyond the altitude and temperature range of the flight data. This is evident from the singularity in figure 42, appendix F. To avoid this type of convergence at a point, a modification of the above method is also described which deletes the P/P_o x CIT cross-product term.

24. Although elimination of the cross-product term separates the effects of altitude and temperature, in reality, they are not independent. This difficulty is overcome by using referred shp as the measure of available power, which depends on both pressure and temperature. Using pressure altitude directly, the defining function becomes:

$$\text{Max available shp}_{ref} = A_o + A_1 \text{ CIT} + A_2 H_P \qquad (25)$$

Where:

Hp = Pressure altitude (ft)

Shaft horsepower is usually referred to sea-level standard conditions (subscript o) from compressor inlet conditions (subscript ci) by the equation:

$$shp_{ref} = \frac{shp}{\frac{P_{ci}}{P_o}\sqrt{\frac{T_{ci}}{T_o}}} \qquad (26)$$

Where:

T_{ci} = measured compressor inlet total temperature, °K

T_o = 288.15°K, sea-level standard temperature

P_{ci}/P_o = ratio of total compressor inlet pressure to standard sea-level pressure

(The pressure ratio term is a function of measured ambient static pressure ratio and airspeed; at hover, P_{ci}/P_o = .992 P/P_o, and the value varies between .9895 and .9965 for airspeeds to 120 knots calibrated airspeed (KCAS). This ratio is based on the external inlet configuration of the UH-1B/540 (ref 7, app A), corrected for effects of particle separator and louvers from inlet data of the UH-1H as shown in figure 114 in reference 14.)

25. Generalized power available is then defined by finding the best-fit coefficients for equation 25 from the topping data. Using both measured CIT and OAT + 2 for the temperature term yields the following sets of coefficients in equation 25:

Using:	CIT	OAT + 2
A_o	1526.563	1525.957
A_1	-15.19031	-14.79035
A_2	2.0576×10^{-3}	3.1878×10^{-3}

26. By transforming shp_{ref} to shp, this function defines engine performance for any combination of pressure and temperature; the power-available curves generated by these coefficients are shown in figures 44 and 45, appendix F. The intent of using a referred parameter is to define a single-valued function of both pressure and temperature; *ie* the referred quantity does not vary with temperature when plotted against pressure and remains invariant with pressure when plotted against temperature. While equation 25 results in reasonable power-available engine characteristics, the referred power parameter it produces does not conform to the single-valued function characteristics just described. To overcome this difficulty, it is more appropriate to employ a separate referred power technique to define engine performance.

Referred Power Method:

27. This method refers both shp and gas producer speed (N_1) to sea-level conditions from compressor inlet conditions. The exponents of the pressure and temperature ratios are not fixed at any specific value, but left open to be determined by flight data. The applicable equations are:

$$shp_{ref} = \frac{shp}{\left(\frac{P_{ci}}{P_o}\right)^{pexp} \left(\frac{T_{ci}}{T_o}\right)^{texp}} \tag{27}$$

$$N_{1\ ref} = \frac{N_1}{\left(\frac{T_{ci}}{T_o}\right)^{texp}} \sim percent \tag{28}$$

Where:

pexp, texp = Exponents of the pressure and temperature ratios. Nominal values are usually given by 1.0 and 0.5, respectively.

T_{ci} = Measured compressor inlet total temperature (°K)

T_o = 288.15°K, sea-level standard temperature

N_1 = Measured gas producer speed (percent)

P_{ci}/P_o = Ratio of total compressor inlet pressure to standard ambient pressure.

28. Measured N_1 varied between 87.0 and 100.8 percent over the full range of recorded flight conditions and power-demanded data. When plotted against observed power, no flattening trend of shp at high or low values of the N_1 range is observed, and a straight line provides the best fit to the data. With this condition of a linear fit, the best values for the exponents of the pressure and temperature terms in the referred power and gas producer speed quantities can be determined.

29. These are found by varying texp and pexp, using them to calculate N_{1ref} and shp_{ref} for all the points, and then observing how the standard deviation of a linear fit to this referred data changes with the chosen values of pexp and texp. The pressure exponent, appearing only in shp_{ref}, was varied first to minimize any altitude influence on the fit to the referred quantities. Standard deviation was not greatly affected by variations from the nominal value of 1.0 for pexp, so the pressure exponent was fixed at one. Changing the temperature exponent in both shp_{ref} and $N_{1_{ref}}$ had a more significant effect, as shown in figure 4, minimizing the standard deviation for a value of texp at approximately 0.47.

Figure 4. Variation of Standard Deviation to a Linear Fit of N_{1ref} vs SHP_{ref} With Change in the Temperature Exponent Ratio

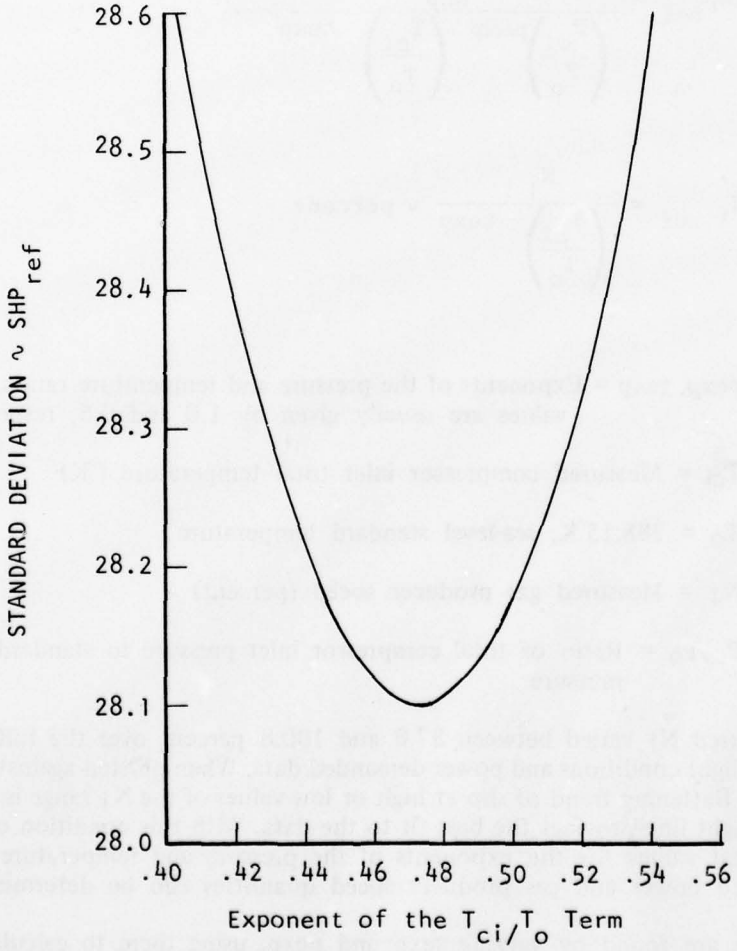

This fit is given by:

$$shp_{ref} = -6579.968 + 79.479\ N_{1_{ref}} \qquad (29)$$

Where referred N_1 and shp were calculated from equations 27 and 28 using:

pexp = 1.00

texp = 0.47

The resulting referred data are shown plotted in figures 48 through 51, appendix F.

30. Equation 29 provides the means to calculate power available for all conditions of temperature and altitude, when combined with the CIT versus N_1 characteristics of the engine. To get power available for the full range of temperatures beyond those recorded for the flight data toppings, the engine specification N_1 deviation from topping as a function of CIT was used, as shown in figure 52, appendix F. The base-line N_1 in this figure was defined at 99.5 percent by the test engine acceptance run. Since the CIT probe measurements obtained are not considered reliable, a constant temperature rise above OAT was taken as the best indication of the actual compressor inlet conditions for this analysis, and using the data of figure 54, the temperature rise chosen was 2.9°C. The flight data topping points are also shown on figure 52, with the CIT given by measured OAT + 2.9°C.

31. Power available was then derived by defining topping N_1 from figure 52, appendix F, for any OAT, referring this N_1 for the chosen OAT and Hp with equation 28, and obtaining the corresponding shp_{ref} from equation 29. Actual shp for the chosen ambient condition is then extracted from this by applying the temperature rise and compressor inlet pressure loss to equation 27, which results in:

$$shp = shp_{ref}\ .992\ \left(\frac{P}{P_o}\right)\ \left(\frac{OAT + 273.15 + 2.9}{288.15}\right)^{.47} \qquad (30)$$

The power-available matrix generated by equation 30 is shown in figure 46, appendix F.

32. Equation 30 also defines actual available lift for comparison with the HLMS-calculated MAL. The available shp is nondimensionalized to Cp by equation 4; this represents the required power for the available lift. Equation 18 can be solved for the available lift:

$$C_T^{3/2} = \frac{-B_1 + \sqrt{B_1^2 - 4\ (B_2)\ (B_o - C_P)}}{2B_2} \qquad (31)$$

Available lift is then immediately found from equation 31. Use of nondimensional coefficients allows incorporating effects of wind speed, density (pressure altitude, temperature, and humidity), and rotor speed.

HLMS EQUATION TRANSFORMATIONS

33. Equations used to calculate performance parameters from the HLMS output variables and to transform dimensional and nondimensional flight data results to comparable HLMS variables are given below.

34. Starting with the HLMS lift expression of equation 1, appendix D, and using the HLMS coefficient notation given in appendix D, we have

$$\text{Lift} = K_7 \, K_6 \, N_2 \, Q_E + K_8 \, \sigma_c \qquad (32)$$

Where:

Lift = gross weight in hover (lb)

N_2 = engine speed, fixed at 6600 rpm

Q_E = engine torque (psi)

σ_c = density ratio, calculated from measured pressure and temperature (equation 6, app C)

K_6, K_7, K_8 = HLMS coefficients

The above expression relates engine torque to lift at hover and equation 1 relates engine torque to shp; combining the two, we have:

$$\text{shp} = \frac{2\pi}{(60)\ (550)} \, \frac{K_Q}{K_6 \, K_7} \, (\text{Lift} - K_8 \, \sigma_c) \qquad (33)$$

Where:

K_Q = torque constant for the test aircraft (18.8 ft-lb/psi)

By using MAL and Q_{ma}, power available is calculated, and use of EGW and Q_E determines power required. This expression can be nondimensionalized by using equation 4 of this appendix to find the corresponding C_P:

$$C_P = \frac{2\pi}{60} \frac{K_Q}{K_6 K_7} \frac{(\text{Lift} - K_8 \sigma_c)}{\rho A (\Omega R)^3} \quad (34)$$

Where:

ρ = ambient air density, slug/ft^3

A = rotor disc area, 1520.53 ft^2

R = rotor radius, 22 ft

Ω = rotor rotational speed (rad/sec) (at 324 rpm, Ω = 33.9292 rad/sec)

Nondimensional HLMS thrust is found by simply using EGW as the thrust term in equation 5; because N_2 is fixed in the HLMS model, main rotor speed has to remain constant at 324 rpm.

35. The difference between actual gross weight and the HLMS EGW due to various factors can be found by applying the nondimensional and analytical power-required functions (equations 4, 5, and 18) to define the shp seen over a range of gross weights. The observed torque at each gross weight is then defined by:

$$Q_E = \frac{(60)\ (550)}{2} \frac{\text{shp}}{K_Q N_2} \quad (35)$$

This torque can be substituted into equation 32 to calculate the HLMS EGW and compared to actual gross weight at the condition evaluated. Use of the flight-determined Cp and C_T functions readily defines torque variations due to wind speed, density (pressure altitude, temperature, and humidity), and rotor speed.

36. While compressibility effects are a recognized factor in helicopter performance, rotor tip speed mach numbers tested were too low to influence the data. Existing tip mach number can be calculated using:

$$a = 65.7702 \sqrt{\text{OAT} + 273.15} \quad (36)$$

$$M_{tip} = \frac{\Omega R}{a} (1 + \mu) \quad (37)$$

Where:

a = speed of sound ~ ft/sec

OAT = outside air temperature ~ °C

Critical mach number is defined as the free stream speed at which the velocity at anv point along the surface of the airfoil reaches the local velocity of sound. For the NACA 0012 airfoil (the blade section of the test aircraft), reference 15, App A, shows a linear variation of critical mach number with lift coefficient, changing from M_{cr} = .725 at C_L = 0.0 to M_{cr} = .639 at C_L = .20. Tip lift coefficient is an empirical function of C_T, as given by reference 16:

$$C_L = \frac{2\ C_T}{\text{rotor solidity}} \qquad (38)$$

Where:

Rotor solidity = .0651 for the test aircraft

The lowest critical mach number over the range of test data was M_{cr} = 0.642. The drag divergence mach number where compressibility begins to affect power required measurably is somewhat higher than M_{cr}. For the test aircraft, drag divergence onset occurs at M_{tip} = 0.83, as reported in reference 17. Over the range of temperatures, airspeeds, and rotor speeds tested, the highest values of M_{tip} fell considerably below this value (M_{tip} = .69 at hover to M_{tip} = .73 at 30 KTAS).

APPENDIX F. TEST DATA

INDEX

FIGURE 1

NON-DIMENSIONAL OGE HOVERING PERFORMANCE SUMMARY

NUH-1H USA S/N 63-8684 T53-L-13B S/N LE 14420

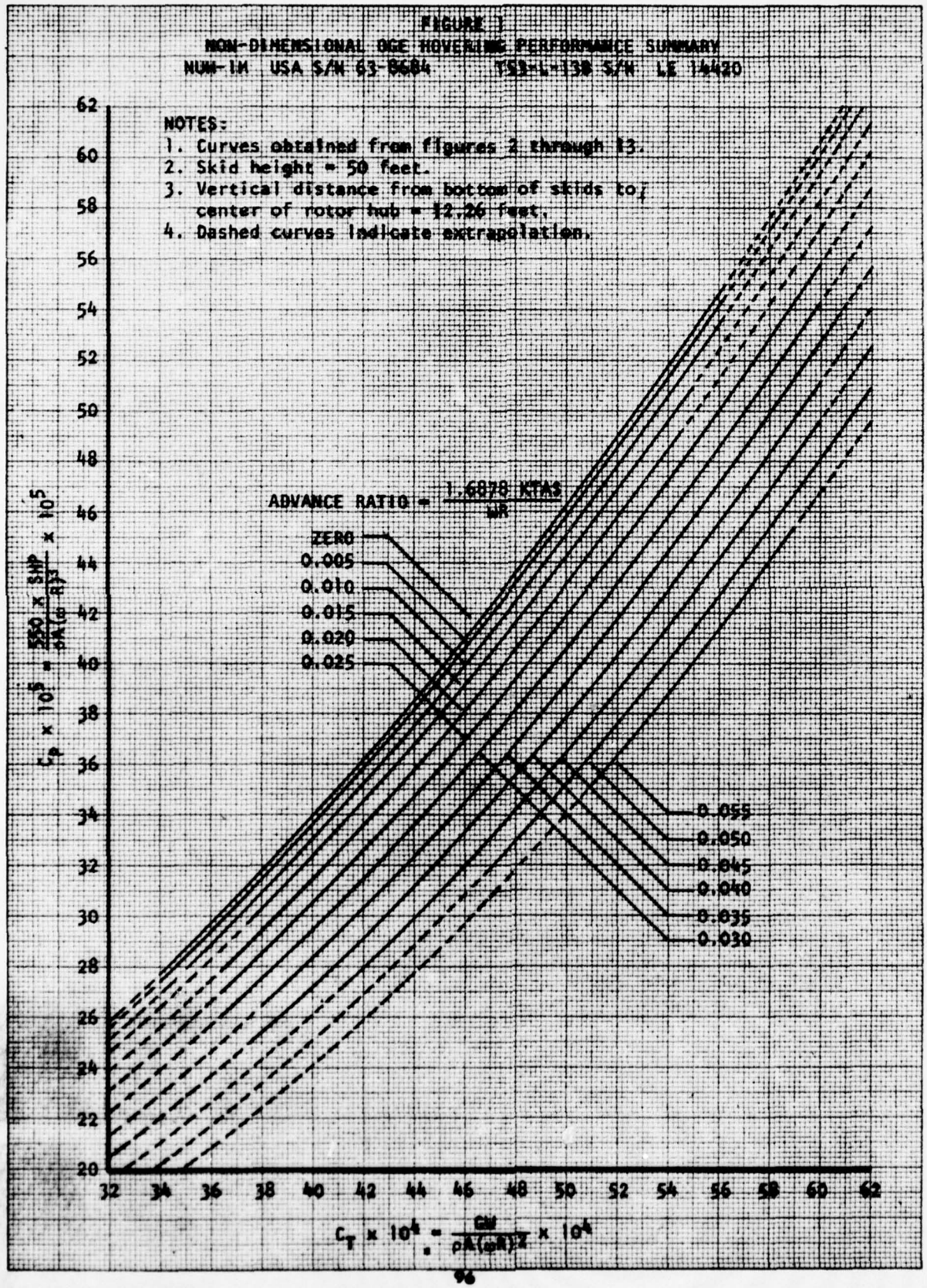

FIGURE 2
NON-DIMENSIONAL OGE HOVERING PERFORMANCE
NUH-1N USA S/N 63-8684 T53-L-13B S/N LE 14420
ADVANCE RATIO = ZERO

SYMBOL ROTOR SPEED 300	314	324	PRESSURE ALTITUDE RANGE ~FEET	TEMPERATURE RANGE ~DEG C
◐	◑	○	-200 to +50	+5 to 20
△	▲	▲	2200 to 2500	15 to 30
▣	▣	□	3900 to 4250	-5 to +20
◆	◆	◇	9300 to 9650	-5 to +10

NOTES:
1. See appendix E for curve function
2. Skid height = 50 feet
3. Vertical distance from bottom of skids to center of rotor = 12.26 feet
4. Dashed curves indicate extrapolation
5. Flagged symbols indicate free hover
6. Advance ratios obtained from measured wind speed

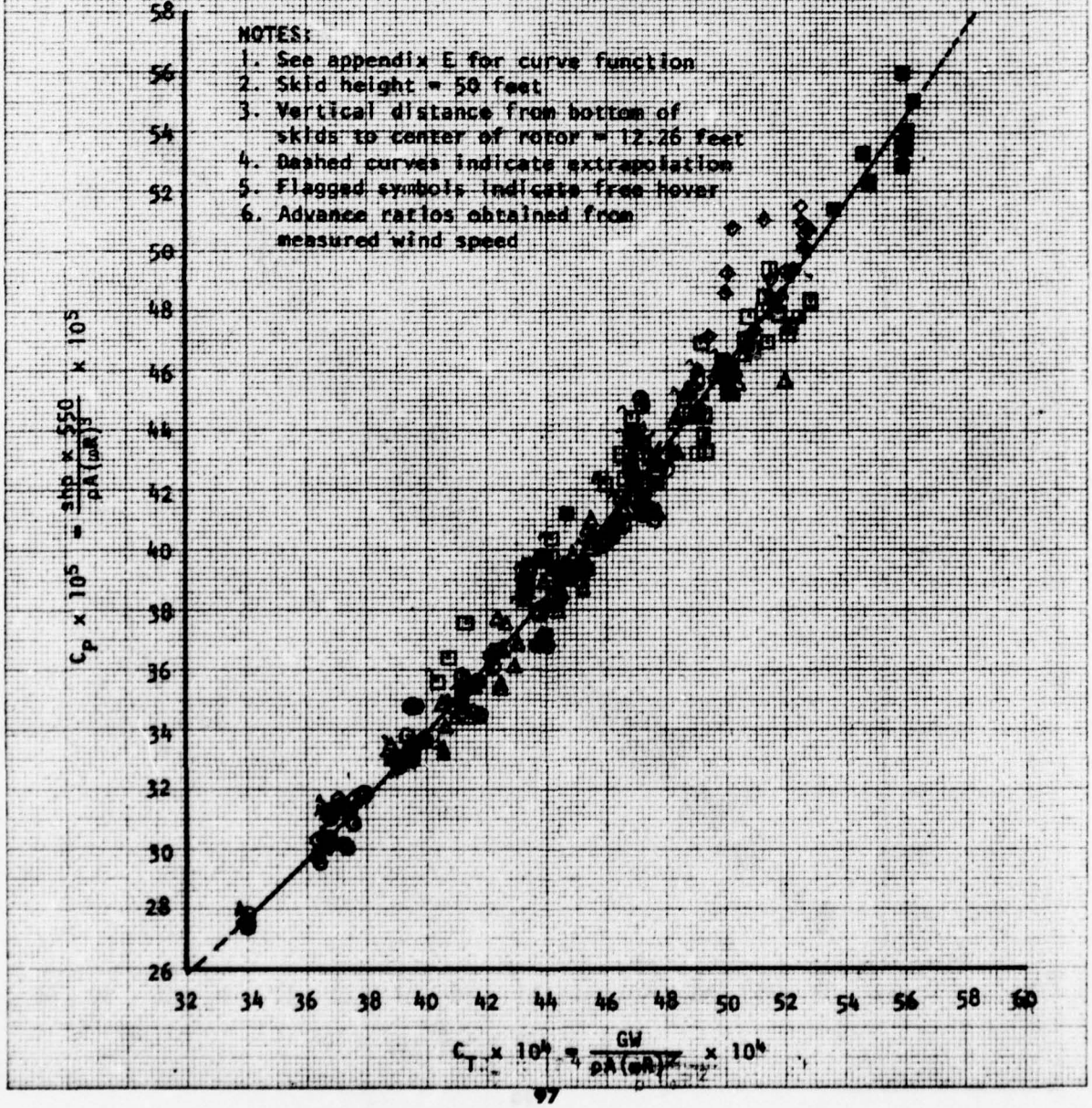

FIGURE 3
NON-DIMENSIONAL OGE HOVERING PERFORMANCE
NUH-1H USA S/N 63-8684 T53-L-13B S/N LE 14420
ADVANCE RATIO = 0.005

SYMBOL ROTOR SPEED 300	314	324	PRESSURE ALTITUDE RANGE ~FEET	TEMPERATURE RANGE ~DEG C
●	●	○	-200 to +50	+5 to 20
▲	▲	△	2200 to 2500	15 to 30
■	■	□	3900 to 4250	-5 to +20
◆	◆	◇	9300 to 9650	-5 to +10

NOTES:
1. See appendix E for curve function
2. Skid height = 50 feet
3. Vertical distance from bottom of skids to center of rotor = 12.26 feet
4. Dashed curves indicate extrapolation
5. Flagged symbols indicate free hover
6. Advance ratios obtained from measured wind speed

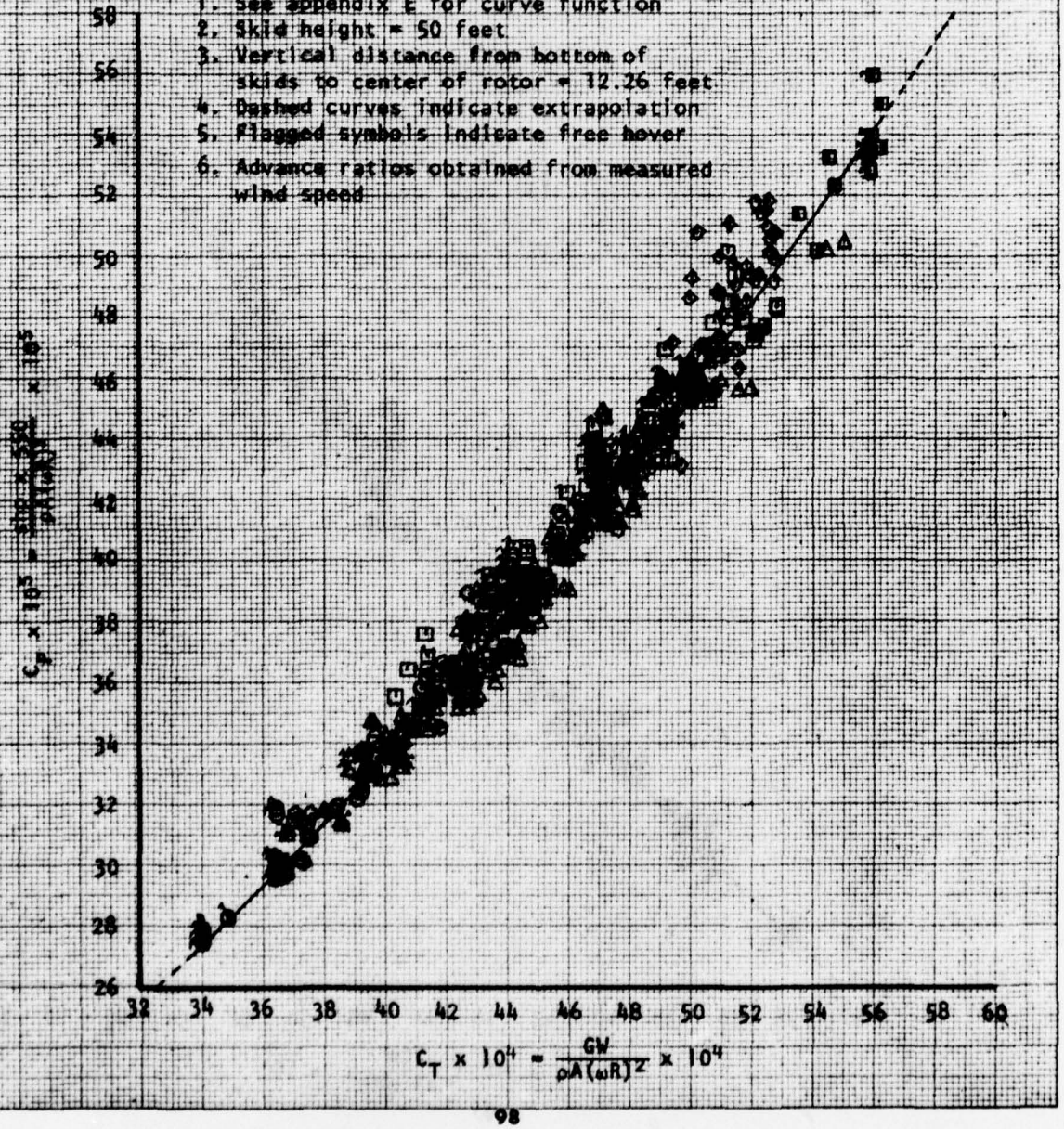

FIGURE 4
NON-DIMENSIONAL OGE HOVERING PERFORMANCE
NUH-1M USA S/N 63-8684 T53-L-13B S/N LE 14420
ADVANCE RATIO = 0.010

SYMBOL ROTOR SPEED 300	314	324	PRESSURE ALTITUDE RANGE ∿FEET	TEMPERATURE RANGE ∿DEG C
●	●	○	-200 to +50	+5 to 20
▲	▲	△	2200 to 2500	15 to 30
■	■	□	3900 to 4250	-5 to +20
◆	◆	◇	9300 to 9650	-5 to +10

NOTES:
1. See appendix E for curve function
2. Skid height = 50 feet
3. Vertical distance from bottom of skids to center of rotor = 12.26 feet
4. Dashed curves indicate extrapolation
5. Flagged symbols indicate free hover
6. Advance ratios obtained from measured wind speed

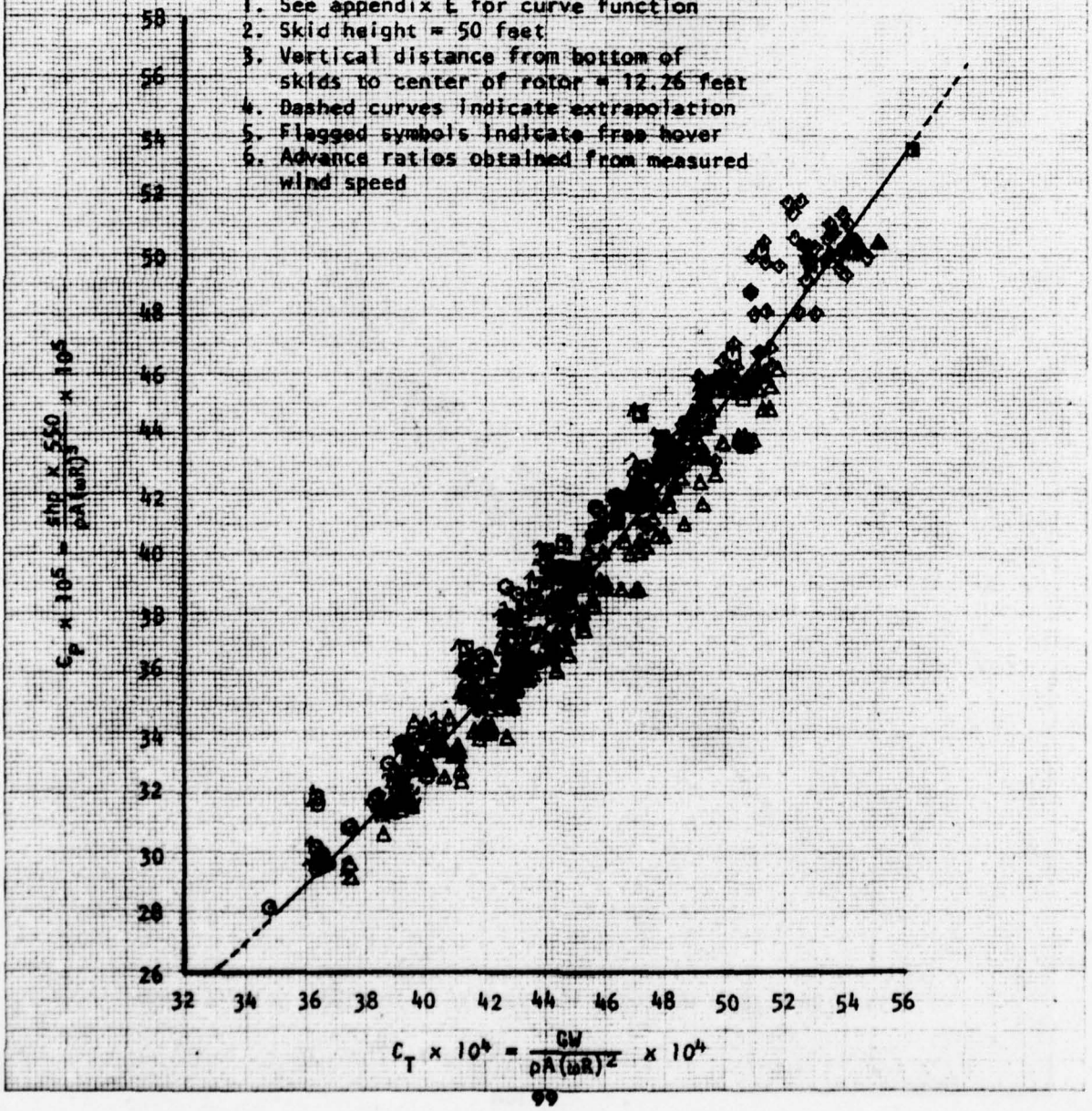

FIGURE 5

NON-DIMENSIONAL OGE HOVERING PERFORMANCE

NUH-1H USA S/N 63-8684 T53-L-13B S/N LE 14420

ADVANCE RATIO = 0.015

SYMBOL ROTOR SPEED 300	314	324	PRESSURE ALTITUDE RANGE ~FEET	TEMPERATURE RANGE ~DEG C
◐	◑	○	-200 to +50	+5 to 20
△	▲	△	2200 to 2500	15 to 30
◧	◨	□	3900 to 4250	-5 to +20
◆	◆	◇	9300 to 9650	-5 to +10

NOTES:

1. See appendix E for curve function
2. Skid height = 50 feet
3. Vertical distance from bottom of skids to center of rotor = 12.26 feet
4. Dashed curves indicate extrapolation
5. Flagged symbols indicate free hover
6. Advance ratios obtained from measured wind speed

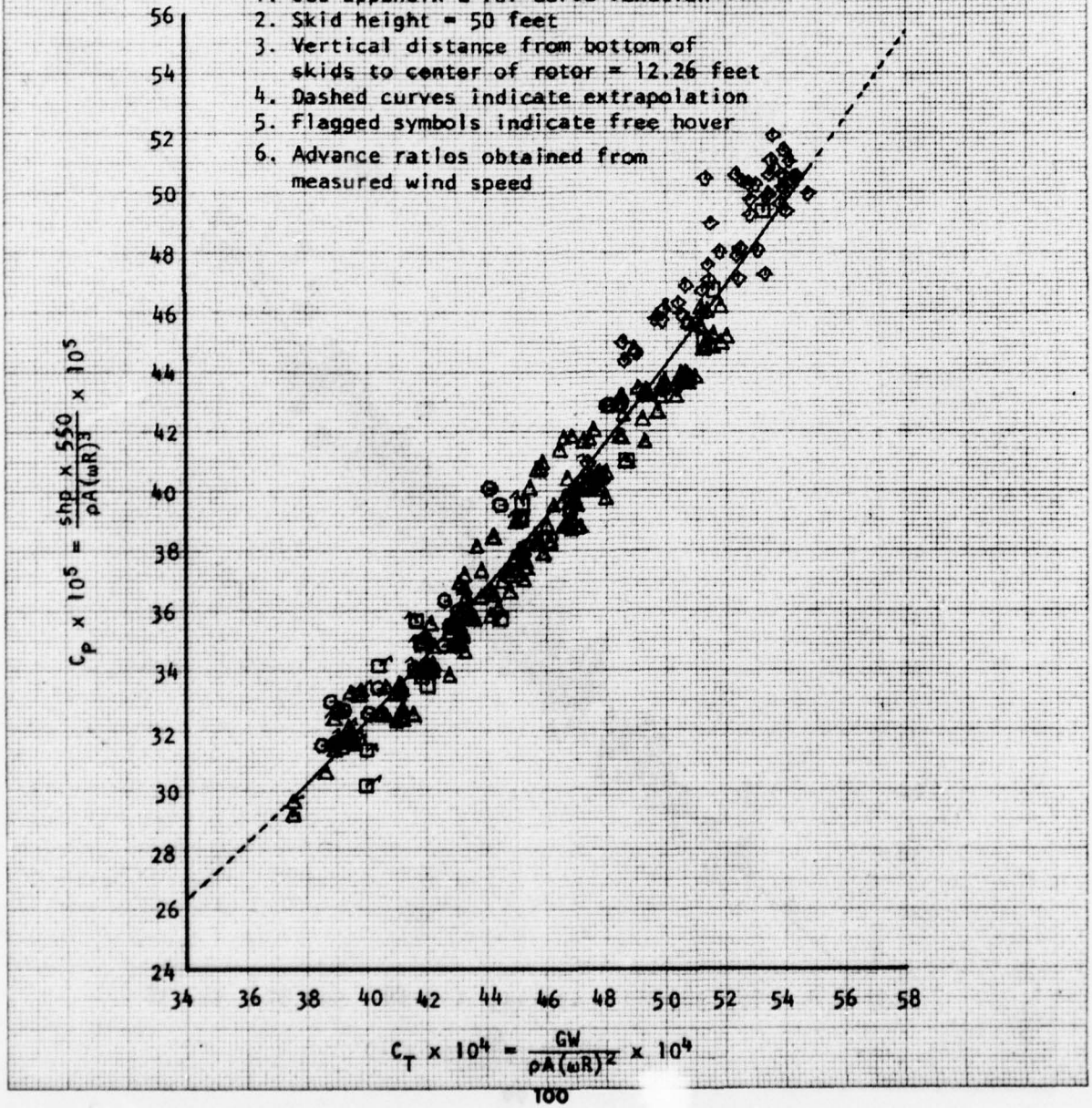

100

FIGURE 6
NON-DIMENSIONAL OGE HOVERING PERFORMANCE
NUH-1M USA S/N 63-8684 T53-L-13B S/N LE 14420
ADVANCE RATIO = 0.020

SYMBOL ROTOR SPEED 300	314	324	PRESSURE ALTITUDE RANGE ~FEET	TEMPERATURE RANGE ~DEG C
◐	●	○	-200 to +50	+5 to 20
▲	▲	△	2200 to 2500	15 to 30
■	■	□	3900 to 4250	-5 to +20
◆	◆	◇	9300 to 9650	-5 to +10

NOTES:
1. See appendix E for curve function
2. Skid height = 50 feet
3. Vertical distance from bottom of skids to center of rotor = 12.26 feet
4. Dashed curves indicate extrapolation
5. Flagged symbols indicate free hover
6. Advance ratios obtained from measured wind speed

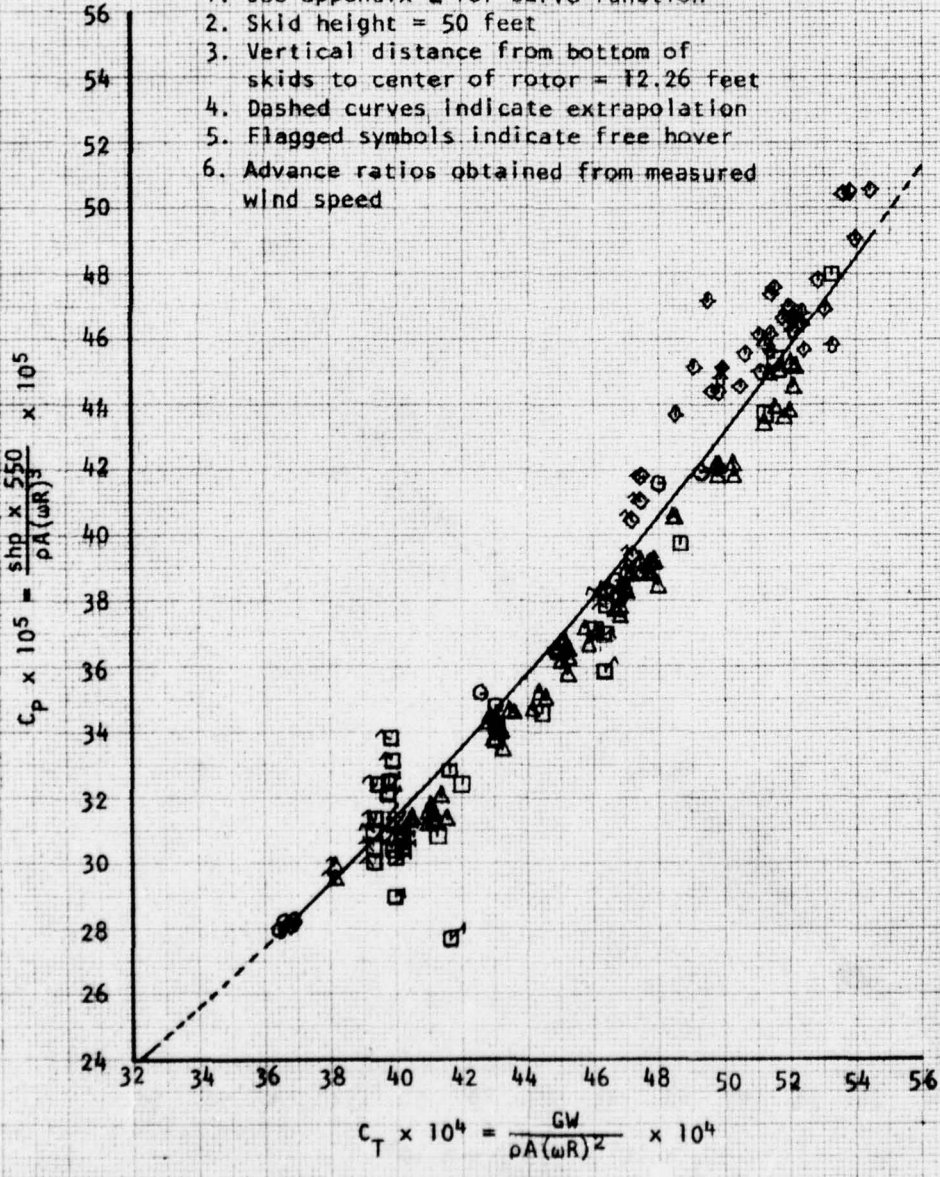

FIGURE 7

NON-DIMENSIONAL OGE HOVERING PERFORMANCE

NUH-1M USA S/N 63-8684 T53-L-13B S/N LE 14420

ADVANCE RATIO = 0.025

SYMBOL ROTOR SPEED 300	314	324	PRESSURE ALTITUDE RANGE ~FEET	TEMPERATURE RANGE ~DEG C
●	◐	○	-200 to +50	+5 to 20
▲	▲	△	2200 to 2500	15 to 30
■	■	□	3900 to 4250	-5 to +20
◆	◆	◇	9300 to 9650	-5 to +10

NOTES:

1. See appendix E for curve function
2. Skid height = 50 feet
3. Vertical distance from bottom of skids to center of rotor = 12.26 feet
4. Dashed curves indicate extrapolation
5. Flagged symbols indicate free hover
6. Advance ratios obtained from measured wind speed

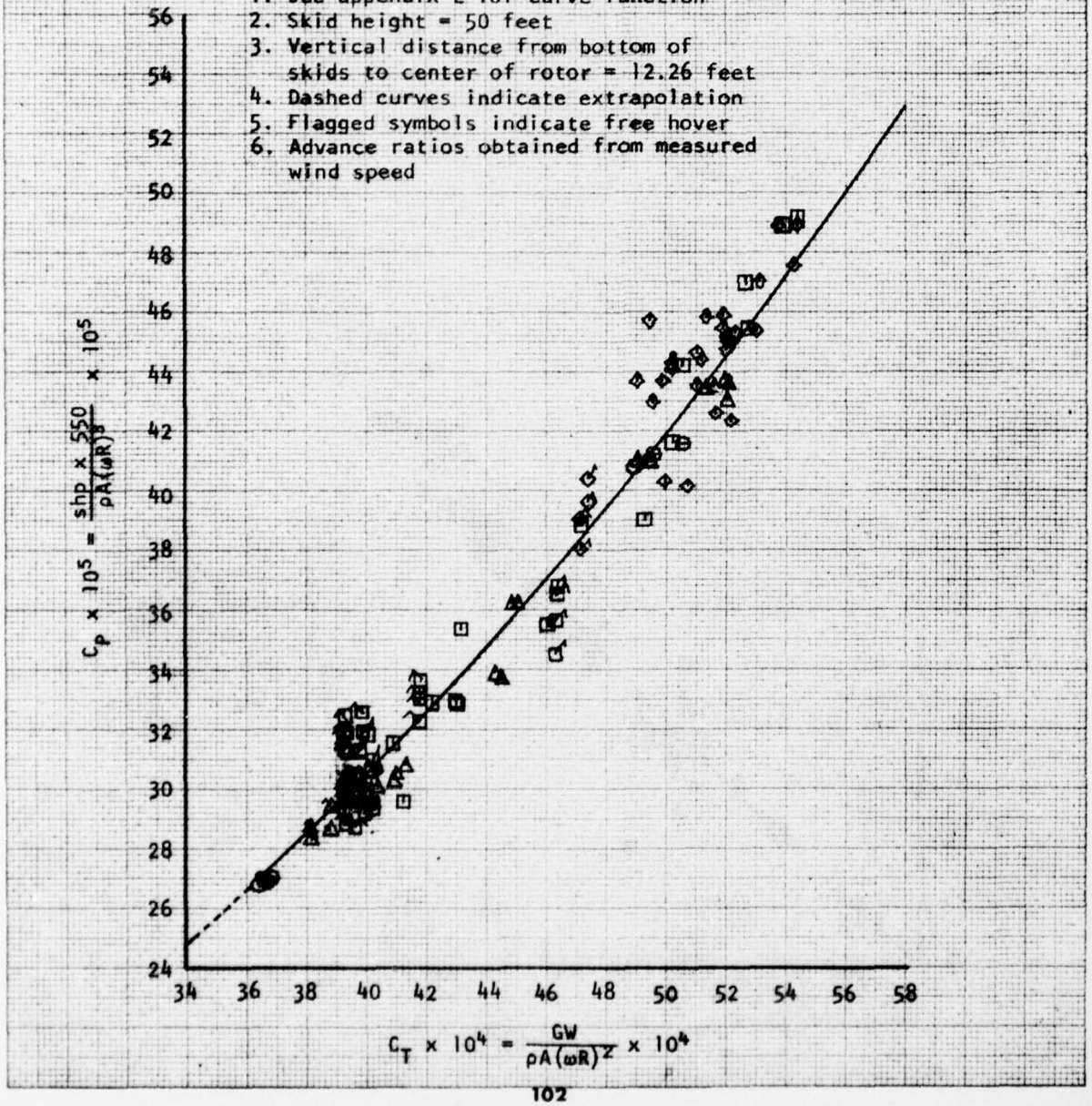

FIGURE 8
NON-DIMENSIONAL OGE HOVERING PERFORMANCE
NUH-1M USA S/N 63-8684 T53-L-13B S/N LE 14420
ADVANCE RATIO = 0.030

SYMBOL ROTOR SPEED 300	314	324	PRESSURE ALTITUDE RANGE ~FEET	TEMPERATURE RANGE ~DEG C
●	●	○	-200 to +50	+5 to 20
▲	▲	△	2200 to 2500	15 to 30
■	■	□	3900 to 4250	-5 to +20
◆	◆	◇	9300 to 9650	-5 to +10

NOTES:
1. See appendix E for curve function
2. Skid height = 50 feet
3. Vertical distance from bottom of skids to center of rotor = 12.26 feet
4. Dashed curves indicate extrapolation
5. Flagged symbols indicate free hover
6. Advance ratios obtained from measured wind speed

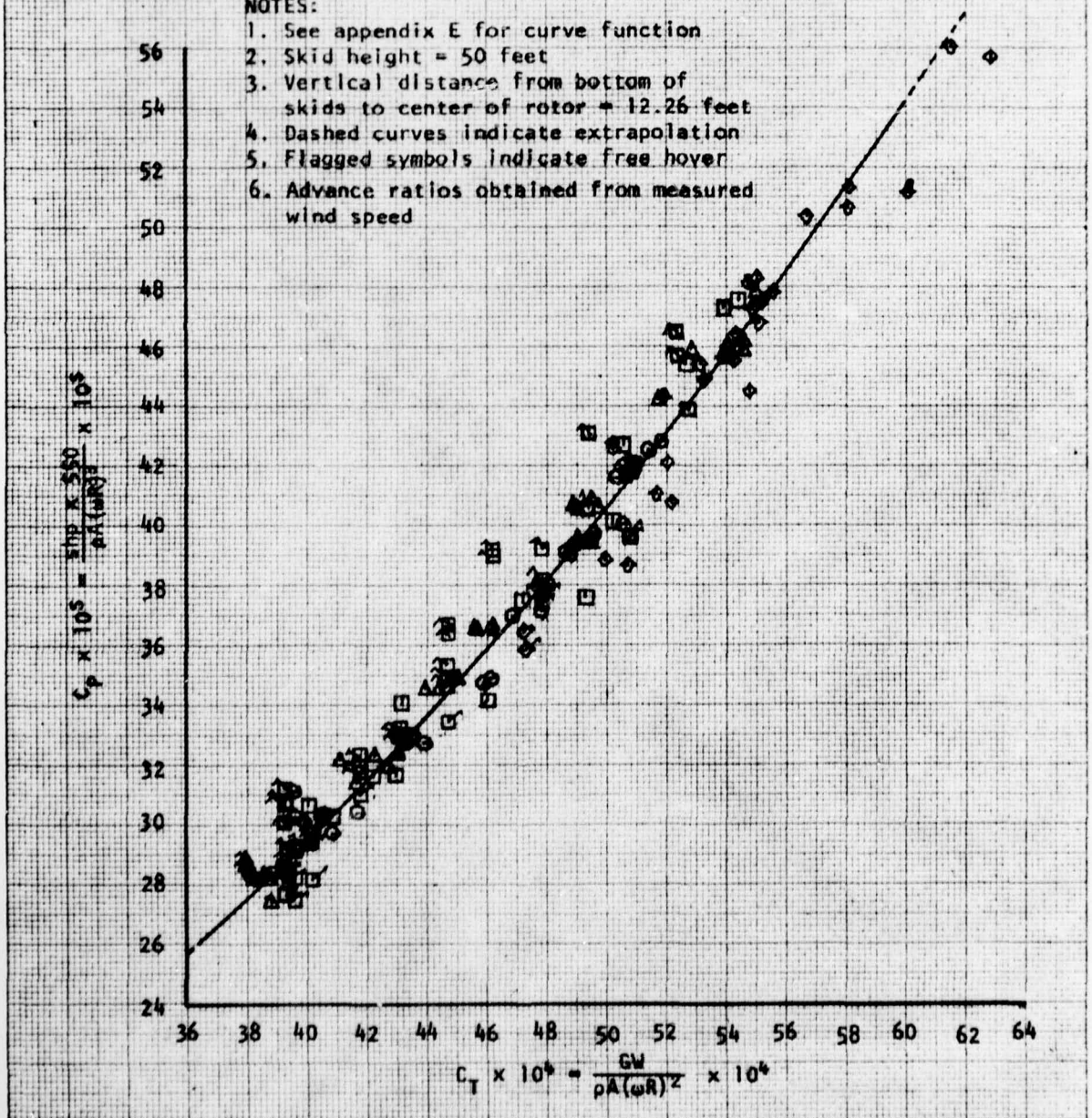

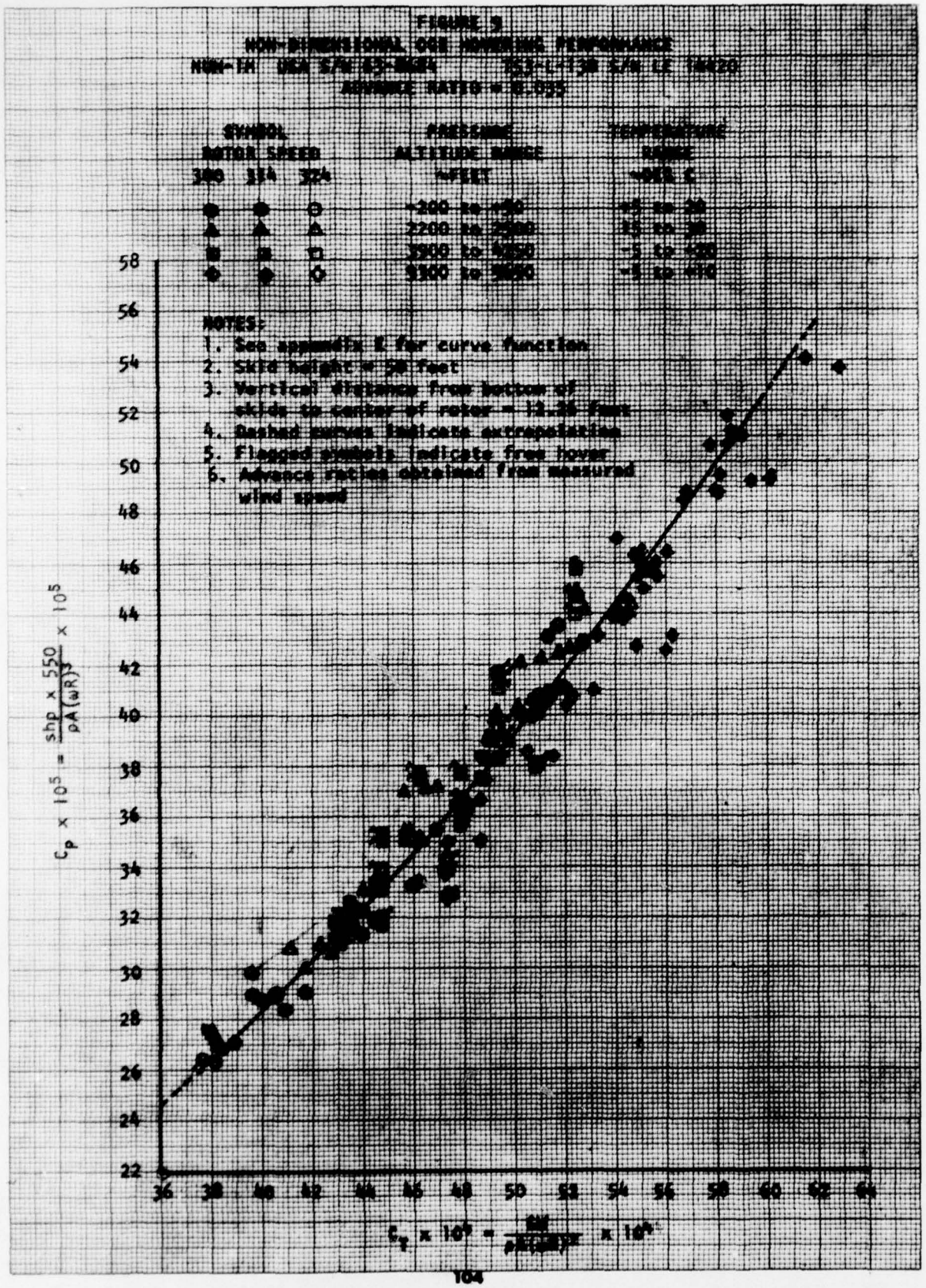
FIGURE 9
NON-DIMENSIONAL OGE HOVERING PERFORMANCE
NOTES:
1. See appendix E for curve function
2. Skid height = 20 feet
3. Vertical distance from bottom of skids to center of rotor = 13.36 feet
4. Dashed curves indicate extrapolation
5. Flagged symbols indicate free hover
6. Advance ratios obtained from measured wind speed
$C_p \times 10^5 = \frac{shp \times 550}{\rho A(\omega R)^3} \times 10^5$
$C_T \times 10^5 = \frac{GW}{\rho A(\omega R)^2} \times 10^5$

FIGURE 10
NON-DIMENSIONAL OGE HOVERING PERFORMANCE
NUH-1N USA S/N 63-8684 T53-L-13B S/N LE 14420
ADVANCE RATIO = 0.040

SYMBOL ROTOR SPEED 300	314	324	PRESSURE ALTITUDE RANGE ~FEET	TEMPERATURE RANGE ~DEG C
◐	●	○	-200 to +50	+5 to 20
▲	▲	△	2200 to 2500	15 to 30
■	■	⊡	3900 to 4250	-5 to +20
◆	◆	◇	9300 to 9650	-5 to +10

NOTES:
1. See appendix E for curve function
2. Skid height = 50 feet
3. Vertical distance from bottom of skids to center of rotor = 12.26 feet
4. Dashed curves indicate extrapolation
5. Flagged symbols indicate free hover
6. Advance ratios obtained from measured wind speed

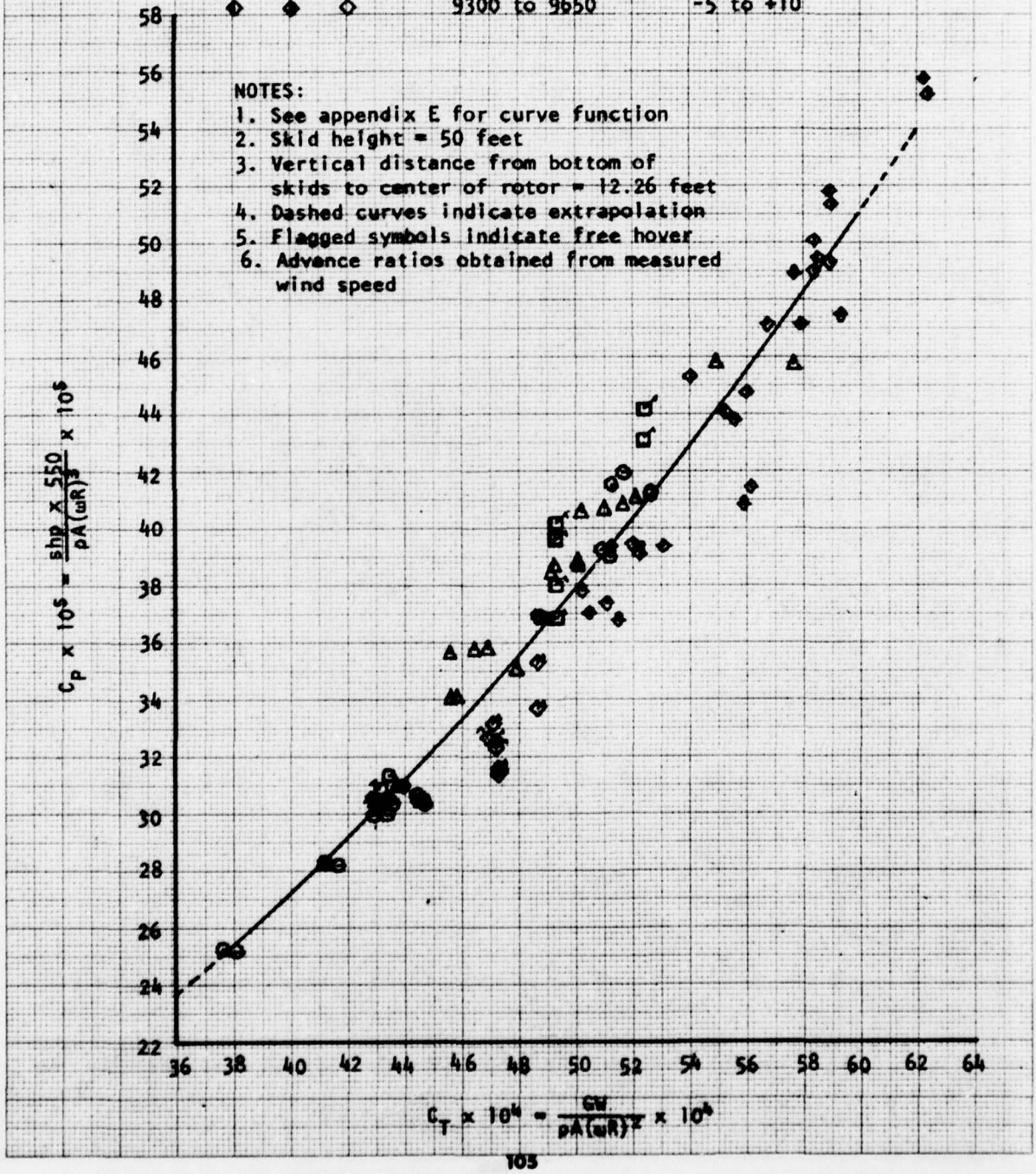

FIGURE 11

NON-DIMENSIONAL OGE HOVERING PERFORMANCE

NUH-1H USA S/N 63-8684 T53-L-13B S/N LE 14420

ADVANCE RATIO = 0.045

SYMBOL ROTOR SPEED 300	314	324	PRESSURE ALTITUDE RANGE ~FEET	TEMPERATURE RANGE ~DEG C
●	◐	○	-200 to +50	+5 to 20
▲	▲	△	2200 to 2500	15 to 30
■	■	□	3900 to 4250	-5 to +20
◆	◆	◇	9300 to 9650	-5 to +10

NOTES:

1. See appendix E for curve function
2. Skid height = 50 feet
3. Vertical distance from bottom of skids to center of rotor = 12.26 feet
4. Dashed curves indicate extrapolation
5. Flagged symbols indicate free hover
6. Advance ratios obtained from measured wind speed

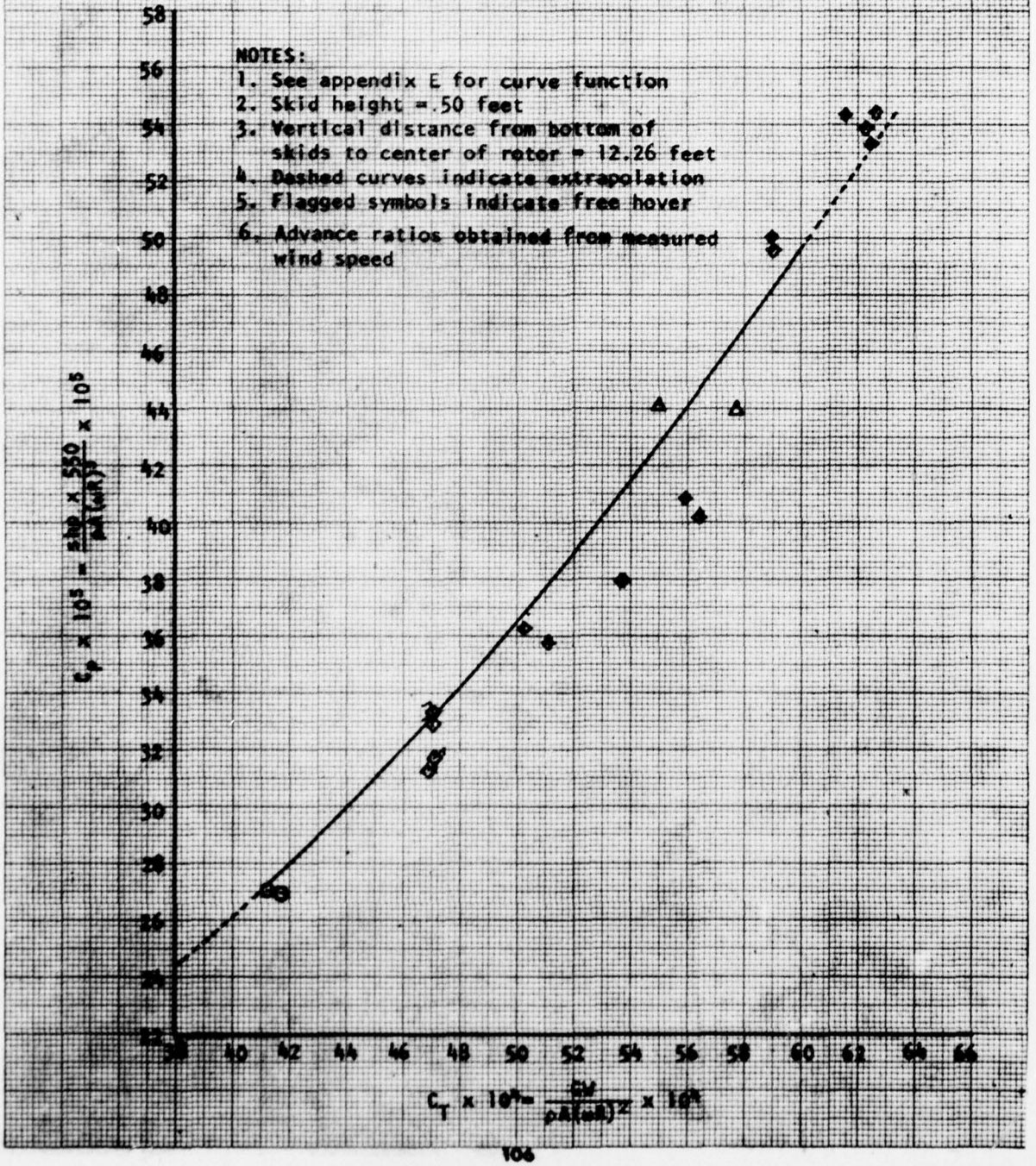

FIGURE 12

NON-DIMENSIONAL OGE HOVERING PERFORMANCE

NUH-1M USA S/N 63-8684 T53-L-13B S/N LE 14420

ADVANCE RATIO = 0.050

SYMBOL ROTOR SPEED 300	314	324	PRESSURE ALTITUDE RANGE ~FEET	TEMPERATURE RANGE ~DEG C
◐	◑	○	-200 to +50	+5 to 20
▲	▲	△	2200 to 2500	15 to 30
◧	◨	□	3900 to 4250	-5 to +20
◆	◆	◇	9300 to 9650	-5 to +10

NOTES:

1. See appendix E for curve function
2. Skid height = 50 feet
3. Vertical distance from bottom of skids to center of rotor = 12.26 feet
4. Dashed curves indicate extrapolation
5. Flagged symbols indicate free hover
6. Advance ratios obtained from measured wind speed

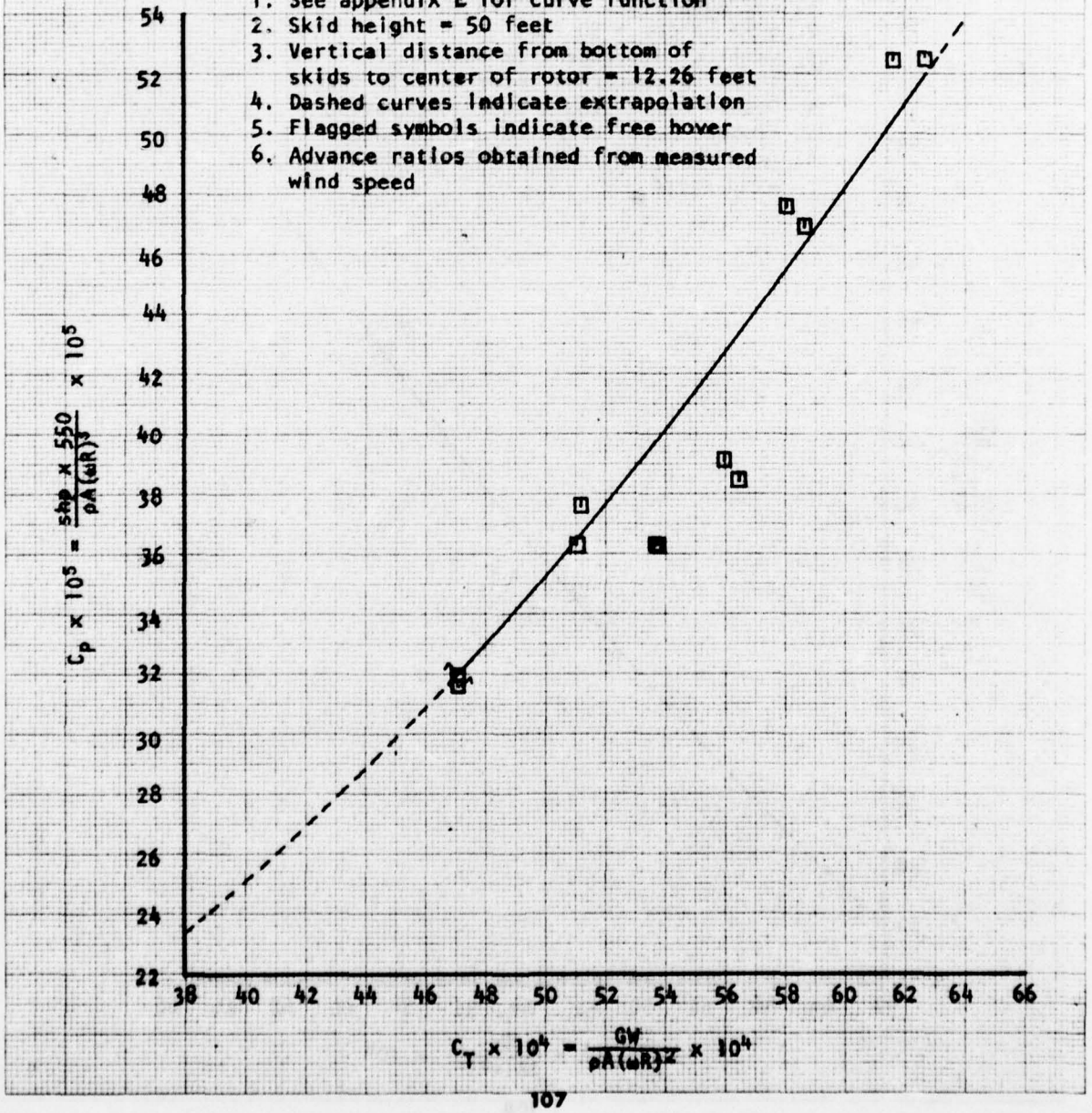

FIGURE 13
NON-DIMENSIONAL OGE HOVERING PERFORMANCE
NUH-1H USA S/N 63-8684 T53-L-13B S/N LE 14420
ADVANCE RATIO = 0.055

SYMBOL ROTOR SPEED 300	314	324	PRESSURE ALTITUDE RANGE ~FEET	TEMPERATURE RANGE ~DEG C
◐	◑	○	-200 to +50	+5 to 20
▲	▲	△	2200 to 2500	15 to 30
◧	◨	□	3900 to 4250	-5 to +20
◆	◆	◇	9300 to 9650	-5 to +10

NOTES:
1. See appendix E for curve function
2. Skid height = 50 feet
3. Vertical distance from bottom of skids to center of rotor = 12.26 feet
4. Dashed curves indicate extrapolation
5. Flagged symbols indicate free hover
6. Advance ratios obtained from measured wind speed

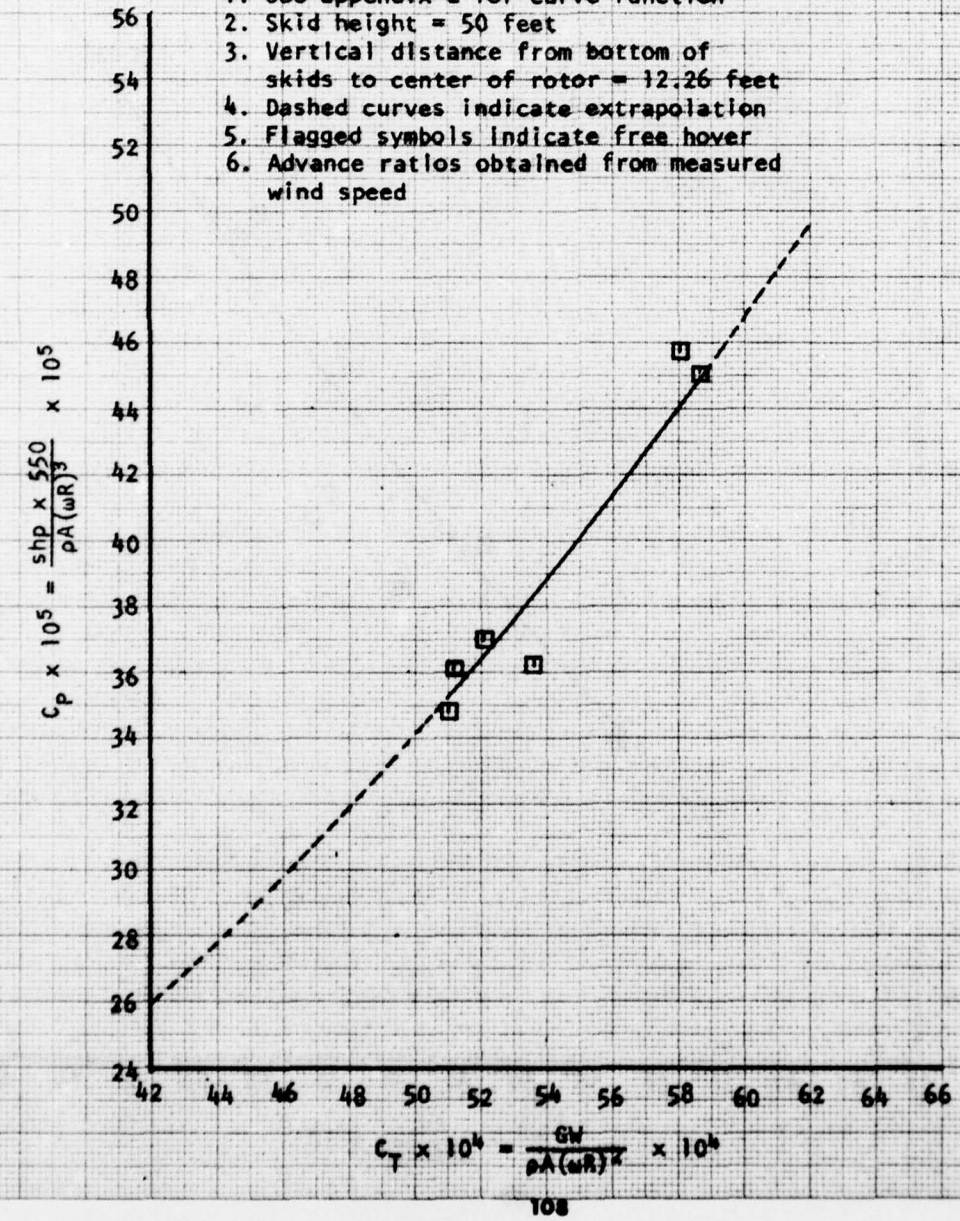

FIGURE 14
NON-DIMENSIONAL OGE LEVEL FLIGHT PERFORMANCE
NUH-1M USA S/N 63-8684 T53-L-13B S/N LE 14420
THRUST COEFFICIENT = 38.5 x 10^{-4}

SYMBOL	PRESSURE ALTITUDE ∿ FEET	TEMPERATURE ∿°C
○	2240	20
△	2230	16
□	2260	16

NOTES:
1. Airspeed obtained from wind measurement and ground pace vehicle speed
2. Skid height = 50 feet
3. Vertical distance from bottom of skids to center of rotor = 12.26 feet
4. Rotor speed = 324 rpm

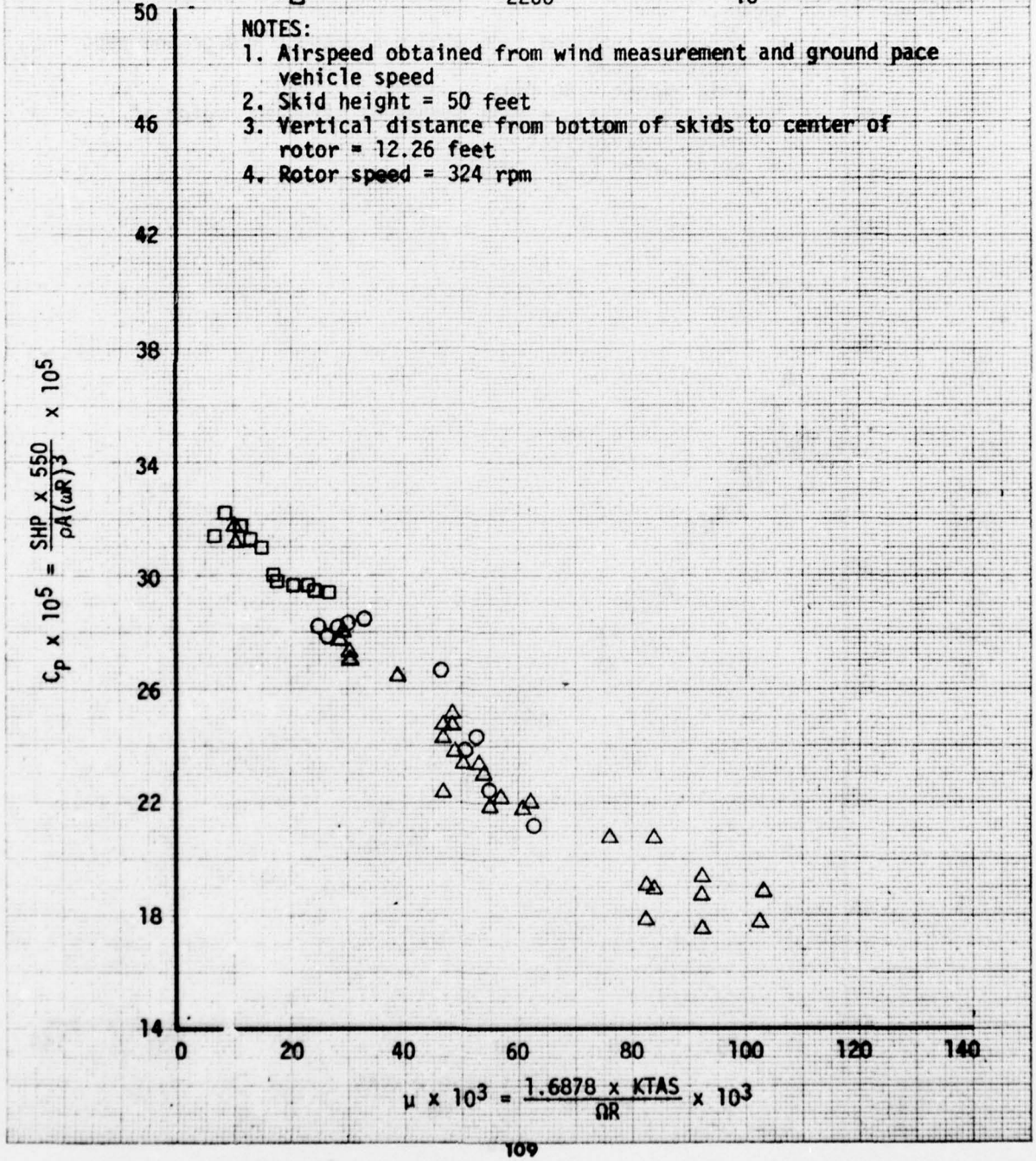

FIGURE 15

NON-DIMENSIONAL OGE LEVEL FLIGHT PERFORMANCE

NUH-1M USA S/N 63-8684 T53-L-13B S/N LE 14420

THRUST COEFFICIENT = 41.0 x 10^{-4}

SYMBOL	PRESSURE ALTITUDE ~ FEET	TEMPERATURE ~°C
○	2220	25
△	2240	24

NOTES:

1. Airspeed obtained from wind measurement and ground pace vehicle speed
2. Skid height = 50 feet
3. Vertical distance from bottom of skids to center of rotor = 12.26 feet
4. Rotor speed = 324 rpm

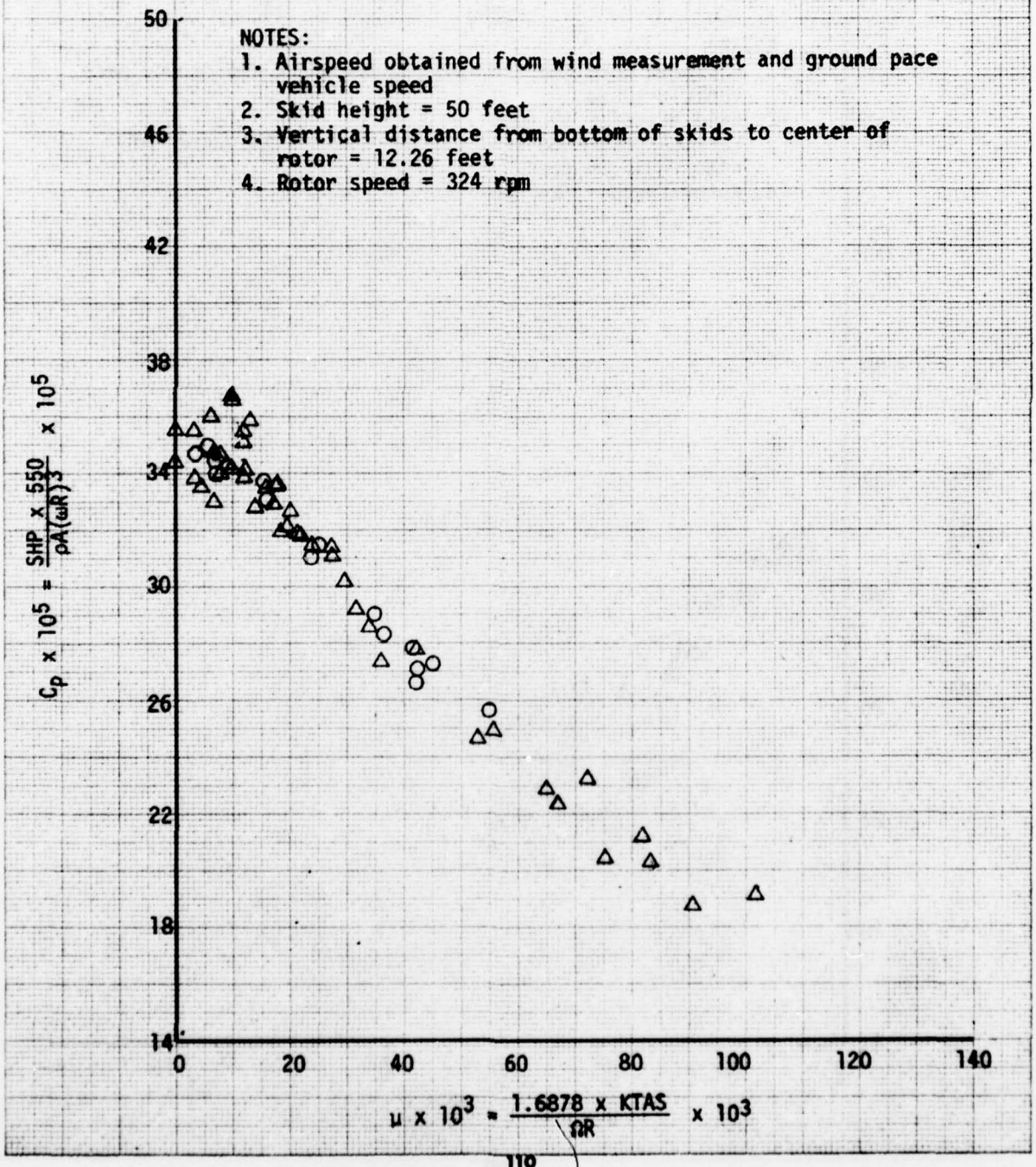

FIGURE 16

NON-DIMENSIONAL OGE LEVEL FLIGHT PERFORMANCE

NUH-1N USA S/N 63-8684 T53-L-13B S/N LE 14420

THRUST COEFFICIENT = 45.0 x 10^{-4}

SYMBOL	PRESSURE ALTITUDE ~ FEET	TEMPERATURE ~ °C
○	2310	17
△	2370	24

NOTES:
1. Airspeed obtained from wind measurement and ground pace vehicle speed
2. Skid height = 50 feet
3. Vertical distance from bottom of skids to center of rotor = 12.26 feet
4. Rotor speed = 324 rpm

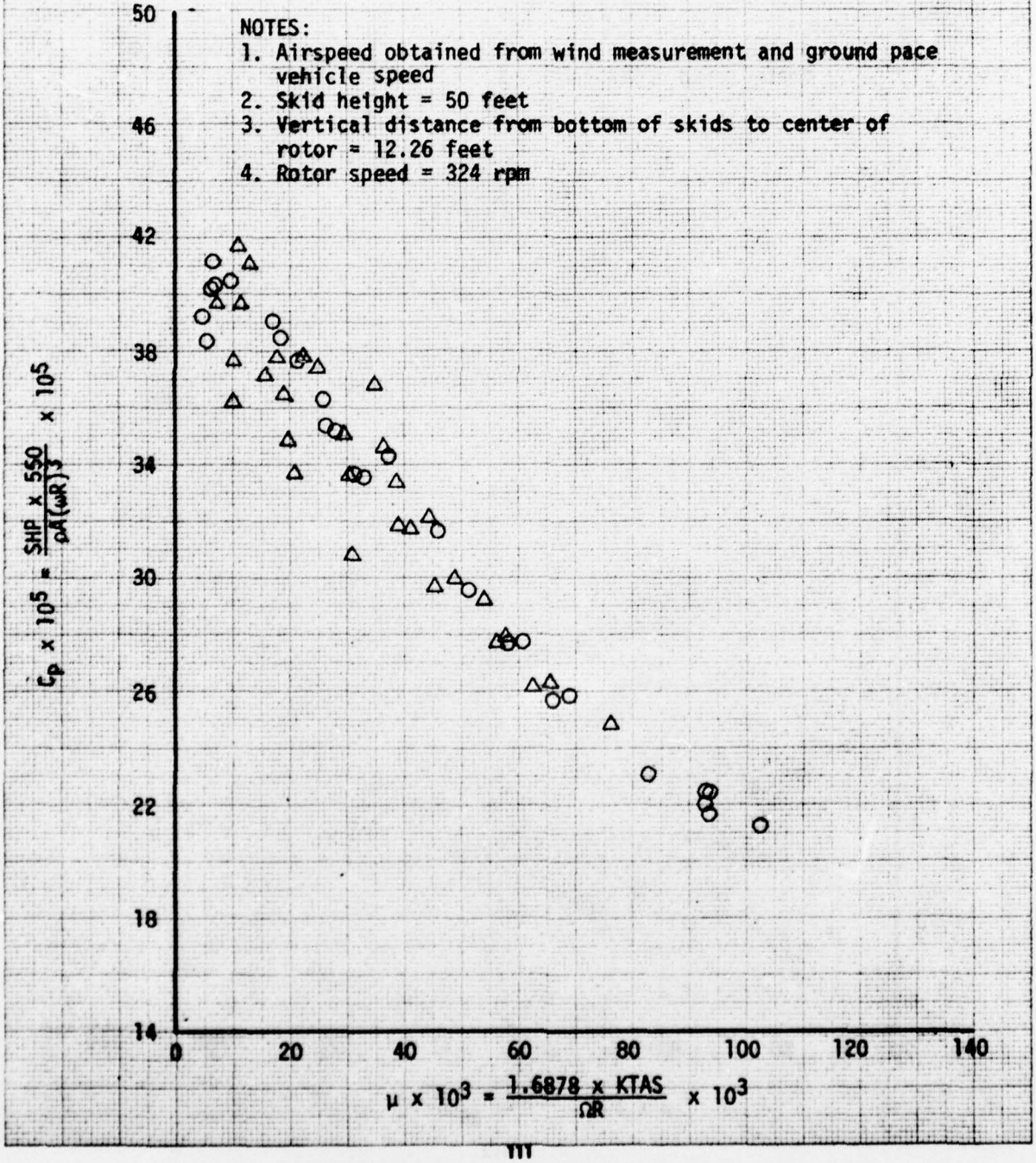

FIGURE 17
NON-DIMENSIONAL OGE LEVEL FLIGHT PERFORMANCE
NUH-1H USA S/N 63-8684 T53-L-13B S/N LE 14420
THRUST COEFFICIENT = 41.0 x 10^{-4}

SYMBOL	PRESSURE ALTITUDE ~ FEET	TEMPERATURE ~ °C
○	2990	24
△	3020	24

NOTES:
1. Aircraft altitude greater than 500 feet above ground level
2. Rotor speed = 324 rpm

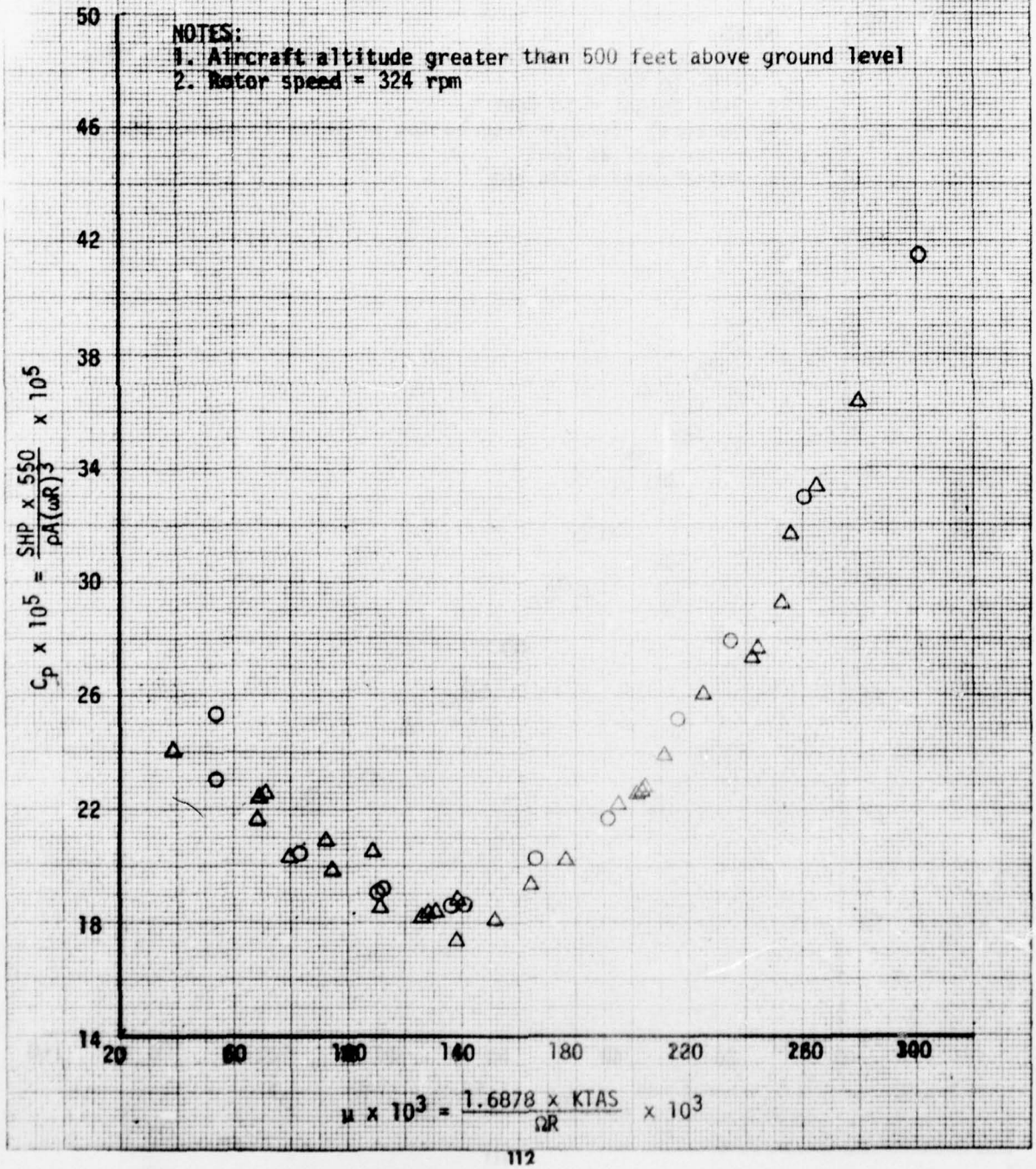

FIGURE 18
NON-DIMENSIONAL IGE HOVERING PERFORMANCE SUMMARY
NUH-1M USA S/N 63-8684 T53-L-13B S/N LE-14420

NOTES:
1. Curves obtained from figures 19 through 26
2. Skid height = 2 feet
3. Vertical distance from bottom of skids to center of rotor hub = 12.26 feet
4. Dashed curves indicate extrapolation

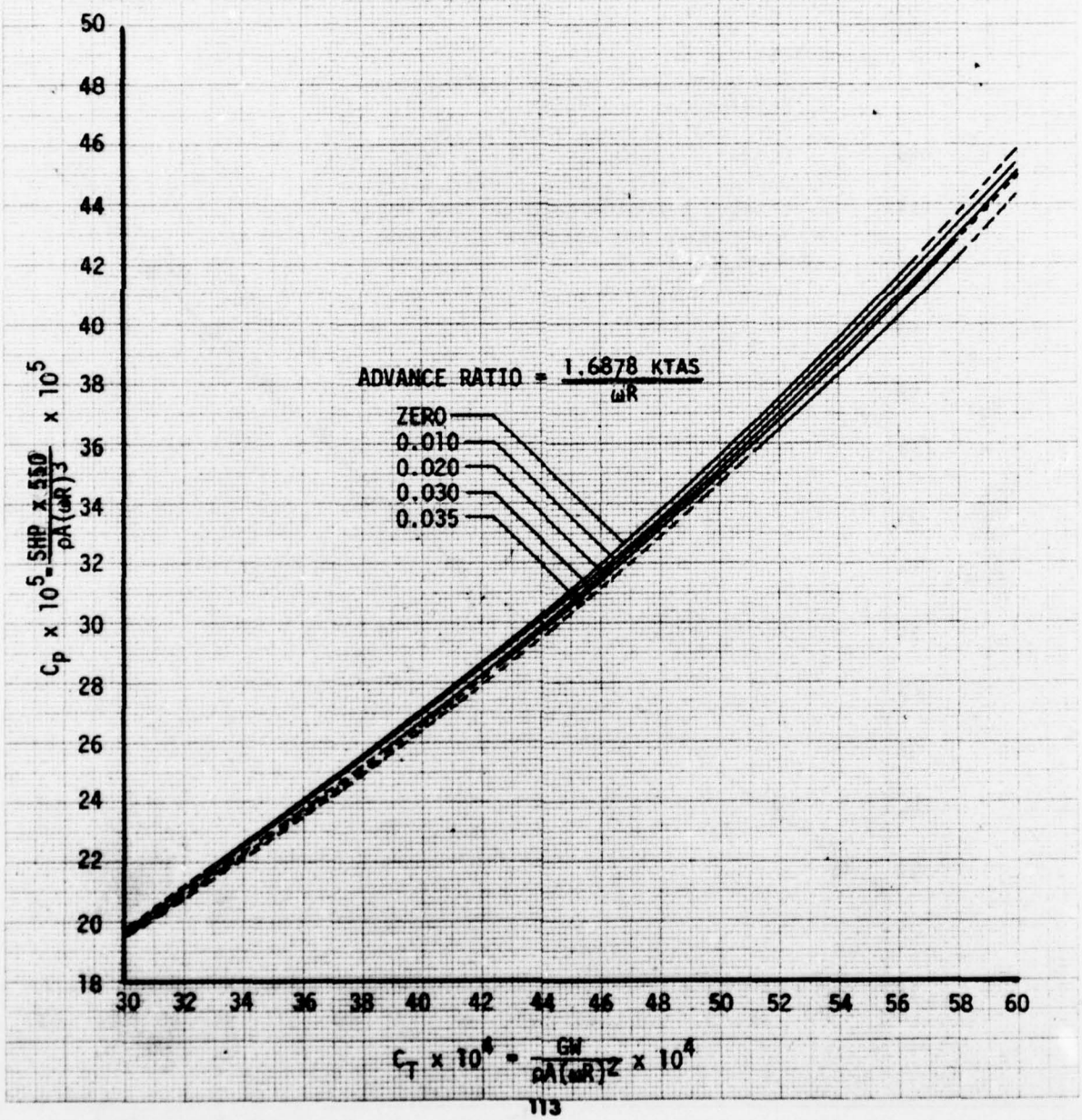

Figure 19

NON-DIMENSIONAL IGE HOVERING PERFORMANCE

NUH-1M USA S/N 63-8684 T53-L-13B S/N LE 14420

ADVANCE RATIO = ZERO

SYMBOL ROTOR SPEED			PRESSURE ALTITUDE RANGE	TEMPERATURE RANGE
314	321	324	∿FEET	∿DEG C
◐	◑	○	-200 to +50	+5 to 20
▲	▲	△	2200 to 2500	15 to 30
▣	◨	□	3900 to 4250	-5 to +20
◆	◆	◇	9300 to 9650	-5 to +10

NOTES:

1. See appendix E for curve function
2. Skid height = 2 feet
3. Vertical distance from bottom of skids to center of rotor = 12.26 feet
4. Dashed curves indicate extrapolation
5. Flagged symbols indicate free hover
6. Advance ratios obtained from measured wind speed

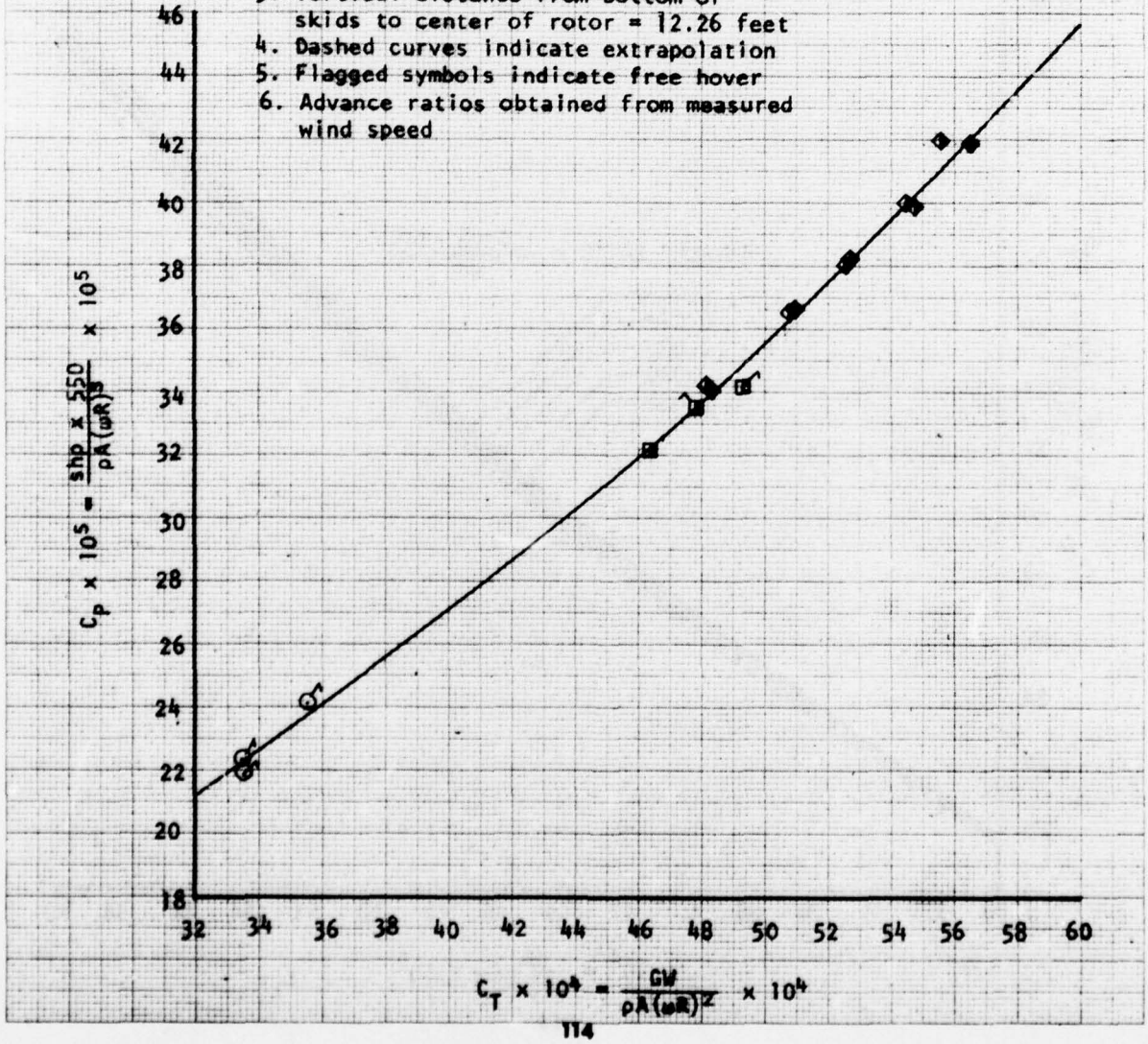

FIGURE 20
NON-DIMENSIONAL IGE HOVERING PERFORMANCE
NUH-1M USA S/N 63-8684 T53-L-13B S/N LE 14420
ADVANCE RATIO = 0.005

SYMBOL ROTOR SPEED 314	321	324	PRESSURE ALTITUDE RANGE ~FEET	TEMPERATURE RANGE ~DEG C
◐	◑	○	-200 to +50	+5 to 20
▲	▲	△	2200 to 2500	15 to 30
◧	◨	□	3900 to 4250	-5 to +20
◆	◆	◇	9300 to 9650	-5 to +10

NOTES:
1. See appendix E for curve function
2. Skid height = 2 feet
3. Vertical distance from bottom of skids to center of rotor = 12.26 feet
4. Dashed curves indicate extrapolation
5. Flagged symbols indicate free hover
6. Advance ratios obtained from measured wind speed

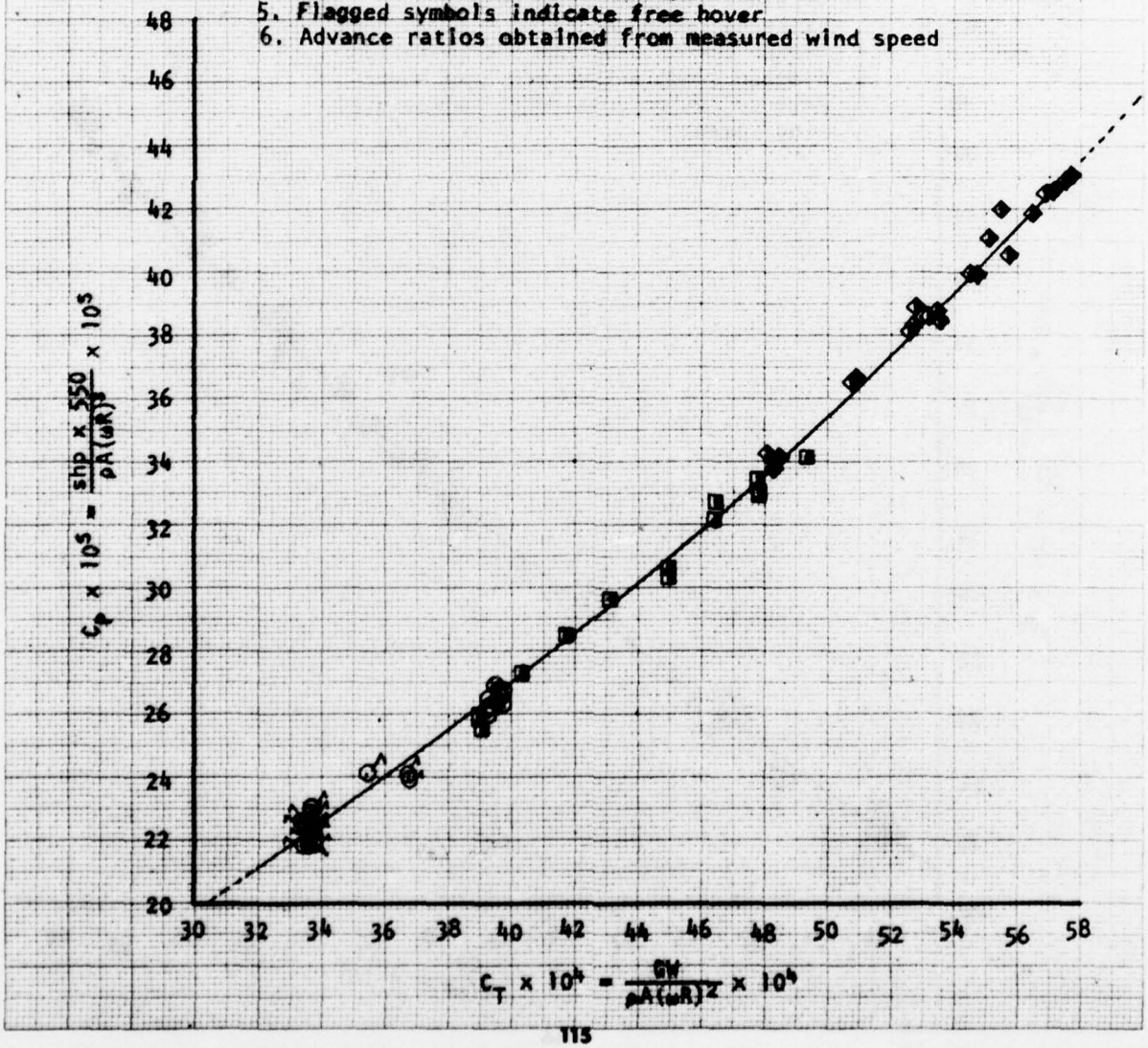

FIGURE 21
NON-DIMENSIONAL IGE HOVERING PERFORMANCE
NUH-1M USA S/N 63-8684 T53-L-13B S/N LE 14420
ADVANCE RATIO = 0.010

SYMBOL ROTOR SPEED			PRESSURE ALTITUDE RANGE	TEMPERATURE RANGE
314	321	324	~FEET	~DEG C
◐	◑	○	-200 to +50	+5 to 20
▲	▲	△	2200 to 2500	15 to 30
◧	◨	□	3900 to 4250	-5 to +20
◆	◆	◇	9300 to 9650	-5 to +10

NOTES:
1. See appendix E for curve function
2. Skid height = 2 feet
3. Vertical distance from bottom of skids to center of rotor = 12.26 feet
4. Dashed curves indicate extrapolation
5. Flagged symbols indicate free hover
6. Advance ratios obtained from measured wind speed

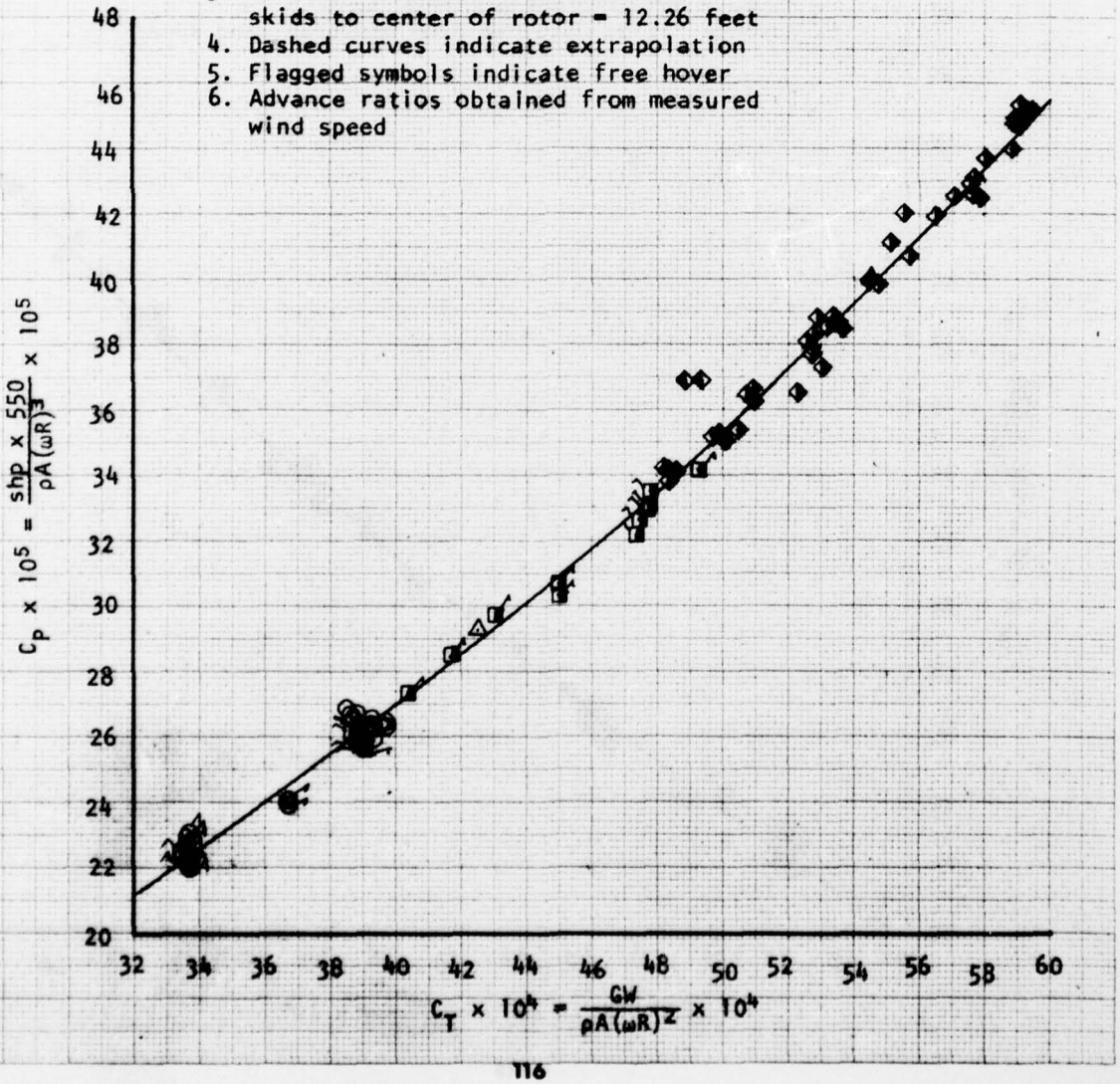

FIGURE 22
NON-DIMENSIONAL IGE HOVERING PERFORMANCE
NUH-1N USA S/N 63-8684 T53-L-13B S/N LE 14420
ADVANCE RATIO = 0.015

SYMBOL ROTOR SPEED			PRESSURE ALTITUDE RANGE	TEMPERATURE RANGE
314	321	324	~FEET	~DEG C
●	◑	○	-200 to +50	+5 to 20
▲	◭	△	2200 to 2500	15 to 30
■	◧	□	3900 to 4250	-5 to +20
◆	◈	◇	9300 to 9650	-5 to +10

NOTES:
1. See appendix E for curve function
2. Skid height = 2 feet
3. Vertical distance from bottom of skids to center of rotor = 12.26 feet
4. Dashed curves indicate extrapolation
5. Flagged symbols indicate free hover
6. Advance ratios obtained from measured wind speed

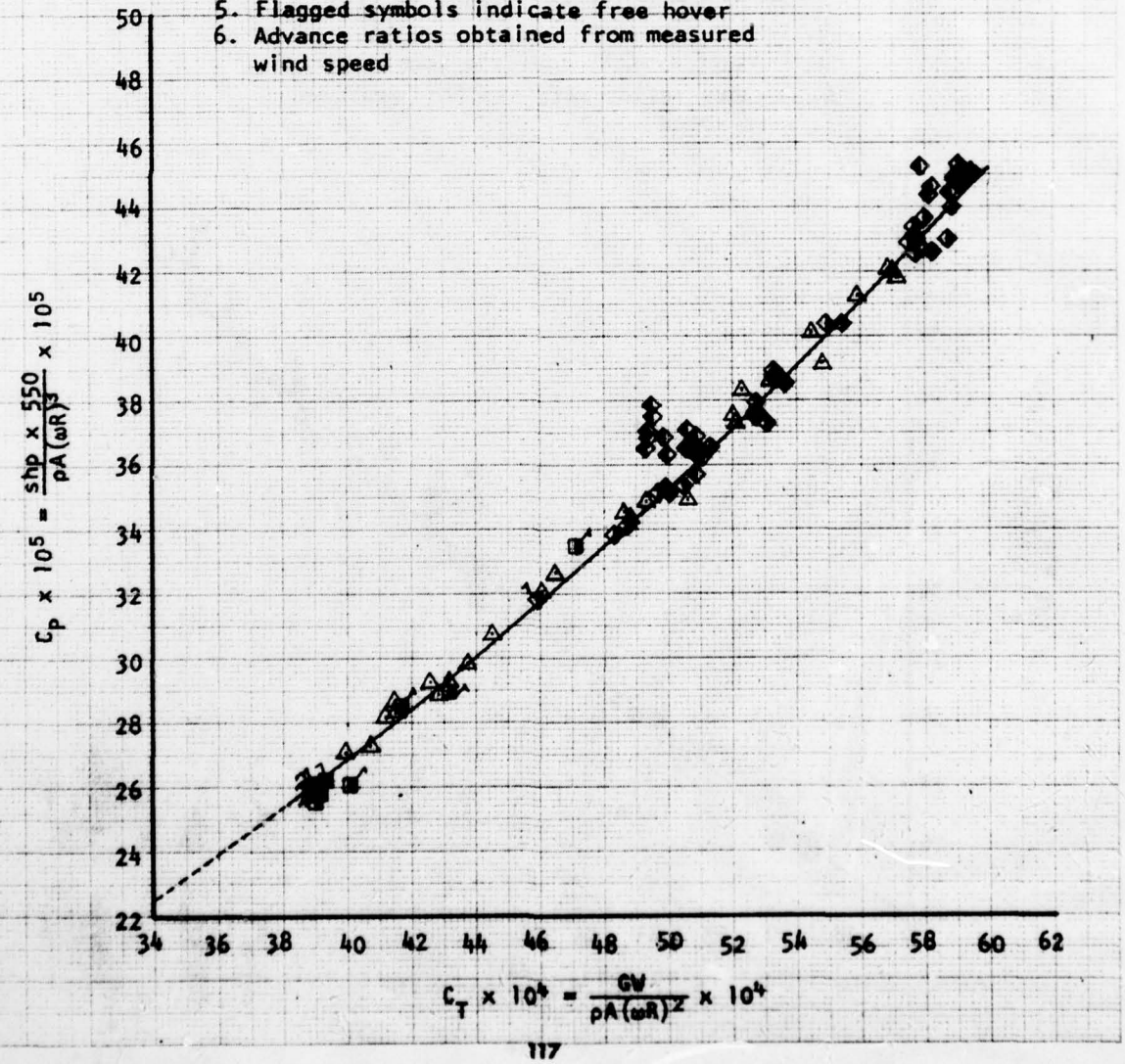

FIGURE 23
NON-DIMENSIONAL IGE HOVERING PERFORMANCE
NUH-1M USA S/N 63-8684 T53-L-13B S/N LE 14420
ADVANCE RATIO = 0.020

SYMBOL ROTOR SPEED 314	321	324	PRESSURE ALTITUDE RANGE ~FEET	TEMPERATURE RANGE ~DEG C
◐	◑	○	-200 to +50	+5 to 20
▲	▲	△	2200 to 2500	15 to 30
◧	◨	□	3900 to 4250	-5 to +20
◆	◆	◇	9300 to 9650	-5 to +10

NOTES:
1. See appendix E for curve function
2. Skid height = 2 feet
3. Vertical distance from bottom of skids to center of rotor = 12.26 feet
4. Dashed curves indicate extrapolation
5. Flagged symbols indicate free hover
6. Advance ratios obtained from measured wind speed

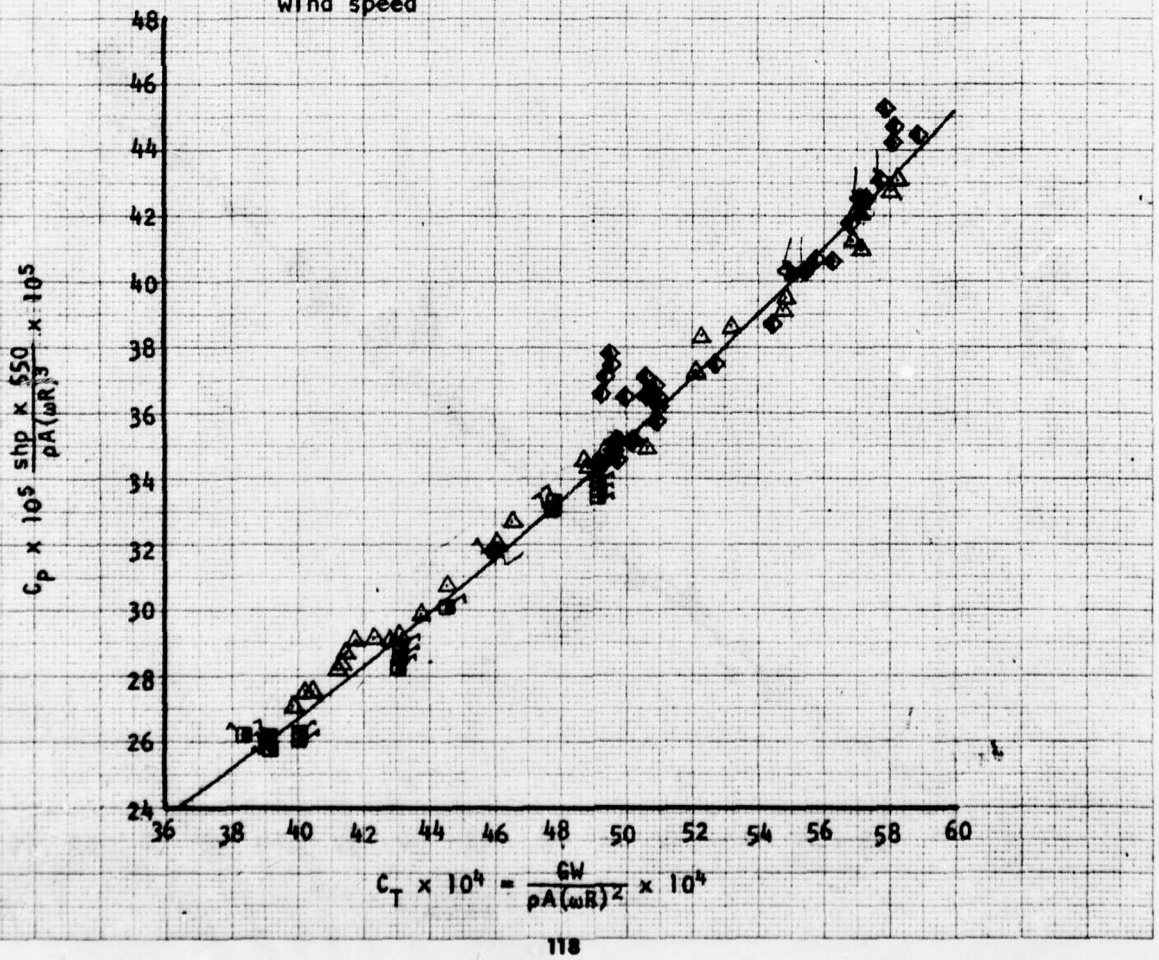

FIGURE 24
NON-DIMENSIONAL IGE HOVERING PERFORMANCE
NUH-1M USA S/N 63-8684 T53-L-13B S/N LE 14420
ADVANCE RATIO = 0.025

SYMBOL ROTOR SPEED			PRESSURE ALTITUDE RANGE	TEMPERATURE RANGE
314	321	324	~FEET	~DEG C
◐	◑	○	-200 to +50	+5 to 20
▲	▲	△	2200 to 2500	15 to 30
◧	◨	□	3900 to 4250	-5 to +20
◆	◆	◇	9300 to 9650	-5 to +10

NOTES:
1. See appendix E for curve function
2. Skid height = 2 feet
3. Vertical distance from bottom of skids to center of rotor = 12.26 feet
4. Dashed curves indicate extrapolation
5. Flagged symbols indicate free hover
6. Advance ratios obtained from measured wind speed

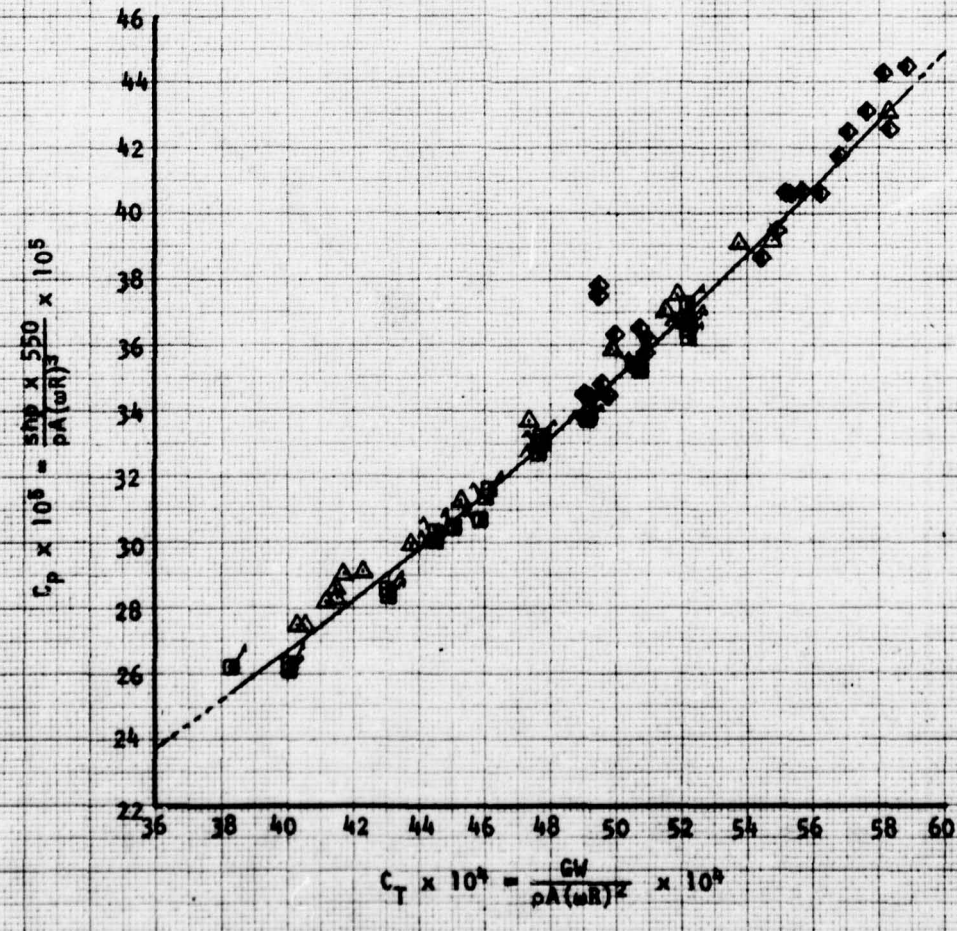

FIGURE 25
NON-DIMENSIONAL IGE HOVERING PERFORMANCE
NUH-1H USA S/N 63-8684 T53-L-13B S/N LE 14420
ADVANCE RATIO = 0.030

SYMBOL ROTOR SPEED 314	321	324	PRESSURE ALTITUDE RANGE ~FEET	TEMPERATURE RANGE ~DEG C
●	●	○	-200 to + 50	+5 to 20
▲	▲	△	2200 to 2500	15 to 30
■	■	□	3900 to 4250	-5 to +20
◆	◆	◇	9300 to 9650	-5 to +10

NOTES:
1. See appendix E for curve function
2. Skid height = 2 feet
3. Vertical distance from bottom of skids to center of rotor = 12.26 feet
4. Dashed curves indicate extrapolation
5. Flagged symbols indicate free hover
6. Advance ratios obtained from measured wind speed

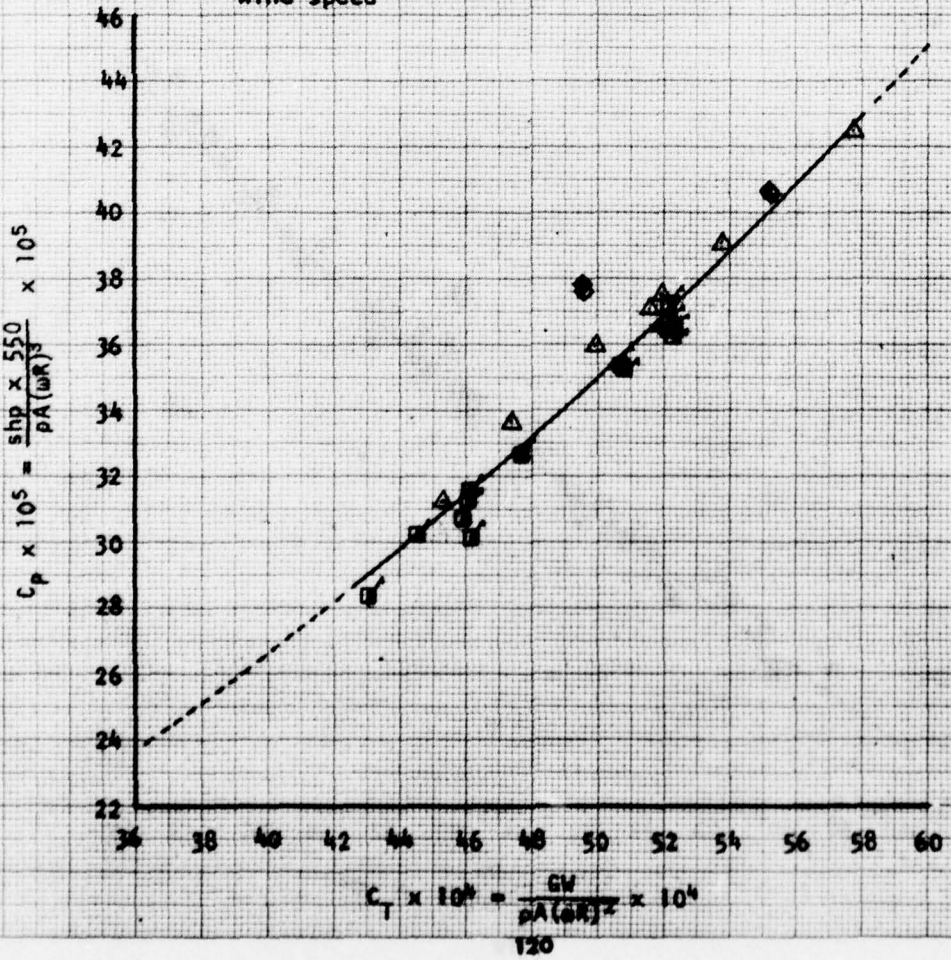

FIGURE 26

NON-DIMENSIONAL IGE HOVERING PERFORMANCE

NUH-1H USA S/N 63-[illegible] T53-L-13B S/N LE 14420

ADVANCE RATIO = 0.035

SYMBOL ROTOR SPEED			PRESSURE ALTITUDE RANGE	TEMPERATURE RANGE
314	321	324	FEET	DEG C
●	◑	○	-200 to +50	+5 to 20
▲	◭	△	2200 to 2500	15 to 30
■	◨	□	3900 to 4250	-5 to +20
◆	◈	◇	9300 to 9650	-5 to +10

NOTES:

1. See appendix E for curve function
2. Skid height = 2 feet
3. Vertical distance from bottom of skids to center of rotor = 12.26 feet
4. Dashed curves indicate extrapolation
5. Flagged symbols indicate free hover
6. Advance ratios obtained from measured wind speed

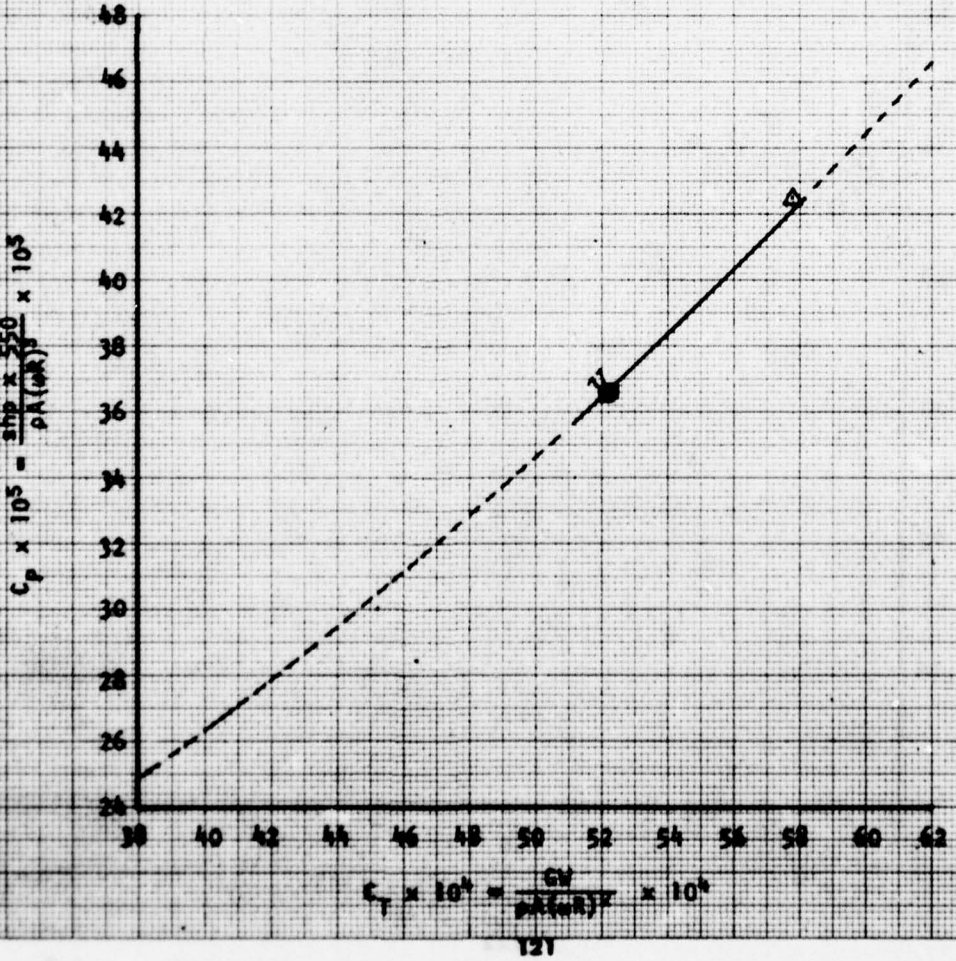

FIGURE 27
NON-DIMENSIONAL IGE LEVEL FLIGHT PERFORMANCE
NUH-1M USA S/N 63-8684 T53-L-13B S/N LE 14420

SYMBOL	PRESSURE ALTITUDE ~ FEET	TEMPERATURE ~ °C	THRUST COEFFICIENT
○	2330	23	45.7×10^{-4}
△	2280	18	44.6×10^{-4}

NOTES:
1. Airspeed obtained from wind measurement and ground pace speed.
2. Skid height = 5 feet
3. Vertical distance from bottom of skids to center of rotor = 12.26 feet
4. Rotor speed = 324 rpm

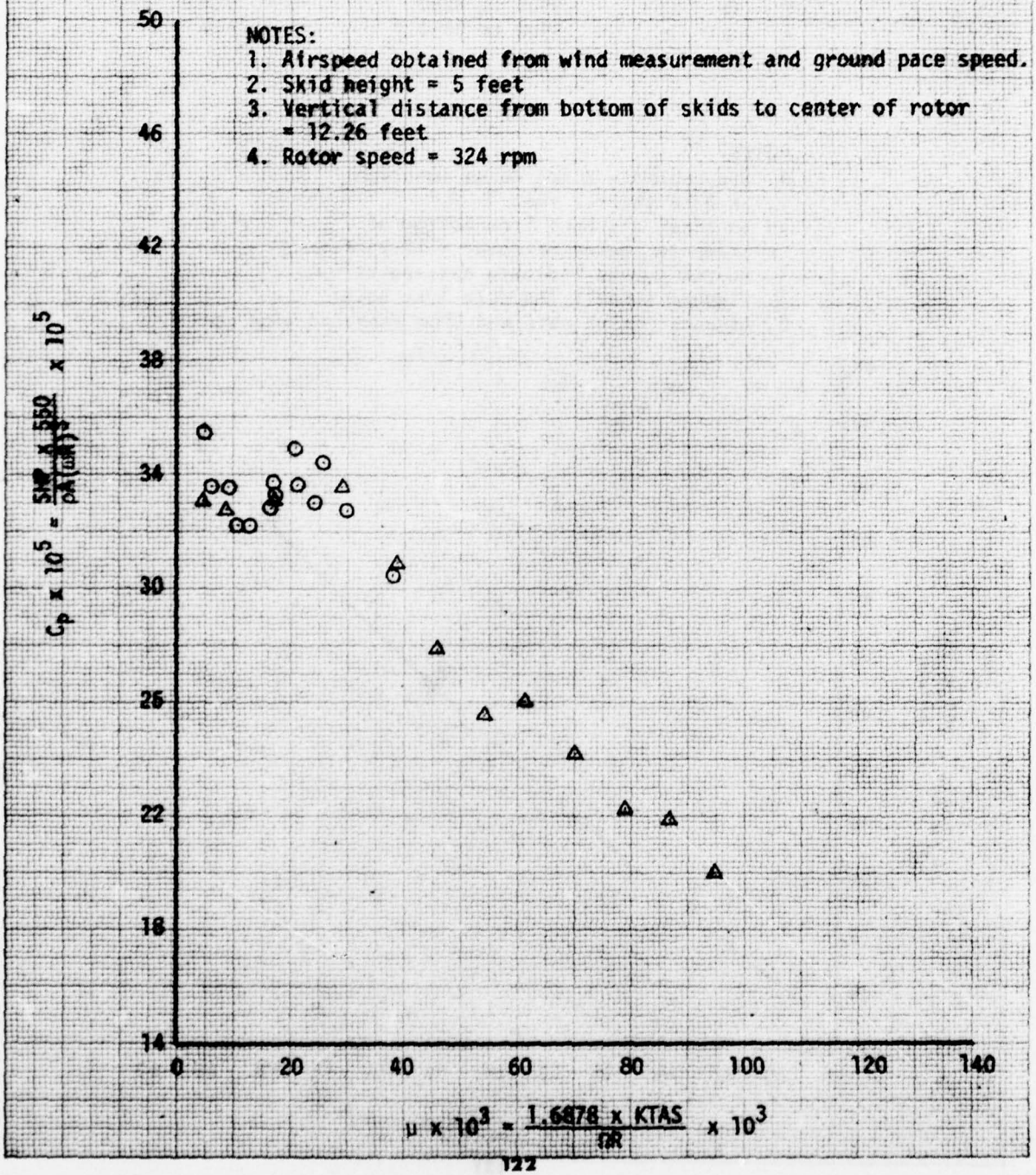

FIGURE 28
NON-DIMENSIONAL IGE LEVEL FLIGHT PERFORMANCE
NUH-1M USA S/N 63-8684 T53-L-13B S/N LE-14420

SYMBOL	PRESSURE ALTITUDE ~ FT	TEMPERATURE ~ °C	ROTOR SPEED ~ RPM	THRUST COEFFICIENT
○	2250	25	322	41.0×10^{-4}
□	2780	23	322	48.0×10^{-4}

NOTES:
1. Airspeed obtained from wind measurement and ground pace vehicle speed
2. Skid height = 5 feet
3. Vertical distance from bottom of skids to center of rotor = 12.26 feet

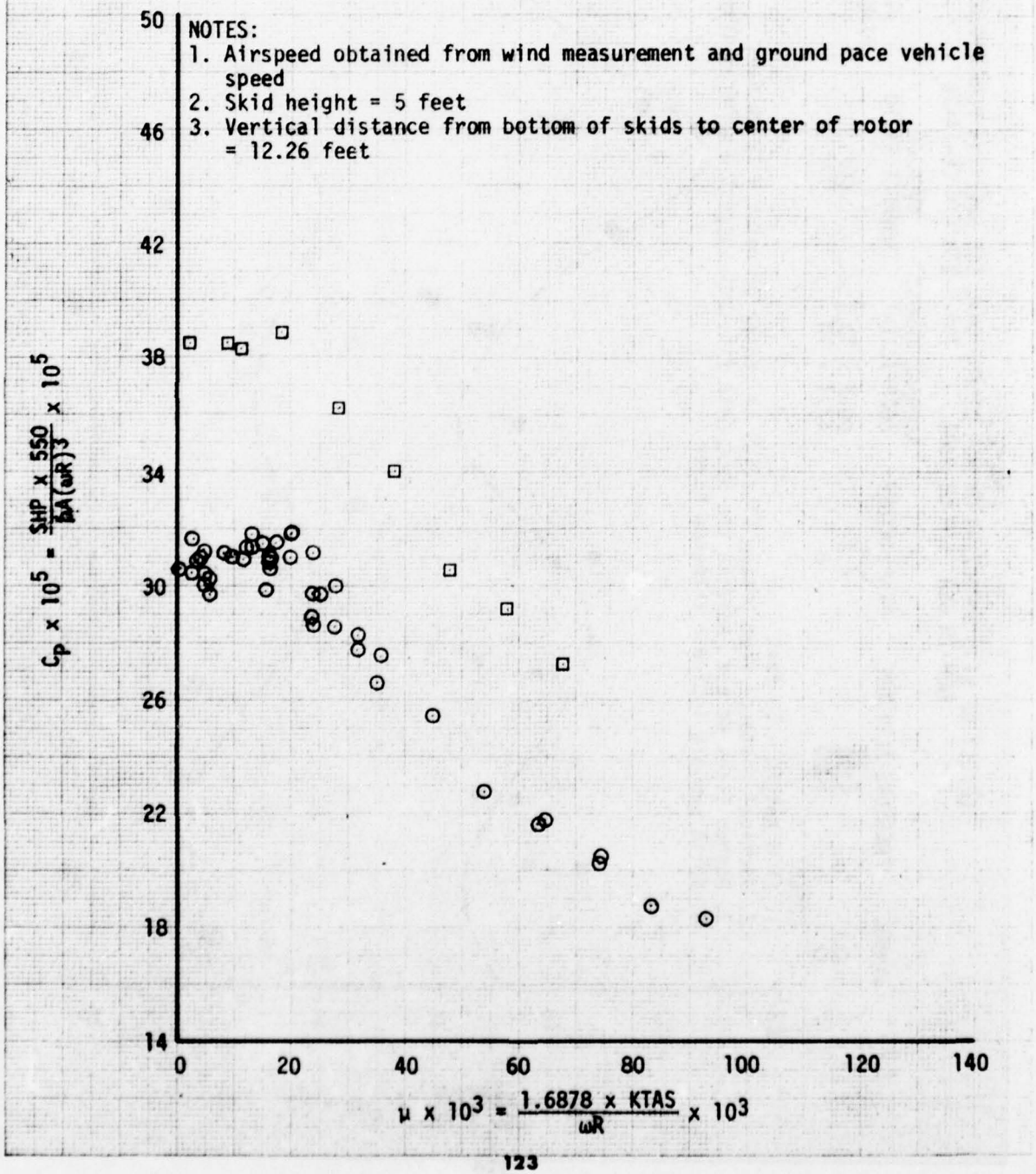

FIGURE 29

EFFECT OF WIND DIRECTION ON NON-DIMENSIONAL OGE HOVERING PERFORMANCE

NUH-1M USA S/N 63-8684 T53-L-13B S/N LE-14420

SYMBOL	PRESSURE ALTITUDE ~ FT	TEMPERATURE ~ °C	AVERAGE THRUST COEFFICIENT	AVERAGE ADVANCE RATIO	WIND SPEED RANGE ~ KTAS
■	9370	6.5	50.7×10^{-4}	.007	1.5 to 4
○	4040	8	47.4×10^{-4}	.003	0 to 2.5

NOTES:
1. Skid height = 50 feet
2. Vertical distance from bottom of skids to center of rotor = 12.26 feet
3. Dashed lines do not indicate the best data fit, but suggest a general trend from combined data
4. Solid symbols indicate tethered hover

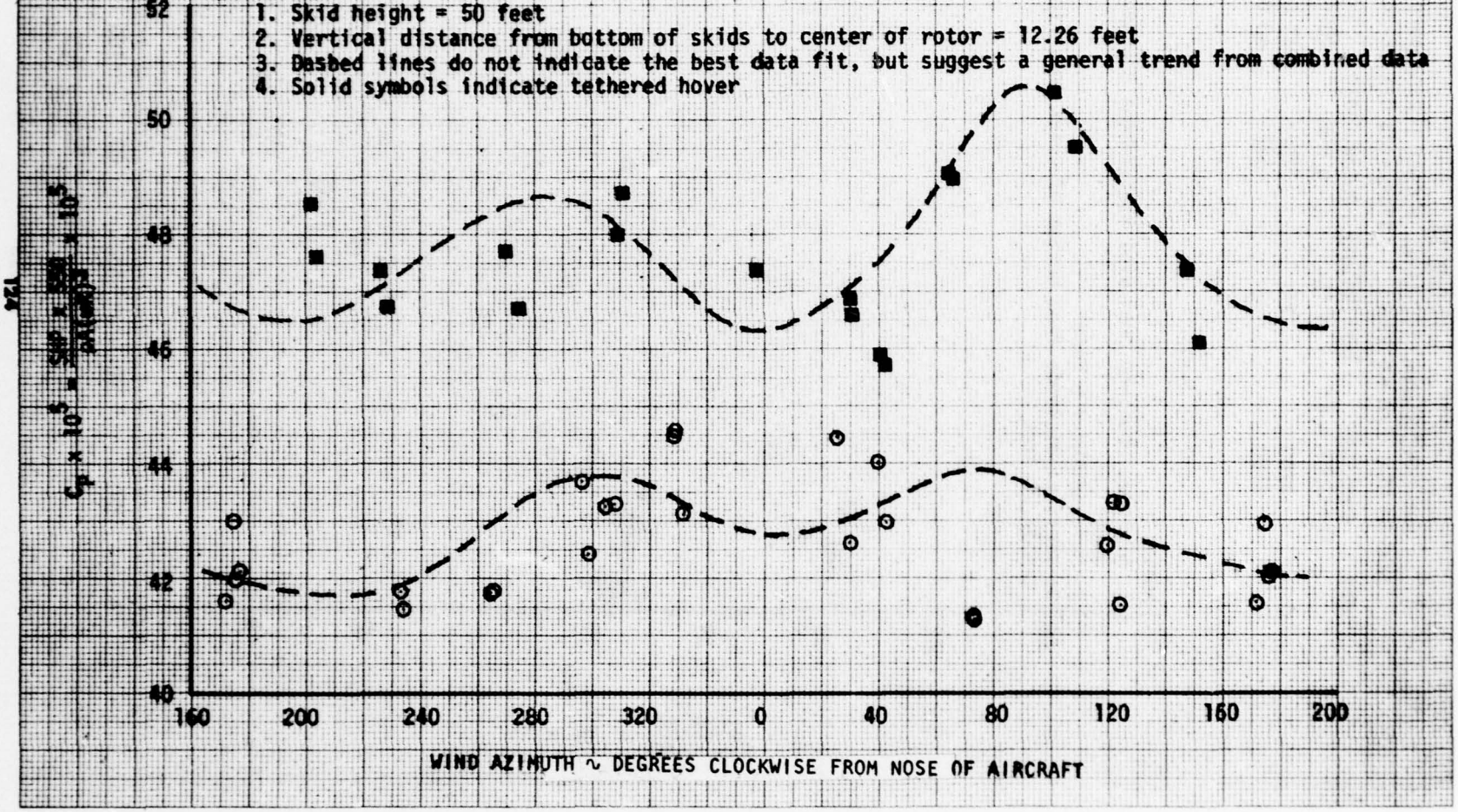

FIGURE 30

EFFECT OF WIND DIRECTION ON NON-DIMENSIONAL OGE HOVERING PERFORMANCE

NGH-1M USA S/N 63-8684 T63-L-13B S/N LE-14420

SYMBOL	PRESSURE ALTITUDE ~ FT	TEMPERATURE ~°C	AVERAGE THRUST COEFFICIENT	AVERAGE ADVANCE RATIO	WIND SPEED RANGE ~ KTAS
○	-10	13.	43.9×10^{-4}	.008	3 to 4
□	-10	13.5	38.8×10^{-4}	.007	2.5 to 3.5
△	-10	13.5	32.9×10^{-4}	.008	3 to 4

NOTES:

1. Skid height = 50 feet
2. Vertical distance from bottom of skids to center of rotor = 12.25 feet
3. Dashed lines do not indicate the best data fit, but suggest a general trend from combined data
4. Solid symbols indicate outboard hover

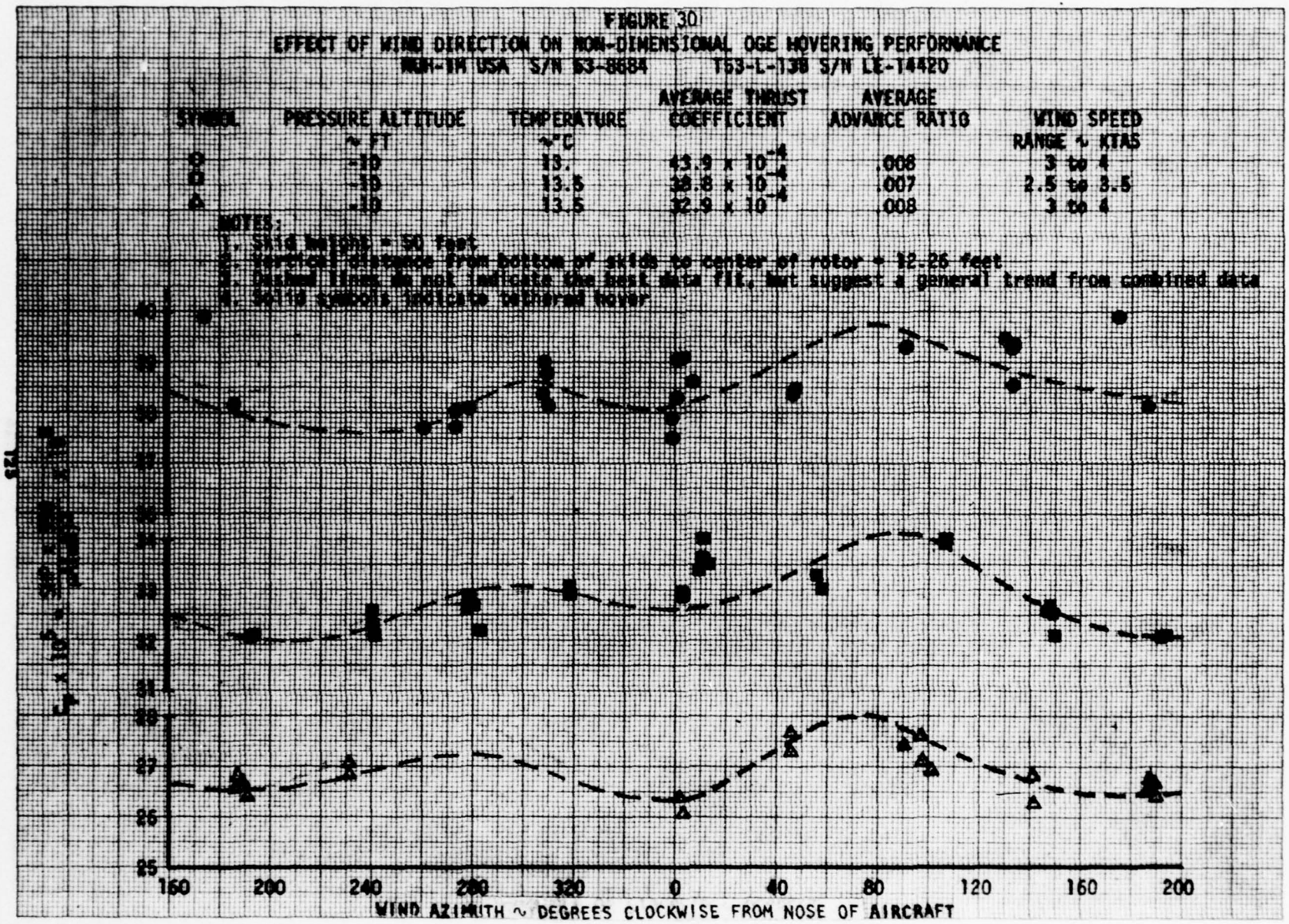

FIGURE 31

EFFECT OF WIND DIRECTION ON NON-DIMENSIONAL OGE HOVERING PERFORMANCE
NUH-1M USA S/N 63-8684 T53-L-13B S/N LE-14420

SYMBOL	PRESSURE ALTITUDE ~ FT	TEMPERATURE ~°C	AVERAGE THRUST COEFFICIENT	AVERAGE ADVANCE RATIO	WIND SPEED RANGE ~ KTAS
■	2410	23.5	47.5×10^{-4}	.017	6 to 8.5
○	2370	25.	45.7×10^{-4}	.016	6 to 7.5

NOTES:
1. Skid height = 50 feet
2. Vertical distance from bottom of skids to center of rotor = 12.26 feet
3. Dashed lines do not indicate the best data fit, but suggest a general trend from combined data
4. Solid symbols indicate tethered hover

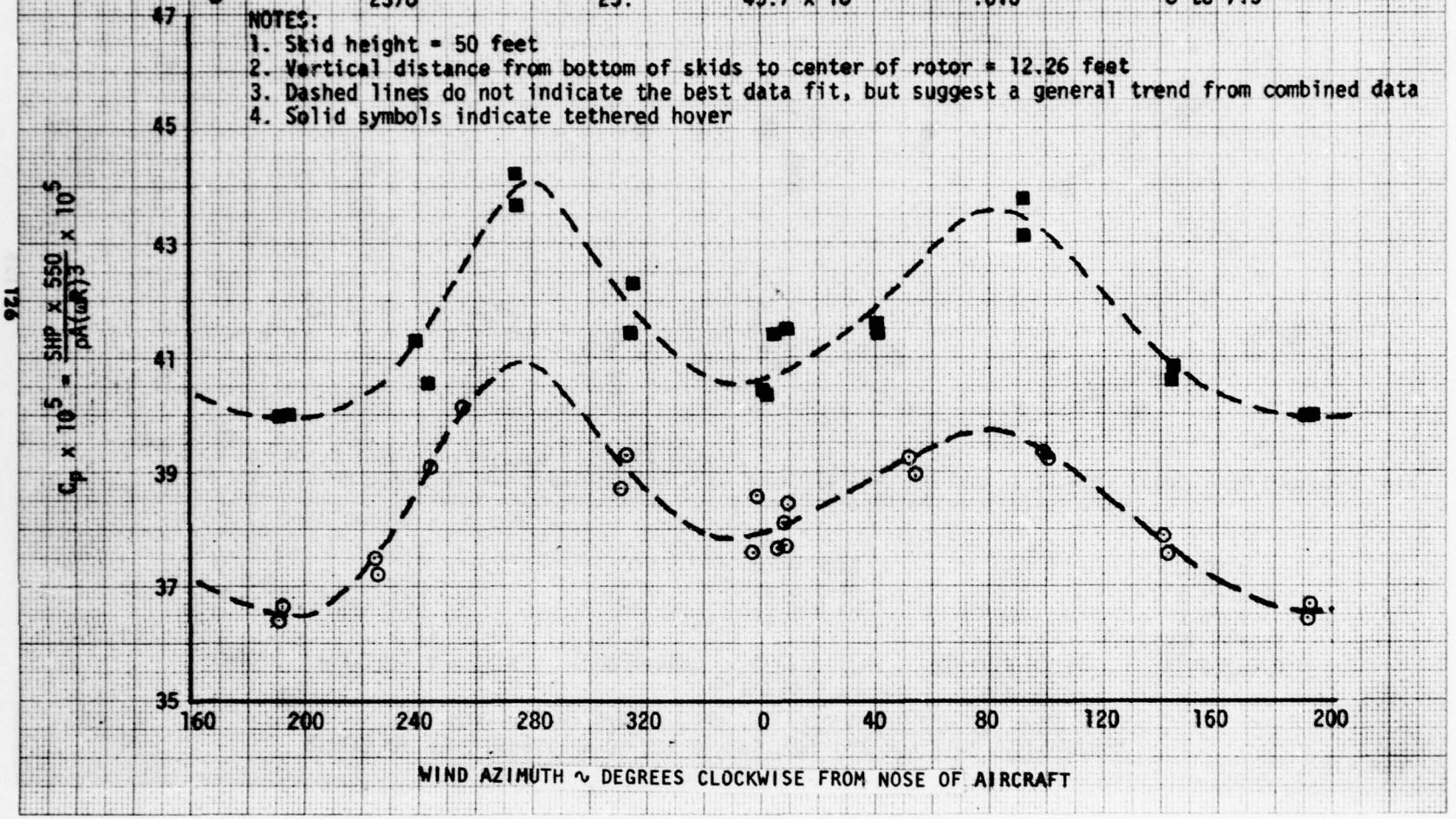

FIGURE 32

EFFECT OF WIND DIRECTION ON NON-DIMENSIONAL OGE HOVERING PERFORMANCE
NUH-1N USA S/N 63-8684 T53-L-13B S/N LE-14420

SYMBOL	PRESSURE ALTITUDE ~ FT	TEMPERATURE ~°C	AVERAGE THRUST COEFFICIENT	AVERAGE ADVANCE RATIO	WIND SPEED RANGE ~ KTAS
□	2410	23.	44.7×10^{-4}	.021	8.5 to 9.5
○	2320	22.	44.4×10^{-4}	.026	10 to 12

NOTES:
1. Skid Height = 50 feet
2. Vertical distance from bottom of skids to center of rotor = 12.26 feet
3. Dashed lines do not indicate the best data fit, but suggest a general trend from combined data
4. Solid symbols indicate tethered hover

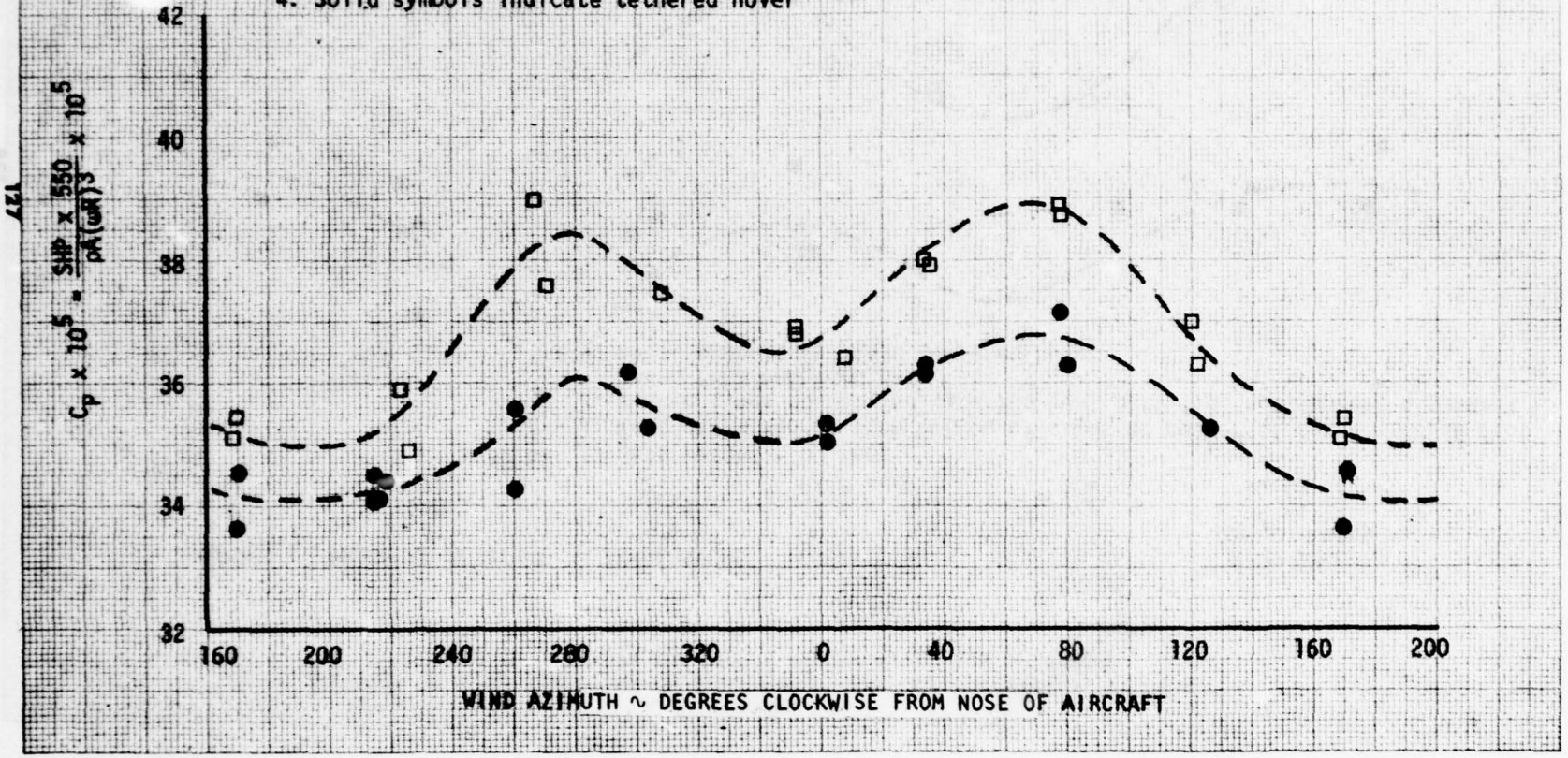

FIGURE 33
EFFECT OF WIND DIRECTION ON NON-DIMENSIONAL OGE HOVERING PERFORMANCE
NUH-1M USA S/N 63-8684 T53-L-13B S/N LE-14420

SYMBOL	PRESSURE ALTITUDE ~ FT	TEMPERATURE ~ °C	AVERAGE THRUST COEFFICIENT	AVERAGE ADVANCE RATIO	WIND SPEED RANGE ~ KTAS
□	4240	13.5	44.5×10^{-4}	.023	8 to 12
○	2320	21.	41.8×10^{-4}	.024	10 to 11

NOTES:
1. Skid Height = 50 feet
2. Vertical distance from bottom of skids to center of rotor = 12.26 feet
3. Dashed lines do not indicate the best data fit, but suggest a general trend from combined data
4. Solid symbols indicate tethered hover

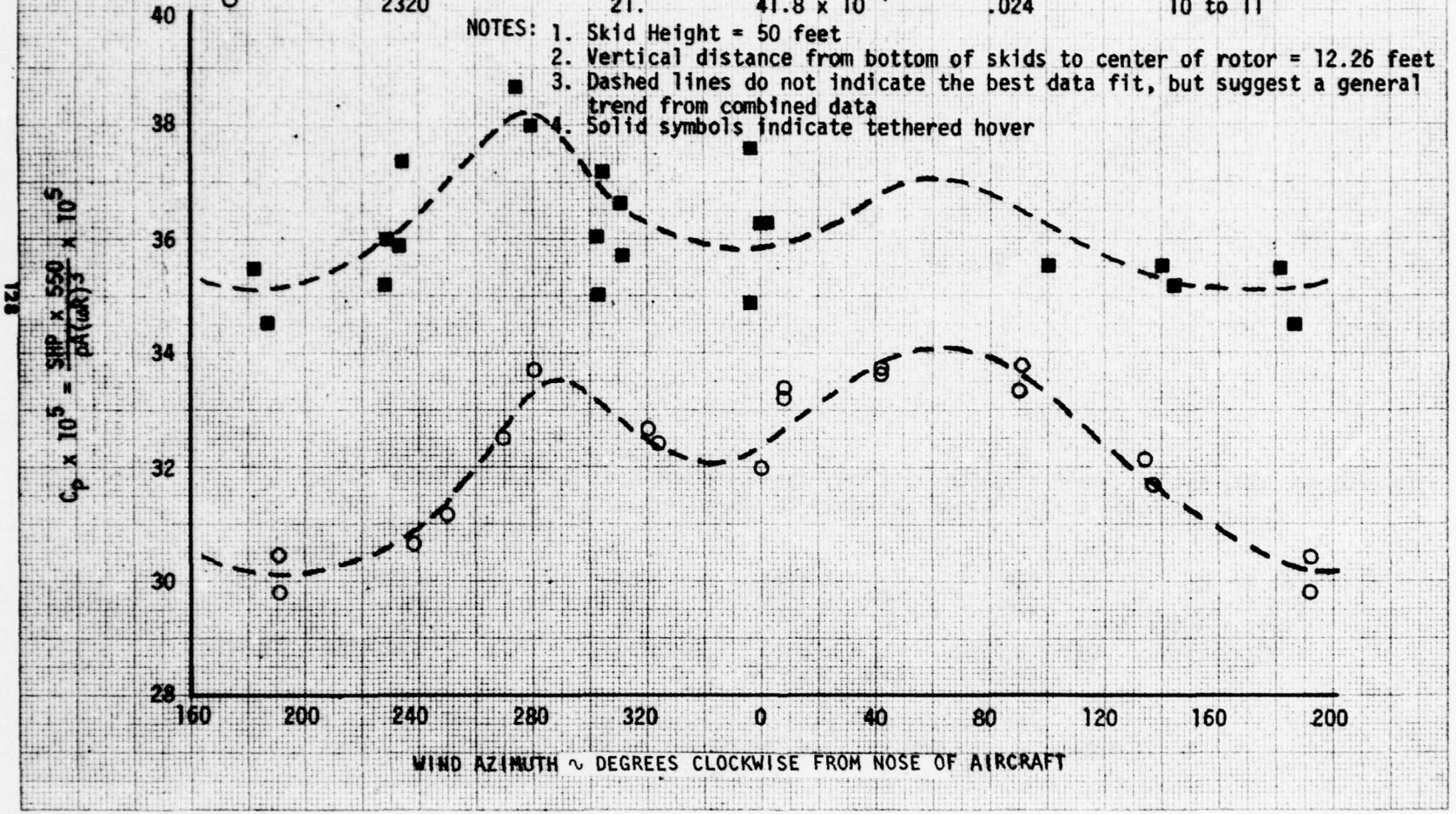

FIGURE 34
EFFECT OF WIND DIRECTION ON NON-DIMENSIONAL OGE HOVERING PERFORMANCE
NUH-1M USA S/N 63-8684 T53-L-13B S/N LE-14420

PRESSURE ALTITUDE ∿ FT	TEMPERATURE ∿°C	AVERAGE THRUST COEFFICIENT	AVERAGE ADVANCE RATIO	WIND SPEED RANGE ∿ KTAS
2340	21.5	37.4×10^{-4}	.039	16 to 19

NOTES:
1. Skid height = 50 feet
2. Vertical distance from bottom of skids to center of rotor = 12.26 feet
3. Dashed lines do not indicate the best data fit, but suggest a general trend from combined data

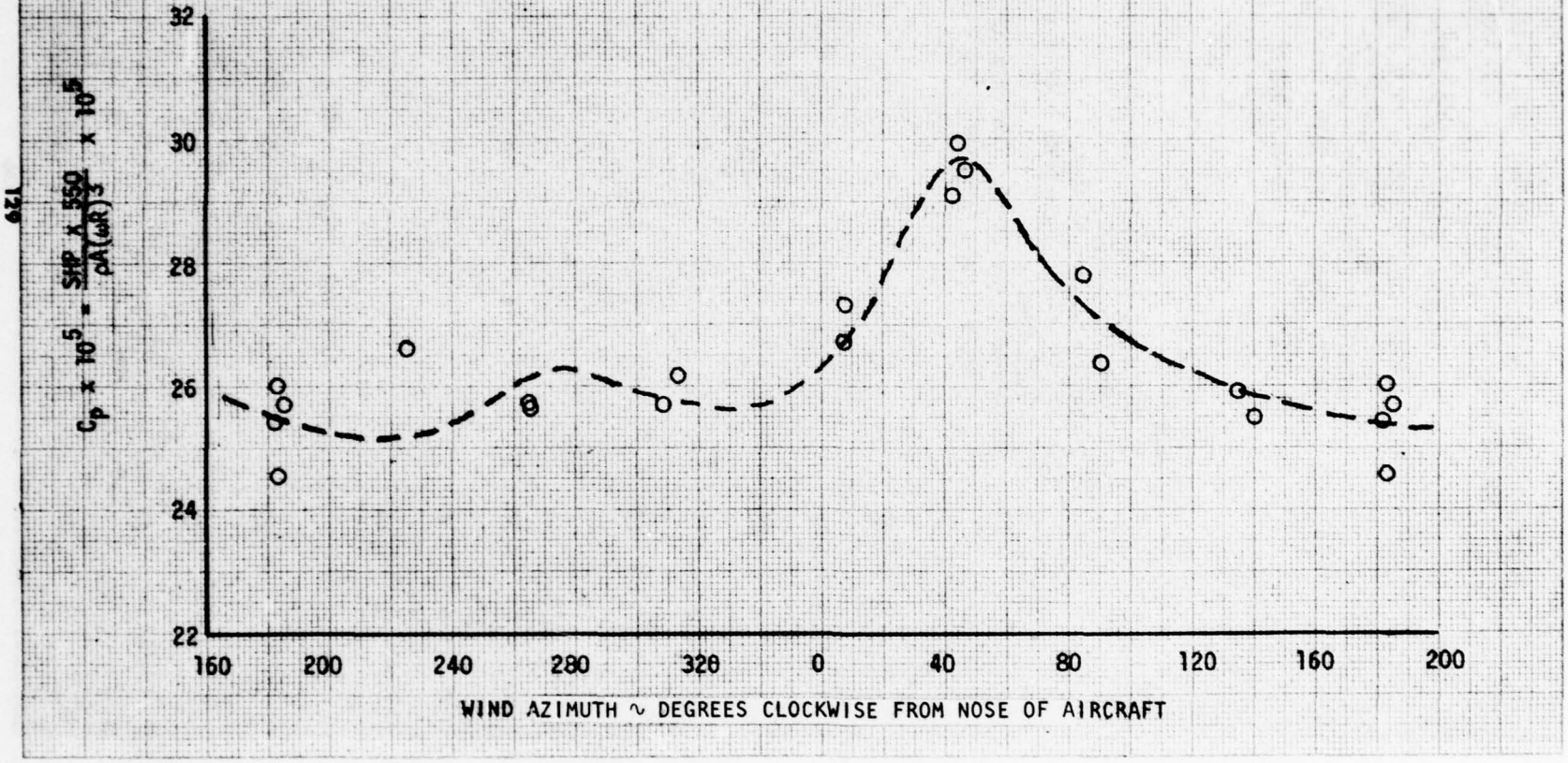

FIGURE 35
SIDESLIP EFFECT ON NON-DIMENSIONAL OGE LEVEL FLIGHT PERFORMANCE
NUH-1M USA S/N 63-8684 T53-L-13B S/N LE-14420

AVERAGE FLIGHT CONDITIONS

THRUST COEFFICIENT = 39.0×10^{-4}
PRESSURE ALTITUDE = 2280 FEET
AMBIENT TEMPERATURE = 15°C
ROTOR SPEED = 324 RPM

SYMBOL	ADVANCE RATIO
□	.020
△	.040
○	.060

NOTES:
1. Airspeed obtained from wind measurement and ground pace vehicle speed
2. Skid height = 50 feet
3. Vertical distance from bottom of skids to center of rotor = 12.26 feet
4. Dashed lines do not indicate the best data fit, but suggest a general trend from combined data.

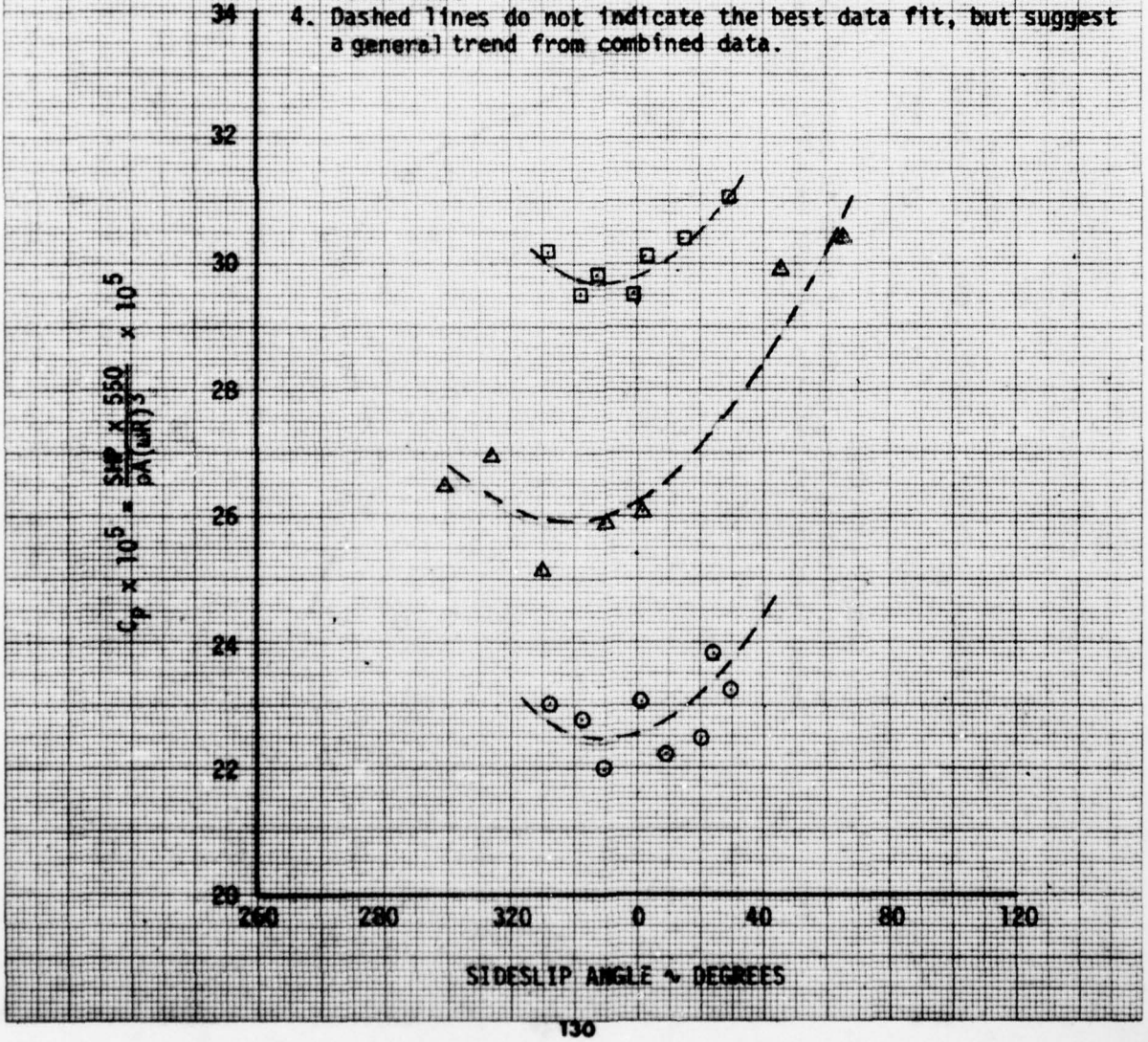

FIGURE 36

NON-DIMENSIONAL DGE PERFORMANCE IN SIDEWARD FLIGHT

NUH-1H USA S/N 63-8684 T53-L-13B S/N LE-14420

SYMBOL	PRESSURE ALTITUDE ~FEET	TEMPERATURE ~°C	THRUST COEFFICIENT
○	2440	23	46.0×10^{-4}
□	2260	19	40.0×10^{-4}

NOTES:
1. Airspeed obtained from wind measurement and ground pace vehicle speed
2. Skid height = 50 feet
3. Vertical distance from bottom of skids to center of rotor = 12.26 feet
4. Rotor speed = 324 rpm

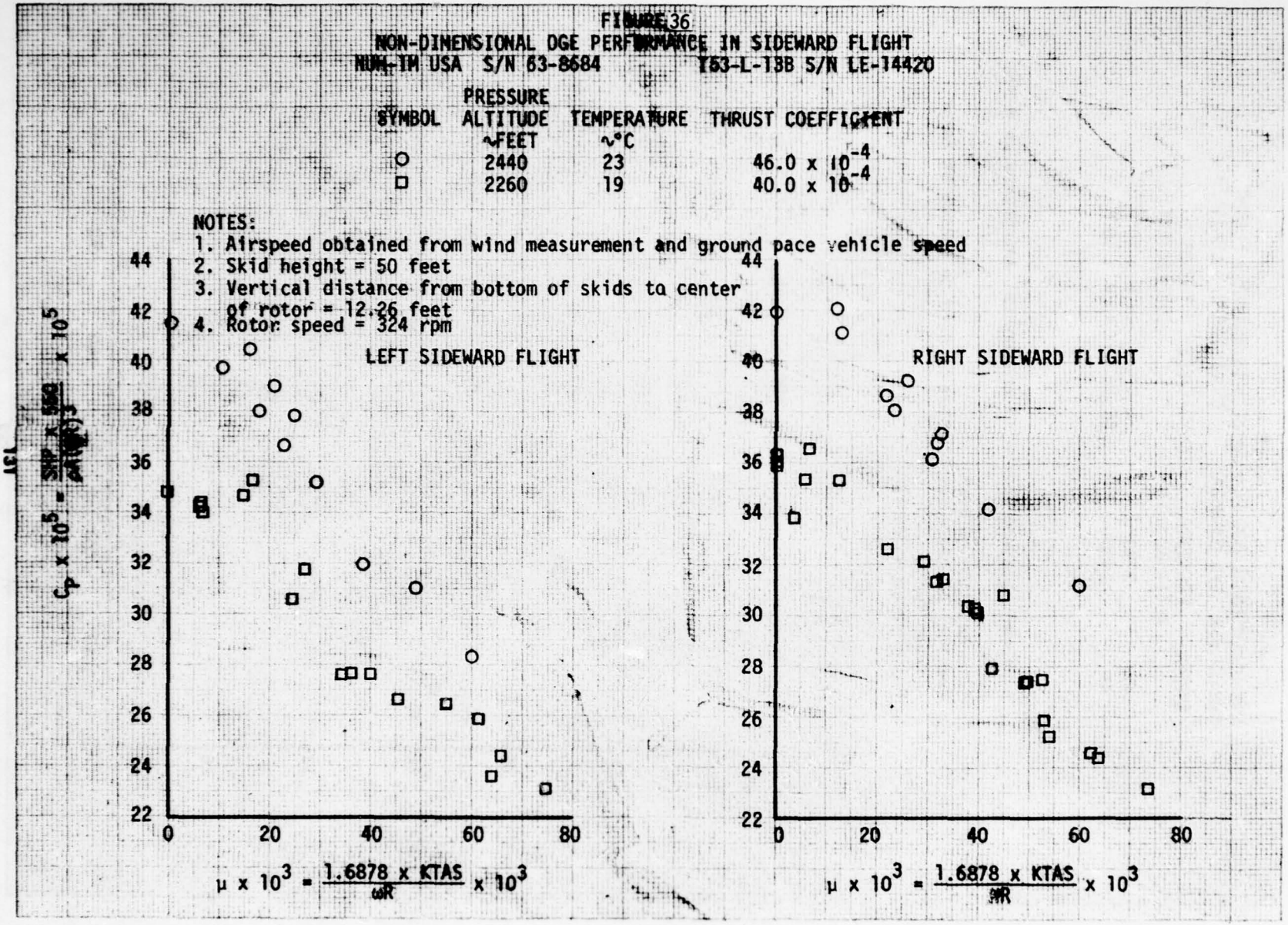

FIGURE 37
NON-DIMENSIONAL OGE PERFORMANCE IN REARWARD FLIGHT
NUH-1H USA S/N 63-8684 T53-L-13B S/N LE-14420

SYMBOL	PRESSURE ALTITUDE ~ FT	TEMPERATURE ~ °C	THRUST COEFFICIENT
○	2290	24.5	40.5×10^{-4}
□	2420	24.5	46.4×10^{-4}

NOTES:
1. Airspeed obtained from wind measurement and ground pace vehicle speed
2. Skid height = 50 feet
3. Vertical distance from bottom of skid to center of rotor = 12.26 feet
4. Rotor speed = 324 rpm

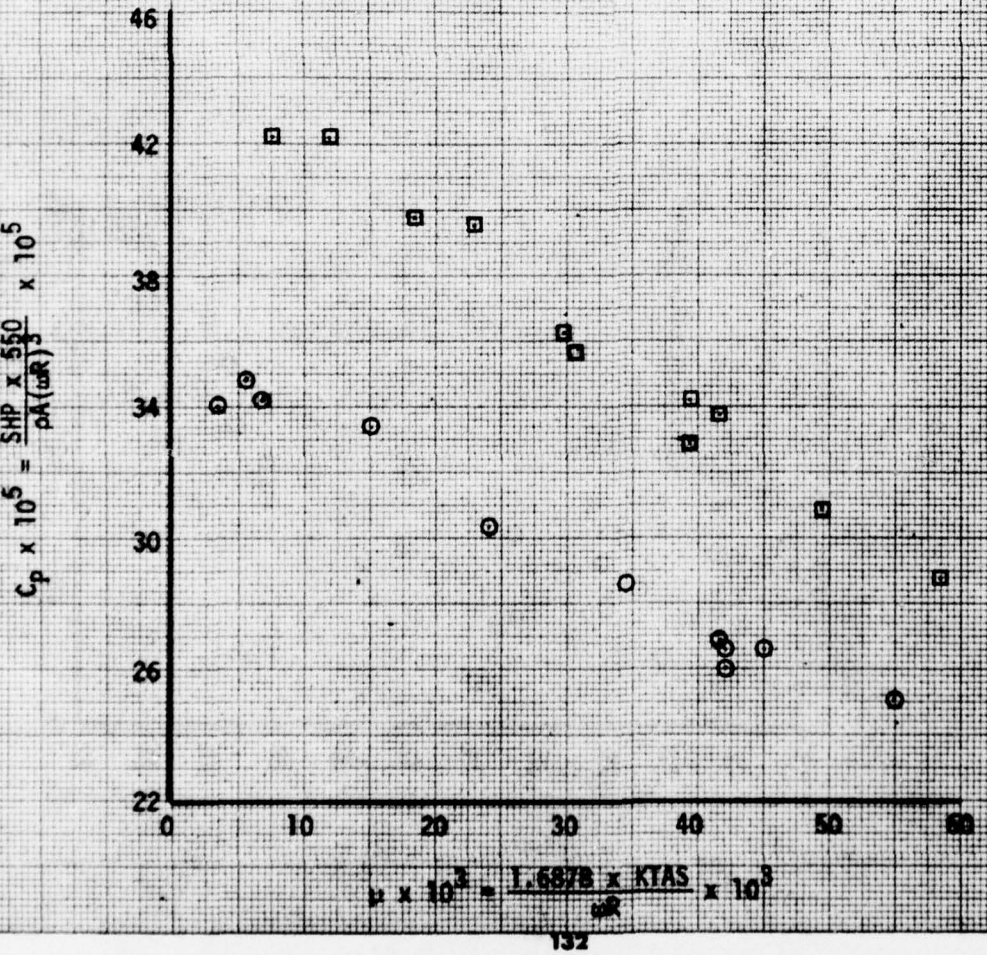

FIGURE 38
RATE OF CLIMB AND CHANGE IN REQUIRED POWER AT LOW AIRSPEED
NUH-1M USA S/N 63-8684 T53-L-13B S/N LE-14420

SYMBOL ADVANCE RATIO x 10^3			PRESSURE ALTITUDE ~FEET	TEMPERATURE ~°C	THRUST COEFFICIENT
0.5 to 8.0	10. to 15.	22. to 23.			
○	□	△	2910	27	40.0×10^{-4}
●	■	▲	2880	28	45.0×10^{-4}

NOTES:
1. Aircraft altitude greater than 500 feet above ground level
2. Rotor speed = 324 rpm
3. See appendix E for function used to calculate power required for zero rate of climb
4. Lines calculated from momentum theory for zero forward airspeed

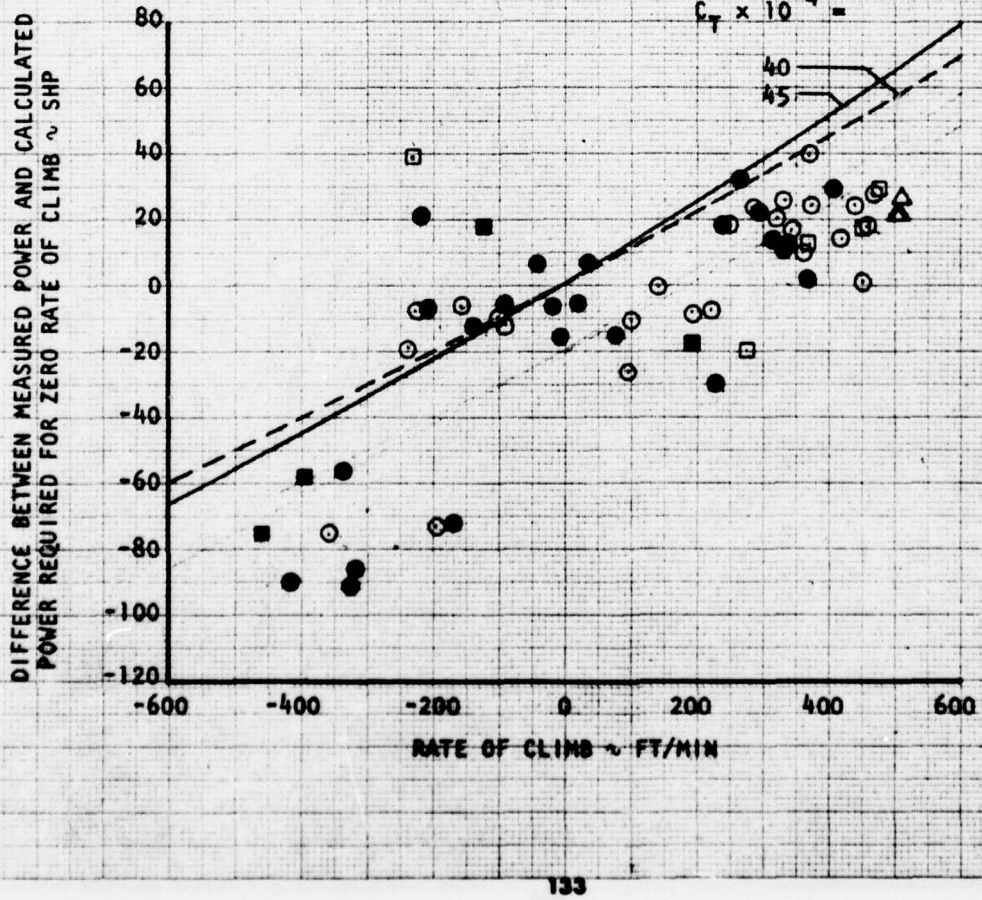

FIGURE 39

SPECIFICATION FUEL FLOW AND THE HELICOPTER LIFT MARGIN SYSTEM FUEL FLOW MODEL

[redacted]-1M
STANDARD DAY

T53-L-13B
6600 OUTPUT SHAFT RPM

NOTES:
1. Solid lines based on Model LTCK-4 Specification 104.33
2. Dashed lines based on [redacted] equation for integrating fuel used as a function of engine torque and pressure ratio

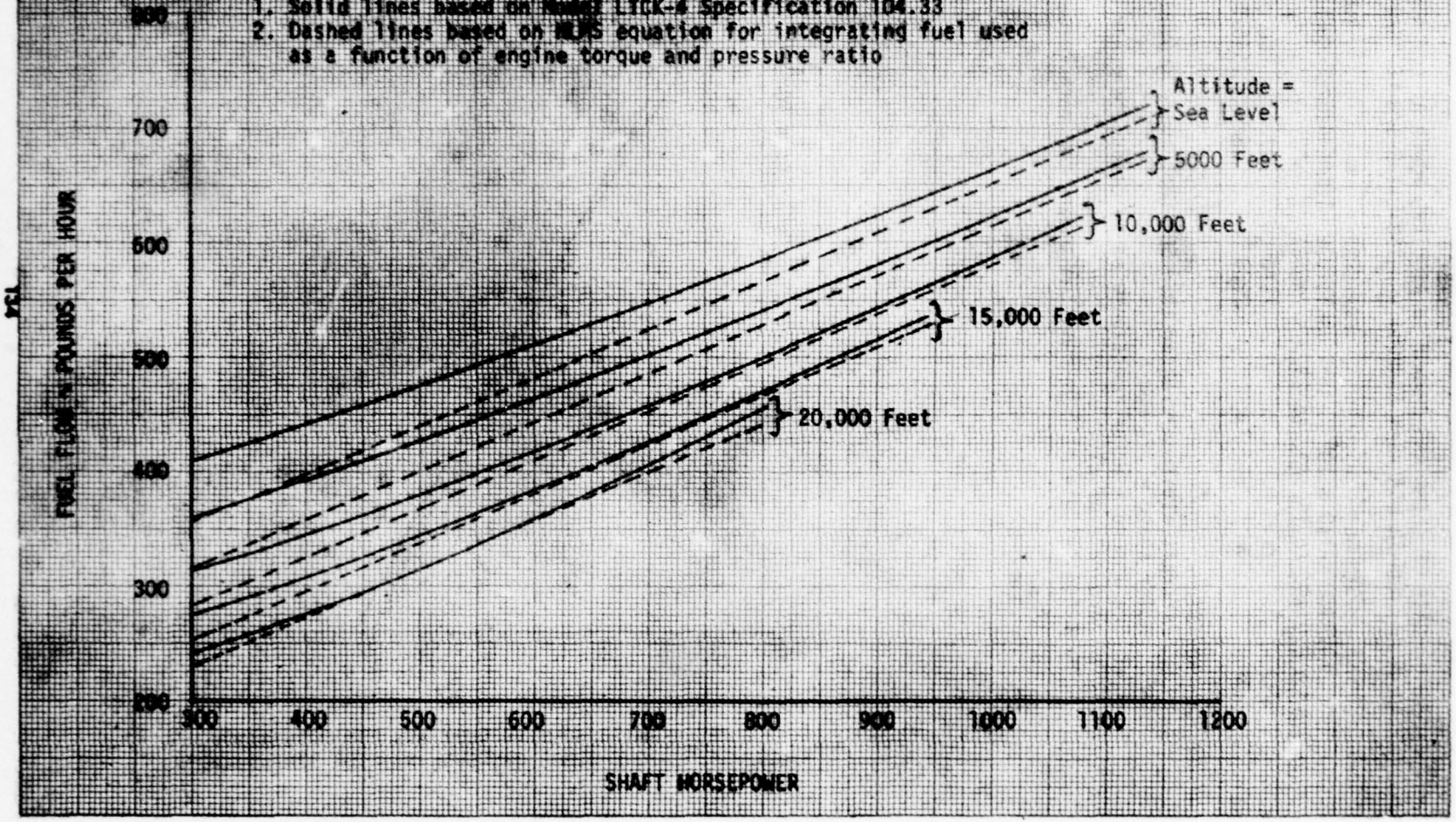

FIGURE 40
MILITARY POWER AVAILABLE
NUH-1M T53-L-13
6600 ENGINE OUTPUT SHAFT RPM

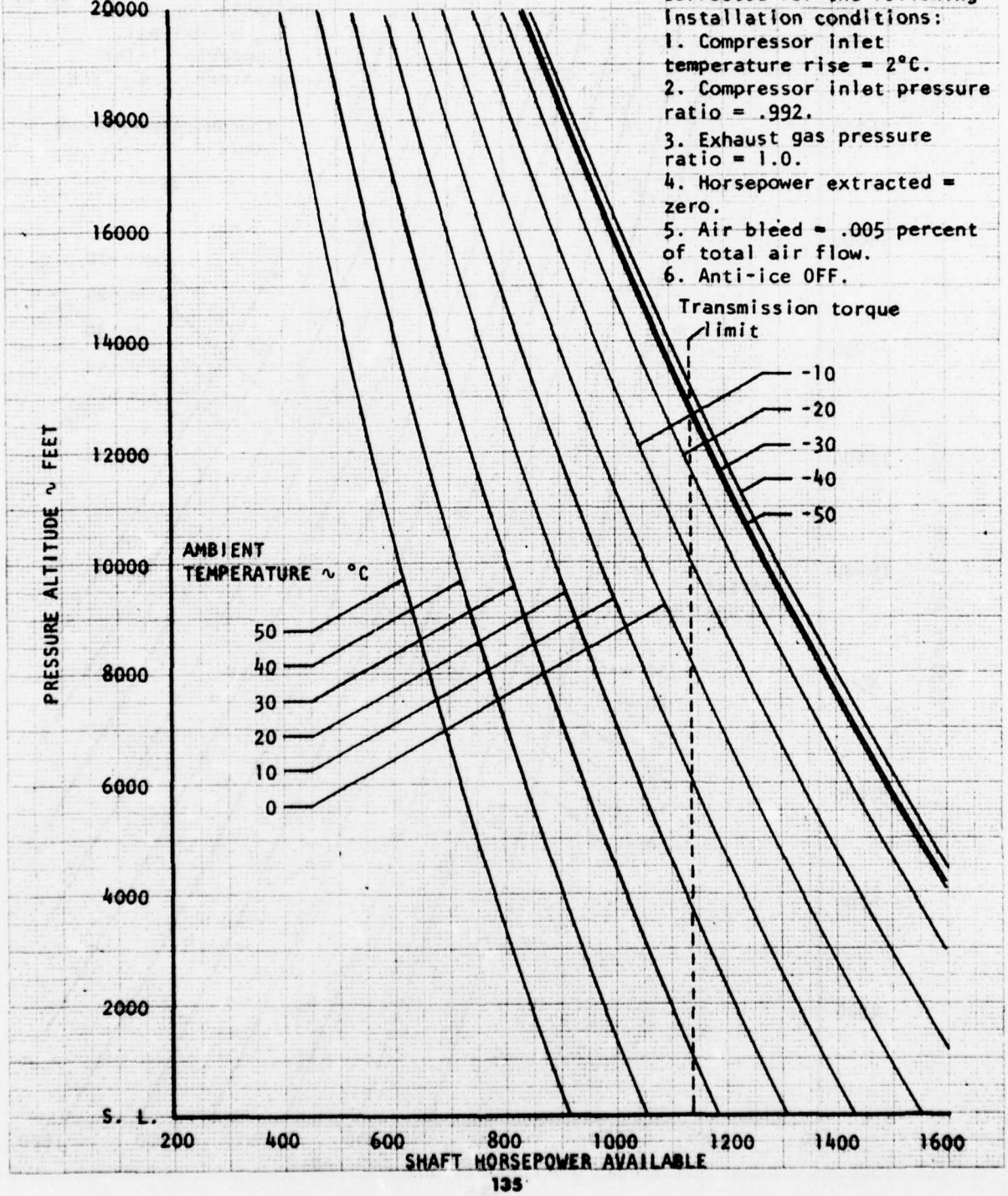

FIGURE 41
MILITARY POWER AVAILABLE
NUH-1M T53-L-13
6600 ENGINE OUTPUT SHAFT RPM

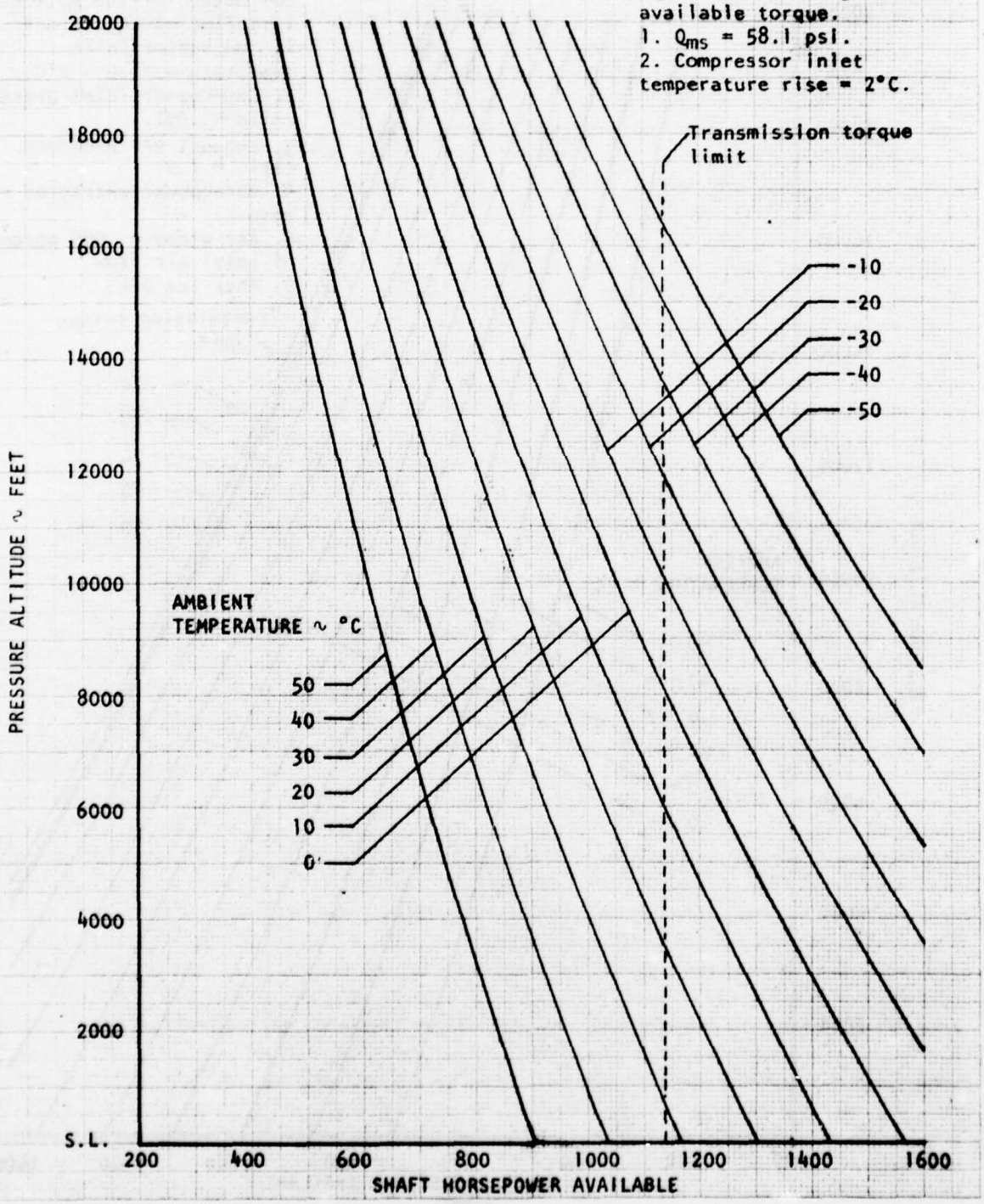

FIGURE 42

MILITARY POWER AVAILABLE

NUH-1H S/N 63-8684 T53-L-13 S/N LE-14420

6603 ENGINE OUTPUT SHAFT RPM

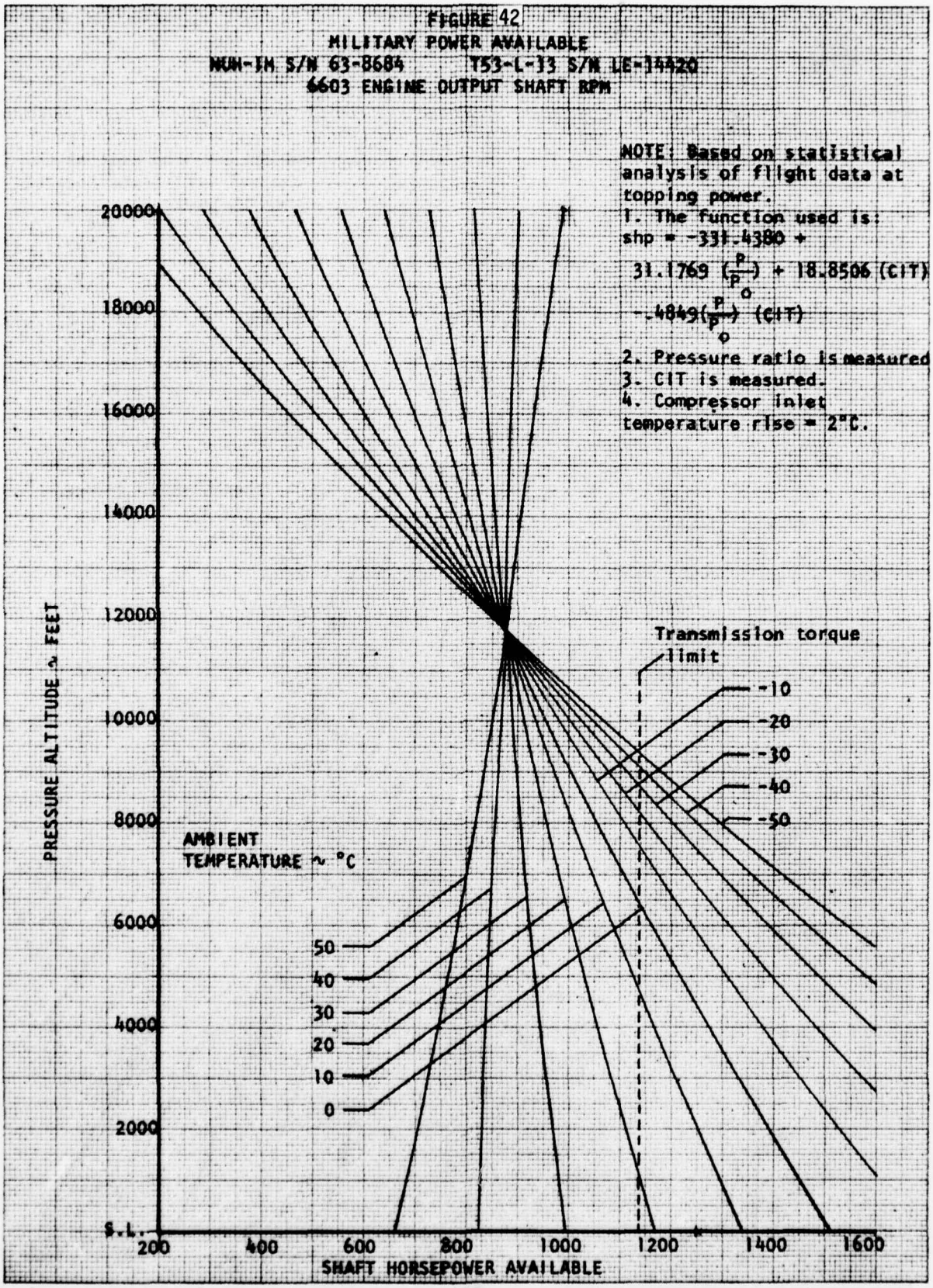

FIGURE 43
MILITARY POWER AVAILABLE
NUH-1H S/N 63-8684 T53-L-13 S/N LE-14420
6603 ENGINE OUTPUT SHAFT RPM

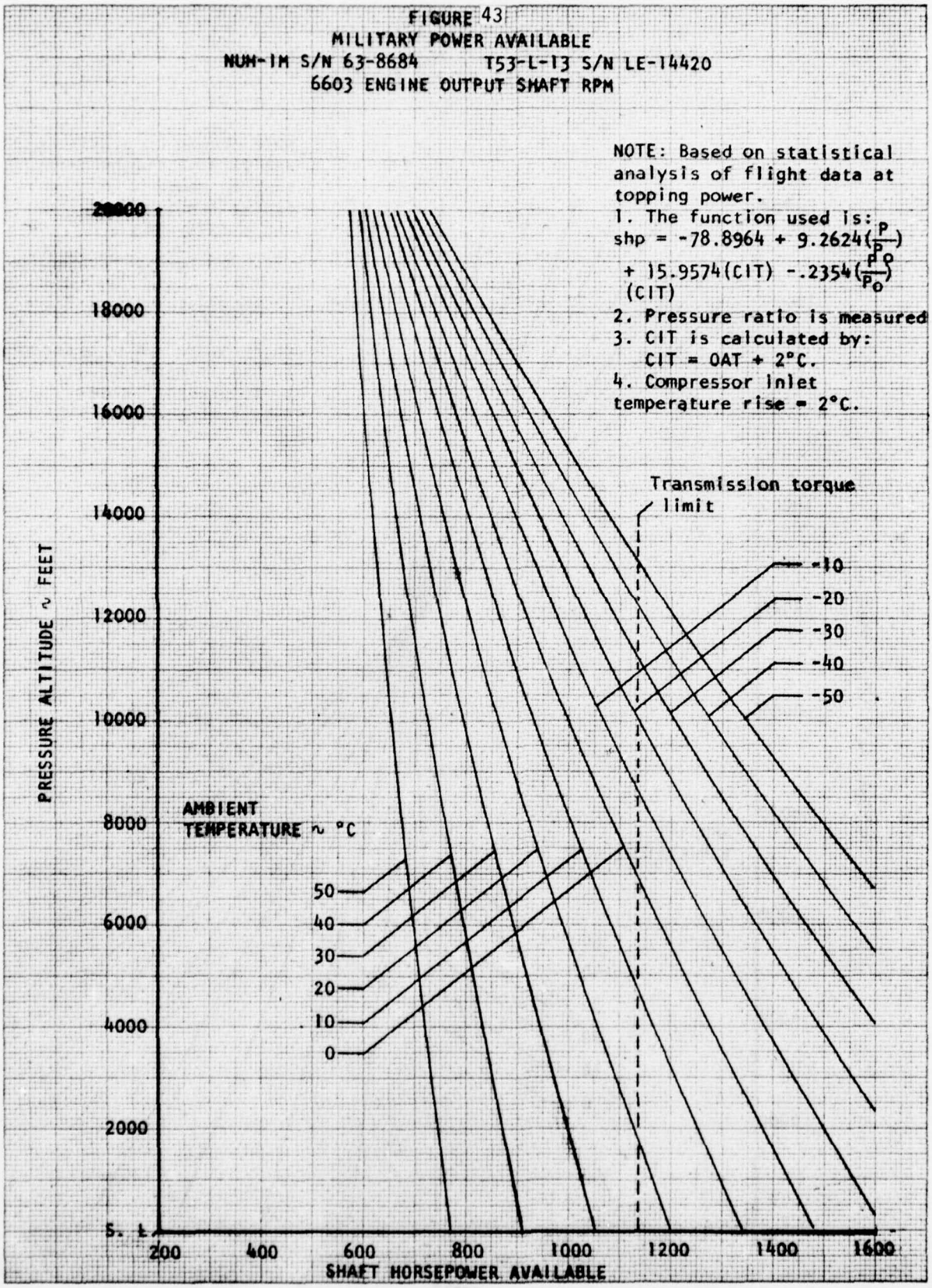

FIGURE 44

MILITARY POWER AVAILABLE

NUH-1M S/N 63-8684 T53-L-13 S/N LE-14420

6603 ENGINE OUTPUT SHAFT SPEED

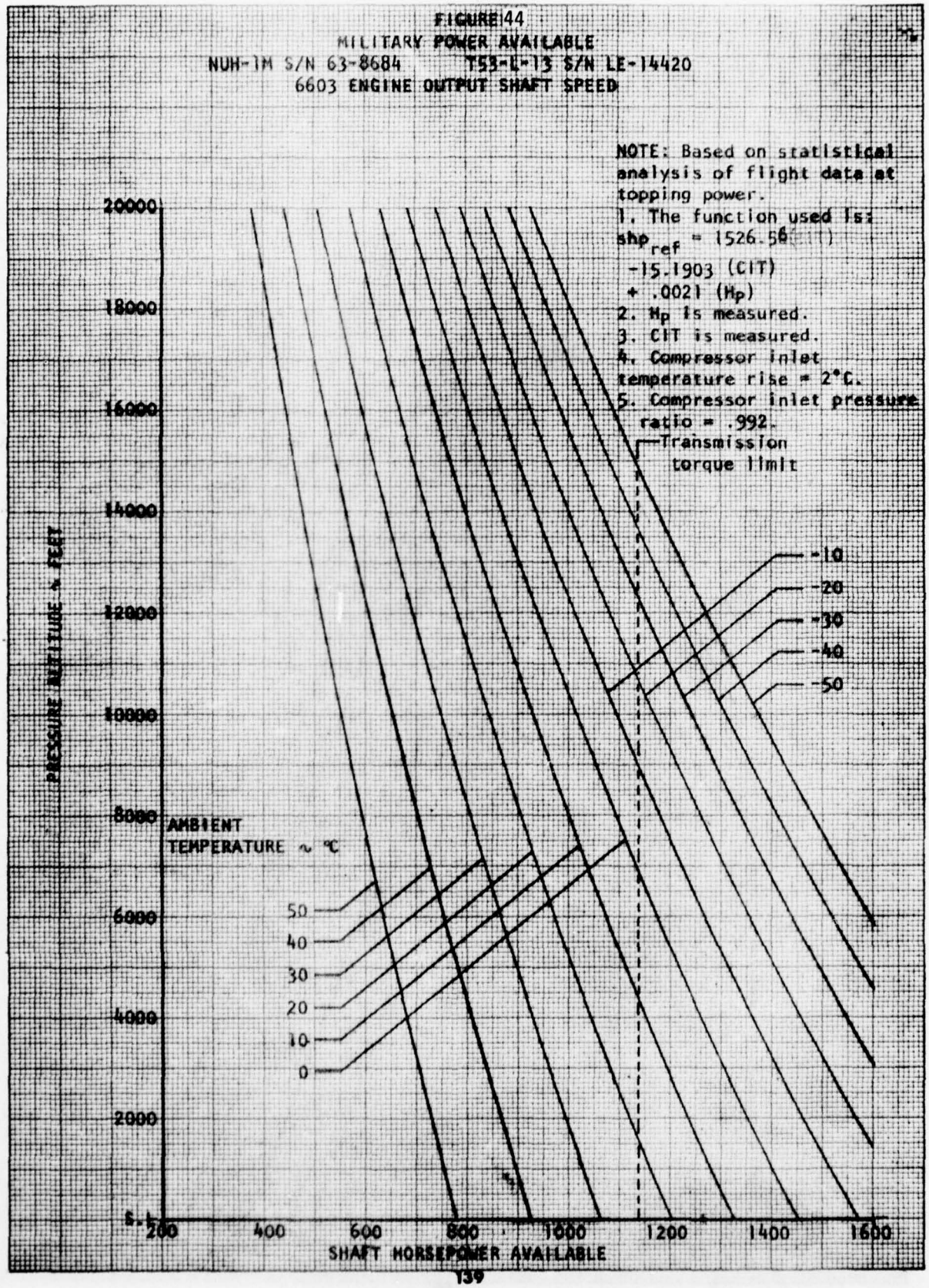

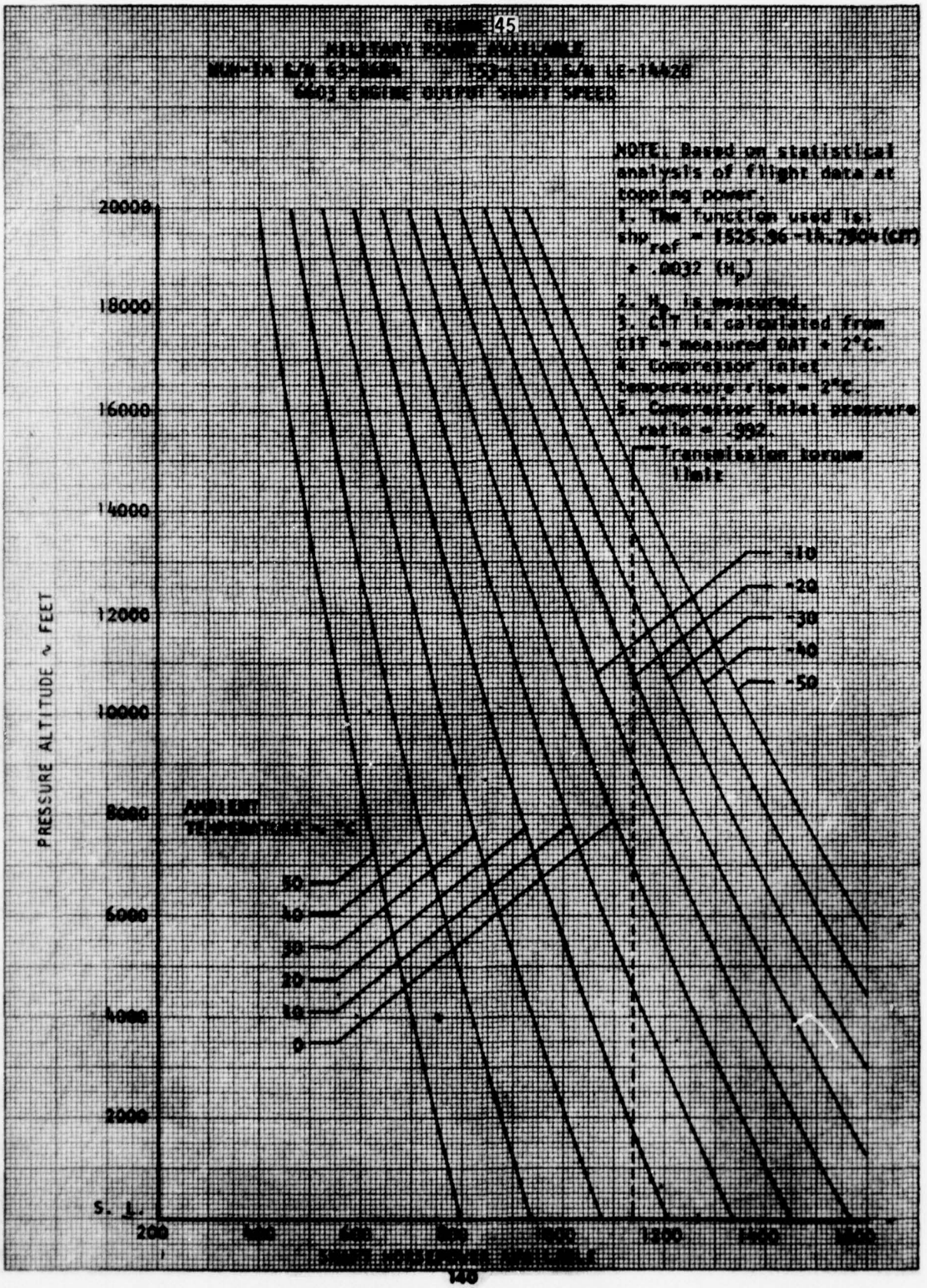
NOTE: Based on statistical analysis of flight data at topping power.
1. The function used is:
shp_ref = 1525.96 -18.290*(Cff) + .0032 (Hp)
2. Hp is measured.
3. CIT is calculated from CIT = measured OAT + 2°C.
4. Compressor inlet temperature rise = 2°C.
5. Compressor inlet pressure ratio = .992.
Transmission torque limit
-10
-20
-30
-40
-50
AMBIENT TEMPERATURE - °C
50
40
30
20
10
0
PRESSURE ALTITUDE - FEET
20000
18000
16000
14000
12000
10000
8000
6000
4000
2000
S. L.
200
1200
1400

FIGURE 46
MILITARY POWER AVAILABLE
NUH-1M S/N 63-8684 T53-L-13 S/N LE-14420
6603 ENGINE OUTPUT SHAFT RPM

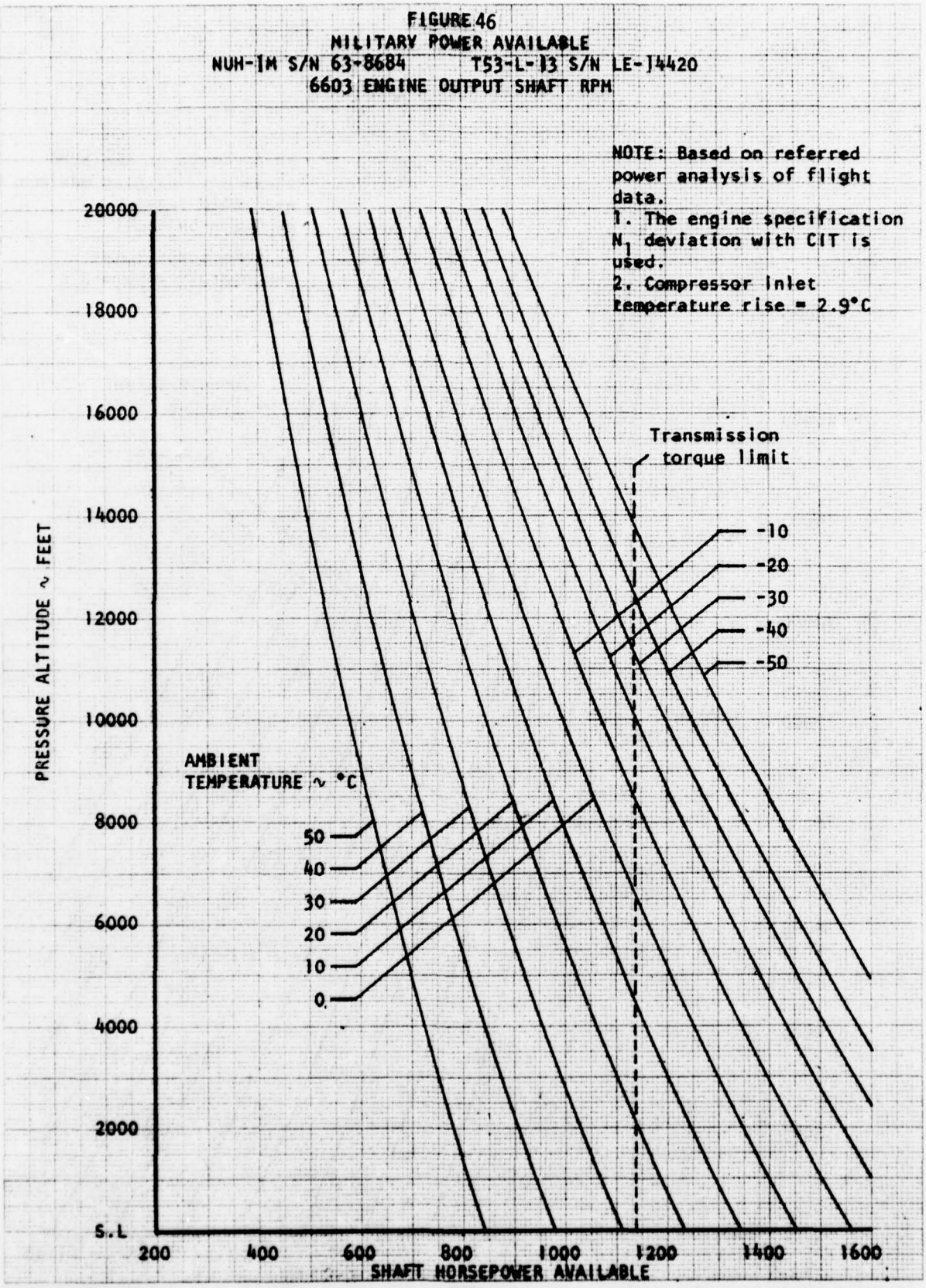

FIGURE 47
MILITARY POWER AVAILABLE
NUH-1H T53-L-13
6600 ENGINE OUTPUT SHAFT RPM

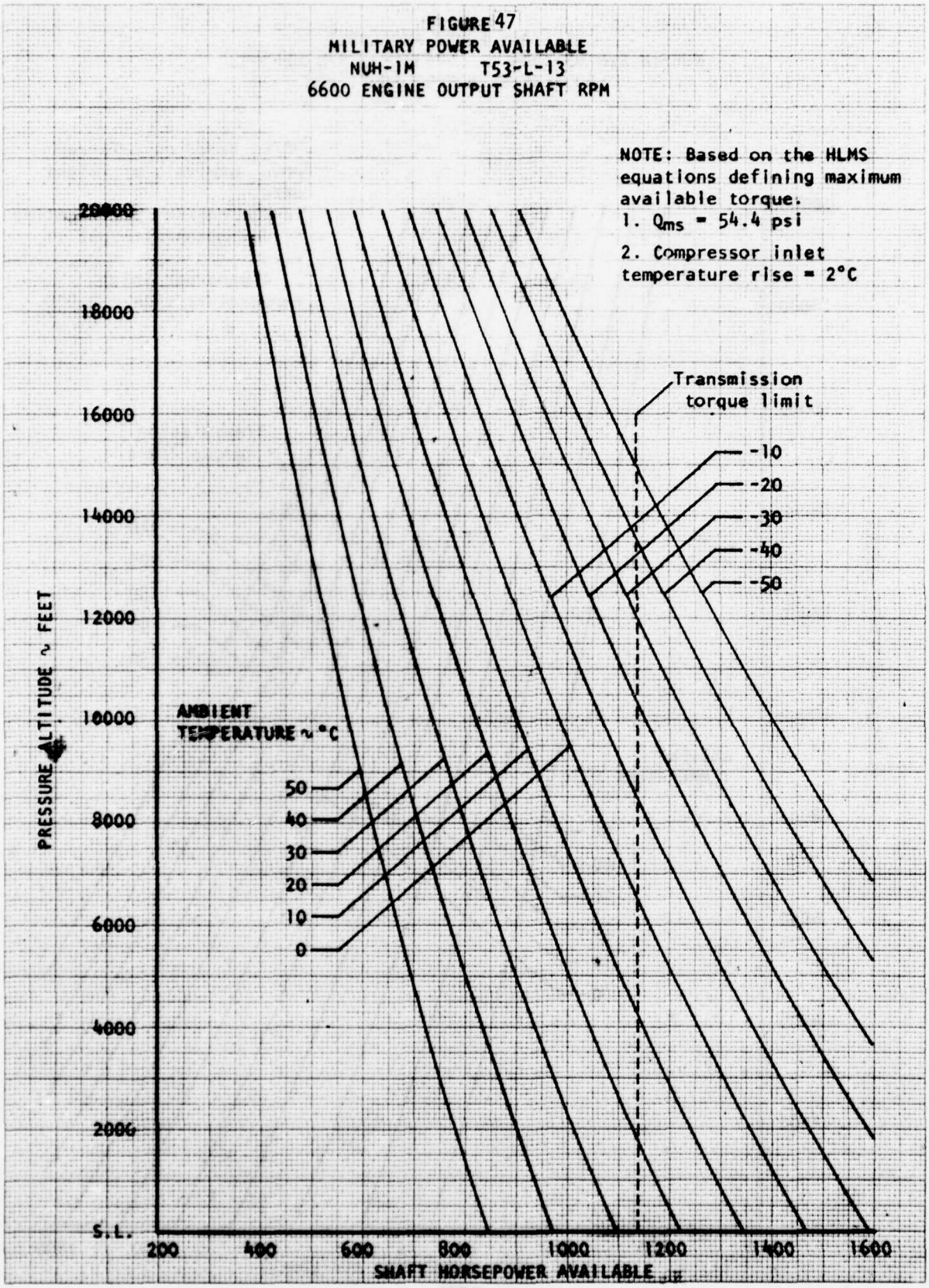

FIGURE 48

REFERRED GAS PRODUCER SPEED AND POWER

NUH-1M USA S/N 63-8684 T53-L-13B S/N LE-14420

PRESSURE ALTITUDE RANGE = -200 to 50 FEET

SYMBOL	TEMPERATURE RANGE ∿ °C
○	5 to 10
□	10 to 15
△	15 to 20
◇	20 to 25

NOTES:

1. 100 percent N_1 = 25,150 rpm
2. Solid line based on the function: $SHP_{ref} = -6579.9 + 79.48\ N_{1_{ref}}$

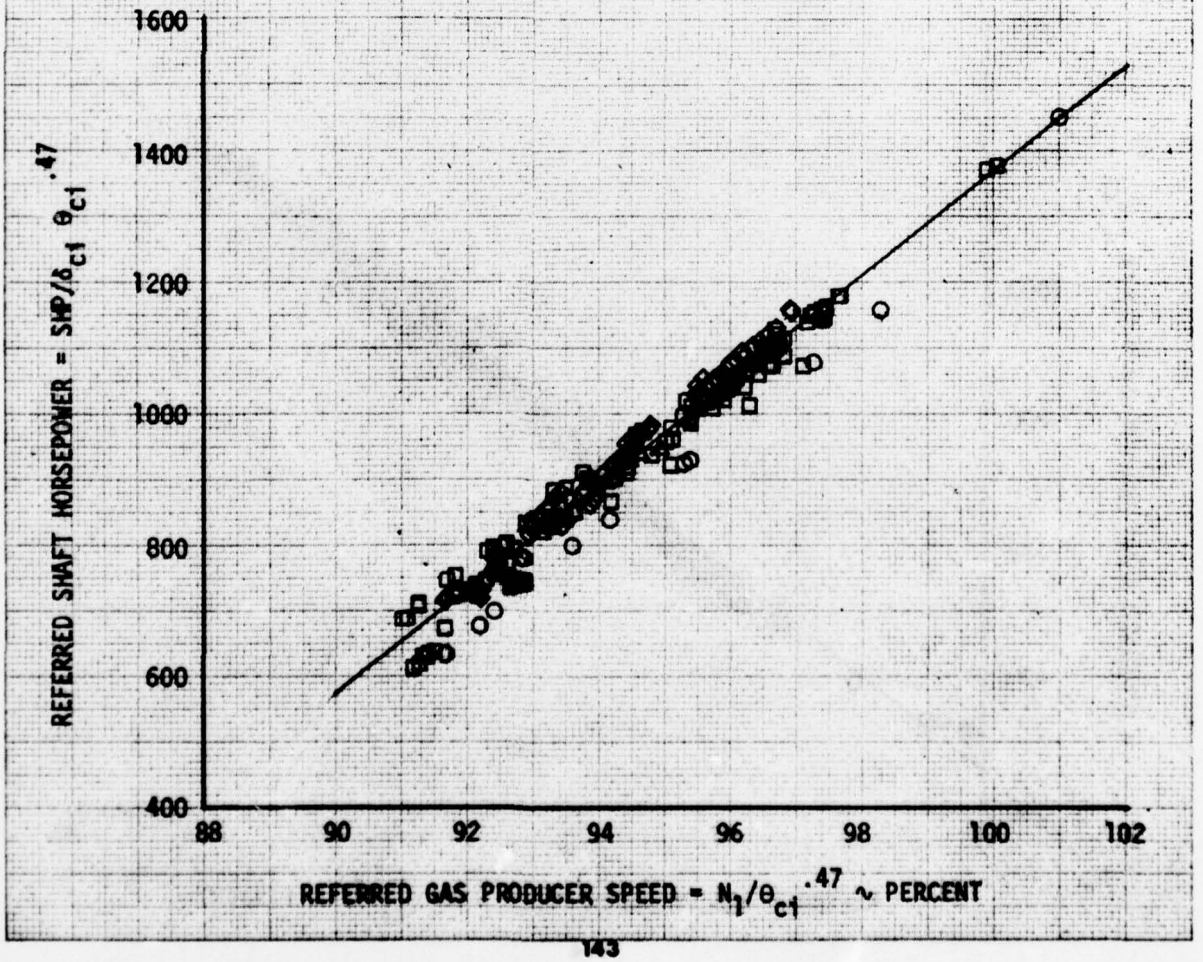

FIGURE 49
REFERRED GAS PRODUCER SPEED AND POWER
NUH-1M USA S/N 68-8684 T53-L-13B S/N LE-14420

PRESSURE ALTITUDE RANGE = 2200 to 2500 FEET

SYMBOL	TEMPERATURE RANGE ∿ °C
○	10 to 15
□	15 to 20
△	20 to 25
◇	25 to 30

NOTES:
1. 100 percent N_1 = 25,150 rpm
2. Solid line based on the function: $SHP_{ref} = -6579.9 + 79.48\ N_{1_{ref}}$

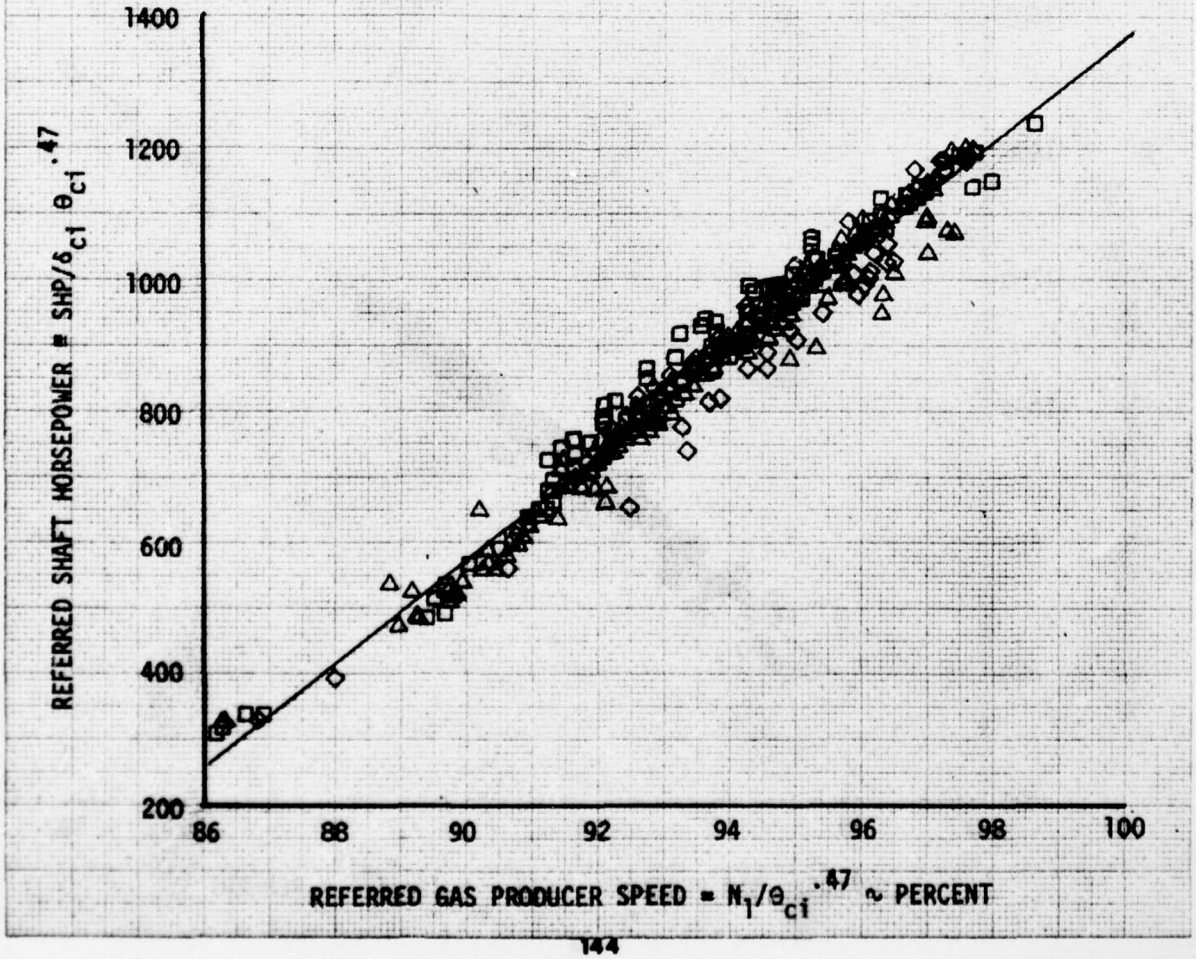

FIGURE 50
REFERRED GAS PRODUCER SPEED AND POWER
NUH-1M USA S/N 68-8684 T53-L-13B S/N LE-14420
PRESSURE ALTITUDE RANGE = 3950 to 4250 FEET

SYMBOL	TEMPERATURE RANGE ~ °C
○	5 to 0
□	0 to 5
△	5 to 10
◇	10 to 15
▷	15 to 20

NOTES:
1. 100 percent N_1 = 25,150 rpm
2. Solid line based on the function: $SHP_{ref} = -6579.9 + 79.48\ N_{1_{ref}}$

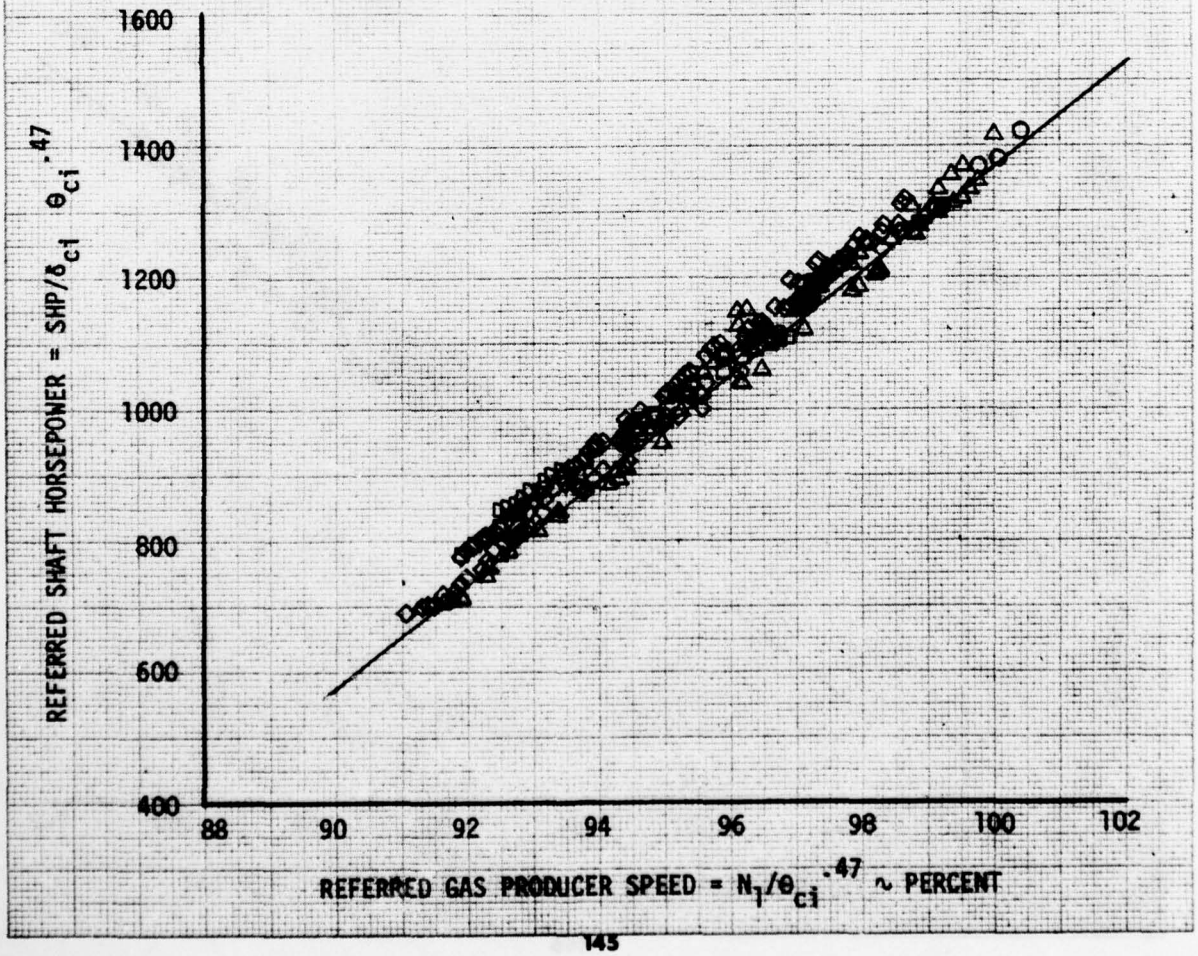

FIGURE 51
REFERRED GAS PRODUCER SPEED AND POWER
NUH-1M USA S/N 63-8684 T53-L-13B S/N LE-14420

PRESSURE ALTITUDE RANGE = 9300 to 9650 FEET

SYMBOL	TEMPERATURE RANGE ~ °C
○	-5 to 0
□	0 to 5
△	5 to 11

NOTES:
1. 100 percent N_1 = 25,150 rpm
2. Solid line based on the function $SHP_{ref} = -6579.9 + 79.48N_{1ref}$

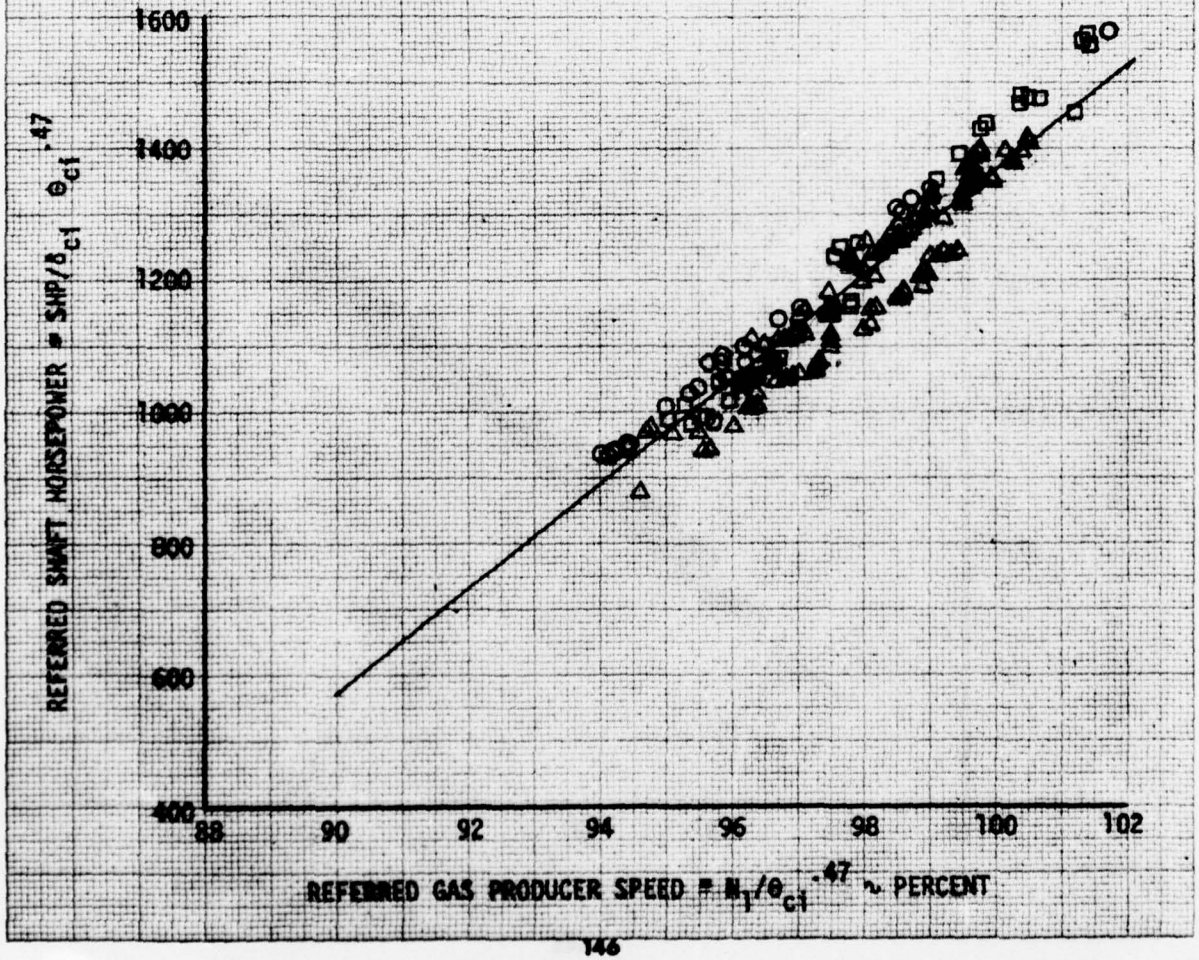

FIGURE 52
DEVIATION IN REGULATED GAS PRODUCER SPEED
(N_1 TOPPING SPEED)

NUM-1M USA S/N 63-8684 T53-L-13B S/N LE-14420

NOTES:
1. 100 percent N_1 = 25,150 rpm
2. Curve obtained from engine manufacturer
3. Test engine zero gas producer speed deviation corresponds to 99.5 percent of N_1
4. Compressor inlet temperature values calculated from CIT = OAT + 2.9

SYMBOL	PRESSURE ALTITUDE RANGE ~ FT
○	2220 to 2340
□	3950 to 4200
⬭	4700 to 5400
◇	5700 to 5900
▱	6000 to 6250
△	6700 to 7100
◿	7800 to 8200
▲	9370 to 9440

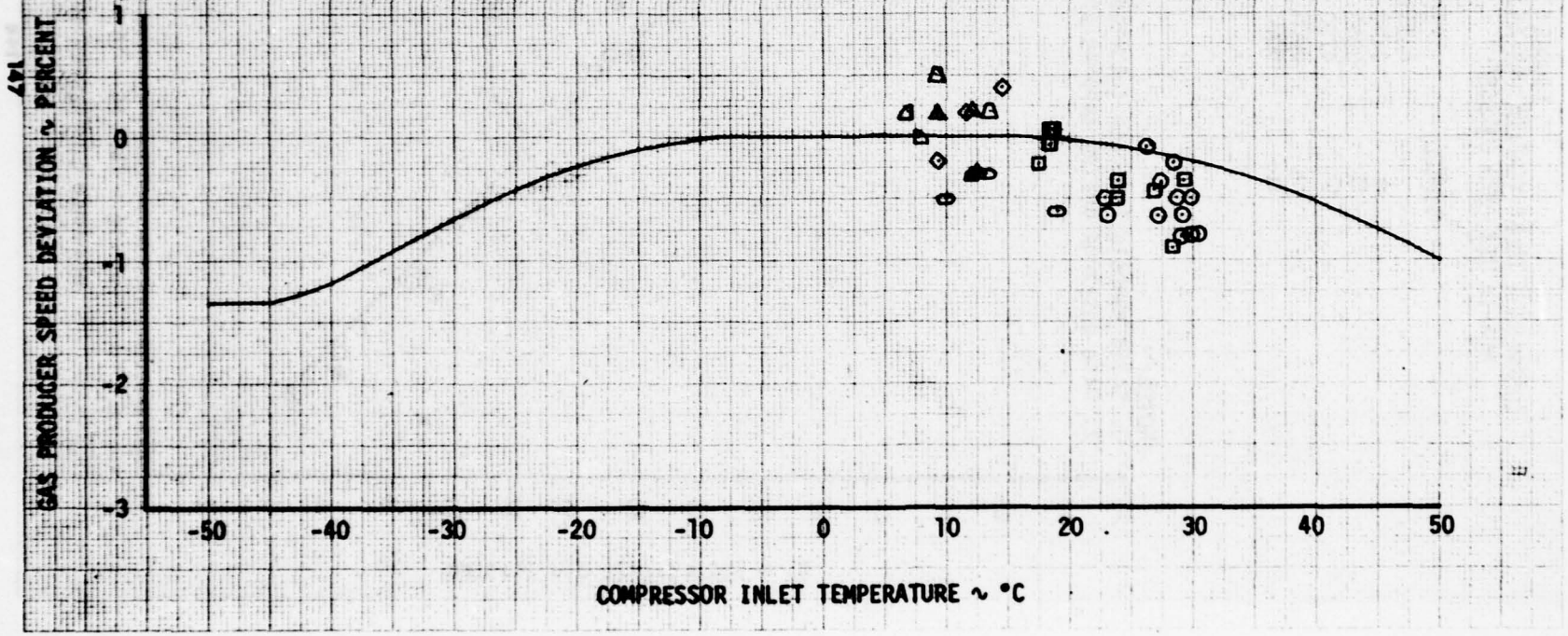

FIGURE 53
COMPRESSOR INLET TEMPERATURE AND OUTSIDE AIR TEMPERATURE
NUH-1H USA S/N 63-8684 T53-L-13B S/N LE-14420

SYMBOL	PRESSURE ALTITUDE ~ FT
△	2200 to 2340
□	3950 to 4200
○	4700 to 6000
◇	6000 to 8000
▷	8000 to 10,000

NOTES:
1. Solid symbols indicate tethered hover
2. Data obtained during topping power conditions

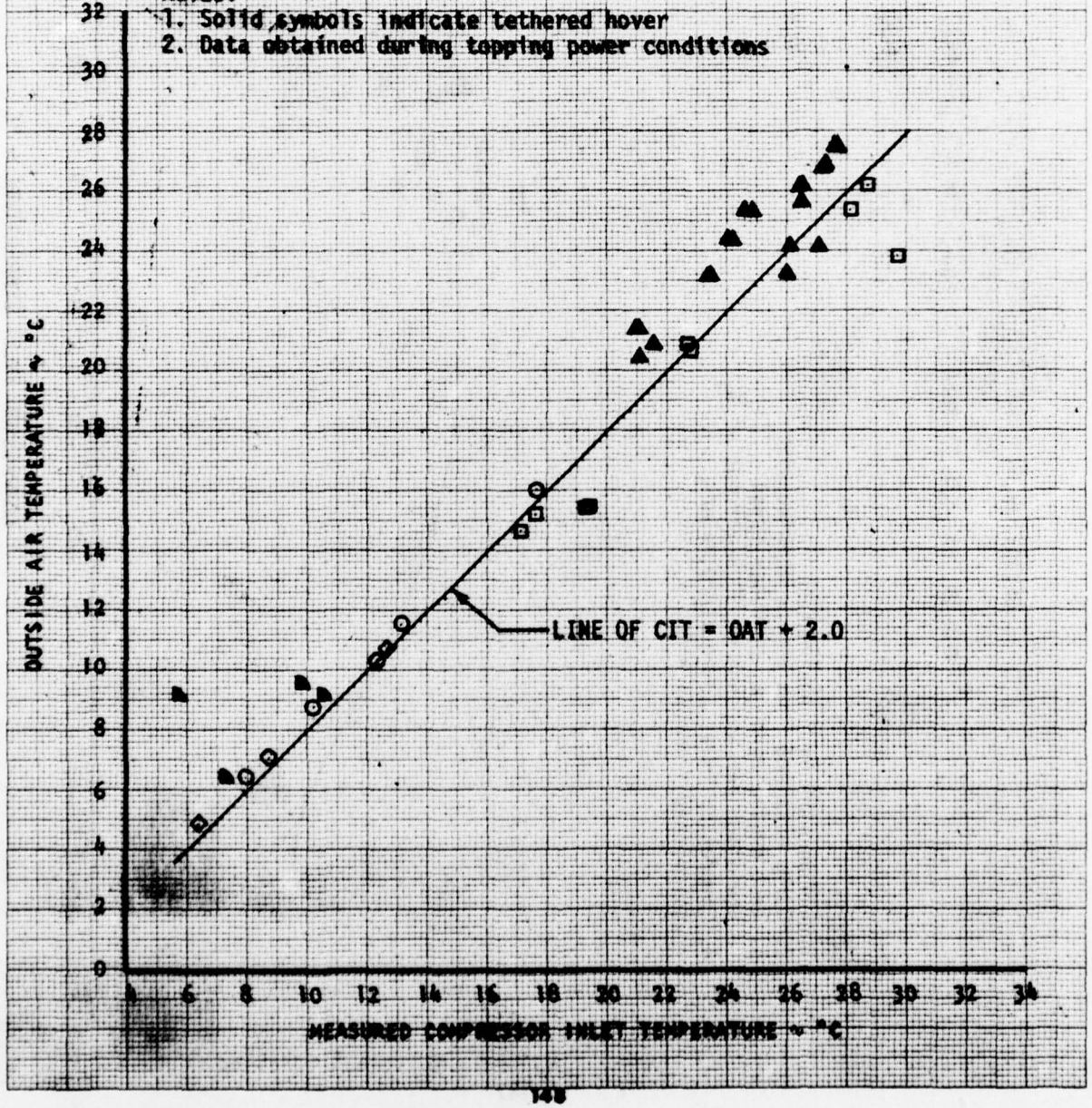

FIGURE 54
COMPRESSOR INLET TEMPERATURE AND OUTSIDE AIR TEMPERATURE
NUH-1M USA S/N 63-8684 T53-L-13B S/N LE-14420

SYMBOL	PRESSURE ALTITUDE RANGE ~ FT
△	5000 to 7000
□	7000 to 9000
◇	9000 to 11,000
○	11,000 to 13,000

NOTES:
1. MEASURED CIT CORRECTED BY $CIT_{total} = CIT_{measured} + (1-K) V^2_{T_{ci}} /7592.1$
2. DATA OBTAINED DURING OGE LEVEL FLIGHT
MEASURED CIT CORRECTED USING K = 0.5
1.0

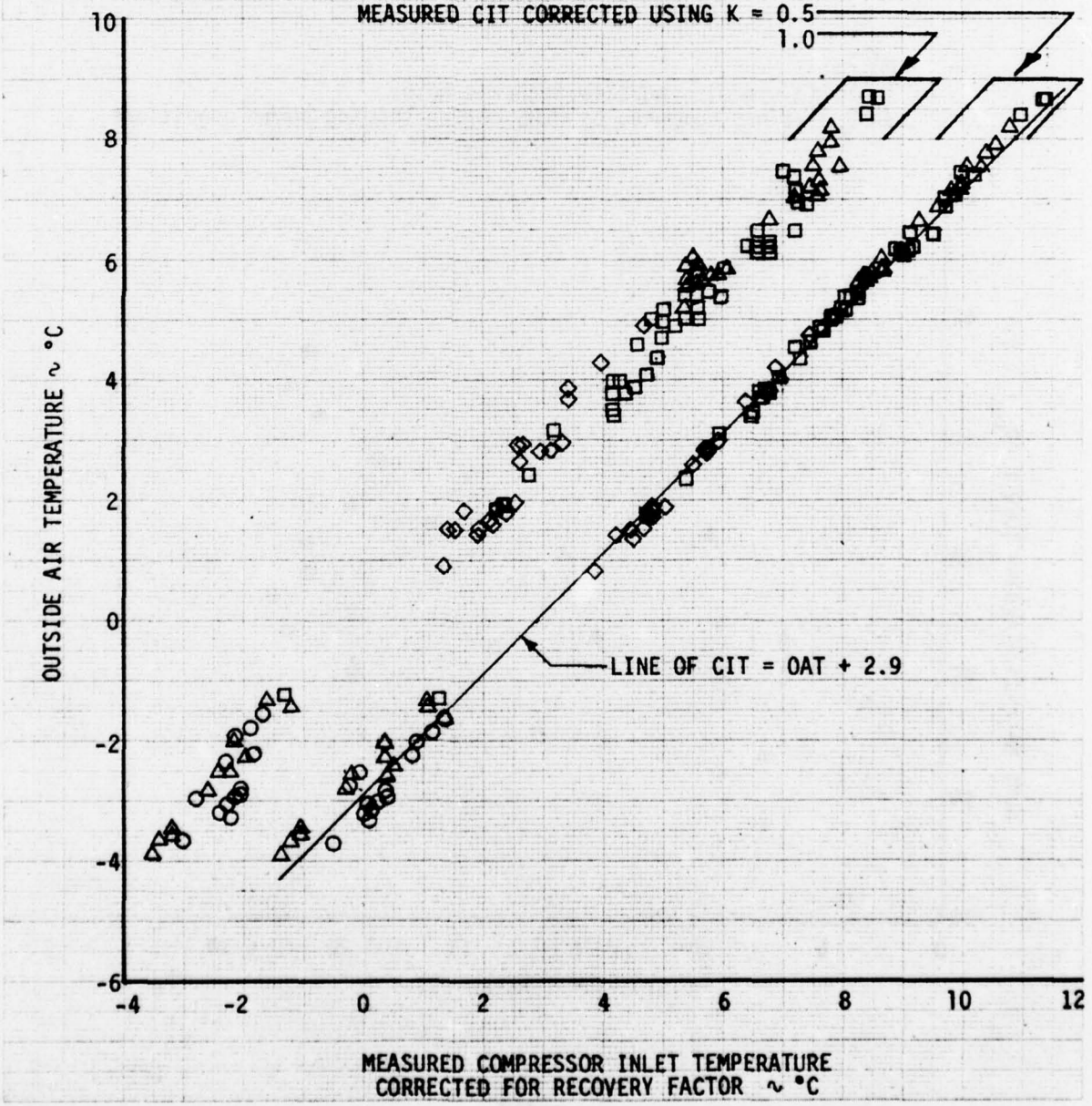

FIGURE 55

HELICOPTER LIFT MARGIN SYSTEM MAXIMUM STANDARD TORQUE COMPUTED AT TOPPING POWER

NUH-1M USA S/N 63-8684 T53-L-13B S/N LE-14420

SYMBOL	PRESSURE ALTITUDE RANGE ~ FT
○	2220 to 2340
□	3950 to 4200
⬭	4700 to 5400
◇	5700 to 5900
◺	6000 to 6250
△	6700 to 7100
◿	7800 to 8200
▲	9370 to 9440

NOTES:

1. Solid symbols indicate tethered hover
2. Q_{ms} values computed by HLMS during topping power conditions.

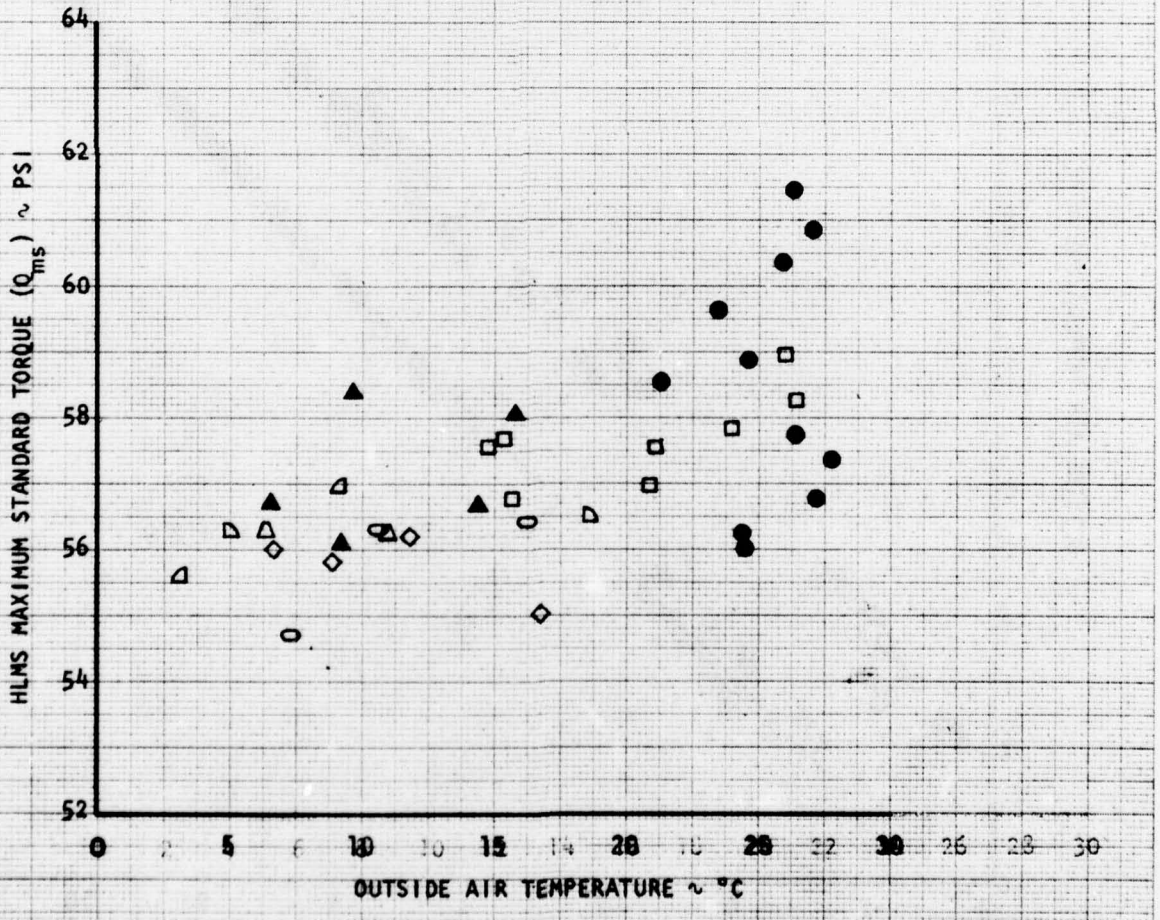

FIGURE 56
HELICOPTER LIFT MARGIN SYSTEM ALTITUDE MEASUREMENT
NUH-1M USA S/N 63-8684 T53-L-13B S/N LE-14420

SYMBOL	TEMPERATURE RANGE ~ °C
○	0 to 5
▱	5 to 10
□	10 to 15
◇	15 to 20
△	20 to 25
○	25 to 30

NOTES:
1. Solid symbols indicate tethered hover
2. Data obtained during topping power conditions

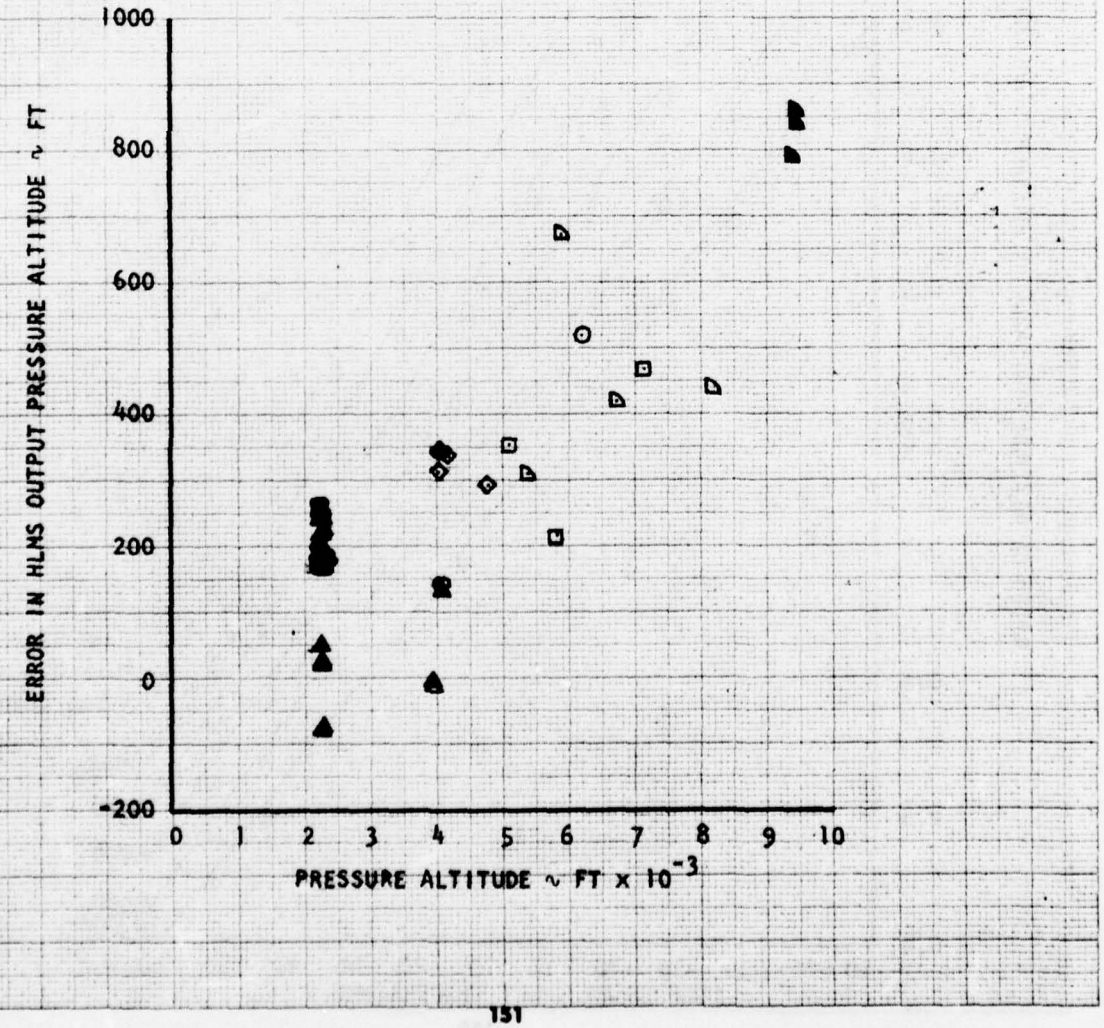

FIGURE 57
HELICOPTER LIFT MARGIN SYSTEM RATIO OF MAXIMUM AVAILABLE TO MAXIMUM STANDARD TORQUE
NUH-1M T53-L-13B

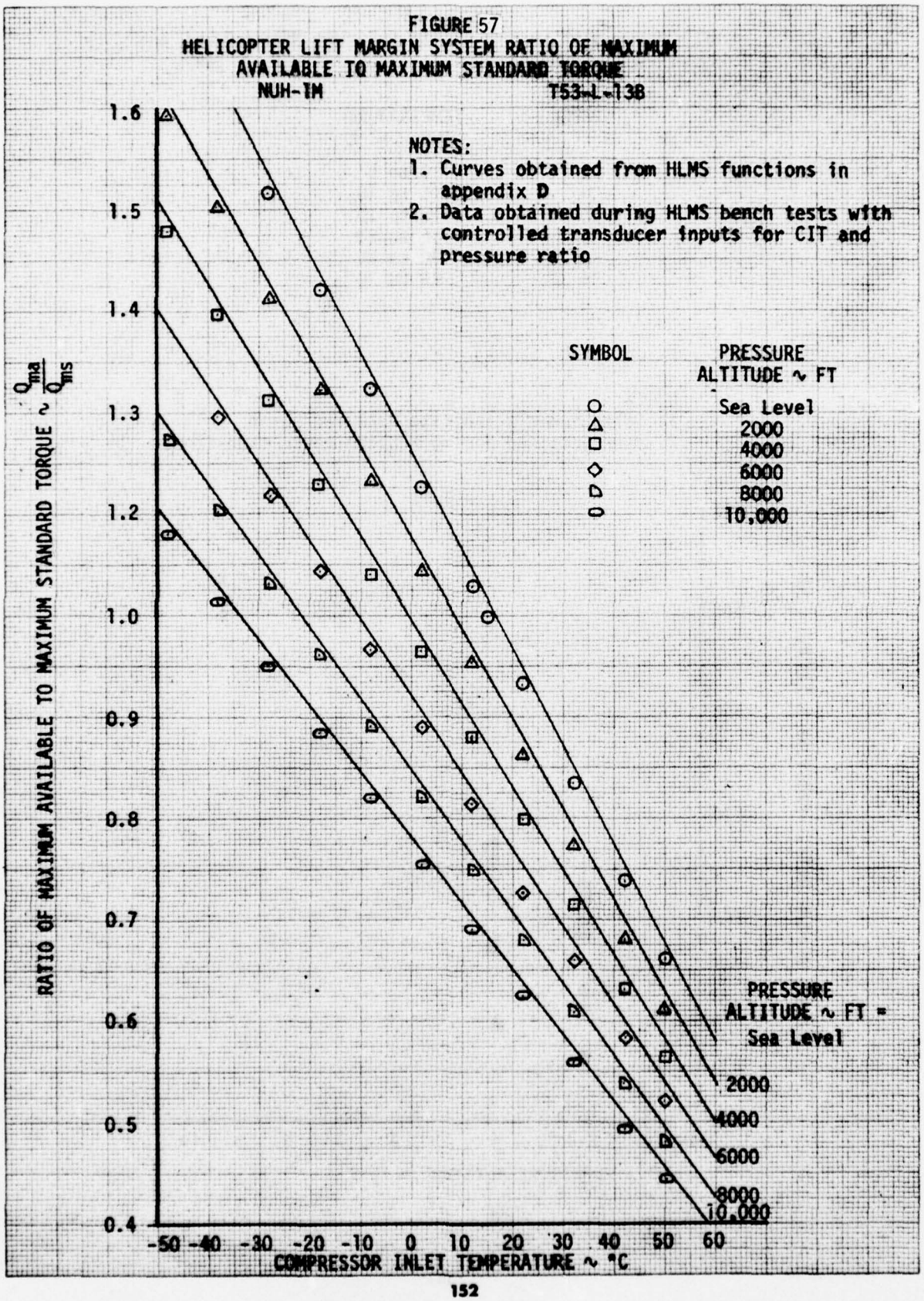

FIGURE 58
HELICOPTER LIFT MARGIN SYSTEM MODEL OF MAXIMUM AVAILABLE LIFT
NUH-1M T53-L-13B

SYMBOL	HLMS MAXIMUM STANDARD TORQUE
- - - - - - - - - -	56.1
———————	58.1
——— - - ——— - -	60.1

NOTE: See appendix D for HLMS functions used

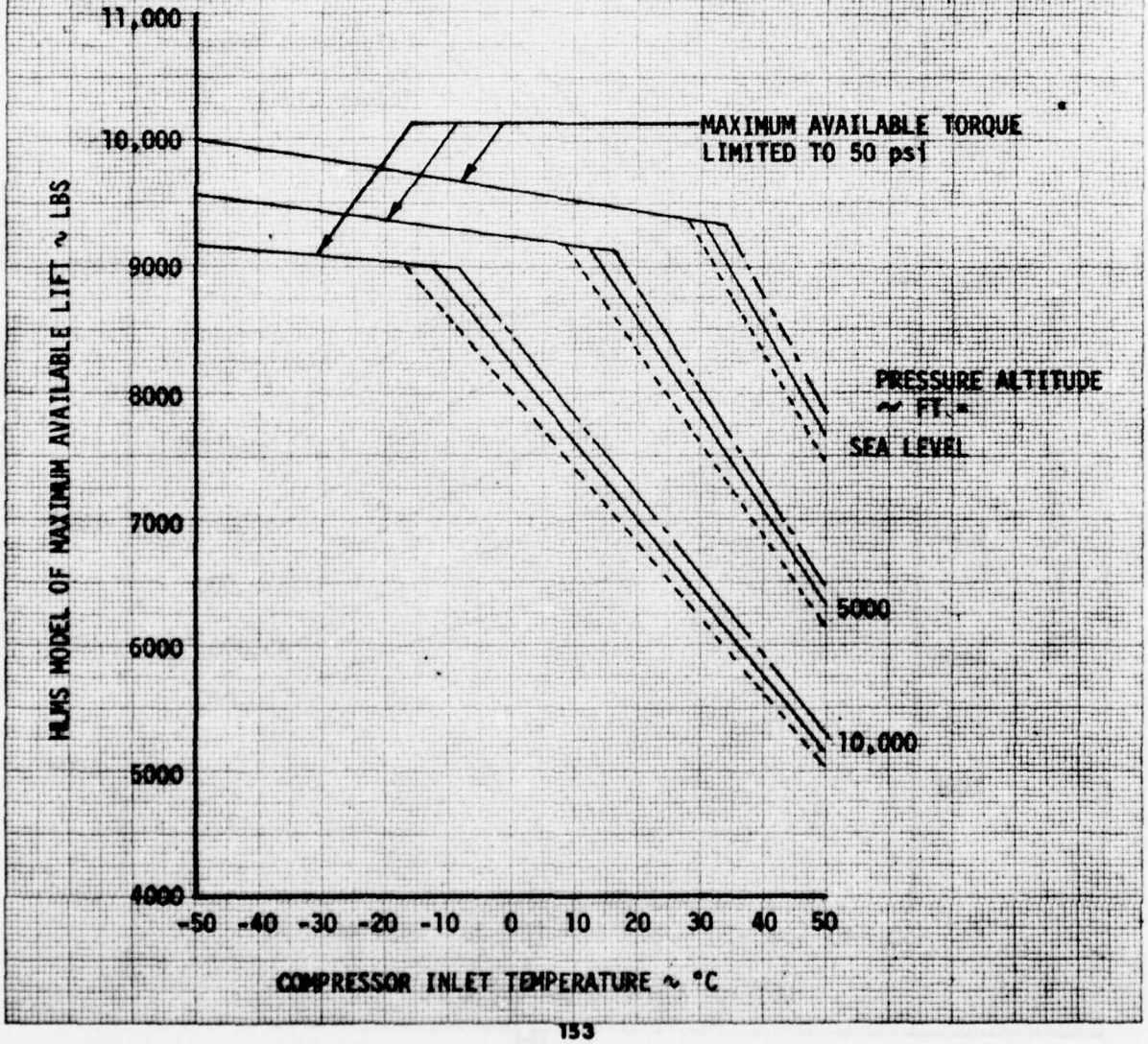

FIGURE 59
DIMENSIONAL OGE HOVERING PERFORMANCE
NUH-1M USA S/N 63-8684 T53-L-13B S/N LE-14420

NOTES:
1. Power required to hover at zero airspeed obtained from figure 1
2. Power available obtained from figure 46
3. Compressor inlet temperature rise = 2.9°C
4. Rotor speed = 324 rpm

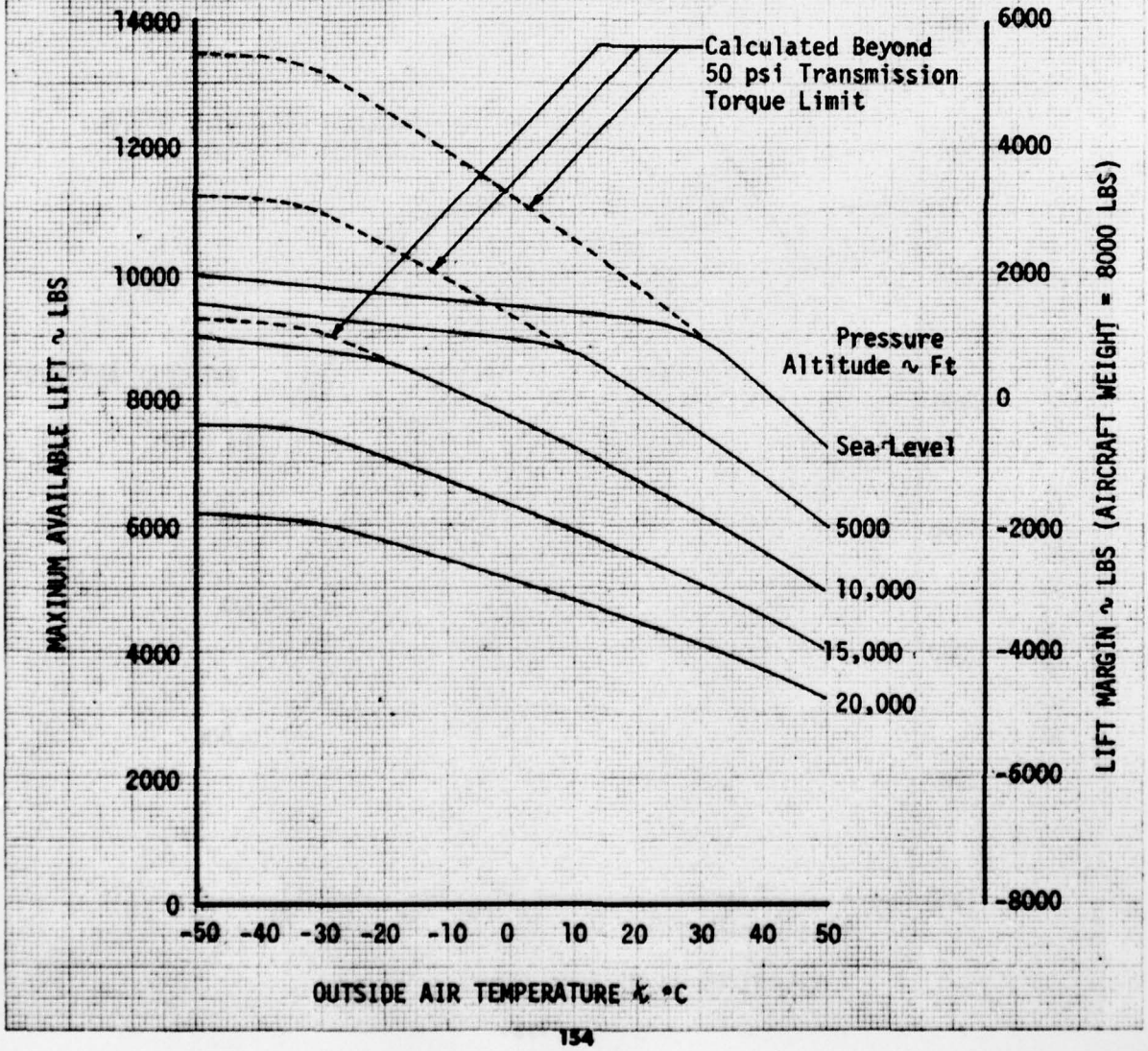

FIGURE 60
HELICOPTER LIFT MARGIN SYSTEM MODEL OF MAXIMUM AVAILABLE LIFT
NUH-1M T53-L-13B

SYMBOL	HLMS MAXIMUM STANDARD TORQUE ~ PSI
———	55.5
- - - - - -	53.5

NOTE: See appendix D for HLMS functions used

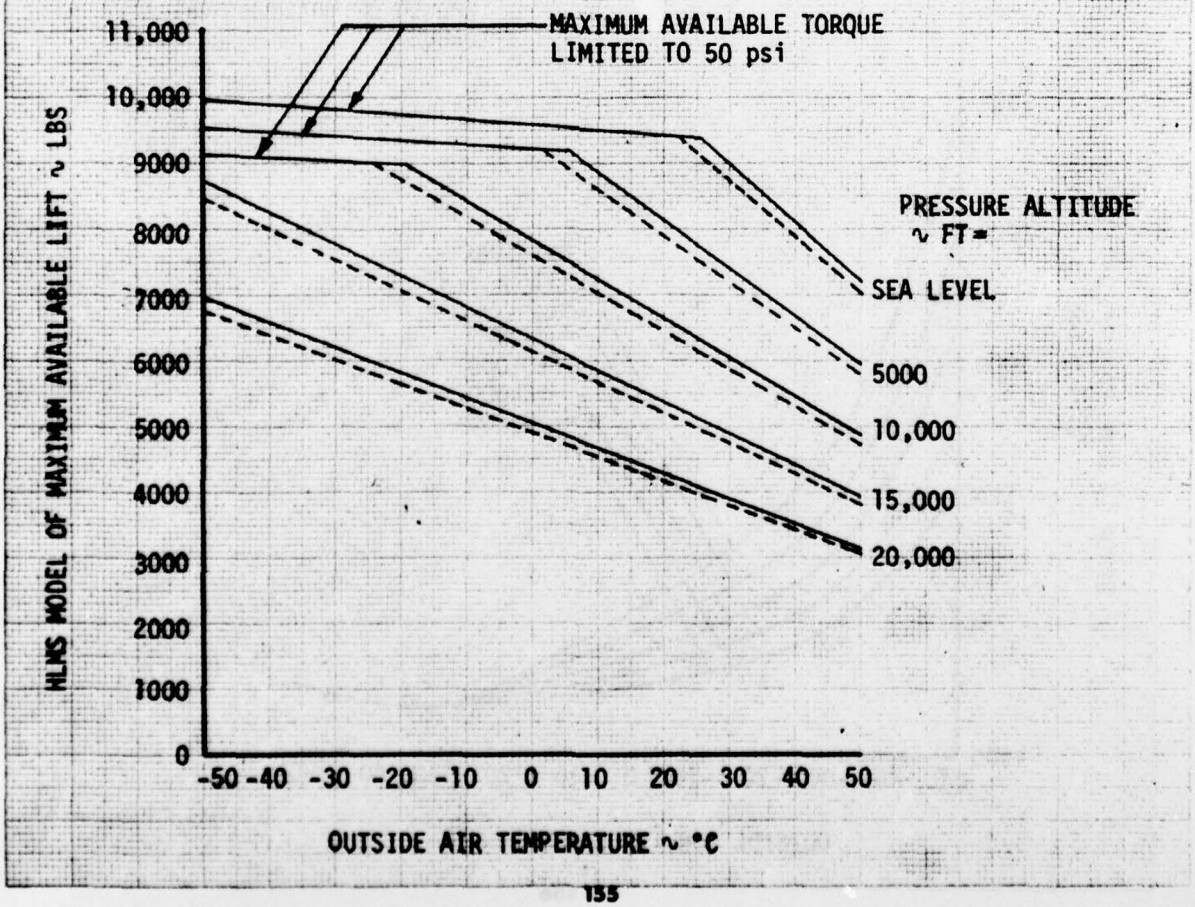

FIGURE 61

HELICOPTER LIFT MARGIN SYSTEM MAXIMUM AVAILABLE LIFT MODELING ERROR

NUH-1M T53-L-13B

HLMS MAXIMUM STANDARD TORQUE = 53.5 PSI

NOTES:
1. Baseline performance obtained from figure 59
2. HLMS model obtained from figure 60

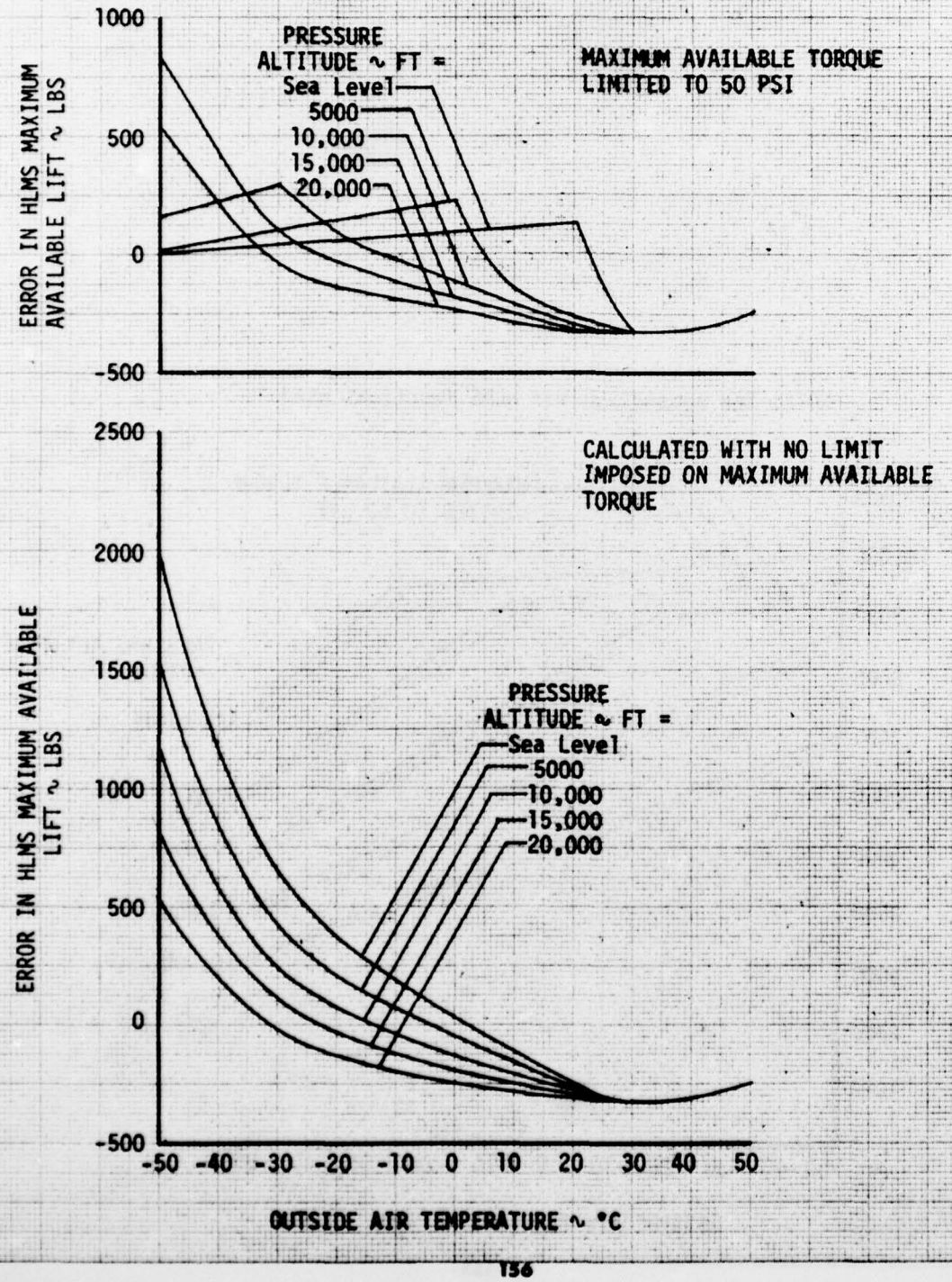

FIGURE 62

HELICOPTER LIFT MARGIN SYSTEM MAXIMUM AVAILABLE LIFT MODELING ERROR

NUH-1M T53-L-13B

HLMS MAXIMUM STANDARD TORQUE = 55.5 PSI

NOTES:
1. Base line performance obtained from figure 59
2. HLMS model obtained from figure 60

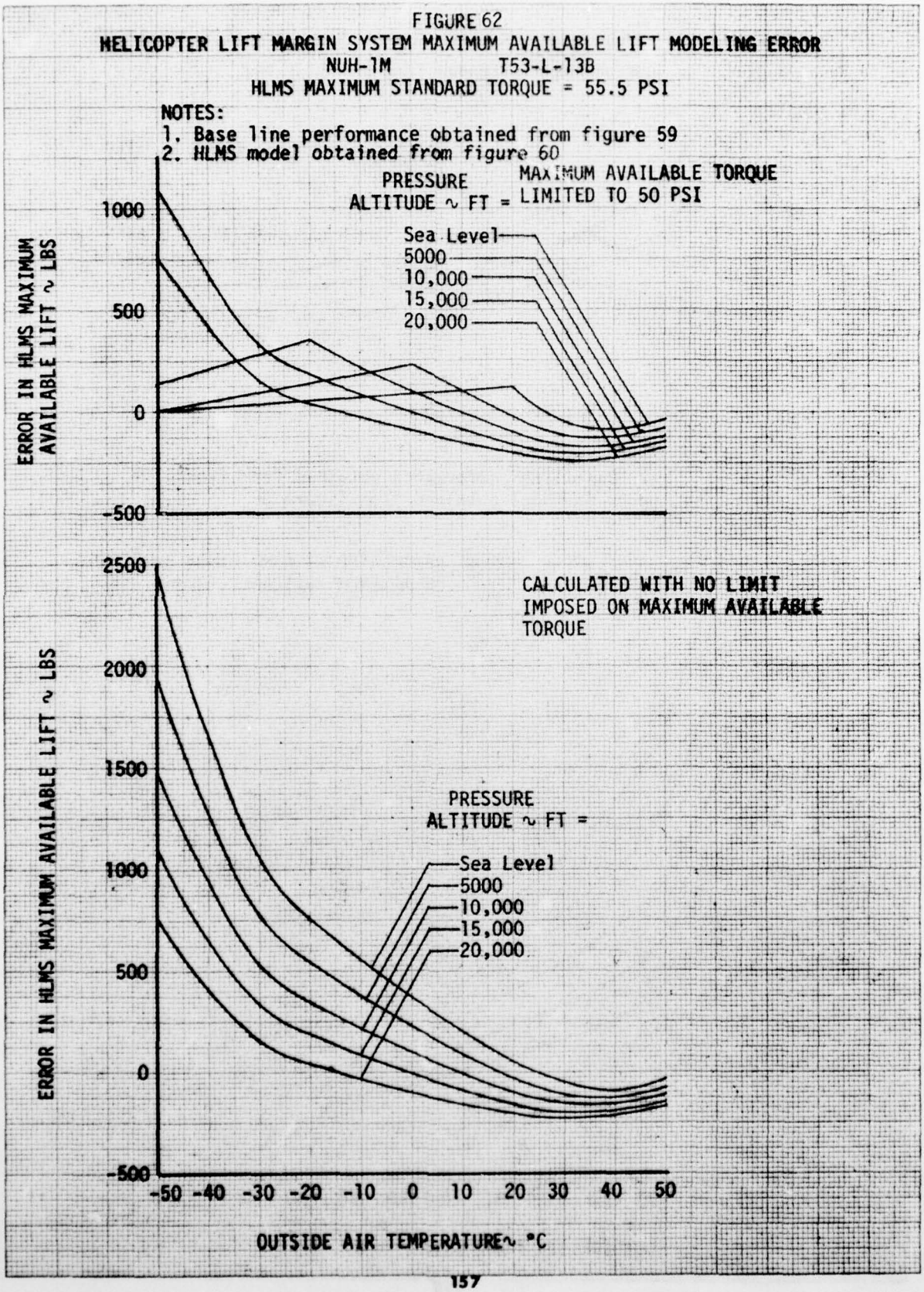

FIGURE 63

HELICOPTER LIFT MARGIN SYSTEM MAXIMUM AVAILABLE LIFT MODELING ERROR

NUH-1M T53-L-13B

HLMS MAXIMUM STANDARD TORQUE = 58.1 PSI

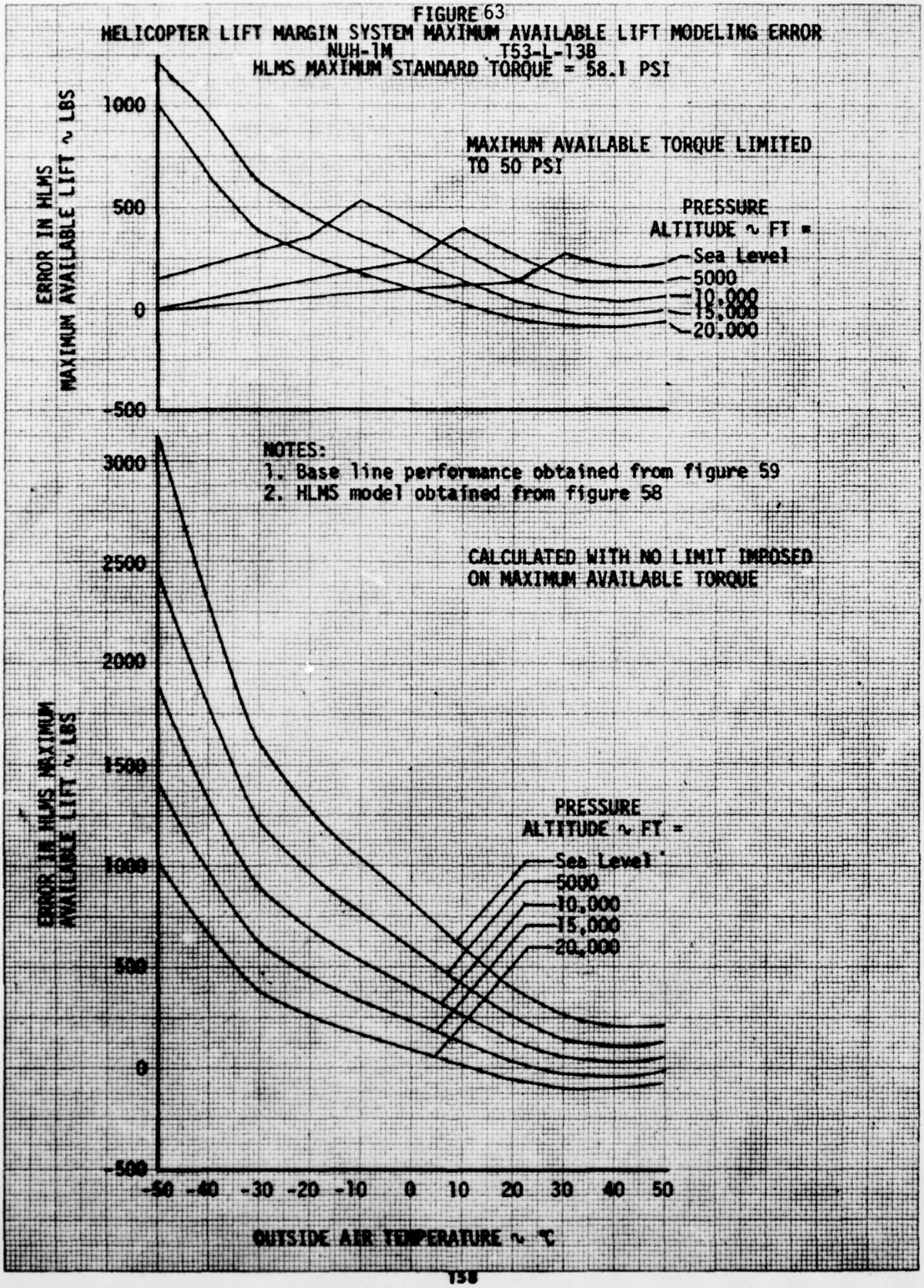

FIGURE 64
HELICOPTER LIFT MARGIN SYSTEM MODEL OF LIFT MARGIN
NUH-1M T53-L-13B

AIRCRAFT GROSS WEIGHT = 8000 LBS

SYMBOL	HLMS MAXIMUM STANDARD TORQUE ~ PSI
- - - - - - - - - - - -	53.5
————————	55.5
—.—.—.—	58.1

NOTES:
1. HLMS Lift Margin = Maximum Available Lift - Effective Gross Weight
2. Effective Gross Weight is initialized (weighing maneuver) at each pressure and temperature condition presented
3. See appendix D for HLMS functions used

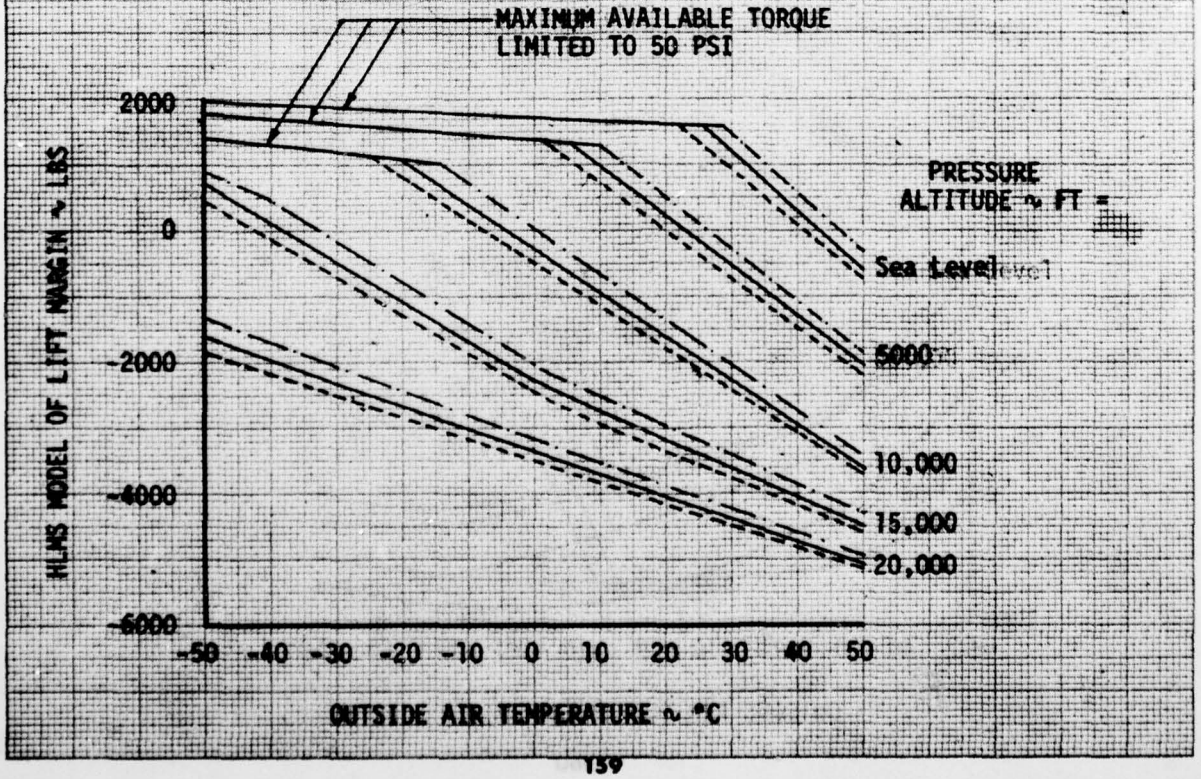

FIGURE 65
HELICOPTER LIFT MARGIN SYSTEM LIFT MARGIN MODELING ERROR
NUH-1M T53-L-13B
AIRCRAFT GROSS WEIGHT = 8000 LBS
HLMS MAXIMUM STANDARD TORQUE = 53.5 PSI

NOTES:
1. Base line performance obtained from figure 59
2. HLMS model obtained from figure 64

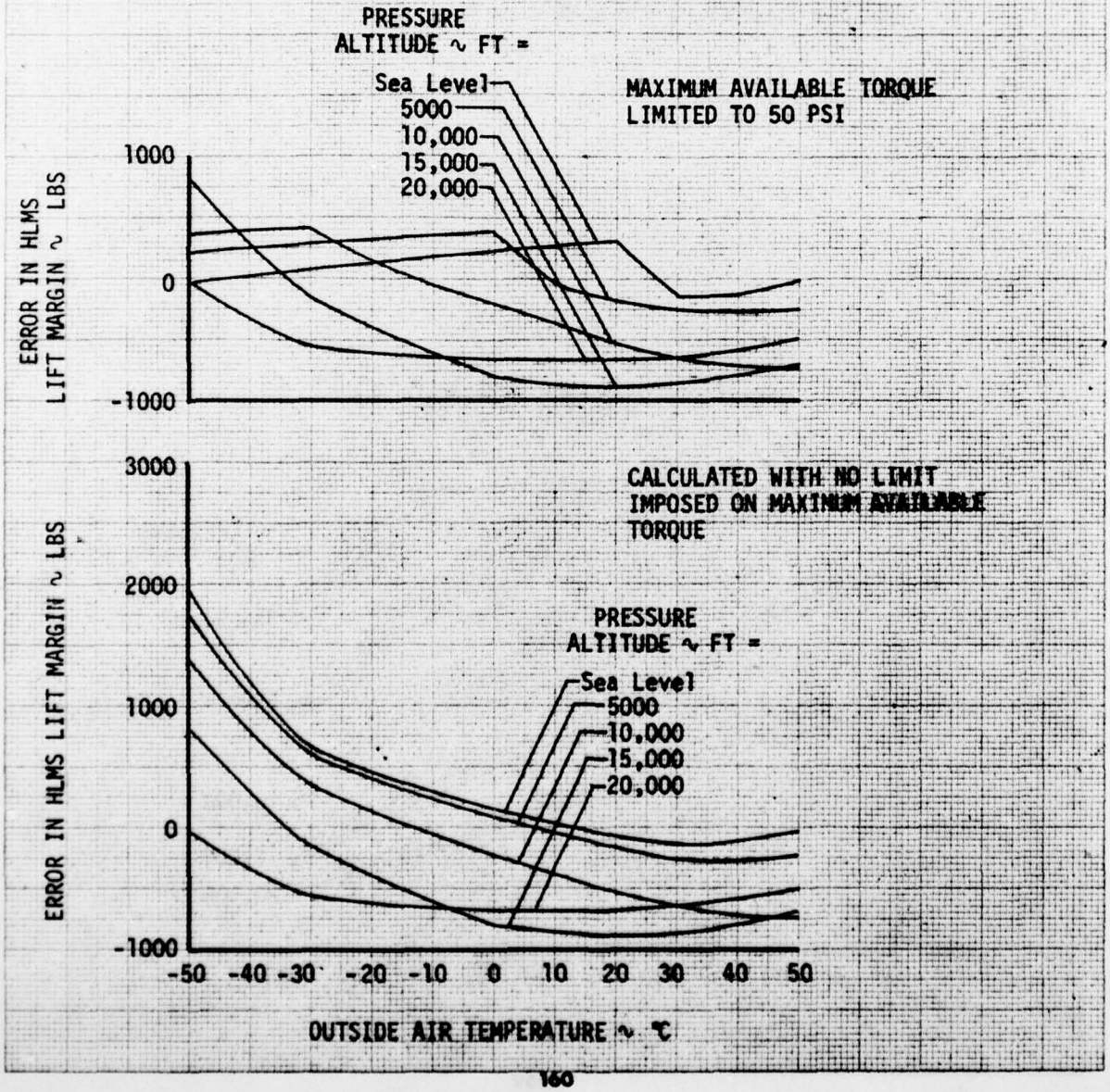

FIGURE 66
HELICOPTER LIFT MARGIN SYSTEM LIFT MARGIN MODELING ERROR
UH-1M T53-L-13B
AIRCRAFT GROSS WEIGHT = 8000 LBS
HLMS MAXIMUM STANDARD TORQUE = 55.5 PSI

NOTES:
1. Base line performance obtained from figure 59
2. HLMS model obtained from figure 64

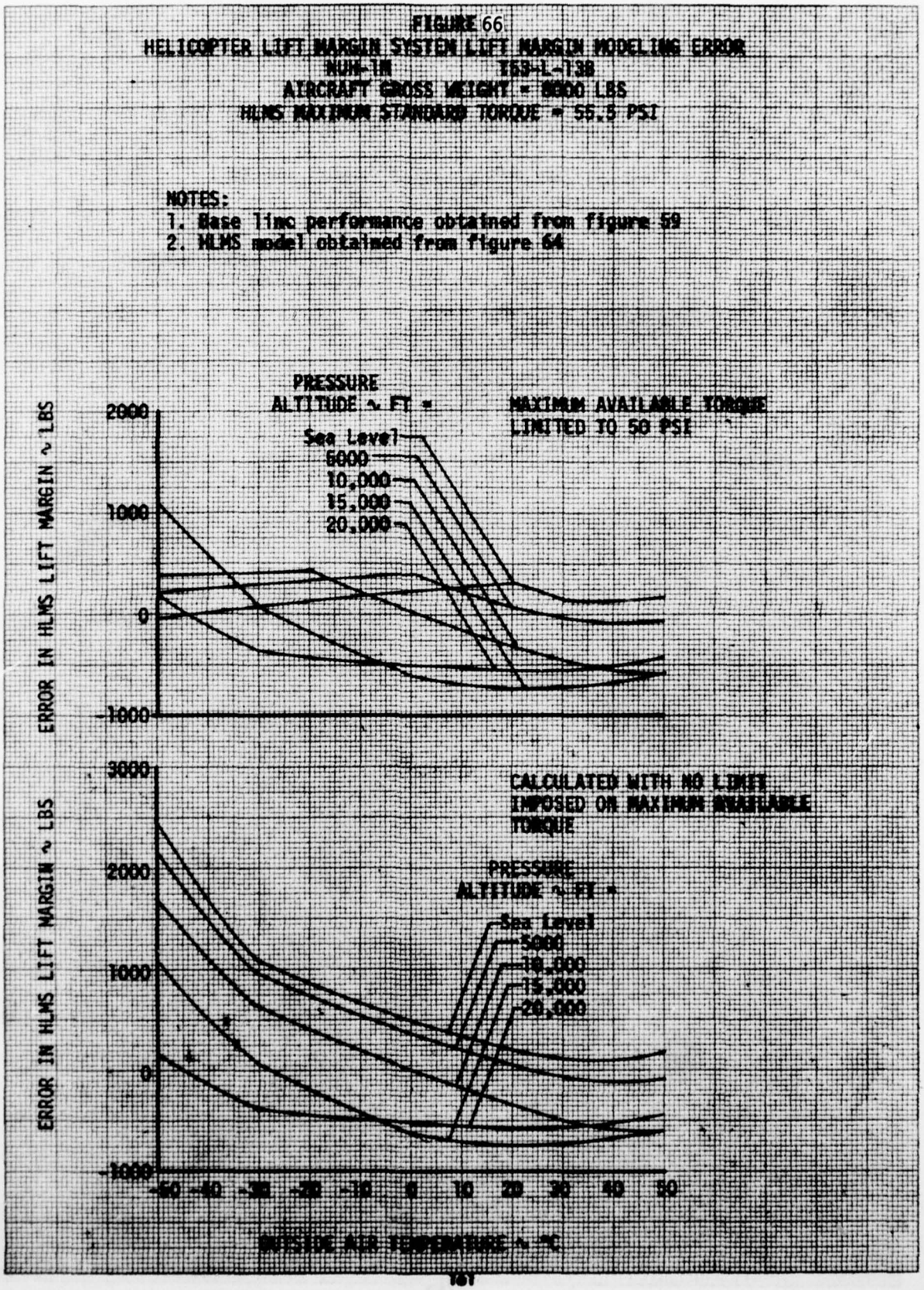

FIGURE 67
HELICOPTER LIFT MARGIN SYSTEM LIFT MARGIN MODELING ERROR
NUH-1M T53-L-13B
AIRCRAFT GROSS WEIGHT = 8000 LBS
HLMS MAXIMUM STANDARD TORQUE = 58.1 PSI

NOTES:
1. Base line performance obtained from figure 59
2. HLMS model obtained from figure 64

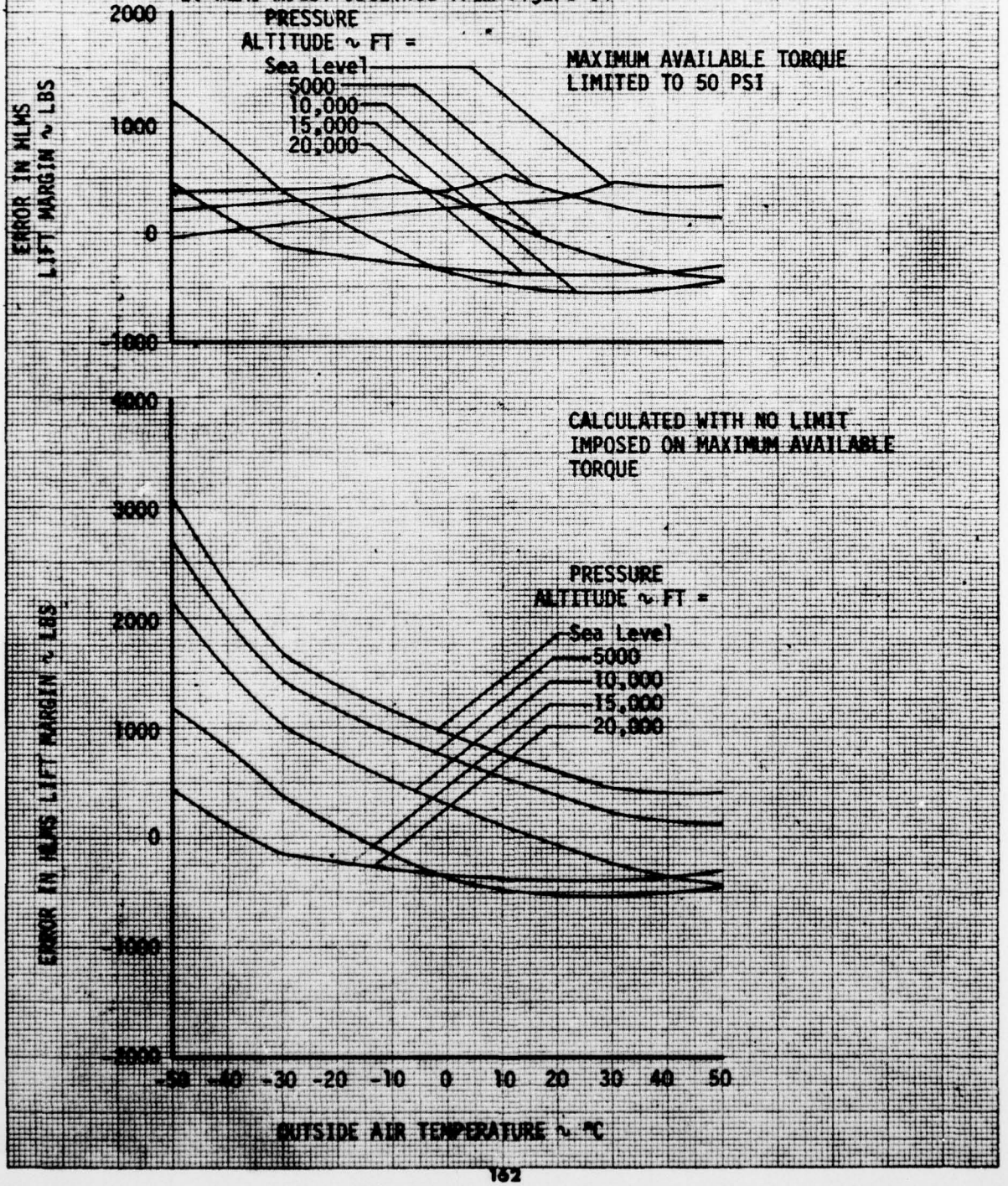

APPENDIX G. SYMBOLS AND ABBREVIATIONS

A	Main rotor disc area ~ 1520.63 ft^2
a	Speed of sound ~ ft/sec
A_n, n = 0,1.2,...11	Polynomial coefficients determining B_n as a function of μ
B_n, n = 0,1,2	Polynomial coefficients determining C_P as a function of C_T
C_P	Power coefficient (nondimensional power) ~ 550 $shp/\rho A(\Omega R)^3$
C_T	Thrust coefficient (nondimensional weight) ~ $GW/\rho A(\Omega R)^2$
C&D	Computer and display unit of the HLMS
CIT	Compressor inlet total temperature ~ °C or °K, as specified
dt	Differential time increment
e	Base of the natural logarithm system ~ 2.71828...
EGW	Equivalent gross weight, the aircraft weight at hover calculated by the HLMS based on the measured engine output shaft torque ~ pounds
$F_{(QE)}$	On/off parameter permitting calculation of fuel-consumed weight in the HLMS
ft	Feet
GW	Gross weight, pounds
hr	Hour
H_D	Density altitude ~ feet
H_P	Pressure altitude ~ feet
HLMS	Helicopter lift margin system

IGE	In-ground-effect conditions, with skid height less than approximatelv 2 main rotor diameters
K_n, n = 1,2.3	Unspecified proportionality constants representing relations between the quantities of an equation
K_Q	Torque constant relating hydraulic engine torque indication (psi) to actual torque units (ft-lb) ~ ft-lb/psi
K_{1i}, K_2, K_{51}, K_{52}	Coefficients of the HLMS equations, as defined in appendix C
K_6, K_7, K_8, K_{91}, K_{92}, K_{11}, K_{12}	
KCAS	Knots calibrated airspeed ~ knots
KTAS	Knots true airspeed ~ knots
kt	Knots
lb	Pounds
LM	Lift margin, the remaining available lift for a particular flight condition ~ pounds
ln ( )	Natural (base e) logarithm of quantity ( )
M	Mach number
MAL	Maximum available lift for a particular flight condition ~ pounds
N_1	Engine gas producer rotational speed ~ rpm or percent of maximum, as specified
N_2	Engine output shaft speed ~ rpm
OAT	Ambient outside air temperature ~ °C or °K, as specified
OGE	Out-of-ground effect conditions, with skid height greater than approximately 2 main rotor diameters.
P	Pressure ~ psi or inches of mercury, as specified

PCM	Pulse code modulation, with signals having discrete instead of continuous values
pexp	Exponent of the pressure ratio in calculation of a referred parameter
psi	Pounds per square inch
P/P_O	Ratio of specified pressure to sea level standard pressure
QE	Engine output shaft torque ~ ft-lb or psi, as specified
Q_{ma}	Maximum available torque at specified flight condition ~ psi
Q_{ms}	Maximum standard torque, a reference quantity representing available engine torque at sea-level standard conditions ~ psi
QMS	Display on the HLMS C&D unit, identical to Q_{ms} ~ psi
R	Main rotor radius, 22.0 feet
rpm	Revolutions per minute
shp	Shaft horsepower
S&M	Simulation and monitor unit of the HLMS
T	Temperature ~ °C or °K, as specified
TDP	Dew point temperature ~ °C or °K, as specified
texp	Exponent of the temperature ratio in calculation of referred parameter
V_T	True airspeed ~ knots
α	Exponential element of the humidity effect equations
β	Angle of sideslip. positive value when aircraft is nose left of the relative wind ~ degrees
Δ	Incremental difference in the specified quantity

δ	Ratio of ambient air pressure to sea-level standard pressure
δ	Partial incremental change of one variable with respect to another
θ	Ratio of ambient air temperature to sea-level standard temperature
μ	Advance ratio (nondimensional airspeed), 1.6878 $V_T/\Omega R$
π	3.14159...
ρ	Air density ~ slug/ft^3
σ	Ratio of ambient air density to sea-level standard density
σ_C	HLMS calculated density ratio
Ω,ω	Main Rotor rotational speed
$\int( )$	Integration of the quantity ( ) with respect to a specified variable

Subscripts

ci	At compressor inlet conditions
cr	Critical
O	At standard ambient sea-level conditions (H_P = 0, H_D = 0, OAT = 15°C)
ref	Quantity referred from existing to standard ambient sea-level conditions
tip	At the main rotor blade tip
WET	Quantity corrected for humidity effects

DISTRIBUTION

Director of Defense Research and Engineering	2
Deputy Director of Test and Evaluation, OSD (OAD(SSST&E))	1
Assistant Secretary of the Army (R&D), Deputy for Aviation	1
Deputy Chief of Staff for Research, Development, and Acquisition (DAMA-WSA,)	2
US Army Materiel Development and Readiness Command (DRCPM-BH, DRCPM-AAH-TM-T, DRCPM-CO, DRCPM-CH-47M, DRCDE-DW-A, DRCSF-A, DRCQA)	20
US Army Aviation Research and Development Command (DRDAV-EQ)	12
US Army Training and Doctrine Command (ATCD-CM-C)	1
US Army Materiel Systems Analysis Activity (DRXSY-CM, DRSXY-MP)	3
US Army Test and Evaluation Command (DRSTE-AV, USMC LnO)	3
US Army Electronic Research and Development Command (AMSEL-VL-D, AMSEL-VL-E)	2
US Army Forces Command (AFOP-AV)	1
US Army Armament Command (SARRI-LW)	2
US Army Missile Command (DRSMI-QT)	1
Director, Research & Technology Laboratories/Ames	2
Research & Technology Laboratory/Aeromechanics	2
Research & Technology Laboratory/Propulsion	2
Research & Technology Laboratory/Structures	2
Research & Technology Laboratories/Applied Technology Laboratory (DAVDL-EU-TSD, Tech Library)	1
US Army Human Engineering Laboratory (DRXHE-HE)	1
US Army Aeromedical Research Laboratory	1
US Army Infantry School (ATSH-TSM-BH)	1
US Army Aviation Center (ATZQ-D-MT)	3
US Army Aviation Test Board (ATZQ-OT-C)	2
US Army Aviation School (ATZQ-AS, ATST-CTD-DPS)	3
US Army Aircraft Development Test Activity (PROV) (STEBG-CO-T, STEBG-PO, STEBG-MT)	5
US Army Agency for Aviation Safety (IGAR-TA, IGAR-Library)	2
US Army Maintenance Management Center (DRXMD-EA)	1

US Army Transportation School (ATSP-CD-MS)	1
US Army Logistics Management Center	1
US Army Foreign Science and Technology Center (AMXST-WS4)	1
US Military Academy	3
US Marine Corps Development and Education Command	2
US Naval Air Test Center	1
US Air Force Aeronautical Division (ASD-ENFTA)	1
US Air Force Flight Dynamics Laboratory (TST/Library)	1
US Air Force Flight Test Center (SSD/Technical Library, DOEE)	3
US Air Force Electronic Warfare Center (SURP)	1
Department of Transportation Library	1
US Army Bell Plant Activity (DAVBE-ES)	5
US Army Boeing Vertol Plant Activity (DAVBV)	2
US Army Grumman Plant Activity	2
US Army Hughes Plant Activity	2
AVCO Lycoming Division	5
Beech Aircraft Corporation	5
Bell Helicopter Textron	5
Boeing Vertol Company	5
Detroit Diesel Allison Division of General Motors Corporation	1
General Electric Company, Technical Information Center	2
Grumman Aerospace Corporation	5
Hughes Helicopter Company	5
Lockheed-California Company	1
Sikorsky Aircraft Division of United Technologies Corporation	5
Teledyne CAE	2
United Aircraft of Canada Ltd	5
Defense Documentation Center	12
USDA Forest Service	1
Department of Navy, Office of Naval Research	5
NASA Ames Research Center	1